EXPLORING WNT REGULATION IN GLIOMA-PROPAGATING CELLS, AND WNT INHIBITION AS A THERAPEUTIC STRATEGY

TOH TAN BOON

B.Sc. (Hons.), NUS

A THESIS SUBMITTED FOR THE DEGREE OF DOCTOR OF PHILOSOPHY

DEPARTMENT OF PHYSIOLOGY

NATIONAL UNIVERSITY OF SINGAPORE

2012

DECLARATION

I hereby declare that the thesis is my original work and it has been written by me in its entirety. I have duly acknowledged all the sources of information which have been used in the thesis.

This thesis has also not been submitted for any degree in any university previously.

_____

TOH TAN BOON

12 December 2012

ACKNOWLEDGEMENTS

I would like to express my heartfelt gratitude to my supervisors, Dr Carol Tang Soo Leng and Associate Professor Ang Beng Ti and for their constant guidance, motivation, patience, enthusiasm and excellent mentorship throughout my graduate studies. They have taught me the importance of thinking critically and this has benefitted me tremendously in my work.

I am also grateful to my co-supervisor, Associate Professor Sanjay Khanna for his invaluable support and encouragement.

I wish to extend my thanks and gratitude to my colleagues and peers, Yuk Kien, Lynnette, Kendra, Edwin, Melanie, Mr Lim and ex-colleagues, Geraldene, Joan, Charlene and Esther with whom I have worked with for years, for their company, friendship, help and support.

I want to express my sincere gratitude and thanks to my family, relatives and friends for their constant support and encouragement throughout this journey.

Special acknowledgement to Edwin Sandanaraj (SICS), for his expertise in bioinformatical analysis.

Last but not least, a very big thank you to all those whom I have unintentionally left out and have in one way or another helped in my project.

TABLE OF CONTENTS

Contents

SUMMARY

Brain tumors such as gliomas have poor prognosis despite advanced surgical intervention and adjuvant chemo- and radiotherapies. The highly infiltrative and recurrent nature of this disease has often been attributed to stem-like cells with extensive self-renewal potential. These cells, termed “glioma-propagating cells” (GPCs), can be isolated from clinical material, and we now have a way to cryopreserve them, with maintenance of essential primary tumor hallmarks such as karyotype and transcriptomic profile. Our foundational work established that histologically similar glioblastoma (GBM, grade IV) tumors yield GPCs with very distinct transcriptomic profiles, suggesting molecular heterogeneity and possibly accounting for the frequently observed inter-patient variability to treatment response. Importantly, we were able to show in the major glioma variants, oligodendroglial tumors and GBM, that GPCs contain signaling pathways, manifested as transcriptomic programs which dictate primary tumor behavior, disease progression and patient survival outcome. These findings emphasize that GPCs are clinically relevant and can serve as a valuable cellular platform for further studies. We explored one of these transcriptomic programs, Wnt, in detail. We showed pharmacologically and genetically that Wnt activation promotes GPC growth and tumorigenicity, mediated through the MITF transcription factor. GPCs (oligodendroglial and GBM) with high MITF expression were more sensitive to pathway inhibition, highlighting the limitation of relying solely on histology to diagnose and subsequently treat patients. Our study provides evidence that tumor growth can be mitigated by targeting Wnt signaling.

LIST OF TABLES

LIST OF FIGURES

LIST OF ABBREVIATIONS

ABC	ATP binding cassette
ABCB1	ATP-binding cassette, sub-family B (MDR/TAP), member 1
ABCC2	ATP-binding cassette, sub-family C (CFTR/MRP), member 2
ABCG2	ATP-binding cassette, sub-family G (WHITE), member 2
AO	Anaplastic Oligodendroglioma
APC	Adenomatous polyposis coli
ATCC	American Type Culture Collection
ATM	Ataxia telangiectasia mutated
bFGF	basic Fibroblast growth factor
bHLH/LZ	basic Helix –loop-helix and leucine-zipper
BRCA1	Breast cancer 1, early onset
CBP	CREB-binding protein
CD133	Complementarity determinant 133
CDKN2A	Cyclin-dependent kinase inhibitor 2A
CDKN2C	Cyclin-dependent kinase inhibitor 2C
CI	Confidence interval
CKIα	Casein kinase 1 alpha
CMAP	Connectivity Map
CNS	Central nervous system
CSC	Cancer stem cell
DCT	Dopachrome tautomerase
DKK	Dickkopf
DMEM	Dulbecco's Modified Eagle Medium
DMSO	Dimethylsulfoxide
dsDNA	Double-strand DNA
Dvl	Dishevelled
EG	Ethylene glycol
EGFR	Epidermal growth factor receptor
ES	Embryonic stem
FAP	Familial adenomatous polyposis

FBS	Fetal bovine serum
FL	Firefly luciferase
FoxM1	Forkhead box M1
GBM	Glioblastoma multiforme
G-CIMP	CpG island methylator phenotype
GEMM	Genetically engineered mouse model
GFAP	Glial fibrillary acidic protein
GPC	Glioma-propagating cells
GSEA	Gene Set Enrichment Analysis
GSK3β	Glycogen synthase kinase 3 beta
HEPES	4-(2-hydroxyethyl)-1-piperazineethanesulfonic acid
HM	Holding medium
HOX	Homeobox
HR	Hazard ratios
HRP	Horseradish peroxidase
HTS	High-throughput screen
IL-6	Interleukin-6
Int-1	Integration-1
IWP	Inhibitor of Wnt production
IWR	Inhibitor of Wnt response
L1CAM	L1 cell adhesion molecule
LEF	Lymphoid enhancer binding protein
LIF	Leukemia inhibitory factor
LOH	Loss of heterozygosity
LRP5/6	Low-density lipoprotein receptor-related protein 5/6
MADM	Mosaic analysis with double markers
MAPK	Mitogen-activated protein kinase
MGMT	O-6-methylguanine-DNA methyltransferase
MITF	Microphthalmia-associated transcription factor
MMTV	Mouse mammary tumor virus
MOBP	Myelin-associated oligodendrocyte basic protein

Msi-1	Musashi-1
MTT	3-(4,5-Dimethylthiazol-2-yl)-2,5-diphenyltetrazolium bromide
NBS1	Nijmegen breakage syndrome 1
NF1	Neurofibromatosis type I
NICD	Notch intracellular domain
NOD-SCID	Non-obese diabetic-severe combined immunodeficient
NSC	Neural stem cell
NT	Non-targeting
O4	Oligodendrocyte marker O4
Oct4	Octamer-binding transcription factor 4
OPC	Oligodendroglial precursor cell
PA	Pilocytic astrocytoma
PCA	Principal Component Analysis
PcG	Polycomb group
PCV	Procarbazine, lomustine, and vincristine
PDGF	Platelet-derived growth factor
PDGFRB	Platelet-derived growth factor receptor, beta polypeptide
PEG3	Paternally expressed 3
PI3K	Phosphatidylinositol 3-kinase
PLAGL2	Pleiomorphic adenoma gene-like 2
Porcn	Porcupine
PP2A	Protein phosphatase 2A
PTEN	Phosphatase and tensin homolog
qRT-PCR	quantitative Reverse Transcription Polymerase Chain Reaction
Rb	Retinoblastoma
REMBRANDT	REpository for Molecular BRAin Neoplasia DaTa
RL	Renilla luciferase
RTK	Receptor tyrosine kinase
sFRP	secreted Frizzled-related protein
shRNA	short hairpin RNA
SP	Side population

SSEA-1	Stage-specific embryonic antigen-1
STF	SuperTopFlash
SVZ	Subventricular zone
TCF	T-cell factor
TCGA	The Cancer Genome Atlas
TGFβ	Transforming growth factor beta
TGFβR1	Transforming growth factor, beta receptor 1
TMZ	Temozolomide
TuJ1	Neuron-specific class III beta tubulin
VS	Vitrification solution
Wg	Wingless
WHO	World Health Organization
WIF-1	Wnt-inhibitory factor-1
β-TrCP	Beta-transducin repeat containing protein

LIST OF PUBLICATIONS

Peer-reviewed journal articles

Koh, L.W., Koh, G.R., Ng, F.S., **Toh, T.B.**, Sandanaraj, E., Phong, M., Tucker-Kellogg, G., Kon, O.L., Ng, W.H., Ng, I., Pervaiz S., Ang, B.T., Tang, C., 2013. A Distinct Reactive Oxygen Species Profile confers Chemoresistance in Glioma-Propagating Cells and Associates with Patient Survival Outcome. Antioxidants and Redox Signaling. (Epub ahead of print)

Ng, F.S., **Toh, T.B.**, Ting, E., Koh, G.R., Sandanaraj, E., Phong, M., Wong, S.S., Leong, S.H., Kon, O.L., Tucker-Kellogg, G., Ng, W.H., Ng, I., Tang, C., Ang, B.T., 2012. Progenitor-Like Traits Contribute to Patient Survival and Prognosis in Oligodendroglial Tumors. Clin Cancer Res. (Co-first author)

Foong, C.S., Ng, F.S., Phong, M., **Toh, T.B.**, Chong, Y.K., Tucker-Kellogg, G., Campbell, R.M., Ang, B.T., Tang, C., 2011. Cryopreservation of cancer-initiating cells derived from glioblastoma. Front Biosci (Elite Ed) 3, 698-708.

Chong, Y.K., **Toh, T.B.**, Zaiden, N., Poonepalli, A., Leong, S.H., Ong, C.E., Yu, Y., Tan, P.B., See, S.J., Ng, W.H., Ng, I., Hande, M.P., Kon, O.L., Ang, B.T., Tang, C., 2009. Cryopreservation of neurospheres derived from human glioblastoma multiforme. Stem Cells 27, 29-39. (Co-first author)

Toh, T.B., Chen, M.J., Armugam, A., Peng, Z.F., Li, Q.T., Jeyaseelan, K., Cheung, N.S., 2008. Antioxidants: promising neuroprotection against cardiotoxin-4b-induced cell death which triggers oxidative stress with early calpain activation. Toxicon 51, 964-973.

Peer-reviewed Book chapters

Koh, L. W., **Toh, T. B.**, Tang, C., and Ang, B. T., 2012. Glioma-propagating cells show enhanced chemoresistance and radioresistance (an update). Stem Cells and Cancer Stem Cells: Therapeutic Applications in Disease and Injury. Hayat, M.A. (Ed.). Springer Press.

Toh, T.B., Chong, Y.K., Ang, B.T., Tang, C., 2012. Glioblastoma Multiforme: Cryopreservation of Brain Tumor-Initiating Cells (Method) Tumors of the Central Nervous System, Volume 4, in: Hayat, M.A. (Ed.). Springer Netherlands, pp. 95-101.

Presented abstracts and posters

Toh, T.B., Ng, F.S., Ting, E., Koh, G.R., Sandanaraj, E., Phong, M., Wong, S.S., Leong, S.H., Kon, O.L., Tucker-Kellogg, G., Ng, W.H., Ng, I., Tang, C., Ang, B.T., 2012. Progenitor-Like Traits Contribute to Patient Survival and Prognosis in Oligodendroglial Tumors. Physiology Symposium 2012 (Poster presentation)

Koh, L. W., Ng, F. S., Koh G. R., Phong, M., **Toh, T. B.**, Ng. K., Pervaiz, S., Tucker-Kellogg, G., Ang, B. T., and Tang, C. Glioblastoma-propagating cells: Reactive oxygen species as central modulators of chemoresistance. Frontiers in Cancer Science 2011 Conference (Poster presentation)

Ng, F. S., Ting, E. H., Koh G. R., Phong, M., Wong, S. S., Leong, S. H., Kon, O. L., Lee J. S., **Toh, T. B.**, Foong, C. S., Tucker-Kellogg, G., Ng, W. H., Ng, I., Tang, C., Ang, B. T. Stem-like tumor-propagating cells contribute to molecular heterogeneity and survival outcome in gliomas. Frontiers in Cancer Science 2011 Conference (Poster presentation)

CHAPTER 1

INTRODUCTION

CHAPTER 1 – INTRODUCTION

Preamble

This thesis explores the molecular characteristics of glioma-propagating cells (GPCs) and shows that GPC core activation pathways contribute to primary tumor behavior, glioma disease progression and patient survival outcome. In addition, we explore the Wnt signaling pathway in GPC maintenance, and show that glioma growth can be abrogated by targeting these long-term, self-renewing cells. The "Introduction" chapter is divided into the following sections which form the basis of our exploration:

i. Molecular classification of glioma.
ii. Glioma-propagating cells (GPCs).
iii. Mouse models relevant for glioma studies.
iv. Targeting GPCs for an effective cure – signaling mechanisms.
v. The Wnt signaling pathway.

1.1 Classification of Gliomas

Gliomas are the most common primary brain tumors of the central nervous system with heterogeneous morphology and variable prognosis. Variants such as glioblastoma multiforme (GBM) portend poor prognosis with a mean survival period of 15 months despite advanced surgical intervention, accompanied by adjuvant radio- and chemotherapies (Louis et al, 2007) . The most widely used current classification of human gliomas is that of the World Health Organization (WHO) system (Louis et al, 2007). The WHO system divides diffuse gliomas into astrocytic tumors, oligodendrogliomas, and oligoastrocytomas. These are then graded into histological degrees of malignancy. Two major subtypes are recognized, namely the astrocytic and the oligodendrocytic tumors. Astrocytic tumors are further subdivided into grades I (pilocytic astrocytomas, PA), II (low grade), III (anaplastic), and IV

(glioblastoma multiforme, GBM) (**Table 1.1**). Oligodendrocytic tumors are separated into grades II (low grade) and III (anaplastic). GBM, a WHO grade IV tumor, is characterized by rapid, highly invasive growth, extensive neovascularization and high mortality. The key reason for unsuccessful therapy is the infiltration of tumor cells into the surrounding brain parenchyma cells, preventing complete glioblastoma resection. Furthermore, glioma cells are notoriously resistant to chemotherapies.

Table 1.1. WHO classification of glial tumors based on histology. WHO grading of glial tumors into grades I-IV is based on the presence or absence of four criteria: (1) nuclear atypical, (2) mitoses, (3) endothelial cell proliferation, (4) necrosis. Adapted from Kleihues *et al.* (2002)

WHO Grading	Type of glioma	Criteria
Grade I	Pilocytic astrocytoma	Benign, slow-growing, low cellularity, presence/ absence of microvascular proliferation
Grade II	Diffuse astrocytoma	Well differentiated neoplastic astrocytic cells; increased hypercellularity; absence of mitosis, necrosis and microvascular proliferation
Grade III	Anaplastic astrocytoma	Distinct nuclei atypia; high rate of hypercellularity and mitosis; absence of necrosis and microvascular proliferation
Grade IV	Glioblastoma multiforme	Pleomorphic astrocytic tumor cells with marked nuclei atypia; very high rate of hypercellularity and mitosis; presence of microvascular proliferation and necrosis

Gliomas of better prognosis include the oligodendroglial tumors. These tumors possess genetic indicators such as the 1p/19q co-deletion status which renders the tumors highly sensitive to chemotherapy (Cairncross et al, 1998). Patient survival, time to progression and response to therapy are all associated with subtype and grade of the tumor (Louis et al, 2007). The current WHO classification of glioma, combined with the patient's prognostic features (e.g. age and Karnofsky Performance Score, KPS), guides treatment decisions. Traditional anatomic and pathologic classification of tumors has

very limited ability to stratify patients into meaningful subgroups for prognosis and intervention. Differences between histological subtypes are very subtle, and classifying gliomas is subjected to large inter-observer variability (Murphy et al, 2002). Consequently, this can result in misdiagnosis. Since treatment protocols often depend on the diagnosed histological subtype, accuracy in diagnosis is very important for patients to get optimal treatment (Murphy et al, 2002). Therefore, more accurate methods to diagnose gliomas are urgently required.

1.2 Molecular Classification of Gliomas

There have been extensive studies on the molecular characteristics of gliomas over the years in order to provide more objective and accurate methods of identifying distinct molecular tumor subgroups, and to identify specific molecular tumor markers that can assist diagnosis, and consequently impacting on treatment decisions. In 2006, the National Cancer Institute, USA, initiated a multi-consortial effort to deep profile, as one of the first cancers, glioblastoma multiforme (GBM), because of its dismal prognosis (Louis et al, 2007). *This effort is predicated on the belief that histologically similar tumors can be molecularly heterogeneous, and that distinct pathways drive the biological phenotype.* The first publication arising from The Cancer Genome Atlas (TCGA) effort showed that patients with GBM sustain mutations that can be grouped into 3 major signaling networks: Receptor tyrosine kinases (RTKs), p53 and Retinoblastoma (Rb) tumor suppressor pathways (Atlas, 2008). Importantly, GBM tumors are molecularly heterogeneous, further highlighting the limitations of relying solely on morphology-based histological methods to diagnose and subsequently treat patients. There have been several attempts to molecularly classify GBM (**Table 1.2**). At a transcriptomic level, Philips *et al.* described 3 subclasses of

GBM tumors; Proneural, Proliferative, and Mesenchymal that correspond to different stages of neurogenesis (Phillips et al, 2006a). Notably, proneural GBM comprises of patients with primary diagnosis, younger age, and better prognosis. In contrast, older age patients and patients with tumor relapses more often associate with Mesenchymal GBM (Lee et al, 2008; Phillips et al, 2006a). A follow-up study at a genomic level then showed that GBM tumors can be further molecularly classified into four subgroups; Proneural, Classical, Mesenchymal and Neural, with each subgroup exhibiting unique gene expression, genomic aberrations and clinical profile (Verhaak et al, 2010). To complement the initial molecular sub-classification of GBM by proteomic analysis, Brennan *et al*. identified active platelet-derived growth factor (PDGF) signaling and loss of neurofibromatosis (NF1) tumor suppressor gene expression as characteristic features of proneural and mesenchymal GBM respectively (Brennan et al, 2009). Using an integrative subtype analysis to characterize subtypes with coordinated genomic, epigenomic, and transcriptomic alterations, Shen *et al.* applied the iCluster algorithm on a subset of 55 GBM samples and showed the existence of three distinct integrated tumor subtypes: (1) iCluster1, a subtype that is enriched for the G-CIMP phenotype and displays a proneural expression profile; (2) iCluster2, a subtype that is characterized by near complete association with EGFR amplification, overrepresentation of promoter methylation of homeobox and G-protein signaling genes, and a classical expression profile; (3) iCluster3 is characterized by NF1 and Pten alterations and exhibits a mesenchymal-like expression profile (Shen et al, 2012). With the strength of an integrative clustering analysis, the authors were able to discover and visualize coordinated patterns of genomic alterations, providing a biologically comprehensive context for subtype discovery.

Table 1.2. Molecular classification of GBM tumors. Overview of the molecular subtypes of GBM at genomic, transcriptional, proteomic and integrated levels. Clustering methodology is shown on the left column.

Clustering method	Subtypes identified				References
Transcriptional	Proneural	Proliferative	Mesenchymal	-	Philips et al. (2006a)
Genomic	Proneural	Classical	Mesenchymal	Neural	Verhaak et al. (2010)
Proteomic	PDGF	EGFR	NF1	-	Brennan et al. (2009)
Integrated genomic, transcriptional, and epigenomic	iCluster1	iCluster2	iCluster3	-	Shen et al. (2012)

A major inference from these studies is that GBM patients can now potentially be treated according to their molecular subclasses and pathway activation. Indeed, Wiedemeyer *et al.* recently showed via pharmacological targeting in a panel of GBM cell lines that co-deletion of *CDKN2A* and *CDKN2C* served as a strong predictor of sensitivity to a selective inhibitor of CDK4/6 (Wiedemeyer et al, 2010). This mapped to similar patterns of *CDKN2A* and *CDKN2C* mutations in TCGA patients, leading to hyperactivated CDK4/6. The Wiedemeyer study thus demonstrates that the integration of genomic, functional and pharmacologic data can be exploited to inform the development of targeted therapy directed against specific cancer pathways. Importantly, the TCGA effort emphasizes that gene expression drives GBM disease progression and clinical outcome.

1.3 Glioma-propagating Cells (GPCs)

The understanding of the normal development of the nervous system has dramatically increased in recent decades. The nervous system has a complex cellular hierarchy ranging from a neural stem cell (NSC) that can give rise to all of the major lineages in the brain parenchyma (neurons, astrocytes, and oligodendrocytes) to lineage-committed progenitors that have a more restricted differentiation potential to terminally differentiated cells (Rietze et al, 2001; Uchida et al, 2000). The expression of nestin, a common

marker of neural stem-progenitor cells was subsequently demonstrated in a variety of neuroepithelial brain tumors (Dahlstrand et al, 1992; Tohyama et al, 1992). The interest in applying normal developmental biology to the field of cancers is perhaps fueled by work of John Dick and colleagues on the identification of cancer-initiating cells in leukemia (Bonnet & Dick, 1997). Subsequently, similar identifications of cancer-initiating populations have been found in multiple systemic cancer types including the breast, colon, pancreatic, prostate and brain (Al-Hajj et al, 2003; Collins et al, 2005; Li et al, 2007; O'Brien et al, 2007; Singh et al, 2003).

Conceptually, cancer stem cells (CSCs) define a small, biologically unique subset of cells with the capability to self-renew and generate the diverse cell types that constitute the whole tumor (Reya et al, 2001). These cells are termed cancer stem cells because of their “stem-like” properties shared commonly with normal tissue stem cells. These properties include extensive self-renewal ability (symmetrical and asymmetrical) and differentiation capacity. The latter, however, is not a mandatory feature of CSCs. Nevertheless, the concept of CSC is of considerable importance as it highlights the need to eradicate the CSC populations to achieve an effective cure. In recent years, the several terminologies such as cancer/ tumor-initiating cells (CICs or TICs) and cancer/ tumor-propagating cells (CPCs or TPCs) have emerged in part due to the operational detection of cells with CSC properties in different contexts. CICs or TICs are more accurately referred to the original cells from which the malignancy first arose as shown elegantly by several lineage tracing mouse models (described in Section 1.5) (Alcantara Llaguno et al, 2009; Jacques et al, 2010; Zheng et al, 2008). CPCs or TPCs, on the other hand, refer to cancer cells that can perpetuate and sustain tumor growth, at least in a serial xenotransplantation model, with the

ability to maintain key karyotypic hallmarks, stemness expression and multipotentiality. As such, in the context of our studies in gliomas, we termed glioma-propagating cells (GPCs) as patient-derived cancer cells from gliomas with the ability to serially transplant and perpetuate tumors that recapitulate the original patient pathophysiology in a xenograft model.

1.3.1 Markers to identify GPCs

The seminal work by Singh *et al*. demonstrated that the expression of a putative neural stem cell marker, CD133, in malignant tumor cells derived from gliomas and medulloblastomas, was sufficient and necessary to initiate and recapitulate the tumor upon transplantation into immunodeficient mice (Singh et al, 2003). Since these initial observations, numerous groups have joined the effort in elucidating the role of cancer stem cells in brain tumors. Recent studies have suggested that several additional but not overlapping markers represent the tumor-propagating cells in brain tumors. These include stage-specific embryonic antigen 1 (SSEA-1) or CD15 (Son et al, 2009), nestin (Bar et al, 2007b), aldehyde dehydrogenase (Bar et al, 2007b), Sox2 (Gangemi et al, 2009), CD44 (Anido et al, 2010), integrin-α6 (Lathia et al, 2010), Bmi-1 (Abdouh et al, 2009) and the side population (Bleau et al, 2009; Chua et al, 2008). Since many of these markers are also expressed on normal cellular counterparts, they do not present the best targeting candidates in any therapeutic strategy. In addition, the initial finding that only CD133-positive cells are the tumor-initiating population has been disputed as tumors have been demonstrated to also arise from CD133-negative cells in a subset of GBM tumors (Beier et al, 2007; Sakariassen et al, 2006). Importantly, CD133 expression has been shown to change with surface sialylation according to disease state and progression, further complicating its definition as a marker of *bona fide* tumor-initiating capacity (Kemper et al,

2010; Zhou et al, 2010). Henceforth, the field of cancer stem cell biology is moving away from heavy reliance on surface marker identification of tumor-initiating cells, to complementing findings that measure the *functional activities* of tumor stem cells (**Figure 1.1**).

1.3.2 Functional assays to identify GPCs

The GPC is defined functionally and there are assays to measure this. One such frequently used assay is the neurosphere assay (Reynolds et al, 1992). The neurosphere assay is often used to approximate neural stem cell frequency in the normal neural stem and progenitor cells of the adult central nervous system (CNS). Neurospheres are heterogeneous and comprise of *bona fide* long-term, self-renewing neural stem cells, as well as lineage-committed short-term, transit-amplifying progenitors (Singec et al, 2006). Therefore, sphere-forming frequency defined by sphere number is typically scored over three to four generations to measure the activity of *bona fide* neural stem cells, compared to transit-amplifying progenitors which loses sphere-forming ability typically after one or two generations (Reynolds & Rietze, 2005). Importantly, this sphere forming frequency has been demonstrated to translate to *in vivo* animal survival outcome (Anido et al, 2010; Clement et al, 2007). In addition, the readout of individual neurosphere size, which approximates proliferation, is important as it distinguishes proliferation arising from the *bona fide* stem cell population which would otherwise be masked if general short-term viability assays (e.g. MTT assay) are carried out that also measure the proliferation of progenitor cells.

The central theme of the cancer stem cell hypothesis is the ability of a subpopulation of cells at the apex of the hierarchy to propagate tumors and promote tumor progression in an orthotopic xenograft transplantation model as compared to the non-tumorigenic cells within the tumor bulk (**Figure 1.1**).

The gold standard to identify GPCs functionally is the ability for the GPCs to reform a phenotypic copy of the original tumor in an orthotopic transplantation model, usually performed as a limiting dilution assay. Non-GPCs, by definition, lack this ability and fail in the transplant model. It is important to note that the hierarchy model of the CSC hypothesis may not be ubiquitous for all cancers or be represented in certain experimental cancer models. For instance, Quintana *et al.* challenged the CSC hypothesis by demonstrating that CSC frequency could be altered based on several parameters: (1) addition of extracellular matrix in the form of matrigel; (2) extending the duration for tumor formation; (3) varying the severity of immune-compromised mice depending on strains used. This study demonstrated that the tumor-initiating capacity, at least in melanoma, is an artifactual consequence of the conditions employed in the xenografts model. Despite the lack of ability of *in vitro* cultured stem-like GPCs to reflect the actual transformational cell in tumorigenesis, the use of GPCs remains important for several reasons. First, GPCs have been shown to retain their transcriptomic and karyotypic features commonly found in the primary tumor in contrast to the commercially procured serum-grown glioma cell lines that often contain additional genomic aberrations (Lee et al, 2006; Li et al, 2008). Second, only GPCs establish xenografts tumors that recapitulate the patient's original histopathology (Lee et al, 2006). Finally, transcriptomic analyses suggest that the stemness properties of GPCs and other cancer stem cells are enriched in high grade, malignant tumors, and contributes to disease progression and survival outcome (Shats et al, 2011). These reasons underscore the importance of GPCs as a more reliable and physiologically relevant cellular system to study disease mechanism.

Our work here describes the isolation and characterization of patient-derived GPCs (Chong et al, 2009). We demonstrate that histologically similar GBM tumors yield GPCs with very different transcriptomic profiles, suggesting that these underlying differences may account for the frequently observed inter-patient variability to treatment response. In addition, Shats *et al.* has shown that a stemness signature derived from embryonic stem cells could predict the breast cancer patient cohort sensitive to small molecules linked to this signature using the Connectivity Map (Lamb et al, 2006; Shats et al, 2011), highlighting the clinical contribution of cancer-initiating cells to patient outcome. As with many studies involving the prospective isolation of tumor-initiating cells, only limited amounts of clinical material are available, and this limitation is compounded by the lack of methods to preserve such cells at convenient time points. Although *in vivo* serial passage of GPCs can provide a reliable means to maintain such primary cells, however in practice it is not always possible to have access to immune-compromised animals of suitable ages to continuously maintain these cells. In addition, serial propagation of GPCs in animals has been shown to result in a genetic drift towards highly proliferating genes as evident by the over-representation of the proliferative expression signature (Hodgson et al, 2009; Phillips et al, 2006a). Eventually, the original features and characteristics of these lines will be lost.

Using our novel modified cryopreservation technique, we essentially resolved the bottleneck in maintaining these cells. That is, we now have a reliable repository of different primary patients' lines that can be thawed upon experimental needs, and since these lines are characterized, we now understand how each patient's phenotypic and transcriptomic profiles looks like. This will greatly enhance any projects that deal with larger patient numbers to address the patient stratification hypotheses.

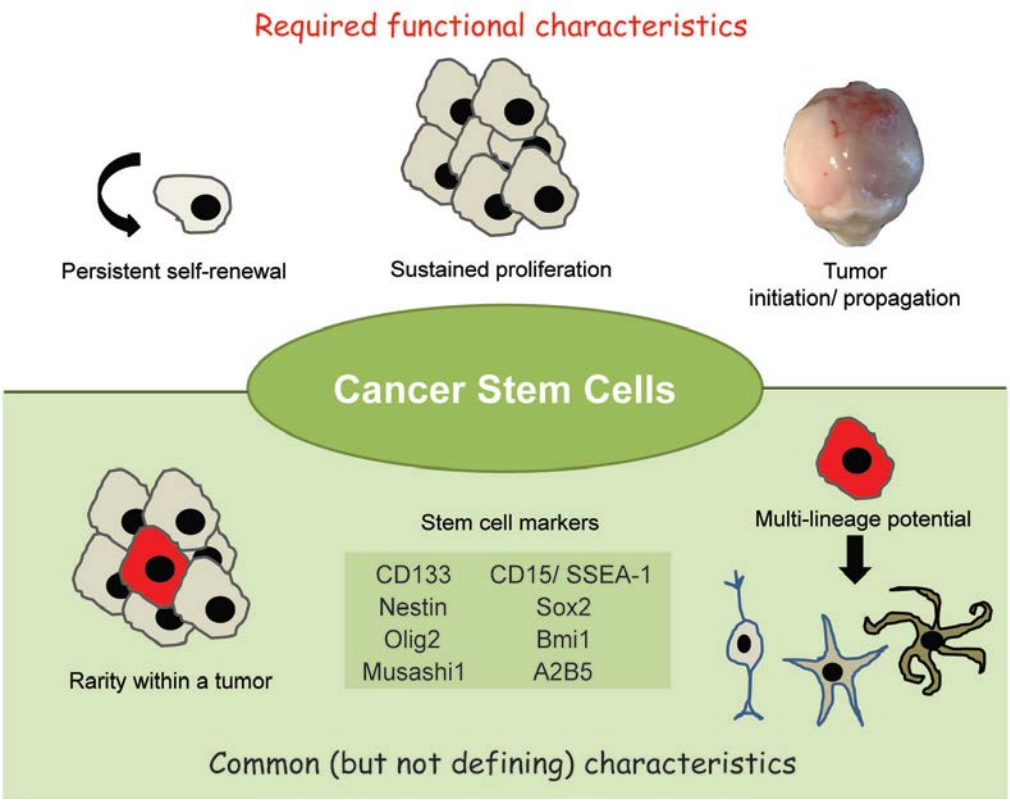

Figure 1.1. Cancer stem cells are defined by a set of functional characteristics. Some of the required functional characteristics that define cancer stem cells include sustained self-renewal, persistent proliferation, and the ability of tumor initiation and propagation. Other characteristics that are often, but not necessarily, associated with cancer stem cells include rarity within a tumor, expression of stem cell markers, and multi-lineage differentiation.

1.3.3 GPCs contribute to primary tumor phenotype

In assessing the contribution of stem-like GPCs to the primary tumor phenotype, several studies have focused on analyzing common GPC marker expression in tissue paraffin sections, often with ambiguous data. This may be reconciled by the fact that GPC properties that sustain the tumor phenotype may reside in more than just specific marker profiles (Bar et al, 2007b; Beier et al, 2007; Sakariassen et al, 2006; Singh et al, 2004; Son et al, 2009). Consequently, pathway activation resembling those functioning in stem-like cells, *represented by a set of genes*, is more likely to correctly

interrogate the clinical contribution of GPCs. An elegant study was carried out by Visvader *et al.* in *BRCA1* mutation-associated breast tumors (Lim et al, 2009). The authors derived differentially regulated genes in subsets of epithelial cells and found that luminal progenitors were highly represented in *BRCA1* mutation-associated breast tumors, even more than the commonly anticipated stem cell population. This suggests that luminal progenitors are more likely the cells-of-origin for *BRCA1* mutation-associated breast cancers, later confirmed in a transgenic mouse model study (Molyneux et al, 2010). Such studies underscore the predictive capability of gene expression mapping of pathway activation, instead of focusing on a specific marker identity. In another separate study, John Dick and colleagues recently demonstrated that serial tumor-initiating (and not marker-defined) acute myeloid leukemia stem cells contribute to disease progression and patient survival outcome (Eppert et al, 2011), highlighting the importance of functionally defining the cancer stem cell.

Two other relevant studies demonstrated that GPCs contribute to GBM patient survival outcome, with preferential activation of core stem cell programs (hematopoietic, neural and embryonic stem cells) (Shats et al, 2011; Yan et al, 2011). Yan *et al.* performed a transcriptomic profiling of CD133+ and CD133- from human GBM and established a CD133 gene expression signature composed of 214 differentially expressed genes. The authors subsequently compared their gene signature with a compendium of published gene expression profiles and found that the CD133 gene signature transcriptomically resembles the human embryonic stem (ES) cells. Most importantly, the CD133 gene signature identifies an aggressive subtype of GBM seen in younger patients with shorter survival who bear excessive genomic mutations as surveyed through TCGA GBM mutation spectrum. Hence, the study by Yan *et al*. provides molecular and genetic support for the

stem-like nature of cells and an objective means for evaluating cancer aggressiveness. In support, Shats *et al.* has shown that a stemness signature derived from embryonic stem cells could predict the breast cancer patient cohort sensitive to small molecules linked to this signature using the Connectivity Map (Lamb et al, 2006), demonstrating the clinical contribution of cancer stem cells to patient outcome.

The key message from these studies is that cancer stem cells perpetuate tumors not merely in terms of their cell numbers or surface marker expression, but more accurately reflected by their pathway activation. Consequently, the primary tumor phenotype is a manifest of cancer stem cell behavior and signaling.

1.4 Mouse models of glioma

Gliomas are heterogeneous, both at the molecular and cellular levels. The complex biology of these tumors makes understanding glioma pathogenesis and the development of novel effective therapies extremely challenging. Unlike *in vitro* culture system using established glioma cell lines or primary cells, tumor development in mice is accompanied by other complex processes such as invasion, angiogenesis and metastasis, similar to those in human cancer. More importantly, mouse models provide a temporally and genetically controlled environment for studying the tumorigenic mechanisms and treatment response. Of note, mouse models of molecularly characterized GBM provide opportunities to determine whether activation of certain pathways can lead to a specific GBM subtype and to generate histologically and genetically accurate mimics of the human disease. Some of the genetically engineered mouse models (GEMMs) that are driven by the genes

known to be key drivers for each clinically distinct glioma subtype are discussed below.

1.4.1 Xenograft Mouse Models

Xenografts are created by implanting tumor cells derived from clinical material or immortalized glioma cell lines into immunocompromised mice. There are two models of xenografts: (1) orthotopic (tumor cells implanted into the original site of occurrence) and (2) heterotypic (non-autochthonous site). The traditional glioma xenograft models uses glioma cell lines (commercially procured and immortalized, usually grown in serum-containing medium) that have been passaged and maintained in tissue culture for long periods of time. Gliomas that are generated from these cell lines do not recapitulate the classical glioma pathophysiology of human gliomas (Lee et al, 2006). In addition, they have not been predictive for response in preclinical trials.

The use of patient-derived tumor cells for orthotopic xenograft transplantation has yielded valuable information on important aspects of GBM histology. In particular, tumor cells derived from freshly isolated human glioma tumors, when cultured in serum-free conditions optimized for tumor stem cell growth and injected orthotopically in animals, more closely mirror the phenotype and genotype of the primary tumor than when cultured in serum-containing medium (Lee et al, 2006). These tumors typically recapitulate the diffuse invasion of glioma cells into the normal brain structures. Moreover, serial passage of these cells in mice can lead to changes in tumor phenotype, suggesting that the progression from lower grade tumor to higher grade GBM may be modeled in such systems (Wang et al, 2009). Furthermore, the importance of recreating the tumor in an anatomically correct site is emphasized in Galli *et al*. where only orthotopic but not subcutaneous tumors

recapitulated the original patient tumor histopathology (Galli et al, 2004). Several groups are currently using these modern xenograft models in preclinical testing. The advantage to such systems is that they are derived from human gliomas. These orthotopic models have also allowed for experiments aimed at studying the biology of glioma-propagating cells (GPCs) and have recently been utilized to recreate the microenvironment and cellular heterogeneity seen in human tumors. Importantly, efforts from TCGA have shown that glioma xenografts established from clinical but not commercially procured material/cells recapitulate the 4 molecular subclasses, each with distinct gene expression, genetic aberrations and clinical profile (Verhaak et al, 2010).

1.4.2 Genetically Engineered Mouse Models (GEMMs)

A second popular cancer model in animals is to use genetically engineered mouse models (GEMMs) with close genetic resemblance to human disease. The advantages of this model includes: (1) the ability to provide appropriate material for comparative onco-genomic studies, which are directed at identifying additional genes that are altered in the development of tumor; (2) tumors derived from these GEMMs can be used to validate the functionality of specific genes in tumorigenesis; (3) GEMMs can also be used to analyze network of genes with specific genetic mutations, hence allowing the assignment of genetic lesions into defined pathways and the testing of drugs targeting these activities. Taken together, GEMMs address the molecular causation of tumor initiation, progression, therapeutic response and histology, contributing to the understanding of the molecular pathways implicated.

Using germline genetic modification techniques, it was demonstrated that GEMMs with activation of receptor tyrosine kinase (RTK) pathways in the

brain along with simultaneous loss of cell cycle-related genes, develop gliomas with high penetrance. This was confirmed by TCGA project which showed that the core signaling pathways are crucial for gliomagenesis. With additional loss of the tumor suppressor phosphatase and tensin homolog (Pten), a higher grade malignancy and reduced survival in mouse glioma models occurred, recapitulating the clinical profile (Kwon et al, 2008).

Mouse modeling that enforces PDGFRB expression produces tumors that ranges from the low-grade oligodendroglioma or oligoastrocytoma to the high-grade GBM with oligodendroglial features (Shih et al, 2004; Uhrbom et al, 2002). The grade of these tumors is regulated by several factors such as the expression levels of PDGF, loss of p53 and Ink4a/arf, and Pten (Dai et al, 2001; Fomchenko et al, 2011; Shih et al, 2004; Uhrbom et al, 2002). Expression profiling of these tumors shows a parallel expression pattern to the human proneural molecular subgroup, which is predominated by PDGF signaling (Lei et al, 2011). In addition, amplification and activating mutation of *EGFR* is the canonical genomic alteration in the classical molecular subgroup of GBM (Brennan et al, 2009; Verhaak et al, 2010). The mouse model of EGFR-driven gliomagenesis, with germline constitutive active variant of EGFR, in conjunction with deletion of Ink4a/arf and Pten, develops high penetrance GBM that histologically resembles the classical GBM in humans (Zhu et al, 2009). Creation of GBM in mice by deletion of NF1 and p53 tumor suppressors shed light on our understanding that NF1 loss is the canonical alteration in the mesenchymal subgroup of GBM (Atlas, 2008; Reilly et al, 2000; Zhu et al, 2005). Furthermore, tumors with NF1 loss often exhibit loss of p53, Ink4a/arf, and Pten (Verhaak et al, 2010).

Recently, variations in genetic mouse models have been used to investigate one of the most important gaps in the knowledge of glioma biology

– the origin of glioma progression and development. With the availability of inducible Cre recombinase transgenes that allow both temporal and spatial induction of Cre recombinase, thereby effecting gene expression or knockout in cell type-specific compartments with a Rosa reporter to trace evolving progeny, the cells of origin alongside with its differentiated progeny, have been elegantly demonstrated in intestinal cancers (Barker et al, 2009; Barker et al, 2007). Recent works have highlighted the importance of neural stem cells as the cells-of-origin with mutations in NF1/Pten/p53, or p53/Pten, as opposed to arising from the more mature progeny such as astrocytes, in contributing to GBM formation (Alcantara Llaguno et al, 2009; Jacques et al, 2010). GEMMS are useful as they offer a window into the events governing the tumorigenic process.

1.5 Cell-of-origin of glioma

One of the major contributing factors to glioma heterogeneity is the tumor cell-of-origin. Cells-of-origin are the normal cells in which tumorigenic mutations first occur and accumulate to form a full-blown malignancy. Cancer stem cells (CSCs), on the other hand, are defined as cells that maintain an already formed tumor. Therefore, the term “tumor-initiating cells” is more in line with the “cells-of-origin”, whereas CSCs would be more accurately be referred to as “tumor-propagating cells” (Visvader, 2011).

There are several theories on the identity of the origin of gliomas. Before the discovery of adult neural stem cells (NSCs), the astrocytes, the only known replication-competent population, were thought to be the cells-of-origin of gliomas. The theory of dedifferentiation of astrocytes to malignant forms is supported by recent findings that reprogramming a panel of transcription factors can turn terminally differentiated cells back to the

pluripotent state (Takahashi & Yamanaka, 2006). Moreover, Verma and colleagues most recently demonstrated that ectopic lentiviral knockdown of key tumor suppressor genes in astrocytes and neurons initiated glioma formation, which later dedifferentiated (Friedmann-Morvinski et al, 2012). However, to-date, definitive evidence supporting that astrocytes are the cells-of-origin are lacking due to the lack of good astrocyte marker. Glial fibrillary acidic protein, GFAP, a widely used marker for astrocytes is also expressed in NSCs (Doetsch et al, 1999).

As NSCs have been shown to be the self-renewing population in postnatal mammalian brains, they were subsequently suspected to be the glioma cell of origin (Zhao et al, 2008). The long-term self-renewal capacity of NSCs offers an advantage to allow accumulation of oncogenic mutations or hits. Recent evidences have supported the NSCs as cells-of-origin. Alcantara *et al.* demonstrated that deleting the tumor suppressors p53, NF1, and Pten specifically in postnatal murine neural stem or progenitor cells resulted in glioma formation with 100% penetrance (Alcantara Llaguno et al, 2009). On the other hand, ablation of these genes in non-neurogenic adult murine brain regions did not produce any tumors. Similarly, Jacques *et al.* showed that ablation of p53, Pten, and/or Rb in stem cells of the subventricular zone (SVZ), but not in the peripheral astrocytes, generated gliomas (Jacques et al, 2010). However, these studies were not able to distinguish between the more quiescent, long-term self-renewing NSCs from the more rapidly dividing progenitor cells. More recently, using mosaic analysis with double markers (MADM), Liu *et al.* demonstrated that the early expanding tumor cells in the Nf1;p53-based mouse oligoastrocytoma model are cells that express oligodendrocyte precursor cell (OPC) markers (Liu et al, 2011a).

An ideal model to study the cell-of-origin should address: (1) whether the cells in question are capable of transformation after harboring a set of oncogenic events; and (2) the kinds of mutations that accumulate in these transformed cells. The development and identification of cell-specific markers and other technologies that enhance precise temporal and spatial somatic gene manipulation would greatly facilitate the study of cell-of-origin.

1.6 Selected signaling pathways regulating GPCs

Key signaling pathways that are crucial for normal neural stem cells, such as Notch, Hedgehog, and the PI3K-Akt axis, have been a focus of increasing interest in cancer therapy as these pathways may underlie GBM therapeutic response and targeting of these pathways may preferentially deplete GPCs. Indeed, our lab's earlier work with Eli Lilly pharmaceutical company utilizing a small molecule screen of several inhibitors against key oncogenic pathways showed that GPCs can be targeted via PI3K/Akt, GSK3β, mTOR, CDK9, PLK1 and TAK1 (Foong et al, 2011; Foong et al, 2012). Certainly, there is much literature supporting our observations that these regulatory pathways promote GPC growth and survival (Bao et al, 2006; Eyler et al, 2008; Kotliarova et al, 2008; Lee et al, 2012). Although the role of these pathways in glioma is not new, their effectiveness against specifically GPCs, the long-term self-renewing population, is of interest in designing a therapy with effective cure, abrogating the infiltrative and recurrent nature of the disease. The targeting of the slowly-dividing population also calls into place the appropriate endpoints for measuring drug effectiveness, since most conventional cancer assays detect short-term and mainly anti-proliferative effects. This would imply that the drugs selected could have been prioritized, paradoxically, against the eventually terminal progenitor population instead of targeting the actual tumor-sustaining fraction.

The cancer stem cell hypothesis thus forces a re-evaluation of endpoints for efficacious drug development.

1.6.1 EGFR/PI3K/AKT axis in GPC regulation

The presence of autocrine and paracrine growth factor loops are common in malignant gliomas and these pathways regulate numerous pro-tumorigenic cellular functions including cellular proliferation, apoptotic resistance, invasion and angiogenesis. Epidermal growth factor (EGF), routinely used in culturing EGF-responsive neural precursors, is a key growth factor used in the maintenance of GPCs (Lee et al, 2006). GBMs frequently display EGFR amplification, with expression of the constitutively active variant EGFRvIII, mediated through PI3K-Akt and Ras/mitogen-activated protein kinase (MAPK) downstream signaling in GBMs and is associated with enhanced tumorigenic potential and more aggressive phenotypes, such as invasiveness and therapeutic resistance (Brandes et al, 2008). Shinojima *et al.* evaluated 87 primary GBM patients and found EGFR amplification to be an independent, unfavorable predictor for overall survival (Shinojima et al, 2003). In this cohort, EGFRvIII overexpression in the presence of EGFR amplification is the strongest indicator of a poor survival prognosis.

Intratumoral heterogeneity plays a major role in contributing to GBM resistance to EGFR targeted therapy due either to pre-existing resistant clones within the tumor or the interaction of non-resistant clones with the tumor cells or the tumor niche. Mazzoleni *et al*. showed that despite both the molecularly and functionally distinct $EGFR^{pos}$ and $EGFR^{neg}$ GPCs being able to form tumors on their own that phenocopy the original tumor sample, only $EGFR^{pos}$ GPCs had elevated tumorigenic proliferation and highly invasive characteristic (Mazzoleni et al, 2010). Hence, the presence of distinct

subpopulations within the same tumor might contribute to GBM resistance and EGFR targeted therapies since $EGFR^{neg}$ GPCs are insusceptible to treatment and will survive to reform the tumor mass. Inda *et al*. demonstrated that EGFRvIII cells secrete IL-6 and LIF, which in turn promote the growth and proliferation of wild-type EGFR cells that form the tumor bulk. This small subset of EGFRvIII cells, driven in a paracrine manner to recruit wild type EGFR cells into accelerated proliferation, enhances the tumorigenic potential of the bulk tumor and actively maintains a heterogeneous expression of both the wild type and the mutant form (Inda et al, 2010). Mice orthotopic tumors overexpressing EGFRvIII are refractory to radiation therapy, with sustained repopulation and nondescript effect on overall survival. The efficacy of EGFR kinase inhibitors have been disappointing so far as silencing of EGFRvIII compels GBM cells to undergo selective pressure *in vivo* to employ alternative compensatory pathways such as upregulating receptor tyrosine kinases (PDGFR, IGF1-R and c-Met) to maintain aggressiveness. These findings suggest that tumor cells are adept at bypassing single EGFR targeted therapies, reforming the tumor after an initial period of stasis, and inhibition of EGFR alone will not be adequate for translation into a beneficial clinical response in GBM patients. An effective therapeutic strategy should take into account the role of residual $EGFR^{neg}$ GPCs or that of the secreted factors in the tumor niche, and the development of a tailored combinatorial therapy targeted at both the aggressive $EGFR^{pos}$ GPCs and the less malignant $EGFR^{neg}$ GPCs or the microenvironment will be imperative to improve the clinical response of GBM patients.

One of the main molecular changes accompanying progression of gliomas to high grade, with simultaneous elevated stem cell expression and resistance to chemotherapy, is the loss of phosphatase and tensin homolog

(PTEN) and consequent elevation of Akt pathway activities (Hu et al, 2005). Deficiency in PTEN modulates Chk1 localization, initiating genetic instability and thereby conferring chemo-radioresistance in GBMs. A number of intracellular signaling cascades are activated upon EGFR stimulation, but the PI3K-Akt module has been predominantly linked to GPC biology and contribution to the resistant phenotype (Dreesen & Brivanlou, 2007; Eyler et al, 2008). Various studies have shown that hyperactivation of the PI3K/Akt and Ras/MAPK signaling pathways in cancer cells promotes tumorigenesis, increases tumor cell survival, proliferation, invasion and is significantly associated with radiotherapy resistance, either through the modulation of cell survival signaling or, by direct regulation of the DNA repair machinery. In human gliomas, there is evidence at genomic, mRNA and protein levels showing that aberrant Akt signaling prognosticates poorer survival (Phillips et al, 2006a). Indeed, chemoresistance in hepatocarcinoma stem cells may be conferred by activation of Akt (Ma et al, 2008), and Akt signaling promotes survival of stem-like tumor cells in the perivascular niche of mouse medulloblastoma models (Hambardzumyan et al, 2008). It has been recently demonstrated that GPCs are more dependent on Akt signaling than their matched non-stem counterparts (Eyler et al, 2008). Chakravati *et al*. observed that GBMs expressed significantly higher levels of phospho-PI3K and phospho-p70s6k, but not of phospho-Akt, compared to their non-GBM counterparts, implying that GBMs display dependency on these pathways possibly for their survival, proliferation and therapeutic resistance (Chakravarti et al, 2004). In addition, inverse correlation between phospho-PI3K, phospho-Akt, and phospho-p70s6k levels with cleaved caspase 3 implicates the likely mechanisms employed by the members of the PI3K family in the inhibition of apoptosis and promotion of radioresistance in GBMs (Chakravarti et al, 2004). Functional inhibition of Akt with the pharmacologic inhibitors

preferentially disrupts GPC neurosphere formation, reduces motility and invasion, induces apoptosis *in vitro*, and significantly prevents intracranial tumor formation of GPCs (Bleau et al, 2009; Eyler et al, 2008). Although *in vitro* targeting of the EGFR-PI3K-Akt signaling cascade may have specific effects on GPC self-renewal and tumorigenic progression, clinical trials of EGFR inhibitors, such as Imatinib, have not resulted in significant survival, suggesting that EGFR inhibition solely is an insufficient therapeutic paradigm, prompting greater focus on PI3K inhibitors.

EGFR/EGFRvIII's cross-interaction with the oncogenic transcription factor STAT3 and receptor tyrosine kinases (c-Met and PDGFR) mediates GPC resistance to anti-EGFR therapy. JAK-STAT3 pathway is constitutively activated in the majority of GBMs and the dynamic interactions between STAT3 and EGFR underlie resistance of GBM cells to Iressa (Lo et al, 2008). Combinatorial inhibition of JAK and EGFR/EGFRvIII abolishes STAT3 activation and synergistically suppresses the GPC proliferation. JSI-124 acts as a highly selective inhibitor of the JAK/ STAT3 signaling pathway (Blaskovich et al, 2003) and has been shown to sensitize malignant glioma and medulloblastoma cells to TMZ, 1,3-bis(2-chloroethyl)-1-nitrosourea, and cisplatin (Lo et al, 2008). In addition, the direct role of EGFR in the regulation of DNA repair was demonstrated by Bandyopadhyay *et al.* where they showed direct physical interaction of EGFR and DNA-dependent protein kinase (DNA-PK), a key component of the nonhomologous end-joining (NHEJ) machinery (Bandyopadhyay et al, 1998). Furthermore, a follow-up observation by Dittmann *et al.* showed that ionizing radiation (IR) and the use of a radiomimetic drug, cisplatin induces the translocation of EGFR into the nucleus, where it interacts and increase the activity of DNA-PK (Dittmann et al, 2005).

Taken together, these findings discussed here suggest that EGFR signaling, either directly through the interaction with the DNA repair machinery or indirectly through the activation of key oncogenic PI3K/ Akt and JAK/STAT signaling pathways, modulates sensitivity to radiation. Therefore, elucidation of the dynamic interactive EGFR networks will enable us to identify mechanisms that circumvent therapeutic resistance in GPCs and improve the modest efficacy of current EGFR-targeted therapy in GBM patients. Given the central role of the EGFR signaling pathway in conferring the aggressive phenotype in tumors, treatment resistance, and poor prognosis, considerable effort has been invested in the development of imaging strategies to non-invasively ascertain EGFR status and therapeutic response to EGFR targeting agents. Such approaches would enable more accurate stratification of the patients who are likely to benefit from EGFR targeting therapeutics and for monitoring treatment efficacy (Hatanpaa et al, 2010).

1.6.2 Notch signaling

Activation of the Notch signaling cascade involves proteolytic cleavage by γ-secretase and is critical for the maintenance of stem and progenitor cells in promoting self-renewal and repressing differentiation (Lathia et al, 2008). Aberrant Notch signaling has been implicated in the pathogenesis of multiple tumors including gliomas, and the overexpression of Notch and its ligands, Delta-like-1 and Jagged-1, is commonly associated with glioma survival and proliferation. The role of Notch signaling in GBMs has been widely characterized and it has been shown that downregulation of *NOTCH1, Delta-like-1, or Jagged-1* leads to glioma cell apoptosis and translates into a prolonged survival in a mouse orthotopic brain tumor model (Purow et al, 2005). Fan *et al*. demonstrated that specific Notch targeting of

patient-derived GPCs by γ-secretase inhibitor (GSI) attenuated neurosphere-forming ability with marked decrease in the expression of stemness-related markers, increased sensitivity to chemotherapeutic agents *in vitro* and blocked tumor propagation *in vivo*, suggesting a potential dependence on Notch signaling in GPCs (Fan et al, 2010). Activation of Notch by upstream oncogenic stimuli and microenvironmental cues is essential for the maintenance of GPCs and the facilitation of tumor propagation, suggesting a role of Notch at the center of key regulatory GPC signaling networks.

Previous reports have demonstrated that exposure to radiation modulated the activation of Notch signaling in the CD44+/CD24-/low breast cancer stem cells (Phillips et al, 2006b). In addition, Notch signaling has been implicated in the radioresistance phenotype of GPCs where knockdown of *NOTCH1* or *NOTCH2* effected radiosensitivity of GPCs but not that of differentiated glioma cells (Wang et al, 2010), suggesting that inhibition of Notch signaling may not only deplete GPC frequency and engraftment potential but also reduce the radioresistance of GPCs. Furthermore, inhibition of the Notch cascade in irradiated GPCs brought about increased apoptotic marker caspase 3/7 and positive labeling of apoptotic marker Annexin V. Thus, these data suggest that, in the case of gliomas, Notch may be a possible target in stem-like glioma cells as GPCs express Notch family genes and gliomaspheres have elevated Notch activity (Lee et al, 2006) and might be involved in evading apoptosis and promoting proliferation. Therefore, targeting Notch and its components underlying the radioresistance of GPCs promise to confer sustained benefit for glioma therapeutics.

1.6.3 Hedgehog-Gli signaling

The Sonic Hedgehog signaling pathway is one of the classic examples of cancer cells regulated by paracrine and autocrine mechanism, supporting

an intimate relationship between tumor cells and their stroma, the microenvironmental niche (Clement et al, 2007; Yauch et al, 2008). Indeed, this pathway is controversial but has been ascribed an autocrine mode of signaling in GPCs (Clement et al, 2007). This pathway is one of key regulatory pathways critical for the maintenance of several types of adult stem cells, including neural stem cells (Clement et al, 2007). The Hedgehog signaling cascade is commonly known to be expressed by tumor-associated endothelial cells and astrocytes in platelet-derived growth factor (PDGF)-driven mouse models of GBM (Becher et al, 2008). The main components of this signaling pathway are the ligands (secreted Hedgehog proteins), the Patched receptor (Ptch, a 12-pass transmembrane protein), the intracellular transducing molecules Smoothened (Smo - a second transmembrane protein) and Gliotactin (Gli, zinc-finger transcription factors). Ligand-binding of Hedgehog to Ptch represses Smo inhibition, allowing the activation of the canonical Hedgehog pathway through Gli-dependent transcription of multiple targets, including N-myc, cyclin D, Ptch, Gli1, and Gli2.

Hedgehog signaling is highly deregulated in a small subpopulation of human medulloblastoma and *Gli1*, a key Hedgehog target, was highly expressed in primary GBMs and CD133+ GBMs (Bar et al, 2007b). Conventional sources of Hedgehog ligands include CD133+ GPCs and tumor-induced vasculature in GBMs (Clement et al, 2007). Several groups have investigated the role of Hedgehog-Gli signaling in GPCs and found that this signaling pathway regulates GPC function, self-renewal and tumorigenesis (Bar et al, 2007a; Clement et al, 2007; Ehtesham et al, 2007). Forced differentiation of gliomaspheres reduced both stemness and Hedgehog activity expression. However, not all GBMs have activated Shh signaling as determined by Gli expression (Bar et al, 2007b), indicating the presence of molecular subgroups of brain tumors in which targeting of Shh

would be ineffective. Treatment of GPCs with the Hedgehog inhibitor cyclopamine or *Gli* knockdown drastically depleted the GPCs by suppressing self-renewal ability and proliferation while increasing apoptotic cell death *in vitro* and inhibiting tumor propagation *in vivo*. Importantly, cyclopamine inhibition of Hedgehog-Gli signaling enhances the efficacy of TMZ to abolish GPC proliferation and improve the effect of radiation on GPCs. Taken together, these studies indicate that the Hedgehog-Gli module is critical for GPC maintenance and targeting this pathway with specific pharmacologic inhibitors may attenuate GPC self-renewal and offer improved therapy efficiency against gliomas.

Gli1 acts at the distal end of the Hedgehog pathway, where it regulates transcription in response to activation or inhibition of the pathway. Moreover, Gli activity correlates with tumor grade in a genetically engineered mouse model (Becher et al, 2008). As such, further investigation must be performed to explore its role in GPC growth, maintenance and GBM recurrence. Cui *et al*. investigated the role of Gli1 in primary and recurrent gliomas and its ability to confer chemosensitivity or chemoresistance of glioma cells (Cui et al, 2010). Overexpression of *Gli1* associated with GPC chemoresistance, resulting in glioma perpetuation. Conversely downregulation of *Gli1* enhanced the susceptibility of GPCs to the synergistic effects of cyclopamine and chemotherapeutic agents, promoting apoptotic cell death, thus suggesting that Gli1 is a key mediator of chemoresistance in GBMs with aberrant Hedgehog signaling. Moreover, the constitutive Hedgehog pathway activity contributes to the resistance of glioma cells to chemotherapeutic agents by promoting self-renewal and tumor regrowth following therapy in an autocrine and/or paracrine manner (Bar et al, 2007b). In contrast, abolishment of Hedgehog pathway activity abrogates tumor growth and restricts tumor recurrence, by downregulation of the expressions

of multidrug resistance protein-1 (*MDR1*), multidrug resistance associated protein-1 (*MRP1*), lung resistance-related protein (*LRP*), O-6-methylguanine-DNA methyltransferase (*MGMT*), B-cell lymphoma 2 (*Bcl-2*) *and* Baculoviral IAP repeat-containing protein 5 (*BIRC5* or *Survivin*), which play important roles in glioma chemoresistance and repopulation, thus providing a mechanism to explain the recurrence of some gliomas.

1.7 WNT Signaling and Regulation

The Wnt proteins are a family of small (39-46 kDa) lipid-modified secreted cysteine-rich glycoproteins (Tanaka et al, 2002). The first Wnt gene was initially discovered by Roeland Nusse and Harold Varmus in 1982 through viral mammary tumorigenesis experiments where they observed integration of the mouse mammary tumor virus (MMTV) into the promoter region of a gene called *Int-1* (integration 1) could induce tumors (Nusse & Varmus, 1982). *Int-1* is orthologous to the *Drosophilia* segment polarity gene Wingless (*Wg*) and the terms were combined to generate the name Wnt (Nusse et al, 1991). Since the identification of Int-1 (now termed *WNT1*), the gene family of *WNT* has grown to 19 paralogous members at present (The Wnt Homepage, http://www.stanford.edu/group/nusselab/cgi-bin/wnt/).

Wnt signaling plays diverse roles both during embryogenesis and normal stem cell development. It is crucial for embryonic patterning through the control of cell proliferation, determining the fate of stem cells, tissue homeostasis and the regulation of stem cell self-renewal. In somatic tissues, Wnt signaling is essential for the maintenance of normal architecture and function of many tissues through the regulation of stem cell renewal (He et al, 2004; Reya et al, 2003; Willert et al, 2003).

In the normal development of CNS, the tight control and regulation of neural stem and precursor cells' proliferation are crucial. The loss of the glycoprotein Wnt1, a protein normally expressed in the caudal midbrain, leads to failure of neural precursor expansion, resulting in malformation and an almost complete loss of the mid/hindbrain region (McMahon & Bradley, 1990). In addition, ectopic expression of Wnt1 in the mid/hindbrain region enhances the proliferation of neural precursors mediated by the induction of cyclin D and the shortening of cell cycle (Panhuysen et al, 2004). These observations suggest the role of Wnt signaling regulation in normal developing brain. Furthermore, Wnt3a mutant mice displayed marked reduction in hippocampal layers due to decreased proliferative expansion of caudomedial cortical progenitor cells (Lee et al, 2000). Recent work by Lie *et al.* demonstrated that Wnt signaling is a crucial regulator of adult hippocampal stem/ progenitor cells (Lie et al, 2005). They showed that *in vitro* and *in vivo* overexpression of Wnt3a in adult hippocampal stem/progenitor cells increased neurogenesis, whereas Wnt inhibition resulted in almost complete abrogation of neurogenesis *in vivo*. In addition, Kalani *et al.* demonstrated the regulatory role of Wnt signaling in the self-renewal of neural stem cells (Kalani et al, 2008). Importantly, the authors showed that Wnt signaling is required for the expansion of single-cell derived neural stem cell populations that are capable of giving rise to neural stem cells and other cells of multipotent lineages. Taken together, these observations highlight the importance of Wnt signaling in the normal development of neural stem/progenitor cells.

Wnt signaling cascades can be broadly classified into canonical and non-canonical pathways as determined by the composition of the Wnt/Frizzled complex. A critical and heavily studied Wnt pathway is the canonical Wnt/β-catenin signaling pathway, which functions by regulating the

amount of transcriptional co-activator β-catenin that controls key downstream developmental gene expression programs. The phosphorylation status and degradation of cytoplasmic β-catenin and its regulation by Wnt proteins are the essence of canonical Wnt/β-catenin signaling. Regulation of Wnt/β-catenin signaling occurs at several different levels to ensure that cytoplasmic levels of free β-catenin protein remain low. For simplicity, the Wnt/β-catenin signaling activity can be viewed as being in a dichotomous state of either “Off” or “On” (**Figure 1.2**).

1.7.1 Wnt/β-catenin signaling: “Off”-state

In the absence of Wnt ligands or stimulus, β-catenin is recruited into a multiprotein “destruction complex”. This destruction complex consists of Axin1 (or Axin2 homologue) that forms the central scaffold of this complex and provides binding sites for β-catenin, adenomatous polyposis coli (APC), glycogen synthase 3β (GSK3β), casein kinase Iα (CKIα), and protein phosphatase 2A (PP2A). Once the complex is formed, it is stabilized by the GSK3β-mediated phosphorylation of Axin and APC. Within the stabilized complex, GSK3β phosphorylates the N-terminus of β-catenin. Phosphorylated β-catenin is then recognized by β-transducin repeat containing protein (β-TrCP), an F-box-containing protein, which together with Skp1, Cullin, and Rbx-1 constitutes the ubiquitin ligase (E3). This, together with ubiquitin conjugating enzyme (E2) and ubiquitin activation enzyme (E1), causes ubiquitination of β-catenin at lysine resides, which is subsequently destroyed by the proteasome system. In the nucleus, prospective Wnt target genes are kept in a repressed state by interacting with T-cell factor (TCF) and lymphoid enhancer-binding protein (LEF) transcription factors, with associated co-repressors. Hence, in the “Off”-state, cells maintain low cytoplasmic and nuclear levels of β-catenin. In addition, extracellular Wnt ligands can interacts

with a variety of endogenous antagonists, including secreted Frizzled-related protein (sFRP), Dickkopf (DKK) family of proteins, and Wnt-inhibitory factor-1 (WIF-1). All these secreted proteins can inhibit Wnt/β-catenin by sequestering Wnt ligands and prevent receptor-mediated activation of the pathway.

1.7.2 Wnt/β-catenin signaling: "On"-state

Wnt/β-catenin signaling is triggered by the interaction of Wnt ligands with Frizzled receptors in the presence of the transmembrane LRP5/6. The association of Wnt ligands with Fz receptors and LRP5/6 initiate the recruitment of phosphoprotein Dishevelled (Dvl) to the cell surface, which subsequently recruits Axin and the "destruction complex" to the cell membrane, where Axin directly binds to the cytoplasmic tail of LRP5/6. Axin is then degraded, which decreases β-catenin degradation and a consequent increase in β-catenin levels in the cytoplasm. The activation of Dvl also leads to the inhibition of GSK3β, which further reduces the phosphorylation and degradation of β-catenin. Therefore, activation of Wnt/β-catenin pathway involves increasing the post-translational stability of β-catenin, via the degradation of Axin and inhibition of GSK3β. As β-catenin levels rises in the cytoplasm, it is translocated into the nucleus where it competes with Groucho (a transcriptional co-repressor of TCF/LEF) for binding with the TCF/LEF proteins. The TCF/LEF proteins allow β-catenin and other co-activators to bind to the DNA, where it forms the basis of a large complex for activating transcription of Wnt target genes.

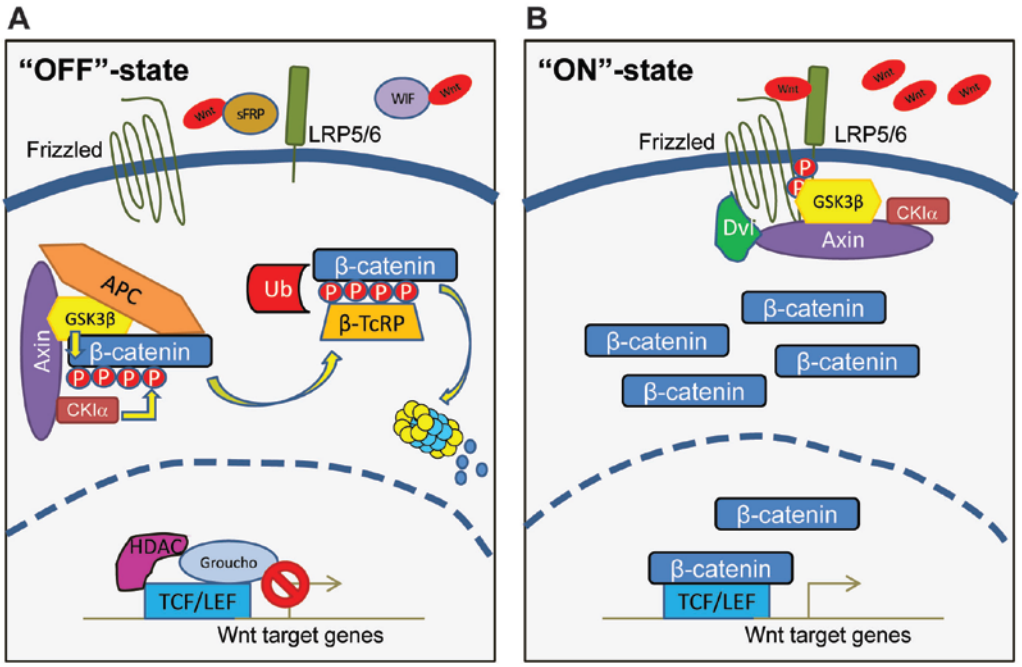

Figure 1.2. Overview of Wnt/β-catenin signaling. A, In the absence of Wnt ("Off"-state), cytoplasmic β -catenin forms a "destruction complex" with Axin, GSK3β, APC, and CKIα. Phosphorylation of β -catenin by CKIα primes subsequent phosphorylation events by GSK3β. Phosphorylated β-catenin is recognized by the E3 ubiquitin ligase β-TrCP, which targets β-catenin for proteosomal degradation. In the nucleus, Wnt target genes are repressed by transcriptional repressors such as Groucho and histone deacetylases (HDAC). **B**, In the presence of Wnt ligand ("On"-state), Fzd and LRP5/6 forrms a receptor complex. The formation of Wnt-Fzd-LRP5/6 complex, together with the recruitment of the scaffolding protein Dvl, results in LRP5/6 phosphorylation and activation and the recruitment of Axin to the cytoplasmic tail of the receptors. This disrupts the formation of the "destruction complex", allowing β-catenin to accumulate in the nucleus where it functions as a coactivator for TCF/LEF to activate Wnt-responsive genes.

1.8 Dysregulation of WNT Signaling in Tumorigenesis

Given the crucial roles of Wnt/β-catenin signaling in development and homeostasis, it came as no surprise that mutations of the Wnt pathway components are associated with many hereditary disorders, including cancers. The Wnt/β-catenin signaling pathway has been demonstrated to be the predominant driving force of stem cells of the colonic crypt, hematopoietic and central nervous system (Barker et al, 2007; Kalani et al, 2008; Reya et al,

2003). In particular, tumor-initiating cells of the colon, breast and hematopoietic system have been shown to promote tumorigenesis through major contributions from aberrant Wnt/β-catenin signaling (Barker et al, 2009; Chen et al, 2007; Woodward et al, 2007; Zhao et al, 2007)

The association of dysregulated Wnt/β-catenin signaling with cancer is perhaps best document with colorectal cancer. *APC* represents the most frequently mutated gene among the Wnt components. Genetic defects in APCs results in a heritable syndrome, familial adenomatous polyposis (FAP), where individuals affected develop hundreds of polyps in the large intestine at an early age and ultimately succumb to colorectal cancer (Clements et al, 2003). Another most commonly mutated proto-oncogene of the Wnt/β-catenin pathway is the β-catenin gene, *CTNNB1*. It is frequently reported that mutations of *CTNNB1* occur in exon 3 and specifically disrupt GSK3β-mediated phosphorylation. The effect of such mutations renders β-catenin not being able to be recognized by the “destruction complex” for degradation.

1.9 WNT Signaling in Glioma

The fact that Wnt signaling is also dysregulated in multiple solid cancers suggests that it may also play a role in the maintenance of GPCs. A study by Pu *et al.* demonstrated that *WNT2*, an activator of the Wnt/β-catenin canonical pathway, was significantly overexpressed in gliomas and their expression levels correlated positively with malignancy (Pu et al, 2009). Similarly, higher grade gliomas were observed to express elevated *CTNNB1* expression (Liu et al, 2011b), which subsequently correlated with poorer prognostic impact in GBM patients (Liu et al, 2011c; Sareddy et al, 2009b). In addition, the expression of other Wnt regulators, including Dvl2, Dvl3, FRAT-1, Pygo-2, TCF4, and LEF-1 and of specific Wnt target genes, CCND1 and

MYC, also increases with glioma grades. Of note, recent reports demonstrated that the knockdown of Dvl2 abrogated both the self-renewal ability and proliferation of gliomas and stimulated the differentiation of patient-derived glioma samples. Tumor propagation in immune-compromised mice was repressed upon Dvl2 depletion.

In addition to regulation of the expression of the Wnt members, antagonists of the Wnt pathway are often repressed in GBMs and their expression is mostly inversely correlated with glioma grades. Frequent aberrant promoter hypermethylation of these Wnt antagonists, such as WIFs, sFRPs, and DKKs is significantly associated with GBMs. Furthermore, Zheng *et al.* identified a novel proto-oncogene *PLAGL2*, which is overexpressed in GBMs and induces GPCs proliferation and tumorigenic potential. PLAGL2 stimulates the expression of Wnt-6, Fz-9 and Fz-2, inhibits differentiation, and increases proliferation of neural progenitors. *PLAGL2* amplification also associates with elevated levels of *CTNNB1* in GBMs, suggesting a possible role of *PLAGL2* in GPCs via the regulation of Wnt signaling. Jiang *et al.* showed that hypermethylation of paternally expressed gene 3 (PEG3) promoter in glioma mitigates expression of PEG3 and correlates with high grade gliomas (Jiang et al, 2010). Upon PEG3 promoter hypermethylation, β-catenin accumulates, resulting in GPC proliferation. A recent study by Zhang *et al.* showed that the interaction between the transcription factor Forkhead box M1 (FoxM1) and β-catenin promotes β-catenin nuclear localization, controls transcriptional activation of Wnt target genes expression and maintains GPC self-renewal (Zhang et al, 2011). Together, these findings validate the role of Wnt and activated β-catenin signaling in mediating GPC self-renewal.

1.10 Gap in knowledge

In following chapters, we will address the following gaps in knowledge in the field of glioma and GPCs:

1. We characterized patient-derived glioma-propagating cells (GPCs) that are enriched in spheroid structures (gliomaspheres) and can be reliably maintained through a combination of in vitro and in vivo serial passaging. We seek to demonstrate that GPCs established from patient tumors with similar histology are transcriptomically distinct, highlighting molecular heterogeneity and the limitation of relying solely on histology to diagnose and subsequently treat patients. In addition, we address the question of whether using our modified method of vitrification if we could reliably preserve and maintain the biological phenotype and transcriptomic profiles of GPCs. This is important, as it will greatly facilitate the study of GPCs as we have a reliable establishment of a GPC repository for subsequent experimental designs and studies.

2. Secondly, we seek to determine the GPC contribution to patient survival and prognosis by analyzing gene expression profiles of GPCs derived from 2 major variant of human gliomas – the oligodendroglial and GBM tumors. This is important as it will provide a direct link between GPCs and disease progression, highlighting the clinical relevance and applicability of GPCs.

3. Next, we will test the hypothesis of whether Wnt/β-catenin signaling (as identified in our oligodendroglial gene signature) is differentially regulated between the oligodendroglial and GBM tumors. We sought to investigate if the Wnt/β-catenin signaling is crucial in the survival

and maintenance of GPCs through the use well-established pharmacological and genetic methods. Importantly, we will investigate the *in vivo* efficacy of β-catenin knockdown to show that Wnt/β-catenin signaling is important in maintaining the tumorigenic capacity of GPCs.

4. Finally, we seek to find potential novel regulators of the Wnt/β-catenin signaling implicated in differential regulation of Wnt/β-catenin signaling and its requirement for the self-renewal, maintenance and survival of GPCs.

CHAPTER 2

MATERIALS AND METHODS

CHAPTER 2 – MATERIALS AND METHODS

2.1 Tissue Collection and Primary Gliomasphere Culture

Graded brain tumor specimens were obtained with informed consent, as part of a study protocol approved by the institutional review board. In this study, NNI-1 was from a patient with recurrent GBM (grade IV) who had received radiation therapy, and NNI-2, 3, 4, 5, 10, 11 and12 were from patients with primary GBM who were treatment naive. NNI-7 and NNI-8 are GPC lines derived from patients with primary anaplastic oligoastrocytoma who were treatment-naive. All GPC lines presented in this thesis except NNI-10 and NNI-11 belong to the proneural subclass. NNI-10 and -11 GPCs represent the mesenchymal subclass based on the molecular classification by Lottaz *et al.* (Lottaz et al, 2010). Tumors were processed according to Gritti *et al.* (Gritti et al, 1996) with slight modifications. Cells were seeded at a density of 2, 500 per cm^2 in chemically defined serum-free selection growth medium consisting of basic fibroblast growth factor (bFGF; 20 ng/ml; Peprotech, New Jersey), epidermal growth factor (EGF; 20 ng/ml, Peprotech), heparin (5 µg/ml; Sigma-Aldrich, St Louis), and serum-free supplement (B27; 1x; Gibco, Grand Island, NY) in a 3:1 mix of Dulbecco's modified Eagle's medium (DMEM; Sigma-Aldrich) and Ham's F-12 Nutrient Mixture (F12; Gibco). The cultures were incubated at 37^{o}C in a water-saturated atmosphere containing 5% CO_2 and 95% air. To maintain the undifferentiated state of the gliomasphere cultures, growth factors were replenished every 2 days. Differentiation was carried out over 14 days in DMEM/F12 without growth factors, supplemented with 5% fetal bovine serum (FBS; Invitrogen, Carlsbad) and 1x B27. Successful gliomasphere cultures (1 to 4 weeks) were expanded by mechanical trituration using a flame-drawn glass Pasteur pipette, and cells were reseeded at 100,000 per ml in fresh medium.

All GPCs except Pollard lines used in this study were cultured as spheroid structures in serum-free media supplemented with bFGF and EGF. Although Pollard lines were cultured on laminin (Pollard et al, 2009), a recent molecular classification study showed that both culture methods preserved the biological and functional signaling pathways (Lottaz et al, 2010). This provides justification for our subsequent analyses.

"Gunther" lines: GS-1, 3, 4, 5, 6, 7, and 8 are GBM-initiating cells whereas GS-2 was derived from a high-grade tumor with oligodendroglial features as previously described (Gunther et al, 2008). Cell lines were cultured for up to 14 passages *in vitro* with preservation of transcriptomic profiles. "Pollard" lines: G144, 144ED, 166, 179, and GliNS2 are GBM-initiating cells whereas G174 was derived from a patient with anaplastic oligoastrocytoma as previously described (Pollard et al, 2009). Pollard lines could be cultured for 1 year (>20 passages) with preservation of key stemness or differentiation expression, karyotypic hallmarks, and tumor propagation.

2.2 Cryopreservation and thawing of gliomasphere cultures for viability count

In the conventional cryopreservation method, 5, 000 gliomaspheres per ml of freezing media (50-100 µm diameter) were frozen in a slow-cooling protocol using a freezing container (Nalgene) in -80^{o}C for 24 hours before transfer into -196^{o}C liquid nitrogen storage for 30 days. Freezing media contained DMEM/F12 media supplemented with 10% dimethylsulfoxide (DMSO; Merck & Co., Whitehouse Station, NY) only; or 10% DMSO and 90% FBS. These samples were thawed at 37^{o}C water bath for 1-2 minutes, washed with excess DMEM/F12 media before being cultured in chemically defined serum-free selection growth medium supplemented with growth factors (DMEM/F12,

20 ng/ml each of bFGF and EGF, 1x B27 and 5 µg/ml heparin). Viability counts were carried out after incubation periods of 1, 5 and 10 days (Gunther et al, 2008).

In the vitrification method (**Figure 2.1 and Table 2.1)**, gliomaspheres from the same passage were subjected to either vitrification or continuous culturing (non-vitrified). Five thousand gliomaspheres (50-100 µm) were frozen in a rapid cooling protocol. Gliomaspheres were resuspended in 100 µl of holding medium (HM) of DMEM/F12 containing HEPES buffer (Gibco) with or without 20% FBS before being transferred by pipetting into sequentially increasing concentrated vitrification solutions (VS1 and VS2). Gliomaspheres were incubated for 1 minute in 100 µl of VS1 consisting of 10% DMSO and 10% ethylene glycol (EG; Merck), followed by a 25-second incubation in 100 µl of VS2 consisting of 20% DMSO, 20% EG and 0.3 M sucrose. The mixture was immediately transferred into 0.78 mm inner diameter borosilicate glass capillaries (Harvard Apparatus), snap-frozen and stored in liquid nitrogen. All procedures were performed in an aseptic manner at room temperature.

The following periods of freezing for vitrified cultures were evaluated prior to thawing: NNI-1 and NNI-2 for 30 days, NNI-5 for 8 months, NNI-4 for 1.5 years and NNI-3 for 2.5 years. Thawing was performed in sucrose solutions of sequentially decreasing concentrations (SS1 and SS2). After removal from liquid nitrogen, the contents of the glass capillaries were released by reverse capillary action into SS1 containing HM supplemented with 0.2 M sucrose for 1 minute. It was then transferred by pipetting into SS2 containing HM supplemented with 0.1 M sucrose and incubated for 5 minutes in HM alone. The mixture was washed with excess HM before being cultured in chemically defined serum-free selection growth medium supplemented with growth factors at abovementioned concentrations (DMEM/F12, bFGF, EGF, B27 and

heparin). Viability counts were carried out after incubation periods of 1, 5 and 10 days (Gunther et al, 2008).

Table 2.1. Materials and solutions used for vitrification and thawing procedures of patient-derived gliomaspheres.

Materials and solutions	Comments
Borosilicate glass capillaries	0.78 mm in diameter
Cryotubes	4.5 ml capacity with holes punched in the upper section through the lid and middle section across the vial to allow liquid nitrogen movement
Liquid Nitrogen	-
DMEM-HEPES (Holding medium)	20% FBS, 1 M HEPES in DMEM medium (Filtered solution through a pre-wet 0.22 µm pore-size filter)
1M sucrose solution	1M sucrose, 20% FBS in DMEM-HEPES medium (Filtered solution through a pre-wet 0.22 µm pore-size filter)
10% Vitrification Solution (VS1)	10% DMSO, 10% Ethylene glycol in DMEM-HEPES medium
20% Vitrification Solution (VS2)	20% DMSO, 20% Ethylene glycol, 30% of the 1 M sucrose solution in DMEM-HEPES medium
0.2 M sucrose solution (SS1)	20% of the 1 M sucrose solution in DMEM-HEPES medium
0.1 M sucrose solution (SS2)	10% of the 1 M sucrose solution in DMEM-HEPES medium

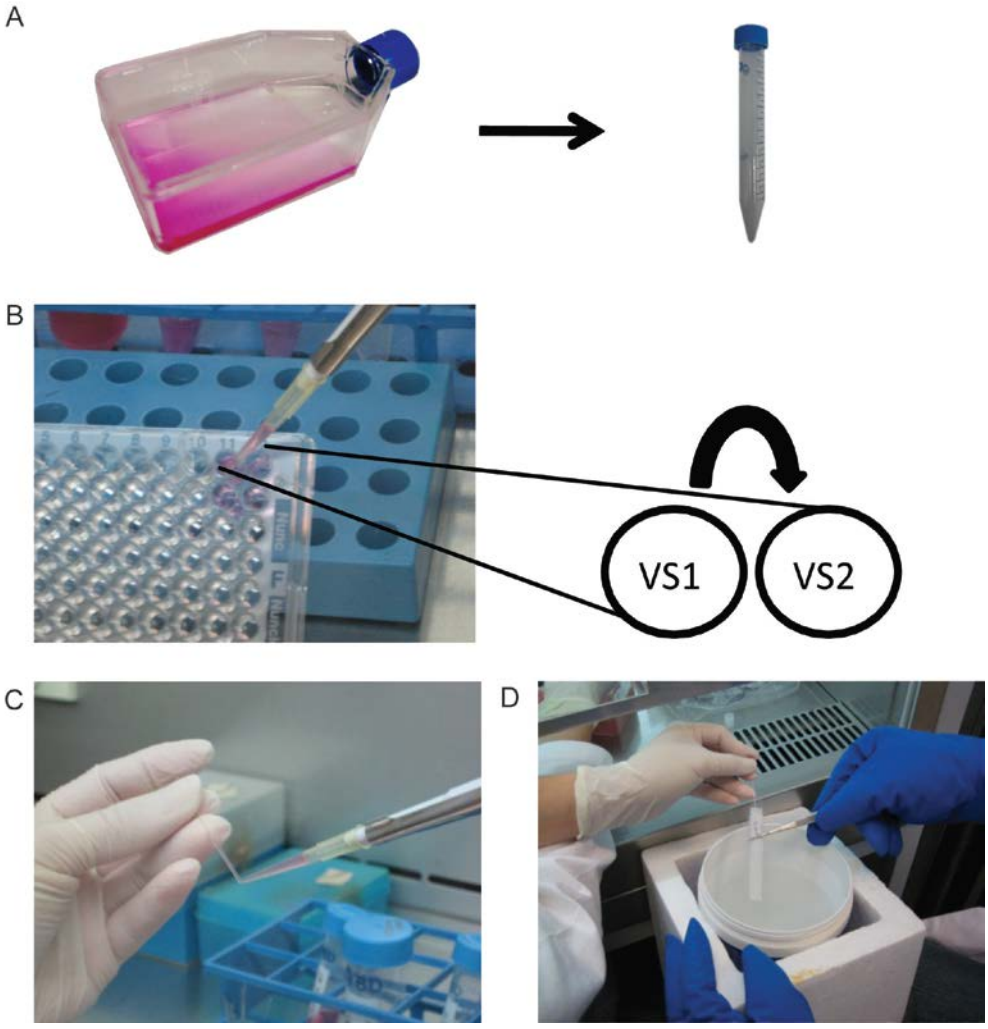

Figure 2.1. Outline of vitrification procedure. A, Gliomaspheres are collected as pellet form by centrifugation. **B**, Gliomaspheres in DMEM-HEPES are transferred into VS1 solution for 1 min and subsequently into VS2 solution for an additional 25 sec. **C**, Suspension of gliomaspheres in vitrification solution is drawn into a fine borosilicate capillary using a micropipettor fitted with a 200 µl pipette tip. **D**, Capillary filled with suspension of gliomaspheres is immediately plunged into a cryovial containing liquid nitrogen.

2.3 Small-molecule inhibitors and reagents

The small-molecule inhibitor of Wnt signaling, Cercosporin (Lepourcelet et al, 2004), IWP2 (Chen et al, 2009), IWR1 (Chen et al, 2009) and XAV939 (Huang et al, 2009) were purchased from Sigma. CCT036477 (Ewan et al, 2010) was manufactured and synthesized by Laviania Corporation according to the published chemical structure. The small-molecule inhibitors of Notch

signaling, γ-secretase inhibitor (Wolfe et al, 1998) and DAPT (Hovinga et al, 2010) were purchased from Sigma. TGFβR1 inhibitor, SB525334 (Grygielko et al, 2005) was procured from TOCRIS bioscience. GPCs were treated at 10 μM for IWP2, IWR1, XAV939, γ-secretase inhibitor, DAPT, and SB525334, and at IC_{50} concentrations for Cercosporin and CCT036477. TGFβR1, used at 200 pM, was obtained from R&D.

2.4 Cell Viability Assays

2.4.1 Dose-response curves and IC_{50} calculations

Gliomaspheres were dissociated into single cells with Accutase™ (eBioscience Inc., San Diego; non-trypsin-based) and seeded into 96-well plates, at a density of 200 cells/μl, with DMEM/F12 medium supplemented with growth factors. Cells were allowed to recover over two to three days prior to drug treatment. Cell viability post-drug treatment was assessed using alamarBlue® (Serotec, Oxford, UK). Briefly, cells were incubated with 10% culture volume of alamarBlue® for approximately 16 hours before absorbance readings were measured at 570 and 600 nm. Dose response curves for each line were generated using GraphPad Prism (GraphPad Software, Inc; USA) and IC_{50} values were computed from 12-point titration curves ranging from 10^{-4} to 10^{2} μM.

2.4.2 Cell viability assessment post lentiviral transduction of GPCs

Lentivirus-infected GPCs were plated into 96-well plates at a density of 2, 500 cells/well. Cell viability was quantified using the alarma Blue® cell viability assay at 5, 10, and 15 days post-infection. Cell viability at each time point was normalized to the cell viability at time zero.

2.5 Quantitative real time RT-PCR

Real-time polymerase chain reaction (PCR) was carried out according to the manufacturer's protocol for the LightCycler Fast- Start MasterPLUS SYBR Green I real-time PCR kit (Roche Diagnostics, Basel, Switzerland, http://www.roche-applied-science.com). A standardized amount of 50 ng of cDNA was used for each PCR. The PCR was carried out with specific oligonucleotide primer pairs at the optimized annealing temperatures stated (supporting information Table 1). Cycle parameters on the LightCycler (Roche Diagnostics) were 38 cycles of 95°C for 10 sec, 55°C for 10 sec, and 72°C for 5 sec. Each real-time PCR was done in triplicate, and the level of expression of each gene was determined relative to the normalizer gene, hypoxanthine phosphoribosyltransferase (HPRT). Gene-specific primers (with melting curve analysis performed to ensure a single product was formed) used in this study are shown in **Table 2.2**.

Table 2.2. Intron-exon-spanning, gene-specific primers used for quantitative real time RT-PCR

mRNA target	Forward primer sequence (5' - 3')	Reverse primer sequence (5' - 3')
APC (Fragment A)	AAC CAA GAA ACA ATA CAG A	CAC TTT TGG AGG GAG ATT T
APC (Fragment B)	AGA ATC AGC CAG GCA CAA AG	GCT TGG TGG CAT GGT TTG T
APC (Fragment C)	GCA GTG GAA TGG TAA GTG G	TCA TCG AGG CTC AGA GCA
AXIN2	CCA AGT GTC TCT ACC TCA	CGA ATT GAG TGT GAG CTC GGA
BIRC5	CAT TCA AGA ACT GGC CCT	CGC AAC CGG ACG AAT GCT TTT T
Bmi-1	AAA GAT ACT TAC GAT GCC CAG	GAA GTG GAC CAT TCC TTC TC
CD133	GAA CAA GTT TAC AGT GAC TGC	TGC GTT GAA GTA TCTT TGA CG
CTNNB1	TAA CAT TTC CAA TCT ACT AAT GC	AGC TAC TTG TTC TTG AGT GAA G
GAPDH	GGA AGG TGA AGG TCG GAG TC	GTC TTG TGG GTG GCA GTG AT
GFAP	GGG ATG GAG AGG TCA TTA AGG	GGG TGA GTT TCT TGT TAG TTG G
HPRT	CAC TGG CAA AAC AAT GCA GAC T	GTC TGG CTT ATA TCC AAC ACT TCG T
MITF	GATGGAAGTCCTTAAGGTGCAGACC	CTCTTTTTCACAGTTGGAGTTAAGC
MOBP	GAC TCA TTG CTT CAC AAC CC	CTT CAA AGT ACT CCA GGC AG
Musashi-1 (Msi-1)	GTT TCG GCT TCG TCA CTT TC	GAG TCA CCA TCT TGG GCT GT
Nanog	AGC TAC AAA CAG GTG AAG AC	CTC CAG GTT GAA TTG TTC CA
Nestin	AGA CAC CTG TGC CAG CCT TTC	CTG CTG CAA GCT GCT TAC CAC
Oct4	GGT TCT ATT TGG GAA GGT ATT CAG	GGT TTC TGC TTT GCA TAT CTC
Sox-2	AGC TGG GAT AGG CCT CAC TT	TGA ATC CAT TTC GGC TTT TC
TCF7L2	TGA AAT GGC CAC TGC TTG ATG	GGT ACT AAC CAT CCT AGC
β-Actin	TTC TAC AAT GAG CTG CGT GTG	GGG GTG TTG AAG GTC TC A AA
β-Tubulin III (TuJ1)	CTT CAT TTC CCG TCA GTG TG	TAT AAT CCT GTC TGG GTA CTC CT

2.6 Immunofluorescence Analyses

Gliomaspheres from vitrified and non-vitrified conditions were dissociated into single cells using Accutase™ (eBioscience Inc., San Diego; non-trypsin-based) and seeded at a cell density of 2 x 10^4 cells per well (stemness markers)/ 1 x 10^4 cells per well (differentiation markers) 1 x 10^4 cells per well (nuclear β-catenin staining) of laminin-coated (Sigma-Aldrich) eight-well culture slides (BD Biosciences, San Diego). Plated cells were fixed with 4% paraformaldehyde (Sigma-Aldrich) for 30 minutes, permeabilized with 0.1% Triton X-100 (Sigma-Aldrich) for 2 minutes, blocked with 5% FBS for 1 hour, all at room temperature and stained for the following markers.

Stemness markers. The undifferentiated cells (stem state) were stained for Nestin (Chemicon), Oct4 (Santa Cruz Biotechnology Inc., Santa Cruz, CA), Musashi-1 (Chemicon), and Ki-67 (Chemicon). As negative controls, isotypes of respective antibodies were used. In events where no appropriate isotype is available, incubation with secondary antibody conjugated to Alexa-Fluor-488 or -594 (Molecular Probes, Eugene, OR) was carried out. The cells were then counterstained with 4'6-diamidino-2-phenylindole (DAPI, 100 mg/ml, Sigma-Aldrich) to visualize the nuclei.

Multipotentiality markers. Induction of differentiation was carried out with DMEM/F12 in the absence of growth factors and supplemented with 5% FBS and 1x B27. After 14 days, differentiated cells were stained for neurons (neuron-specific class III beta-tubulin, TuJ1; Chemicon), astrocytes (glial fibrillary acidic protein, GFAP; Dako, Glostrup, Denmark), and oligodendrocytes (O4; Chemicon).

Nuclear β-catenin staining. Undifferentiated states of GPCs were stained for active β-catenin (8E7, 1:1000; Millipore, #05-665) overnight at 4^{o}C and

incubated with Alexar-Fluor-488 secondary antibody. The cells were then counterstained with 4'6-diamidino-2-phenylindole (DAPI, 100 mg/ml, Sigma-Aldrich) to visualize the nuclei.

2.7 Limiting Dilution Assay

Gliomaspheres were dissociated into single cells by Accutase™. The cells were then dispensed into each well of a 96-well plate at decreasing cell numbers of 100, 80, 60, 40, and 20. Sphere formation was scored 7 days after seeding. To carry out sequential minimal dilution assays, the secondary gliomaspheres were similarly dissociated into single cells and then dispensed into each well of a 96-well plate at similar decreasing numbers. Tertiary gliomasphere formation was scored 7 days after seeding. Sequential minimal dilution experiments were carried out for at least 3 passages.

2.8 Gliomasphere Formation Assay

For analysis of GPC frequency, gliomaspheres were dissociated into single cells by Accutase™ (eBioscience) and 30 cells were subsequently flow-sorted into each well of 96-well plates. Cells were then treated with indicated amounts of drugs, or DMSO as a vehicle control. Gliomasphere-forming ability and gliomasphere sizes were determined after 7, 14, and 21 days. A *bona fide* gliomasphere is defined as a single sphere of diameter exceeding 20 μm. Scoring and diameter measurements were performed using Nikon Eclipse Ti Microscopy, accompanied with digital camera (DS-Qi1) and NIS-Element Imaging Software (Nikon Instruments Incoporation; New York, USA).

2.9 Luciferase Reporter Assay

L-Wnt-STF cells (obtained from A/Prof. Lawrence Lum, Department of Cell Biology, University of Texas Southwestern Medical Center, USA) were

generated by transfecting L-Wnt cells (ATCC) with SuperTopFlash (STF) and SV-40 *Renilla* luciferase plasmids and selecting for clones resistant to G418 and Zeocin. Briefly, 5, 000 L-Wnt-STF cells were seeded into each well of a 96-well plate, and individual Wnt inhibitors were added 24 hr later into each well. Firefly and Renilla luciferase activities, as indicated by relative luminescence units (RLU) were determined 24 hr later using Dual-Glo luciferase assay kit (Promega) according to the manufacturer's instructions.

2.10 Flow Cytometry

Gliomaspheres were dissociated with Accutase™ and stained with anti-CD133/2-allophycocyanin (APC) and IgG1 isotype (negative control) according to manufacturer's instructions (Miltenyi Biotech, Bergisch Gladbach, Germany). Dead cells were distinguished by propidium iodide staining. A total of 10000 events were acquired on the FACSCalibur (BD Biosciences). Data were plotted using FlowJo software (Treestar, Ashland, OR).

2.11 Stereotaxic Intracranial Implantations of NOD/SCID gamma (NSG) Mice

Mice were treated according to the guidelines of the Institutional Animal Care and Use Committee, National Neuroscience Institute, Singapore. Tumorigenicity was determined by injecting GPCs from dissociated gliomaspheres orthotopically in NOD/SCID gamma (NSG, NOD.Cg-*Prkdc*^{scid}*Il2rg*^{tm1Wjl}/SzJ JAX®, The Jackson Laboratory, Maine) mice. Five hundred thousand cells in 2 µl of phosphate-buffered saline were delivered into the right frontal lobe (0.1 µl/ minute) by stereotaxic injection through a glass electrode connected to a Hamilton syringe (Narishige, Toyko). The coordinates used were +2 mm mediolateral, +1 mm anteroposterior and -2.5

mm dorsoventral. Mice were euthanized by means of transcardiac perfusion with 4% paraformaldehyde upon presentation of neurological deficits with ataxia, cachexia, lethargy, or seizure. Where secondary cultures were generated, non-perfused tumors were surgically removed, avoiding mouse tissue and dissociated into single cells using Accutase™ and treated as described in our previous work (Chong et al, 2009). For intracranial transplantation of lentiviral transduced GPCs, 500,000 cells were lentivirally-transduced with pLKO.1-β-catenin knockdown constructs [clones: shβcat1 (TRCN0000003843) and shβcat2 (TRCN0000003844)] from Open Biosystems or a non-targeting (NT) control shRNA (SHC002, Sigma), and packaged with pLenti-X-packaging system according to the manufacturer's instruction (Clontech). Animals were monitored for time to development of neurological deficits. Kaplan-Meier survival analyses were carried out using the log-rank test in GraphPad Prism software.

2.12 Immunohistochemistry

Hematoxylin-and-eosin staining and immunohistochemistry were performed on 5 μm-thick paraffin sections. Antibodies used for primary tumor or tumor xenograft paraffin sections included: (1) Mouse monoclonal anti-active β-catenin (1:300, Millipore, #05-665); and (2) Rabbit polyclonal anti-CD133 (1:500, Abcam, ab19898); anti-activated Notch (1:500, Abcam, ab8925); anti-MITF (1:200, Sigma, HPA003259) and anti-phospho-Smad2 (Ser465/467) (1:50, Millipore, AB3849).

2.13 Karyotypic Analysis of Gliomaspheres

Two million cells from dissociated gliomaspheres were cultured in a T-25 flask (BD Biosciences). The cells were then treated within 3-5 days with 0.1 μg/ml colcemid (Invitrogen) for 24 hours. Metaphase-arrested cells were pelleted

(180g for 10 minutes) and hypotonic-treated with 0.075 M potassium chloride. Chromosomes were fixed in methanol:acetic acid (3:1), re-centrifuged and resuspended in fixative. Twelve µl of the fixed cell suspension was dropped on a clean, moistened glass slide and place on a hot plate at 48^{o}C to obtain chromosome spreads. Spectral karyotyping (SkyPaint; Applied Spectral Imaging, Israel) was performed on metaphases according to the manufacturer's instructions.

2.14 Immunoblot analysis

GPCs were harvested and pelleted prior to lysis with radio-immunoprecipitation assay (RIPA) buffer containing 0.5% sodium deoxycholate, 1% NP-40 detergent, 0.1% sodium dodecyl sulphate, 0.15 M NaCl, 10 mM Tris-HCl (pH 7.4), with protease and phosphatase inhibitor cocktail tablets (Roche). Equal amounts of protein lysate were resolved by SDS-PAGE and electrotransferred onto polyvinylidene difluoride (PVDF) membranes. Membranes were processed according to standard procedures and proteins detected using the imaging system, SYNGENE G:Box, iChemiXT. The following antibodies were used: Anti-active β-catenin (8E7, 1:1000; Millipore, #05-665), anti-β-catenin (1:1000, BD Transduction Laboratories, #610153), anti-cleaved Notch 1 (NICD; 1:1000; Cell Signaling, #2421), anti-phospho-Smad2 (Ser465/467; 1:1000; Cell Signaling, #3108), anti-Smad2 (1;1000; Cell Signaling, #3122), anti-phospho-Smad3 (Ser423/425; 1:1000; Millipore, #07-1389), anti-Smad3 (1:1000; Cell Signaling, #9523), anti-MiTF (C5, 1:1000; Abcam, #ab12039) anti-β-actin (AC-15, 1:10000; Sigma Aldrich, A5441). Goat anti-mouse or anti-rabbit horseradish peroxidase (HRP)-conjugated secondary antibody (1:10000, ECL Amersham Biosciences; Buckinghamshire; UK) was used.

2.15 Co-immunoprecipitation assay

Protein lysates were pre-cleared by incubating 1 mg of protein with sepharose beads (Protein A-Sepharose®; Zymed Laboratories Inc,; San Francisco; USA) for 30 min. Subsequently, protein lysates were incubated overnight with agitation at 4^{o}C using 5 µg anti-β-catenin (E-5, Santa Cruz, #sc-7963) or anti-LEF-1 (N-17, Santa Cruz, #sc-8591). Fresh sepharose beads were then added to the protein-antibody mixture and incubated at 4^{o}C with agitation for another 4 hrs for protein-antibody complex to bind to the beads. Sepharose beads were collected and washed 3 times with lysis buffer. The beads were subsequently resuspended in 5x SDS loading buffer and boiled for 10 minutes prior to gel loading.

2.16 Lentiviral Transduction

Human lentiviral shRNA clones (Sigma Mission RNAi) targeting β-catenin [Clones: shβcat1 (TRCN0000003843) and shβcat2 (TRCN0000003844)], MITF [Clones: shMITF(C1) (TRCN0000019122) and shMITF(C2) (TRCN0000019123)], scrambled non-targeting control (SHC002) and TurboGFP positive control (SHC003) were purchased from Sigma. These vectors were co-transfected using the Lenti-X^{TM} HTX Packaging System (Clontech, CA, USA) into HEK293FT cells according to the manufacturer's instruction (Clontech). Viral titer of supernatant collected was determined using Lenti-X™ p24 Rapid Titer Kit (Clontech) according to manufacturer's instructions.

2.17 Statistical Analysis

Data are expressed as means ± standard error of the mean (SEM) of at least 3 independent experiments. Student's *t* or Mann-Whitney *U* test was used where appropriate. $P \leq 0.05$ was accepted as statistically significant.

Bioinformatics Analyses (with help from Edwin Sandanaraj, SICS)

2.18 Processing of microarray data, gene signature generation and pathway analysis

Affymetrix U133 Plus 2.0 CEL files were mas5 processed and quantile normalized in the R statistical software using the *affy* packages (Gautier et al, 2004; Team, 2009). Probes with 'Absent' call in all samples were removed. Microarray data were obtained from the Gunther (Gunther et al, 2008) and Pollard (Pollard et al, 2009) publications and were processed similarly. To understand the transcriptomic differences between oligodendroglial gliomas and GBM, a linear model was fitted with batch correction using the *limma* package (Gentleman R, 2005). Additionally, a linear model was applied to gene expression data of NNI-8 GPC cells and its primary tumor. For both analyses, probesets with adjusted p-value ≤ 0.05 were considered significant and used as inputs for pathway analysis in MetaCore from GeneGo, Inc. Significantly enriched process networks and canonical pathways were analyzed and top ranking results were reported. All array platform gene annotation was derived from Biomart . Raw and processed data are available on the GEO public database: GSE31545

To further interrogate the oligodendroglial feature of glioma, we defined an "oligodendroglial GPC signature" using a log ratio cut-off of 0.8. Similarly, the "NNI-8 GPC versus tumor" stemness signature was obtained by taking the top ranking differentially expressed probesets using the log ratio cut-off of 6. These signatures were used in the Connectivity Map analysis.

2.18.1 Connectivity Map analysis

We adapted the Connectivity Map method (Lamb et al, 2006) to score glioma gene expression databases based on the extent of pathway activation

associated with our GPC gene signature. (i) First, we defined an "oligodendroglial GPC signature" – a set of genes exhibiting altered expression between two cell states (oligodendroglial GPC versus GBM GPC), (ii) Second, we generated databases of reference gene expression profiles from 2 glioma databases – REMBRANDT and "Gravendeel" (Gravendeel et al, 2009; Madhavan et al, 2009), (iii) Third, using a non-parametric, rank-based pattern matching procedure, we mapped the GPC signature onto each patient gene expression profile and calculated activation scores based on the strength of association to the GPC signature, and finally, (iv) The patients were sorted according to their pathway activation scores. Two patient classes were identified, (+) and (-), where a positive activation score indicates that the patient gene expression profile is positively associated to the gene signature and vice versa. The two-tailed test p-values associated with each activation score were calculated as described in Lamb *et al*. (Lamb et al, 2006). P-values ≤ 0.1 were considered significant.

2.18.2 Reference profile generation for Connectivity Map analysis

Public GBM datasets with clinical data, in terms of survival length, histology, grade and age were obtained from the REMBRANDT database and the GEO database in the case of the Gravendeel dataset (GSE16011). To generate the reference profiles, all raw files were processed separately using the mas5. Expression values less than the threshold value of 50 were replaced with the threshold value. Next, the data was quantile normalized and gene expression values were row-wise median centered. Median centering each probeset allows us to study the range of gene expression values in a large dataset.

2.18.3 Survival analysis

Kaplan-Meier and Cox regression analysis of (+) and (-) groups were done in R using the survival package (Burkhardt et al, 2011). For the REMBRANDT

dataset, only survival ranges were available. Hence, the lower limit of the range was used in this analysis.

2.18.4 Prediction of Phillips Classification in REMBRANDT and Gravendeel datasets

To classify the REMBRANDT and Gravendeel samples according to the Phillips *et al*. classification (Phillips et al, 2006a), Affymetrix U133A probes for the Phillips molecular subtypes were extracted from the publication. A shrunken centroid model was trained and tested on the Phillips dataset (**Supplementary Table S1;** overall error rate 0.12) using the R package *pamr* (Tibshirani et al, 2002). Next, classification of the REMBRANDT and Gravendeel datasets was performed using the trained model.

2.18.5 REMBRANDT SNP array processing and 1p/19q LOH analysis

CEL files from the Affymetrix 100K SNP Arrays of oligodendroglioma and oligoastrocytoma patients were downloaded from the REMBRANDT database and all samples were normalized in dChip (Li & Wong, 2001; Lin et al, 2004). Genotyping calls were generated in the Affymetrix Genotyping Console (Affymetrix Inc.) software using the BRLMM algorithm. Chromosome 1p and 19q loss-of-heterozygosity inference was performed using an HMM algorithm in dChip with default parameters.

2.18.6 Gene Set Enrichment Analysis (GSEA)

The gene signature was further evaluated in molecular signature database using gene set enrichment approach. GSEA tool was downloaded from Broad Institute portal. The significantly enriched genesets in molecular signature database (MSigDB) were further analyzed for phenotypic correlation in the reference datasets.

CHAPTER 3

RESULTS

CHAPTER 3 – CRYOPRESERVATION OF GLIOMASPHERES DERIVED FROM HUMAN GLIOBLASTOMA MULTIFORME

3.1 Introduction and objectives

Gliomas represent the most prevalent of primary adult malignant brain tumors, with GBM exhibiting the worst prognosis and mean survival period of 15 months post-diagnosis (Louis et al, 2007). The highly recurrent, infiltrative and heterogeneous nature of the disease has prompted much research into the origin of gliomas to develop more effective therapeutic targeting. In lineage-tracing mouse modes, a cellular hierarchy exists where neural stem cells propagate tumor-causing mutations or deletions in key tumor suppressor genes (Alcantara Llaguno et al, 2009; Zheng et al, 2008). Such findings underscore the difficulty in eradicating GBM growth at its root. *In vitro*, glioma-propagating cells (GPCs) derived from clinical material are purportedly enriched in tumor-initiating cells (Galli et al, 2004). This makes future studies using GPCs as a cellular platform very important for recapitulating the disease pattern. *We and others have shown that patient-derived GPCs contain phenotypic, karyotypic and transcriptomic information that dictates primary tumor behavior (Chong et al, 2009; Foong et al, 2011; Ng et al, 2012). Importantly, GPCs recreate orthotopic xenograft tumors that mirror the patient's original tumor phenotypically and transcriptomically*. In this chapter, we describe our foundational work at establishing a well-characterized GPC repository.

In many studies involving the prospective isolation of GPCs, only a small amount of clinical material is available, and this limitation is compounded by a lack of methods to preserve such cells at convenient time points. In gliomas for instance, it has been shown that *in vivo* serial passaging of gliomaspheres [spheroid structures containing a heterogeneous mix of

glioma stem and progenitor cells (Reynolds & Rietze, 2005; Singec et al, 2006)] can provide a means to reliably maintain such primary cell lines (Galli et al, 2004). However, in practice it is not always possible to have access to suitably-aged immune-compromised animals to continuously maintain the stem and progenitor cells. Lee *et al.* demonstrated that tumor stem-like cells grown in serum-free condition closely mirrors the genotype, gene expression profile and biology of their parental tumors (Lee et al, 2006). In contrast, the frequently studied, commercially procured serum-grown glioma cells (typically purchased from American Type Culture Collection, ATCC) often contain karyotypic aberrations not found in the primary tumor (Li et al, 2008). Furthermore, we and others showed that xenografts established from patient-derived GPCs, but not serum-grown glioma cells, recapitulate the patient's original pathophysiology (**Figure 3.9**) (Chong et al, 2009; Li et al, 2008; Ng et al, 2012; Wakimoto et al, 2012). These observations bring into question the relevance of standard serum-grown cancer cell lines for studying the biology of human cancers and for screening new therapeutic agents. We therefore sought to explore a novel method of vitrification for gliomaspheres that is effective at preserving the cells' biological and genetic properties. We believe this method could provide many researchers with the means to establish a repository of primary GPCs that can be readily tapped upon for expansion or experimental design. In addition, such a method would also allow investigators to return to the same experimental cell line passages to reduce variability in experimental replication.

We explored vitrification for the following reasons: Vitrification is a process of glass-like solidification in which an aqueous solution is prevented from crystallization by rapid cooling (Rall et al, 1987). Vitrification has been commonly used for the cryopreservation of embryos at different

developmental stages from various species such as murine, rabbit, sheep and bovine (Ali & Shelton, 1993; Kasai et al, 1992; Kasai et al, 1990; Saha et al, 1996). Furthermore, human and mouse multi-cell embryos have been successfully cryopreserved using this strategy (Mukaida et al, 1998). *This highlights the feasibility of cryopreserving cell aggregates*. In addition, it has been demonstrated that vitrified embryonic stem cells retained their pluripotency and viability upon thawing (Reubinoff et al, 2001). Taken together, vitrification could provide an effective means of storage of GPCs cultured as spherical structures (i.e. gliomaspheres). To assess the efficacy of such a method, we compared vitrification with the most commonly and easily utilized method in labs, i.e. serum-containing medium with 10% dimethylsulfoxide (DMSO). We scored for parameters such as sphere-forming ability (GPC frequency) and sphere size (proliferation). The neurosphere assay has been well-studied for the maintenance and propagation of neural stem cells (Reynolds et al, 1992), and has been successfully adapted for GPCs (Galli et al, 2004). Additionally, serial sphere propagation reliably maintains GPC frequency (Reynolds & Rietze, 2005). We also assessed the expression of stemness and differentiation markers, gene expression profiles, as well as the retention of karyotypic hallmarks, and the ability to engraft and form orthotopic tumors that recapitulate the pathophysiology of the patient's original tumor. These criteria define GPCs phenotypically and functionally (Rich & Eyler, 2009).

3.2 Vitrification maintains the morphology, viability and proliferation rate of gliomaspheres

An important criterion for efficacious vitrification is the preservation of cellular properties upon thawing after long-term cryopreservation. We analyzed essential properties such as viability, expression of stem cell markers and multipotentiality. All patients' lines generate free-floating gliomaspheres except for NNI-4 and NNI-11 which generate semi-adherent spheres. Such morphological characteristics have previously been observed by others (Beier et al, 2007). The reasons are unclear but semi-adherent cultures, often displaying cells with neurite outgrowths, may represent more differentiated cells.

Gliomaspheres were frozen either conventionally in a slow-cooling protocol with 10% DMSO in the presence or absence of 90% FBS, or vitrified in 20% serum or serum-free medium by exposing glass capillaries containing gliomasphere aggregates to liquid nitrogen. The cell aggregates were then stored in liquid nitrogen for 30 days to as long as 2.5 years to mimic long-term storage prior to analyses. We assessed the viability of gliomaspheres at 1, 5 and 10 days post-thawing from liquid nitrogen storage by counting the number of gliomaspheres measuring at least 50 – 100 µm in diameter (Gunther et al, 2008). Gliomasphere formation has previously been shown to indicate GPC frequency and proliferation (Diamandis et al, 2007; Gal et al, 2007). A visual scan of cellular morphology indicated that vitrification with low serum best maintains initial frozen gliomasphere size with little or no cell death, with cells remaining relatively undifferentiated for up to 15 days in culture (**Figures 3.1 and 3.2**). Cryopreservation by vitrification lacking serum, or by conventional freezing with 10% DMSO showed greater cell death and vastly smaller gliomaspheres compared to non-vitrified cultures, suggesting

sphere disintegration (**Figure. 3.1**). We could not recover sufficient cells for further analyses due to extensive cell death. Standard freezing with 90% FBS yielded the best viability and preservation of spheroid structures for all the samples except NNI-2 where vitrification with 20% serum yielded the best viability (**Figure 3.2ii**). However, the peripheries of all gliomaspheres cryopreserved in 90% FBS exhibited clear signs of differentiation by 5 and 10 days post-thawing (**Figure 3.1xi and xii**). Our finding indicates that freezing with 10% DMSO + 90% FBS is an attractive alternative that should be explored in future studies. Encouraged by the good viability and lack of visual differentiation demonstrated by vitrified gliomaspheres, we proceeded with our analyses by comparing vitrified and non-vitrified samples. Proliferation rate as determined by using a standard alamarBlue® assay showed that all vitrified and non-vitrified gliomaspheres continued to proliferate at similar rates except for NNI-3 which displayed a moderate but significant change (**Figure 3.3**).

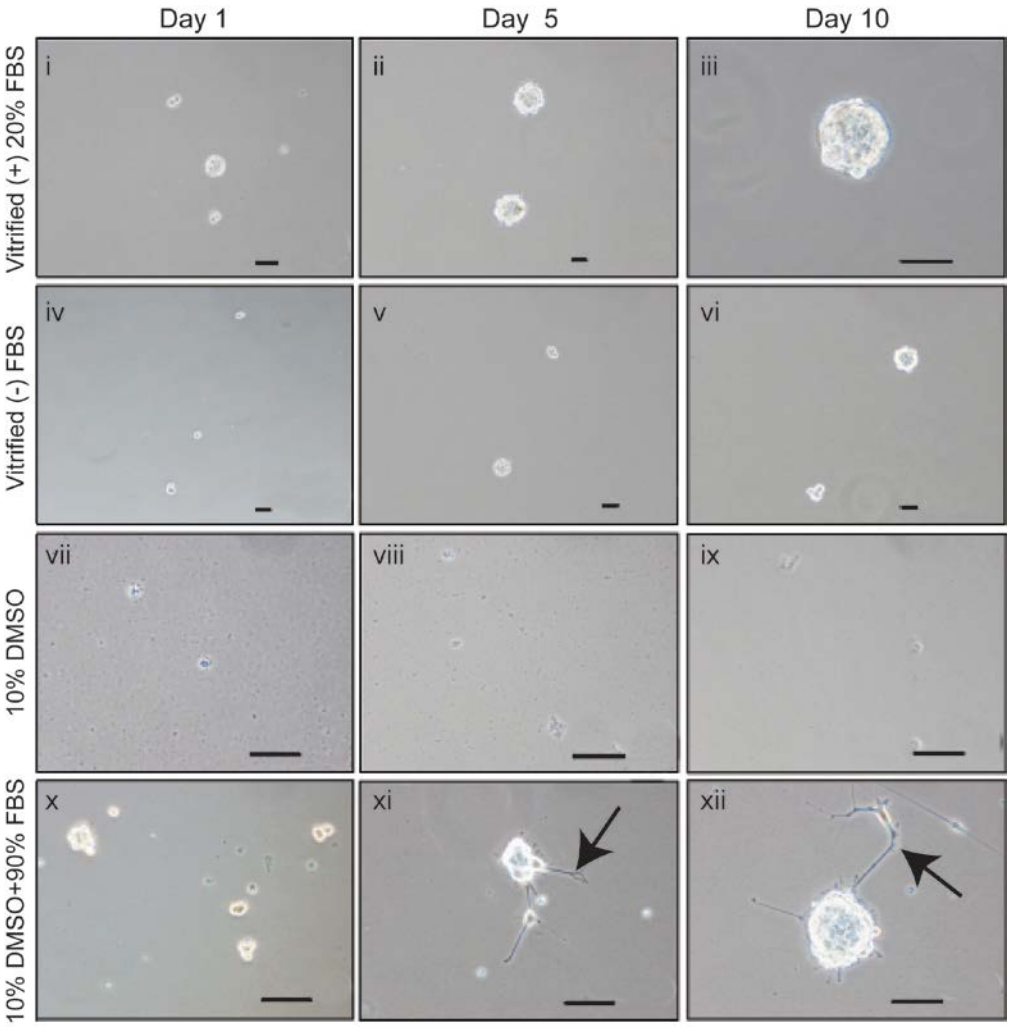

Figure 3.1. Vitrification results in greater viability and absence of differentiation in gliomaspheres after thawing. Gliomaspheres were frozen by various methods: **i-iii**, vitrification with 20% serum; **iv-vi**, vitrification without serum; **vii-ix**, 10% DMSO; **x-xii**, 10% DMSO + 90% serum. After storage in liquid nitrogen for 30 days (vitrification with 20% serum and without serum, 10% DMSO, and 10% DMSO + 90% FBS) and up to 2.5 years (vitrification with 20% serum only), the gliomaspheres were thawed and subjected to morphological analyses while in culture under serum-free conditions supplemented with growth factors. Shown are representative images obtained from one patient's gliomasphere line, NNI-1. Note the appearance of extended processes (indicated by arrows) at the periphery of the spheroid structure (typical signs of differentiation) on days 5 and 10 of the sample frozen with 90% FBS (arrows). Scale bar = 100 µm. Experiments carried out in duplicate.

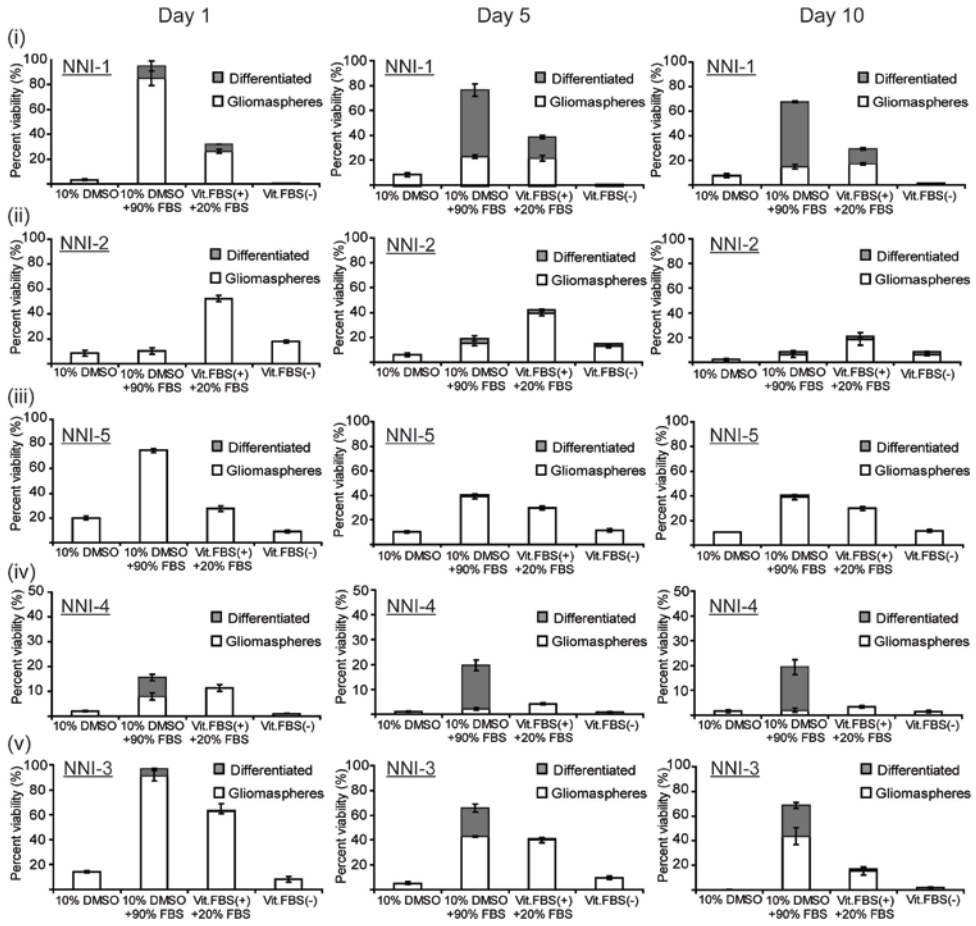

Figure 3.2. Quantitative analysis of viability and signs of differentiation 10 days post-thawing. Conventional cryopreservation with 10% DMSO + 90% FBS yielded best viability post thawing in majority of the gliomasphere lines (**i, iii, iv, v**) except NNI-2 (**ii**). Signs of differentiation post-thawing were scored and the proportions were represented as grey bars for each freezing condition. Cryopreservation with 10% DMSO + 90% FBS showed highest number of differentiated gliomaspheres 10 days post-thawing (**i, iv, v**) compared to vitrification with 20% FBS.

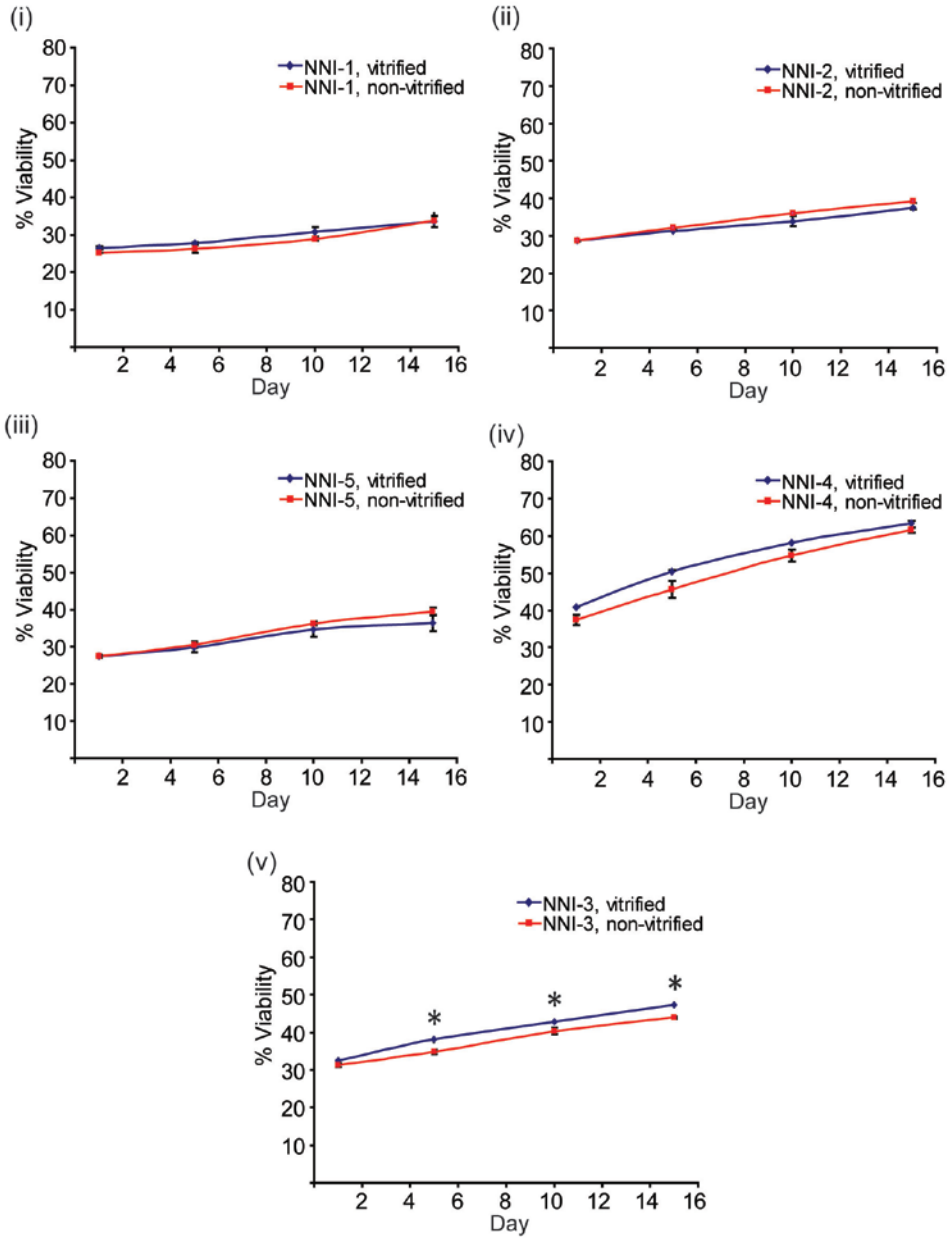

Figure 3.3. Vitrification maintains the proliferative capacity of gliomaspheres. Patient's gliomaspheres (**i-v**) were subjected to vitrification, and proliferation rate compared to gliomaspheres without vitrification (non-vitrified) was determined using a standard alamarBlue® assay. *p<0.05, n=3.

3.3 Vitrification preserves the stemness expression and multipotentiality

Markers of the stemness state such as Nestin, Sox-2, CD133, Musashi-1 (Msi-1), Bmi-1, Nanog and Oct4 were assayed by quantitative real-time qRT-PCR. Differentiation markers such as TuJ1, MOBP and GFAP were also evaluated as gliomaspheres are heterogeneous and comprise of more differentiated progenitors in addition to *bona fide* stem cells (Reynolds & Rietze, 2005; Singec et al, 2006). Nestin is expressed in neural precursors (Cai et al, 2002); Sox-2 is a gene known to play a role in maintenance of the neural progenitor state (Graham et al, 2003); CD133 is a marker for neural stem cells as well as glioma-propagating cells (Singh et al, 2004; Uchida et al, 2000); Msi-1 is a marker for self-renewal (Kaneko et al, 2000) ; Bmi-1 is a Polycomb group (PcG) gene and epigenetic silencer that prevents premature growth arrest in most differentiated tissue cells and is essential for the self-renewal of several types of adult stem cells (Lessard & Sauvageau, 2003; Park et al, 2003); Nanog is a transcription factor essential for the maintenance of an undifferentiated state (Ivanova et al, 2006), and Oct4 is a transcription factor implicated in maintaining the pluripotency of stem cells (Mountford et al, 1998). TuJ1 marks neurons, MOBP represents myelin-associated oligodendrocytes basic protein and GFAP marks astrocytes.

We observed that vitrification preserved the expression of essential stem cell markers for patient samples NNI-2, NNI-4 and NNI-5 (**Figures 3.4A, C and D**). Between vitrified and non-vitrified samples, expressions of Nestin, CD133, Bmi-1, Nanog and TuJ1 for NNI-1 were minimally altered by less than two-fold (**Figure 3.4B**), but there was significant variation in virtually all genes examined for NNI-3 (**Figure 3.4E**). We will provide justification later for this variation (Page 70).

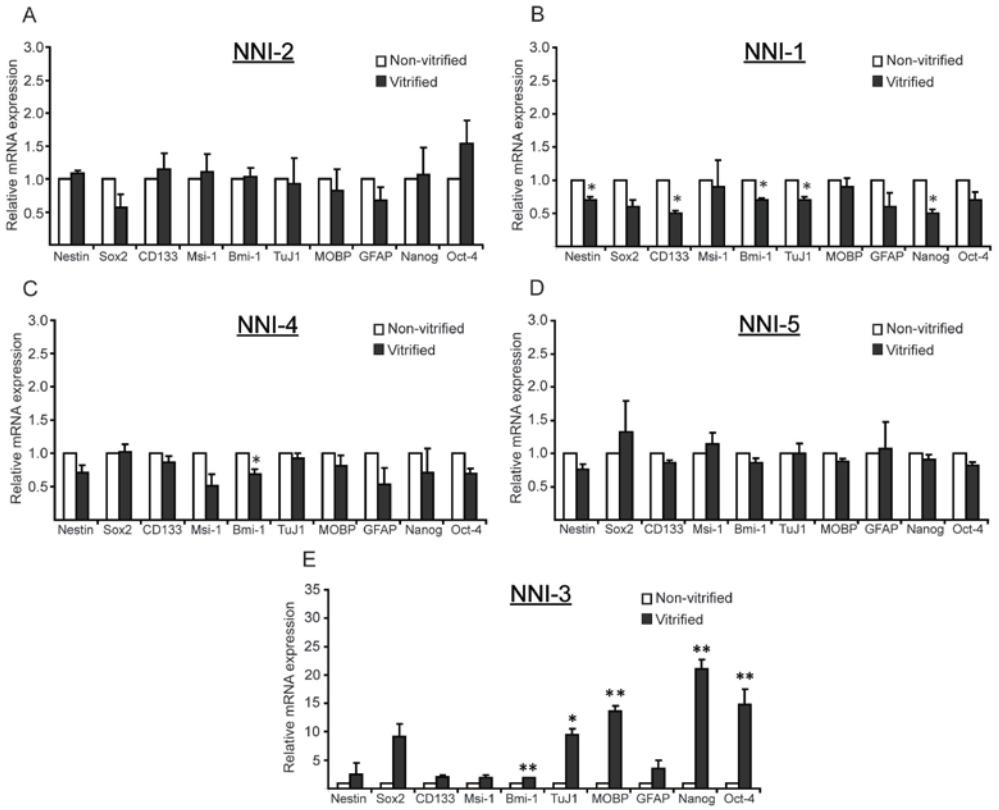

Figure 3.4. Vitrification preserves essential neural precursor gene expression. (**A-E**): Quantitative real-time RT-PCR analysis of five patients' gliomaspheres. The undifferentiated states of both vitrified and non-vitrified gliomaspheres were analyzed for the presence of stem/progenitor and differentiation markers. *p<0.05; **p<0.01, n=3.

Additionally, we carried out immunofluorescent staining experiments to verify the stemness and multipotentiality profiles of the vitrified and non-vitrified samples. All patients' gliomaspheres demonstrated preservation of stem-like characteristics in vitrified and non-vitrified samples (**Figures 3.5A and 3.6**). As cell morphology changes accompany the induction of differentiation of neural stem cells, we assessed multipotentiality by scoring for neurons (TuJ1), astrocytes (GFAP) and oligodendrocytes (O4). All samples displayed the ability to differentiate into neurons, astrocytes and oligodendrocytes (**Figures 3.5B and 3.6**). Furthermore, we scored for differentiated cells staining positively for Nestin and Msi-1 stemness markers

to determine the retention of self-renewal in otherwise normally terminal differentiated neural lineages, an aberrant developmental feature previously observed by others (Galli et al, 2004; Hemmati et al, 2003; Yuan et al, 2004). We also scored for cells co-expressing GFAP and TuJ1. All patients' gliomaspheres when differentiated showed no significant differences between the vitrified and non-vitrified states, supporting that vitrification preserves the multipotentiality property of the cells (**Figure 3.6**). We observed that all samples displayed 70-95% Nestin- and Msi-1-stained cells despite being cultured under differentiating conditions (**Figure 3.5B**). This may in turn reflect an aberrant regulatory pathway in cancer stem cells. Differentiated cells were detected that co-stained for GFAP and TuJ1; notably, NNI-4 differentiated cells expressed the highest proportion of such cells (**Figure 3.6**). Others have also demonstrated the co-existence of such normally distinct neural development pathways (Galli et al, 2004; Hemmati et al, 2003; Singh et al, 2003; Yuan et al, 2004).

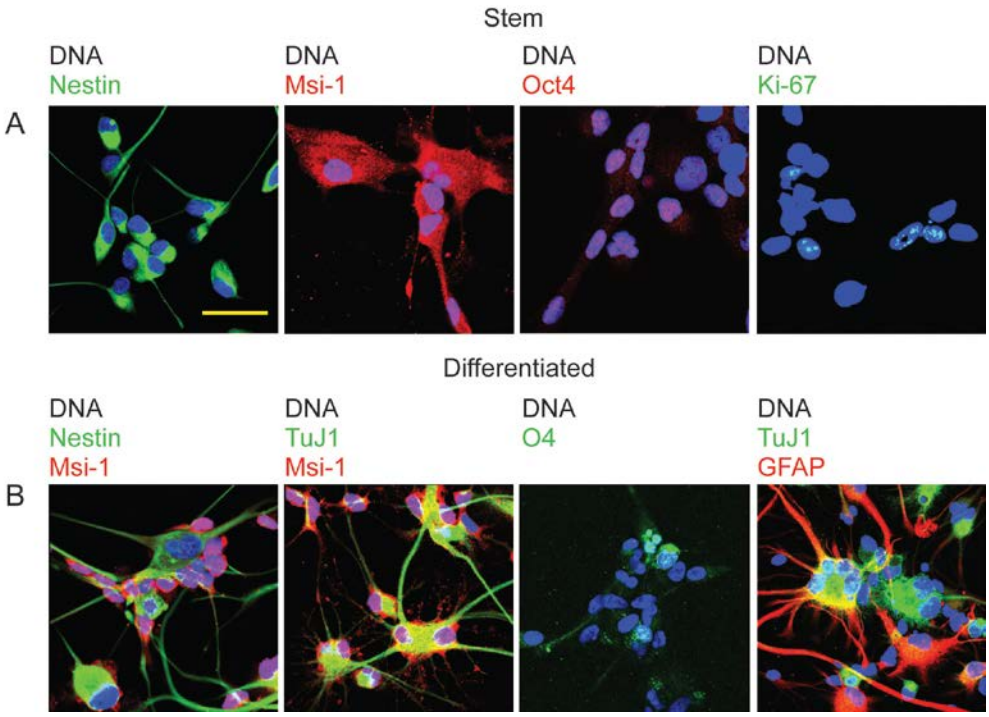

Figure 3.5. Vitrification preserves stemness and differentiation markers expression. Immunofluorescent staining of representative vitrified patient sample NNI-1 with (**A**) stem cell/precursor or proliferative markers (Nestin, Msi-1, Oct4, and Ki-67) and (**B**) multipotentiality markers (TuJ1, GFAP, and O4). Scale bar = 50 µm.

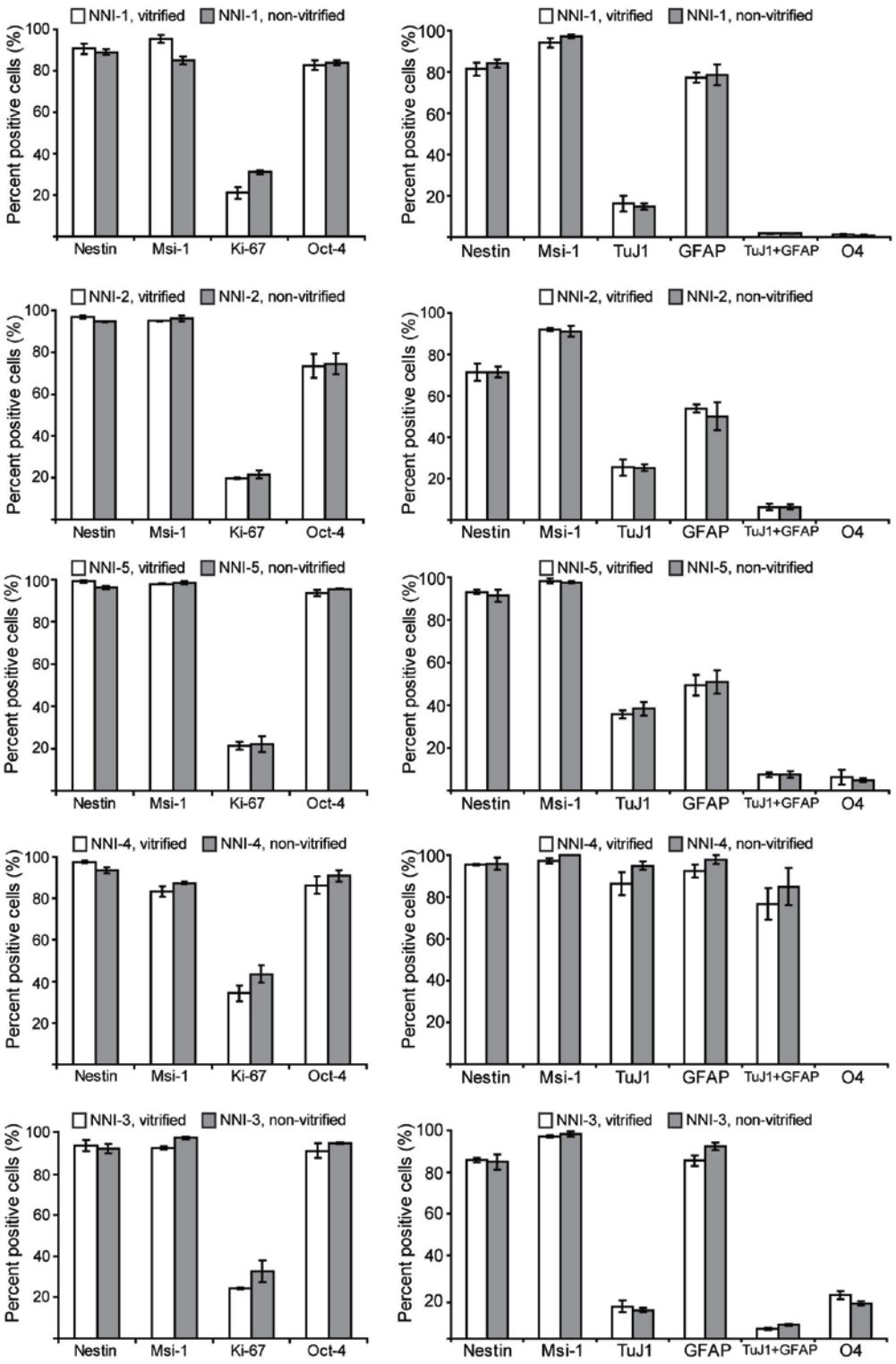

Figure 3.6. Vitrification maintains stemness and multipotentiality in GPCs. Quantification of immunofluorescent staining in five gliomasphere lines (NNI-1, 2, 3, 4, and 5) with or without vitrification. Stemness and multipotentiality markers were scored. $p>0.05$ for all sample pairs, indicating that there was no significant difference between vitrified and non-vitrified samples; n=3.

3.4 Vitrified gliomaspheres demonstrate secondary sphere formation and self-renewal potential

For an effective cryopreservation method, GPCs must be reliably maintained and not subject to cell death upon thawing and expansion. To investigate the stem cell frequency and self-renewal potential of gliomaspheres, we dissociated gliomaspheres into single cells and dispensed into 96-well plates at decreasing cell numbers and then scored for secondary sphere formation after 7 days (**Figure 3.7A**). Cell clustering played no apparent role in sphere formation as cells were plated at clonal densities (Singec et al, 2006). As gliomaspheres are heterogeneous and the neurosphere assay does not distinguish initially proliferating neural precursors from *bona fide* stem cells with self-renewal potential, we sought to carry out sequential minimal dilution assays for at least three passages, which confirmed that these single-cell derived gliomaspheres possess the potential to grow infinitely, underscoring self-renewal as an important criterion for glioma-propagating cells. The proportion of sphere-forming cells remained stable throughout the course of culture (>6 months), indicating asymmetrical cell divisions (Lathia et al, 2011). There was no significant difference between the vitrified and non-vitrified samples of all patients' gliomasphere lines except for NNI-3, indicating that the vitrification procedure does not reduce the secondary sphere-forming ability of these cells (**Figure 3.7A**). This implies that GPC frequency is maintained through vitrification. Moreover, the CD133-expressing population within the spheres that is often associated with tumor-initiating potential was also maintained throughout the course of culture (>6 months; **Figure 3.7B**).

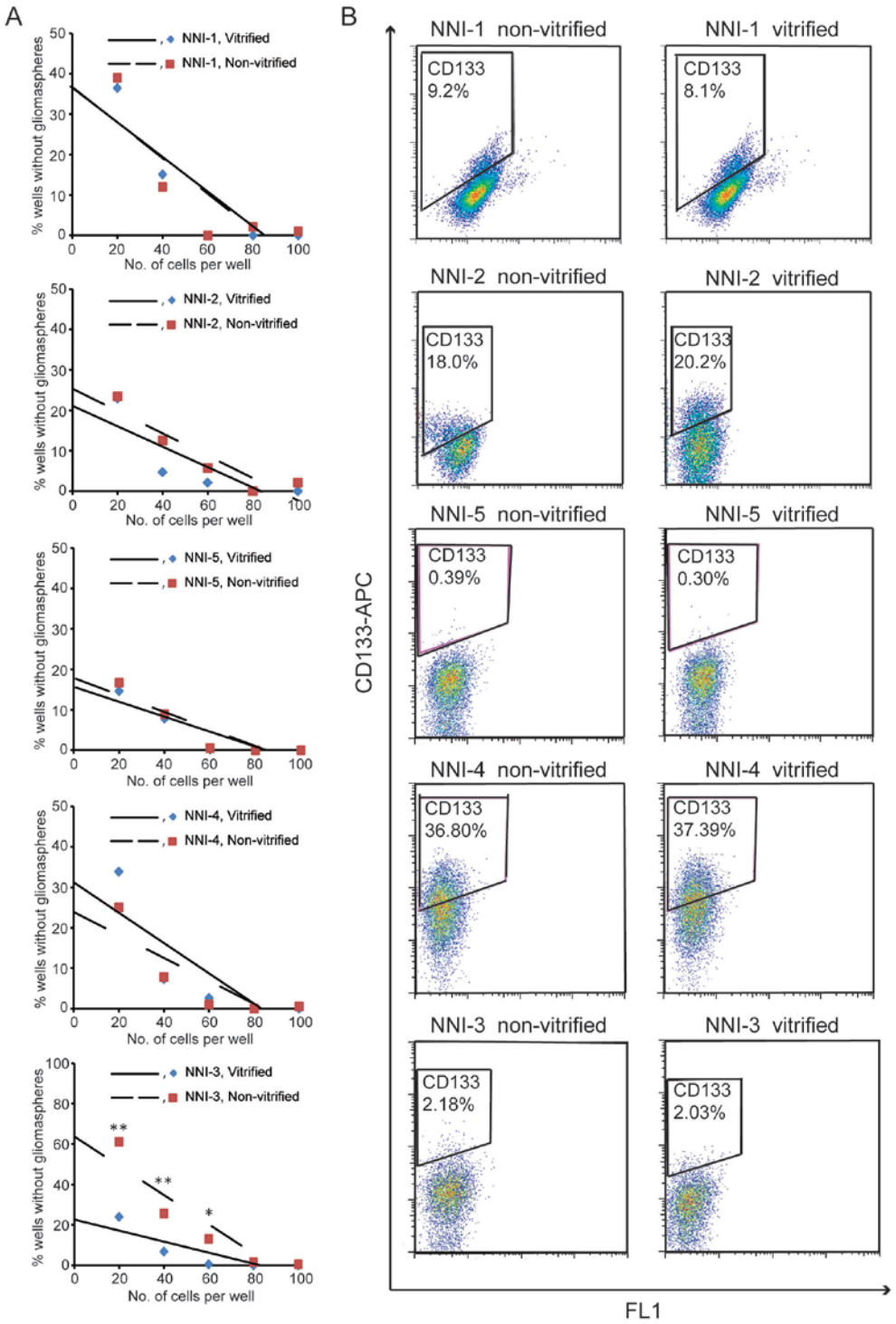

Figure 3.7. Vitrification preserves self-renewal capability and CD133 expression in gliomaspheres. A, Gliomaspheres were dissociated into single cells, plated at decreasing cell numbers, and analyzed for their ability to form secondary gliomaspheres. $p>0.05$ for all sample pairs (except NNI-3, $*p<0.05$; $**p<0.01$) indicating that vitrified and non-vitrified samples maintained self-renewal capability; n=3. **B**, Gliomaspheres were dissociated into single cells and stained with CD133/2 antibody conjugated to APC according to the manufacturer's instructions (Miltenyi Biotec). Percentage of CD133 expression was determined by fluorescence-activated cell sorting. Each vitrified or non-vitrified sample was gated according to its own isotype control; n=3.

3.5 Vitrification preserves the karyotypic hallmarks of glioblastoma multiforme

To conclusively demonstrate the tumor origin of our gliomaspheres, as well as to ascertain if vitrification preserves the karyotypic integrity and hallmarks of GBM, we karyotyped all patients' gliomaspheres before and after the vitrification process. Our data indicate that all gliomaspheres were of tumor origin, preserved their karyotypic integrity as well as maintained the hallmarks of GBM in both vitrified and non-vitrified samples (**Figure 3.8**). Notably, typical GBM primary tumor features such as polysomy of chromosome 7 (where *EGFR* is located) and loss of chromosome 10 (where *PTEN* is located) were present, which is consistent with a previous report by Wakimoto *et al.* (Wakimoto et al, 2012). In addition, Lee *et al.* reported that GPCs cultured under serum-free conditions preserved the karyotypic profiles of the primary tumors (Lee et al, 2006). In contrast, conventional serum-grown cells contained chromosomal aberrations not reflective of the primary tumors (Li et al, 2008). These findings underscore the importance of studying GPCs and we now have a method to reliably cryopreserve these cells. Interestingly, we observed aneusomy of chromosomes 12 and 13 across all five patients' gliomaspheres. We were able to detect additional karyotypic changes in NNI-3 non-vitrified cells (**Supplementary Figure S1**) that had been *in vitro* passaged for the longest period compared to all other lines (> 50 passages). It is probable that this resulted in changes in proliferation rate, surface marker expression, self-renewal potential and gene expression as previously shown, likely resulting in cell line transformation. We believe this highlights the importance of the vitrification method in being able to freeze down low passage cells, and thaw them only when needed for further experiments. Continued passaging *in vitro* to maintain the cells would be deleterious.

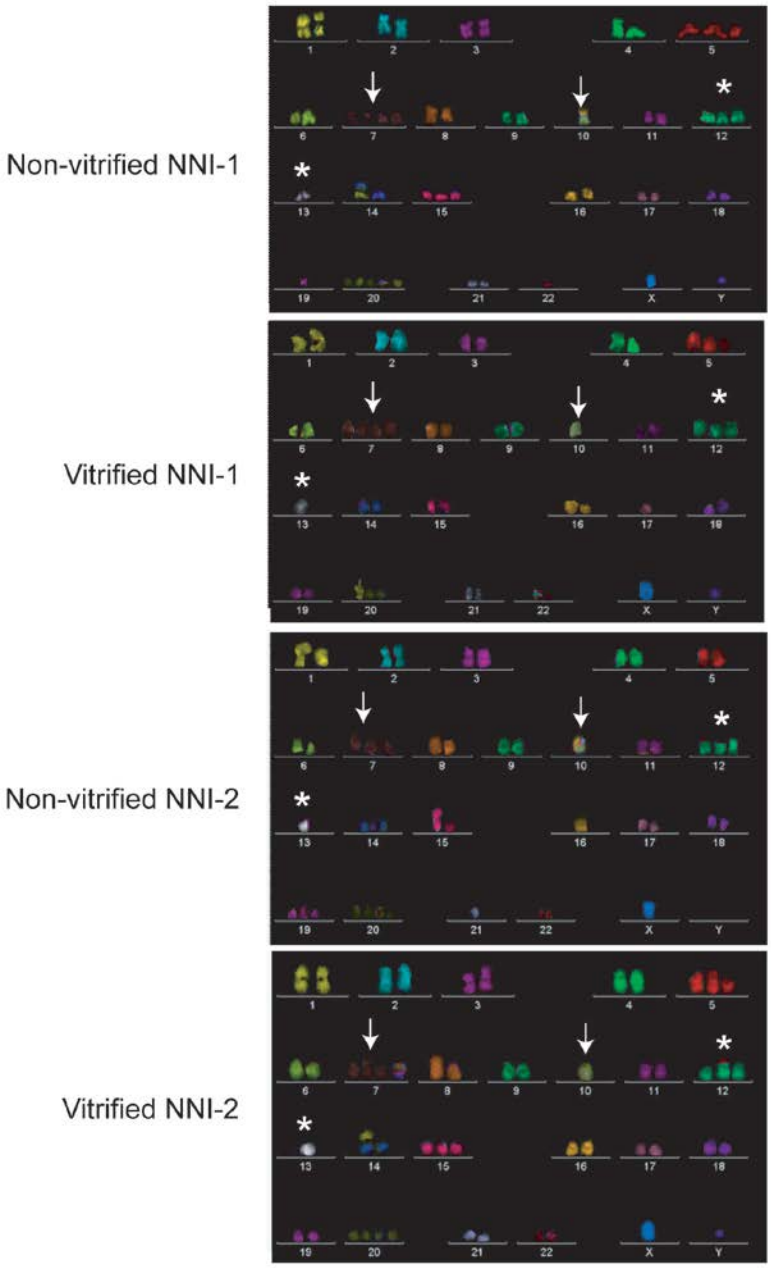

Figure 3.8. Vitrified gliomaspheres maintain karyotypic integrity and GBM hallmarks. Single 2 x 10^5 cells from dissociated gliomaspheres were karyotyped by metaphase-fluorescent *in situ* hybridization (mFISH) analyses according to the manufacturer's instructions (MetaSystems XCyte mFISH). Arrows indicate polysomy of chromosome 7 and loss of chromosome 10. Asterisks denote aneusomy of chromosomes 12 and 13.

3.6 GPC-derived xenograft tumors recapitulate glioma pathophysiology in NOD-SCID gamma mice

The ability of GPCs to serially transplant and reform gliomas that recapitulate the original tumor pathophysiology provides unequivocal evidence for the definition of a cancer-initiating cell (Vescovi et al, 2006). Accordingly, we were able to recapitulate glioma disease patterns when we orthotopically implanted our vitrified gliomaspheres in immune-compromised mice (**Figure 3.9**). In this case, the NOD-SCID gamma (NSG) mouse was chosen for its superior ability at engrafting clinical material (Quintana et al, 2008).

When we implanted NNI-1 and NNI-8 gliomaspheres, we obtained tumors that demonstrated extensive infiltration into the surrounding cerebral cortex, a pathognomonic feature of human GBMs (Galli et al, 2004; Singh et al, 2004) (**Figure 3.9A**). Intriguingly, when we implanted NNI-8 (a GPC line derived from a patient with anaplastic oligoastrocytoma) into NSG mice, we obtained glioma xenografts that were highly infiltrative and displayed the typical “fried egg” histology of oligodendroglial cells with “chicken wire” patterning of the stroma, recapitulating features present in oligodendroglial tumors (Cairncross et al, 1998). This emphasizes the ability of patient-derived GPCs to capture primary tumor behavior. This is further validated in the effort by The Cancer Genome Atlas (TCGA) which demonstrated that orthotopic xenografts established from clinical material, but not commercially procured, serum-grown cells (**Figure 3.9B**), formed xenografts that mirrored the primary tumor phenotype and gene expression profiles (Verhaak et al, 2010).

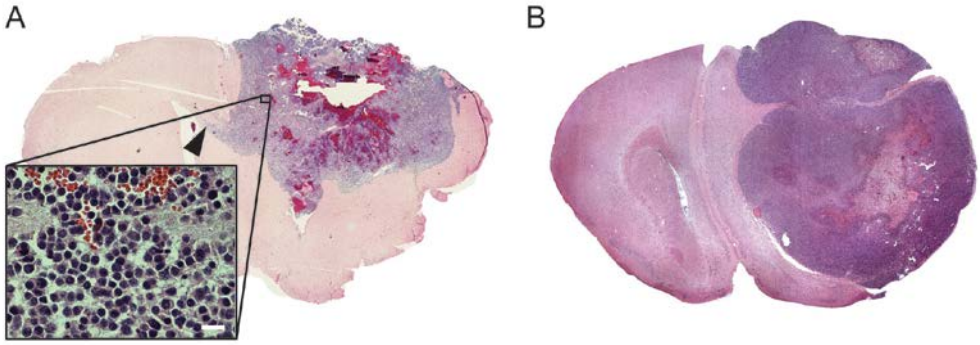

Figure 3.9. Vitrified gliomaspheres form tumor xenografts that recapitulate glioma pathophysiology. A, Anaplastic oligoastrocytoma GPC intracranial xenograft exhibited extensive infiltration, hemorrhaging and displayed the typical “fried egg” morphology and “chicken wire” patterning of stroma. Also note the migration of glioma cells along the white matter tract (black arrow head), typically found in patients with invasive glioma. Scale bar = 20 µm. **B**, Intracranial xenograft established from serum-grown U87MG displayed spatially constrained, well-lineated tumor margins, non-reflective of human GBM disease pathology.

3.7 Gene expression studies demonstrate the clustering of vitrified and non-vitrified gliomaspheres, and histologically similar GBM tumors yield GPCs of very distinct transcriptomic profiles

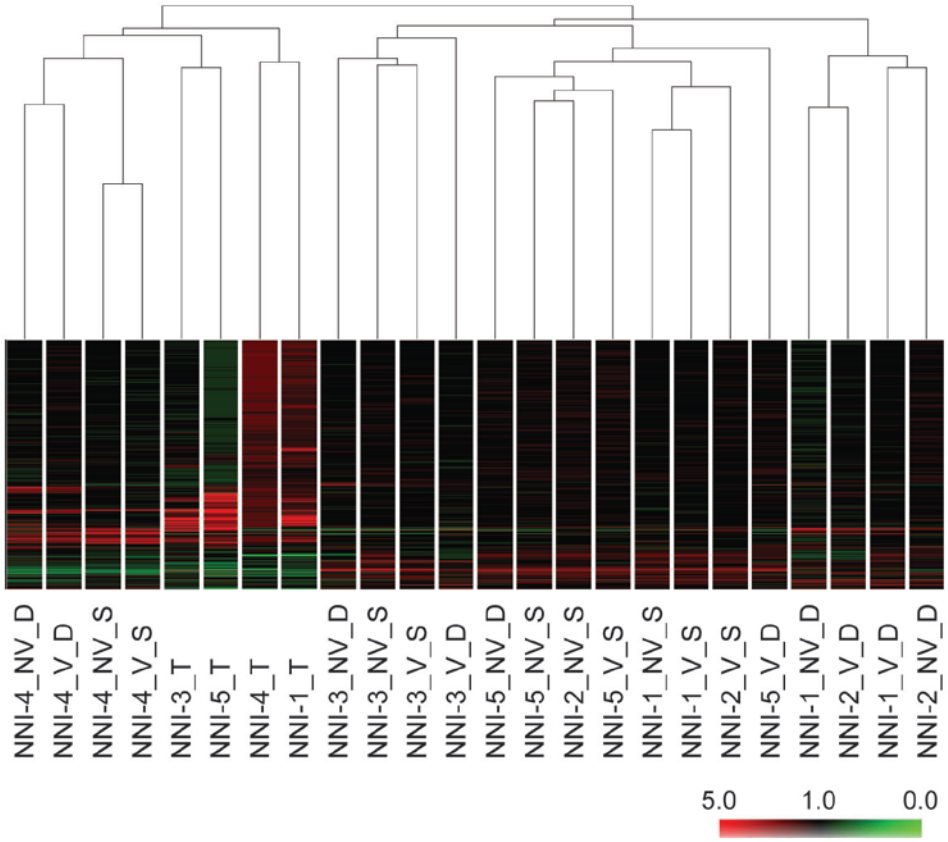

Figure 3.10. Vitrification preserves transcriptomic profiles of gliomaspheres. Dendrogram determined by unsupervised hierarchical cluster analysis of five patients' gliomaspheres (V, vitrified and NV, non-vitrified) cultivated under serum-free conditions supplemented with growth factors (S-suffix) or differentiated by withdrawal of growth factors with addition of serum (D-suffix). Samples with the T-suffix represent the original primary patient tumor specimen.

Verhaak *et al*. showed for the first time that histologically similar GBM tumors can be molecularly classified into four subgroups, each with distinct gene expression, genomic aberrations and clinical history (Verhaak et al, 2010). Such findings indicate that gene expression drives glioma disease progression and outcome. For vitrification to be an efficient cryopreservation method, we would expect that vitrified and non-vitrified gliomaspheres should

generate transcriptomic profiles that cluster together, indicating the genetic stability of the samples. We therefore performed microarray gene expression analyses on all five patient's gliomasphere lines (NNI-1, 2, 3, 4, and 5; vitrified and non-vitrified) as well as on their differentiated counterparts (vitrified and non-vitrified) and primary patient tumor specimens. This gene expression data was also subsequently utilized in Chapter 4. Indeed, unsupervised clustering analysis showed that the vitrified form of each sample in the stem/ progenitor or differentiated state, clustered together with its respective non-vitrified form (**Figure 3.10**). This supports our study that vitrification preserves the transcriptomic profile of GPCs.

Intriguingly, through Principal Component Analysis (PCA) map which allows us to view molecular grouping with a third dimension, thereby separating planes of cell groups, we observed that histologically similar GBM tumors yielded GPCs with very distinct transcriptomic profiles (**Figure 3.11**). This molecular heterogeneity has in recent years been emphasized in many cancer types (Atlas, 2008; Gerlinger et al, 2012; Ooi et al, 2009), and alludes to the likely reason for the frequently observed inter-patient variability to treatment response.

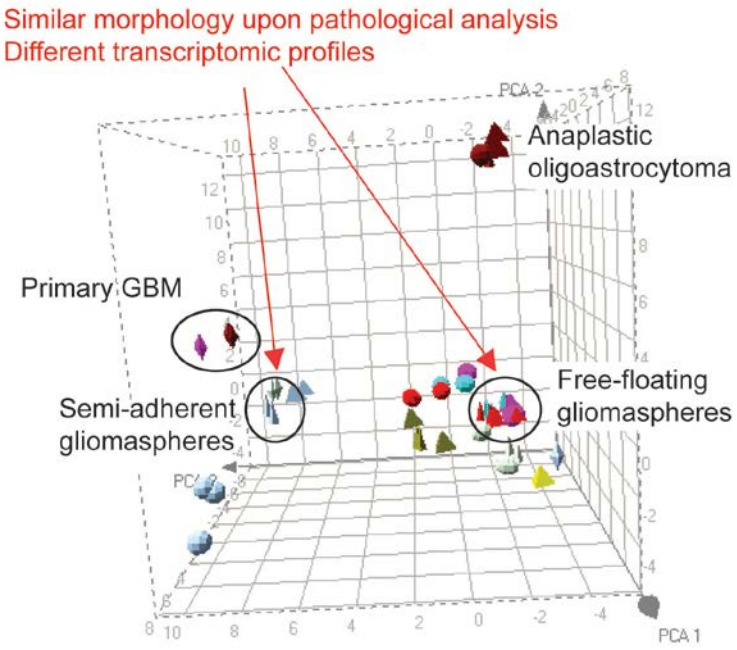

Figure 3.11. Vitrification preserves genetic profiles of gliomaspheres, which are transcriptomically distinct from primary tumors and differentiated cells. Principal component analysis (PCA) map of gliomaspheres (free-floating and semi-adherent) and primary tumors showed that histologically similar GBM tumors yielded GPCs with distinct transcriptomic profiles.

3.8 Summary

Tissue repositories have traditionally been maintained either as frozen samples stored in liquid nitrogen tanks, or embedded in paraffin wax. While both methods of storage allow the retrieval of cellular material, it is static as it does not allow the isolation and subsequent cultivation of live cells from the stored tumor. In our study, we present data for the first time on a modified vitrification method for patient-derived brain tumor gliomaspheres which enriches for tumor-propagating cells, more commonly referred to as “cancer stem cells”. Such a method evaluates essential stem cell-like properties, multipotentiality capacity, genotypic profile and ability to recapitulate glioma pathophysiology. Vitrification now provides a solution to the long-term storage of tumor-propagating cells without the need to maintain a constant supply of suitably-aged immune-compromised animals to *in vivo* serially passage the cells. With the vitrification approach, a glass-like solidification of the freezing solution is achieved by using a high concentration of cryoprotectant and rapid cooling. This method eliminates cell injury due to ice crystal formation. Although various cryopreservation techniques have been developed for a range of cells such as human or mouse embryonic stem cells (Ha et al, 2005; Reubinoff et al, 2001) and mouse neural precursor cells (Hancock et al, 2000; Milosevic et al, 2005; Tan et al, 2007), these studies have largely relied on gross morphological appearances and have ignored examining the genetic profiles and quantitative analysis of cell types (both stem and differentiated forms) of samples. For validation of vitrification as a method of cryopreservation for GPCs, the cellular heterogeneity of tumor cells and their ability to recapitulate glioma pathophysiology would have to be taken into consideration.

Standard freezing techniques with high serum content have been used in many cellular systems due to their less complex preparatory steps. Previous work has evaluated the use of such a method in the cryopreservation of human embryonic stem cells which resulted in differentiated outgrowths (Ha et al, 2005). Here, we demonstrated that although freezing with 90% FBS yielded the best viability of gliomaspheres; it also resulted in differentiated outgrowths. Serum contains many unknown growth factors and cytokines that can induce differentiation of stem cells when applied at high concentrations (Ha et al, 2005; Richards et al, 2004). Nevertheless, given the significantly better viability by the method, slow freezing with high serum presents an attractive alternative that should be explored in future studies.

Taken together, we have demonstrated that vitrification maintains essential stem/progenitor-like properties, multipotentiality and transcriptomic profiles. Importantly, the vitrified cells retain the capacity to form tumor xenografts that recapitulate glioma pathophysiology. This validates GPCs as a useful cellular platform for further studies.

CHAPTER 4

RESULTS

CHAPTER 4 – PROGENITOR-LIKE TRAITS CONTRIBUTE TO PATIENT SURVIVAL AND PROGNOSIS IN OLIGODENDROGIAL TUMORS

4.1 Introduction and objectives

Although our earlier findings indicated that *in vitro* low passage GPCs recapitulate the phenotypic and karyotypic profiles, as well as tumor morphology of the primary tumor, the contribution to patient survival and clinical outcome is unclear. To make sense of targeting GPCs and their self-renewing function in any therapeutic design, we must first show that GPCs are clinically relevant, and that their presence in the primary tumor affects disease progression. In other words, *we ask if GPCs contain genomic and transcriptomic information that dictates primary tumor behavior*. The plausibility of this hypothesis has been shown in lung cancer stem cells using a mouse model (Curtis et al, 2010). In that instance, the combination of *KRAS*, *TP53* and *EGFR* mutations in lung cancer stem cells determines the cell lineage and histotype specificity of the primary tumor, suggesting that the oncogenotype of GPCs drives primary tumor behavior.

We explored this hypothesis in 2 major brain tumor variants, GBM and oligodendroglial tumors, the latter of which has significantly better prognosis and increased chemosensitivity (Cairncross et al, 1998; Louis et al, 2007). Recent works have shown that these 2 tumor types are molecularly heterogeneous, with each subclass distinguished by unique gene expression, genetic aberrations, and clinical profile (Atlas, 2008; French et al, 2005; Gravendeel et al, 2009; Verhaak et al, 2010). These findings highlight that gene expression drives disease progression and survival outcome. Accordingly, we used gene expression analyses to explore the clinical relevance of GPCs isolated from GBM and oligodendroglial tumors, by

tapping into our own data, as well as that from publicly available GPC collections (Chong et al, 2009; Gunther et al, 2008; Pollard et al, 2009) to enlarge the statistical pool of cells. We subsequently interrogated their clinical contribution in 2 large patient glioma databases, REMBRANDT (Madhavan et al, 2009) and "Gravendeel" (Gravendeel et al, 2009). We adapted the Connectivity Map method (Lamb et al, 2006) to determine strengths of association between the GPC gene signature (that distinguished oligodendroglial from GBM GPCs) and individual patient gene expression data. This method is advantageous as it allows us to make connections between different data platforms and biological information through the common vocabulary of genome-wide expression profiling. Since then, the Connectivity Map has been successfully applied to determine the degree of oncogenic pathway activation in gastric cancer (Ooi et al, 2009). We also recently successfully used this method to define the tumor suppressor function of Parkin in glioma (Yeo et al, 2012). Furthermore, as the 1p/19q co-deletion status is currently a clinical indicator for enhanced chemosensitivity of oligodendrogliomas and consequently better prognosis (Cairncross et al, 1998), we asked if our molecularly defined GPC signature performed better. This would shed light on the value of molecular signatures over current clinical indicators in patient prognosis and treatment regimens. Finally, we validated the pathway networks identified by our gene signature using a panel of prospectively collected primary tumors. Our study in this chapter supports that *GPC genomic and transcriptomic information dictates primary tumor behavior, consequently impacting on disease progression and patient survival outcome*.

4.2 An oligodendroglial GPC signature is defined

We first determined differentially regulated genes between 3 oligodendroglial GPCs (NNI-8, GS-2, G174) and 17 GBM GPCs collectively obtained from our study (Chong et al, 2009), as well as that of Gunther *et al.* (Gunther et al, 2008), and Pollard *et al*. (Pollard et al, 2009) (**Figure 4.1**). This differential gene list, "oligodendroglial GPC signature", is shown in **Supplementary Table S2**. An analysis of the associated pathway networks using MetaCore from GeneGo Inc. revealed that the signature is enriched in the Wnt, Notch and TGFβ signaling pathways (**Figure 4.2**). Interestingly, Notch (Fan et al, 2010; Zhu et al, 2011), TGFβ (Anido et al, 2010; Penuelas et al, 2009), and the recently published Wnt (Zhang et al, 2011; Zheng et al, 2010) signaling pathways have been shown to be crucial in maintaining the growth of GBM GPCs.

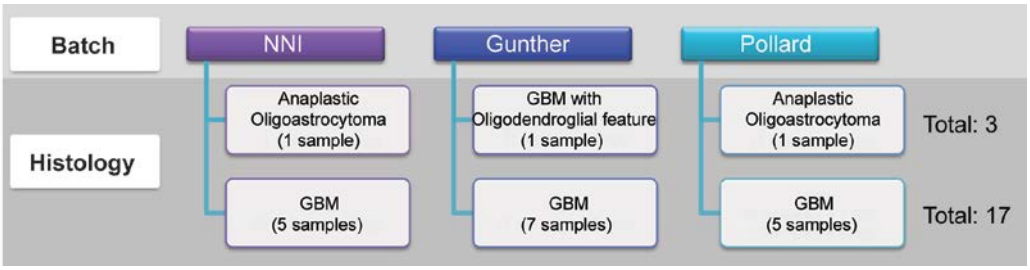

Figure 4.1. Study flowchart. Oligodendroglial GPCs (NNI-8, GS-2, G174) and 17 GBM GPCs were collectively obtained from our study plus Gunther and Pollard.

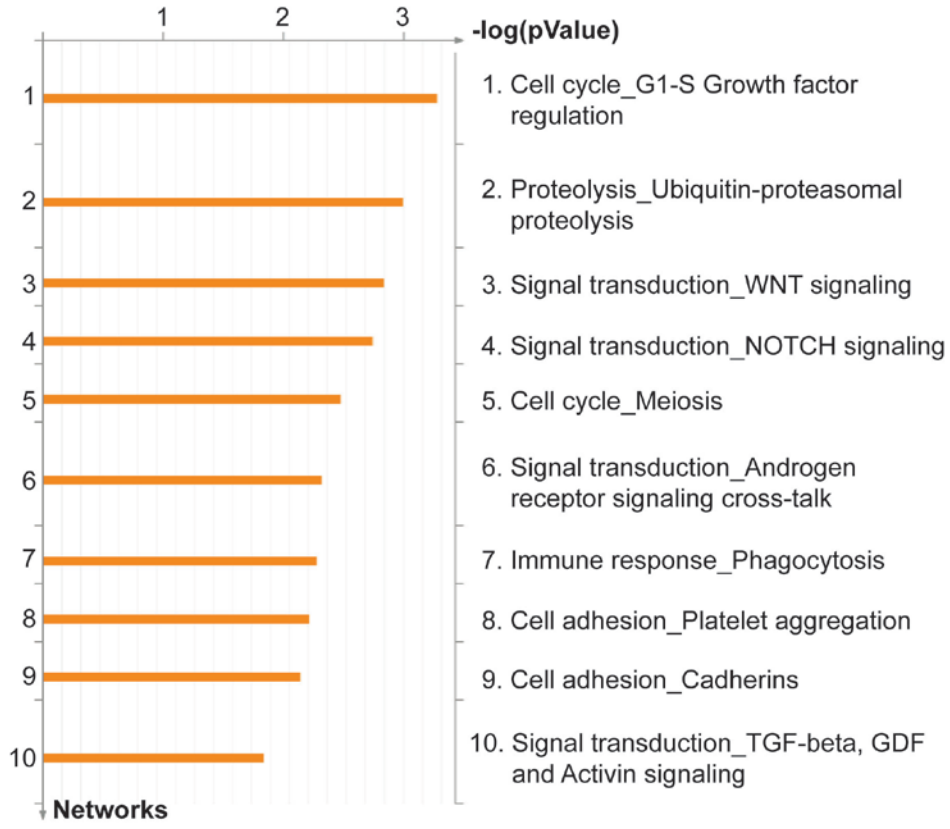

Figure 4.2. GeneGo process networks. Top-ranking process networks include Wnt, Notch and TGFβ signaling pathways.

4.3 Functional validation of the Wnt, Notch, and TGFβ pathways in GPCs

Although the Wnt, Notch, and the TGFβ pathways regulate GBM GPC survival, their relation to the 2 glioma variants – oligodendroglial versus GBM GPCs, is unclear. In the previous section 4.2, we showed that the oligodendroglial gene signature is enriched for the Wnt, Notch, and TGFβ signaling pathways (**Figure 4.2**); however, their precise activation or downregulation remains to be tested. To assess pathway activation in GPCs (NNI-4, 7, 8, 10, 11 and 12), we carried out two assays: (i) immunoblot analysis of key pathway components; and (ii) dependence on pathway by using well-established pharmacological inhibitors. NNI-7 and NNI-8 oligodendroglial GPCs showed increased sensitivity to Wnt pathway

inhibitors, Cercosporin (Lepourcelet et al, 2004) and CCT036477 (Ewan et al, 2010), compared with the other 2 of 3 GBM GPCs (NNI-11 and NNI-12) tested, consistent with the highest level of active β-catenin (nuclear-localized) detected (**Figure 4.3Ai**). Gliomasphere frequency was significantly reduced upon pathway inhibition, indicating that GPCs were effectively targeted (**Figure 4.3Bi**).

Next, we assessed the Notch signaling pathway activation in our GPCs. Using γ-secretase inhibitor (Wolfe et al, 1998) and DAPT (Hovinga et al, 2010), we observed that NNI-7 and NNI-8 oligodendroglial GPCs were more sensitive to pathway inhibition compared with NNI-4, -11, and -12 GBM GPCs (**Figure 4.3Bii**). Again, these findings were consistent with the immunoblot analysis showing the highest level of Notch intracellular domain (NICD) detected in NNI-8 GPCs (**Figure 4.3Aii**).

Finally, we tested the TGFβ signaling pathway by using SB525334 (Grygielko et al, 2005). Interestingly, all three GBM GPCs showed sensitivity to SB525334 with up to 80% inhibition in NNI-4 (**Figure 4.3Biii**). A less clear pattern of phospho-Smad2 and phospho-Smad3 levels was observed upon TGFβ1 stimulation (**Figure 4.3Aiii**). This may reflect the redundant roles of various Smad proteins in GPC regulation (Penuelas et al, 2009). Our data indicate that GPC-forming capacity and gliomasphere size were preferentially targeted in GBM GPCs.

Collectively, our data indicate, albeit a limited panel of GPCs used, that Wnt and Notch signaling pathways are upregulated in NNI-7 and NNI-8 oligodendroglial GPCs, while TGFβ pathway is active in GBM GPCs tested.

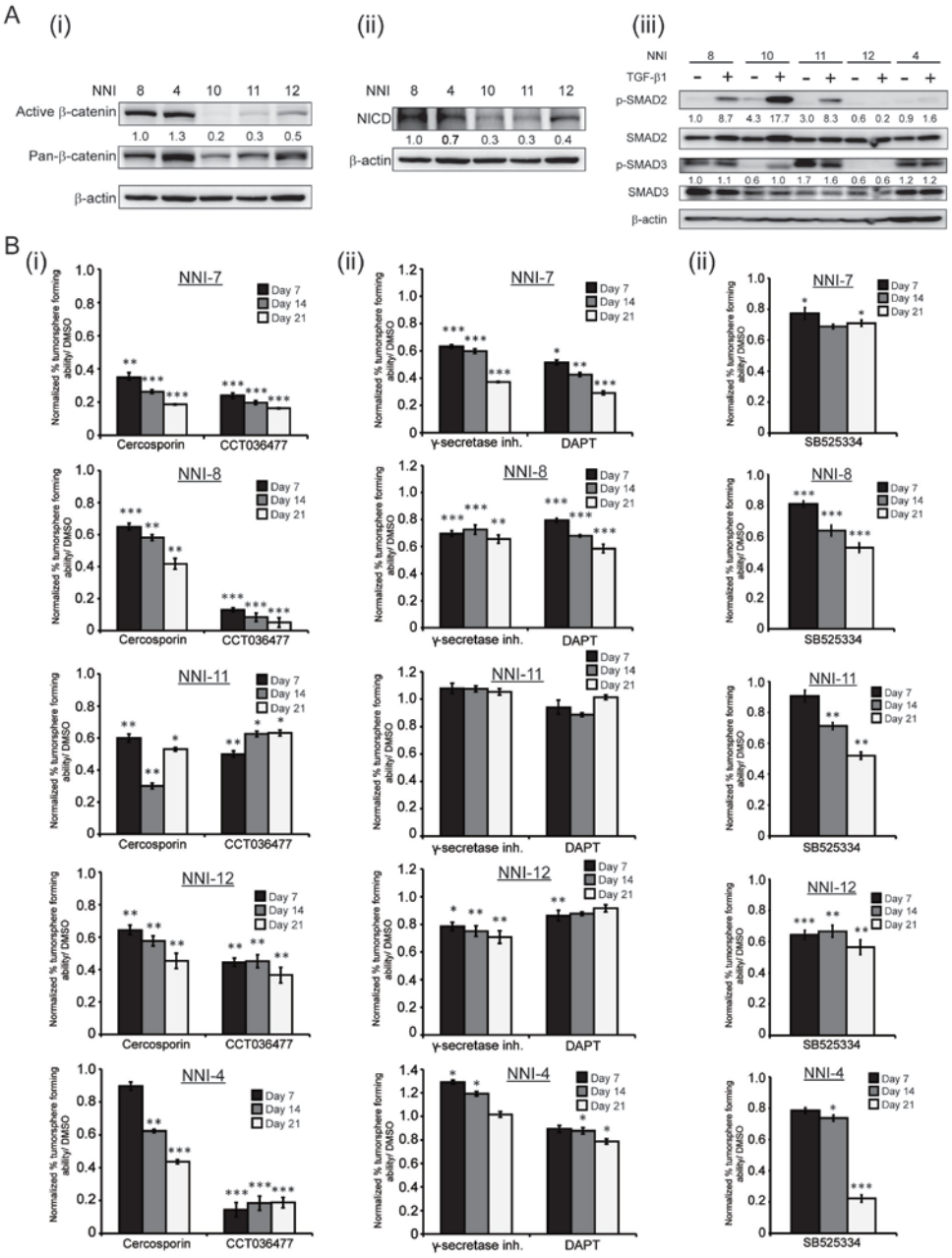

Figure 4.3. Functional validation of the Wnt, Notch and TGFβ signaling pathways in GPCs. A, Representative immunoblot analyses of key signaling components of the Wnt, Notch and TGFβ pathways using (**i**) active β-catenin, (**ii**) NICD, and (**iii**) pSmad2/3 respectively. Densitometric values of activated components compared to their respective controls are shown from representative immunoblots (n=3). **B**, Pathway dependence was assessed using well-established pharmacological agents: (**i**) Cercosporin and CCT036477 for Wnt, (**ii**) γ-secretase inhibitor and DAPT for Notch, and (**iii**) SB525334 for TGFβ signaling pathways in a gliomasphere forming assay over 21 days (to detect slow-growing GPCs). Fresh aliquots of drugs and media supplemented with growth factors were replenished every 7 days; *p<0.05, **p<0.01, ***p<0.001 compared to respective DMSO controls; n=3.

4.4 The oligodendroglial GPC signature stratifies glioma patient survival

We rationalized that our hypothesis would imply that oligodendroglial GPCs confer a better prognosis in their primary tumors compared to GBM GPCs, likely because of pathway activation programs depicted in their transcriptomic profiles [since gene expression drives glioma disease progression (Verhaak et al, 2010)]. Thus, moving forward, we utilized the Connectivity Map to analyze the strength of association of the oligodendroglial GPC signature with individual patient gene expression data from REMBRANDT and Gravendeel. We assigned positive "(+)" and negative "(-)" activation scores with significant *P* values (**Supplementary Table S3**) and observed that the gene signature separated (+) and (-) patient cohorts that make up 30% to 50% of all patients in each database (**Table 4.1**). Most importantly, the gene signature stratified patient survival (**Figure 4.4**).

Table 4.1. Summary of results from Connectivity Map, Logrank and Cox Regression Analysis for all patient samples. (+) represents patients with concordance to oligodendroglial GPC signature; (-) represents patients with inverse gene expression relationship to oligodendroglial GPC signature.

Dataset	Connectivity Maps Analysis						Log Rank	Multivariate Cox		Univariate Cox	
	No. of probes	No. of samples	(+)	(-)	Total (+)(-)	%(+)(-)	*p*-value	Hazard Ratio	*p*-value	Hazard Ratio	*p*-value
REMBRANDT	95	298	86	61	147	49.33	1.93E-05	0.44 (0.301-0.643)	2.22E-05	0.462 (0.322-0.664)	2.90E-05
Gravendeel	95	276	58	34	92	33.33	0.0082	0.851 (0.504-1.436)	0.546	0.535 (0.334-0.856)	0.009

Patients with better survival composed of (+) association (i.e. more oligodendroglial GPC association) whereas poorly surviving patients tended to be of (-) association (i.e. more GBM GPC association; REMBRANDT *P*-value, 1.93 E-05; Gravendeel *P*-value, 0.0082). The (+) activation score also contained more low-grade gliomas, especially enriched for oligodendrogliomas; whereas the (-) activation score enriched for high-grade

gliomas with mainly GBMs. Cox regression analysis indicated that the GPC gene signature served as a significant prognostic indicator and the positive score patients (oligodendroglial GPC-like) in REMBRANDT had 54% lower risk of death; the HR (95% confidence interval, CI) was 0.462 (0.322 - 0.664) in a univariate model (*P* = 2.90 E-05) (**Table 4.1**). Consistently, the positive score patients in Gravendeel were associated with 47% lower risk of death and the HR (95% CI) was 0.535 (0.334 – 0.856) in a univariate model (*P* = 0.009). This association remains significant in REMBRANDT after adjusting for other clinical factors such as age and tumor grade (*P* = 2.22 E-05).

Although we did not detect a significant multivariate analysis *P*-value in the Gravendeel data set, this does not mean the absence of GPC transcriptome contribution to patient survival as shown in the REMBRANDT data set. First, most glioma databases are *retrospectively* generated and therefore, this limits our ability to assess the true *predictive* value of the gene signature. Second, a significant *P*-value was observed in the univariate analysis, highlighting the relevance of the gene signature as an alternative prognostic tool. Collectively, these results suggest that GPCs contribute to disease progression and survival outcome, thus representing that these cells are clinically relevant.

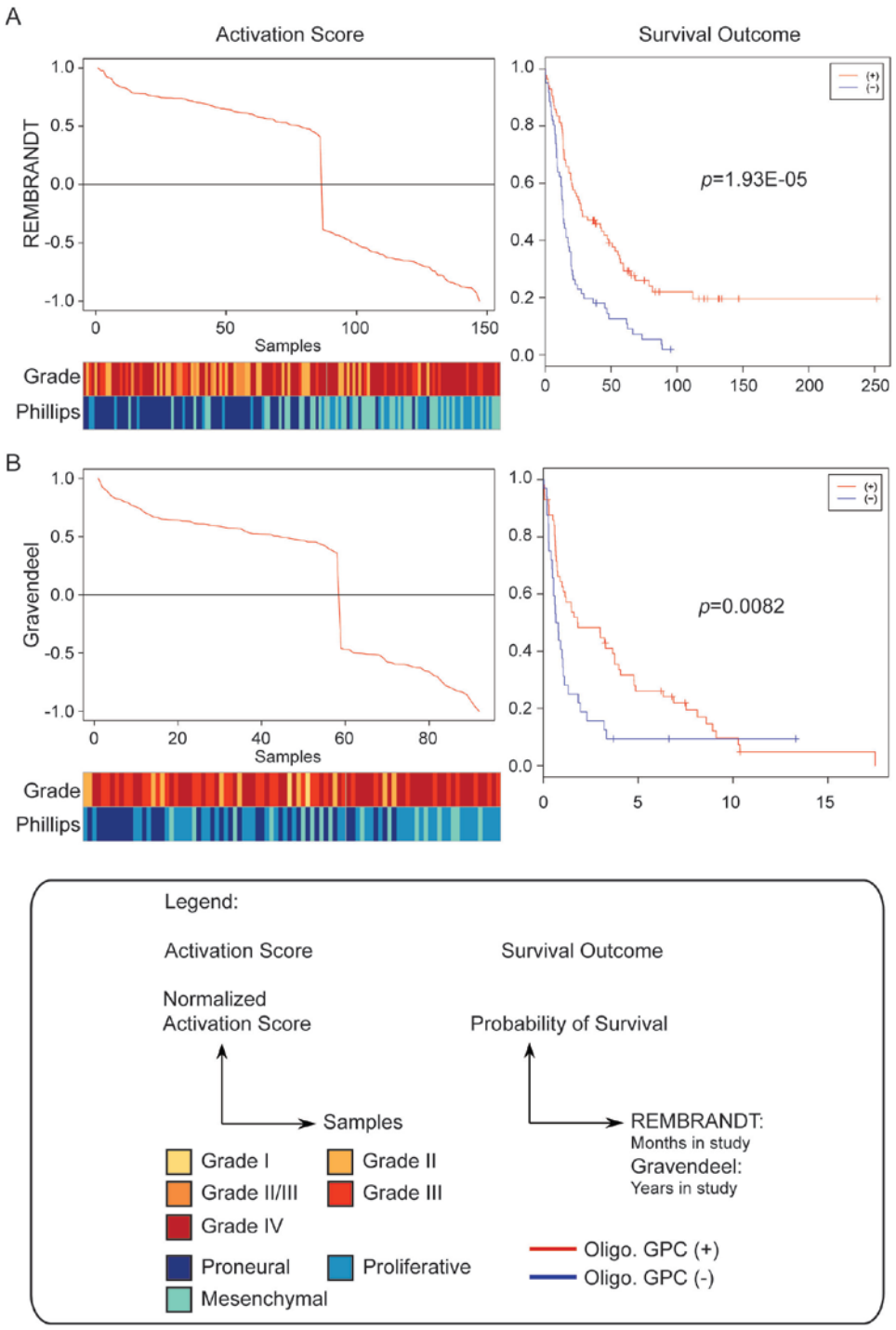

Figure 4.4. Oligodendroglial GPC signature stratifies patient survival. Patient survival is shown in all glioma patients in **A**, REMBRANDT; and **B**, Gravendeel databases. Tumor grade ("Grade") and molecular classification ("Phillips") distribution corresponding to (+) and (-) classes are shown below the activation score graphs.

4.5 The oligodendroglial GPC signature correlates with "Phillips" molecular classification of gliomas

We next attempted to strengthen our findings based on the Connectivity Map by asking whether our GPC-derived gene signature could predict glioma survival outcome similar to other existing molecular-based classification schemes. This would be important to further validate the significance of the GPC-derived gene signature in relation to disease progression. We applied as an independent gene expression-based approach, the "Phillips" classification of gliomas (Phillips et al, 2006a) which molecularly categorizes the tumors into three subclasses: proneural, proliferative, and mesenchymal. We observed that the (+) activation score enriched for the proneural subclass, whereas the (-) activation score tended to be proliferative or mesenchymal (**Figure 4.4; Supplementary Table S4**). The proneural subclass typically consists of lower grade gliomas with oligodendroglial features, frequently associated with better prognosis; in contrast, the mesenchymal subclass characterizes highly aggressive, recurrent gliomas such as GBM. Interestingly, recent work in a transgenic mouse model suggested that oligodendrogliomas are more chemosensitive because their cells-of-origin are oligodendrocyte precursor cells (OPCs), compared with the more resistant neural stem cells and astrocytes in GBM (Persson et al, 2010). We therefore find it intriguing that all cultured patient-derived GPCs from multiple studies are transcriptiomically consistent with this hypothesis; however, we cannot definitively pinpoint the identity of GPCs due to their human origin. It should be noted that we chose the "Phillips" molecular classification scheme since that original work subclassed all gliomas (Grades 1 to IV of astrocytic lineage), a situation analogous to our REMBRANDT and Gravendeel patient glioma databases.

As our method above compared GPCs from a better surviving histology (oligodendroglial tumor) to a worse histology (GBM), we could have artificially biased our findings without assessing the true contribution of the GPC in a primary tumor. We therefore in addition derived a “stemness” gene signature by comparing NNI-8 GPCs to its primary tumor (Note: not comparing to another GPC; **Supplementary Tables S5-7**). This, we rationalized, would allow an assessment of the GPC traits within the bulk tumor mass, and if its presence contributed to eventual disease progression and survival outcome. This “stemness” gene signature similarly stratified patient survival, with the (+) class enriched for lower grade tumors of proneural classification, whereas the (-) class enriched for higher grade tumors with mesenchymal features (**Figure 4.5**). Collectively, our data support that patient-derived oligodendroglial GPC’s contribute to a favorable prognosis, likely mediated by more chemosensitive OPC-like properties (**Figure 4.6**).

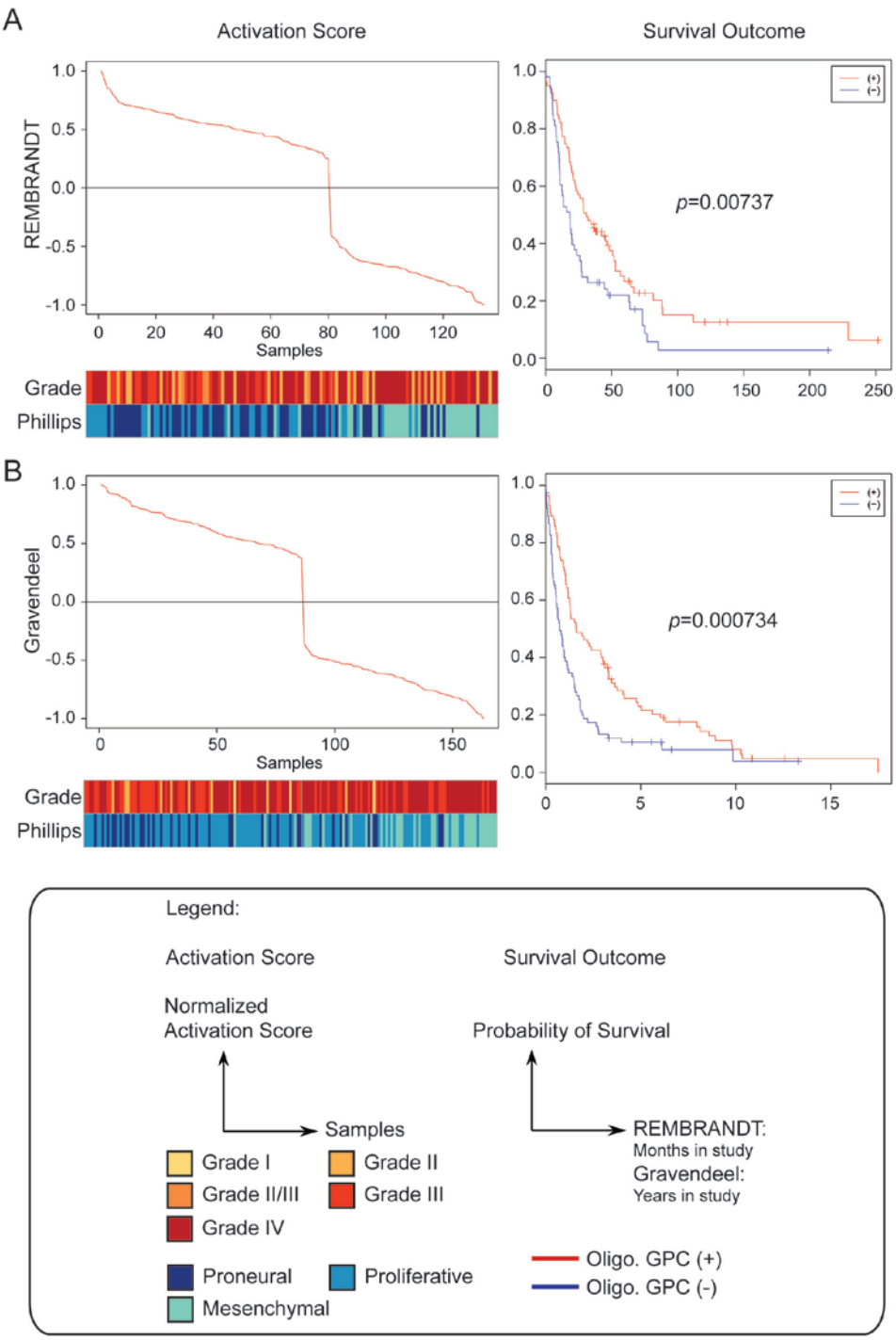

Figure 4.5. "NNI-8 GPC versus primary tumor" gene signature stratifies patient survival. Patient survival is shown in all glioma patients in **A**, REMBRANDT; and **B**, Gravendeel databases. Tumor grade ("Grade") and molecular classification ("Phillips") distribution corresponding to (+) and (-) classes are shown below the activation score graphs.

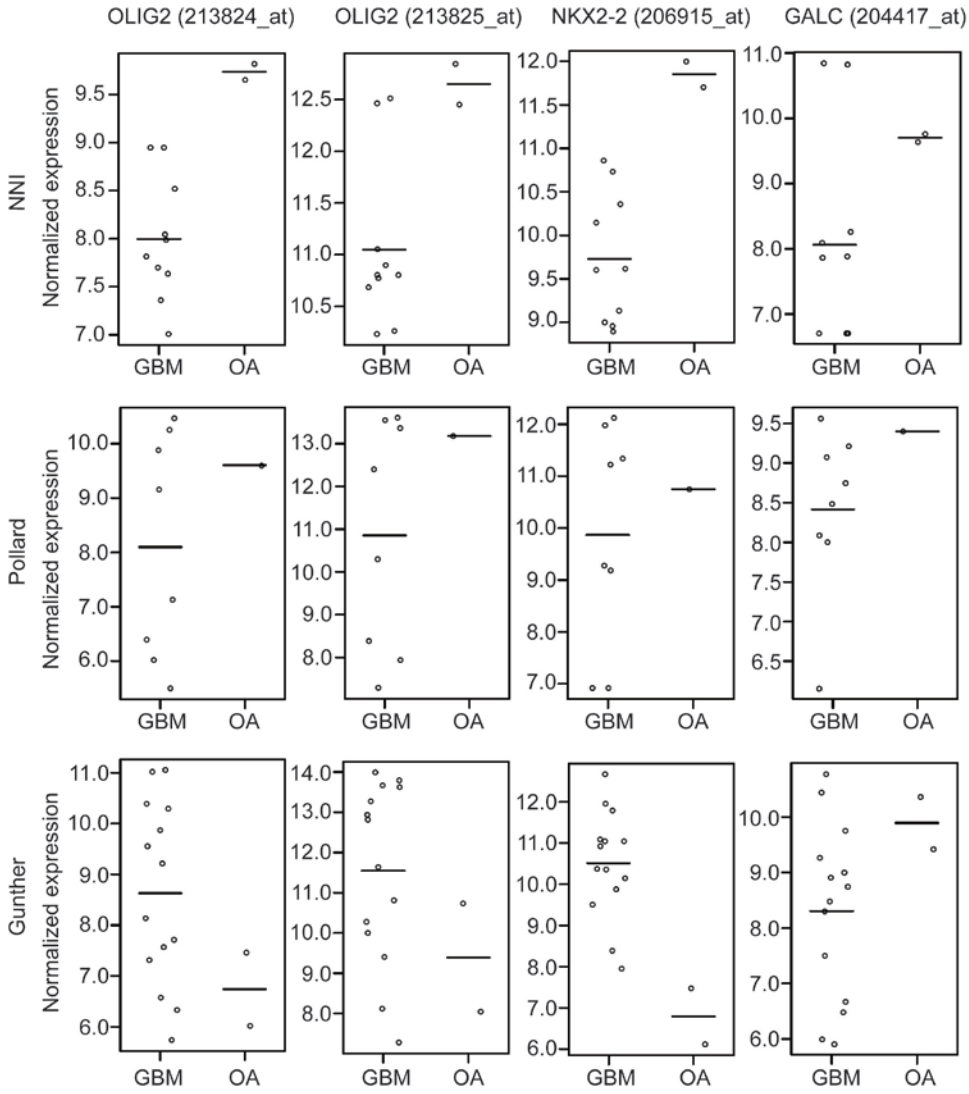

Figure 4.6. Oligodendroglial GPCs express OPC markers. Oligodendroglial tumor GPCs (OA) of NNI-8 and Pollard reflect higher immature OPC marker expression: Olig2, Nkx2.2 and GalC, in comparison to GBM GPCs (GBM). The Gunther line expresses mature oligodendrocyte marker, GalC, and may reflect its diagnosis as a GBM with oligodendroglial features.

4.6 The oligodendroglial GPC signature is enriched in the Wnt, Notch, and TGFβ pathways in patient glioma databases

Our previous findings indicate that the oligodendroglial GPC signature is enriched in the Wnt, Notch, and TGFβ signaling pathways (**Figure 4.2**); however, their precise activation or downregulation remains unclear. On the basis of our *in vitro* data in a limited but unique GPC collection (**Figure 4.3**), we suggested that oligodendroglial GPCs were more sensitive to Wnt and Notch inhibition, whereas GBM GPCs tended to be responsive to TGFβR1 inhibition. In recognizing the limitations posed by a small GPC panel, as with any such studies to-date, we sought to understand whether our GPC-derived conclusions bore similar significance in primary tumors of REMBRANDT and Gravendeel. We rationalized that our hypothesis would suggest the similar regulation of signaling pathways as predicted by our GPCs in **Figure 4.3** and the sheer number of patients in REMBRANDT (*N* = 298) and Gravendeel (*N* = 276) would provide firm evidence. Accordingly, using Gene Set Enrichment Analysis (Subramanian et al, 2005), we observed the following (**Table 4.2**): (i) The (-) activation score patients defined by our Connectivity Map, which correlate inversely with the oligodendroglial gene signature (i.e., more GBM GPC-like) in both databases, showed upregulated TGFβ1 response pathways upon closer analysis of the gene modules, further supported by downregulation of this pathway in Gravendeel (+) cohort. This is consistent with our *in vitro* data which suggest that GBM GPCs respond more strongly to TGFβR1 inhibition than oligodendroglial GPCs (**Figure 4.3Aiii and Biii**). Furthermore, Gravendeel (-) patients showed upregulation of the Nutt_GBM versus AO (anaplastic oligodendrogliomas) gene module, providing an independent verification that our GBM versus oligodendroglial GPCs mirror their primary tumor transcriptomic profile; (ii) The (+) patient cohort in Gravendeel showed upregulation of Wnt signaling pathway, again consistent

with our *in vitro* data where NNI-7 and NNI-8 oligodendroglial GPCs were more sensitive to Wnt inhibition (**Figure 4.3Ai and Bi**); and (iii) The REMBRANDT (-) patients showed upregulation of Notch signaling. Upon closer analysis, this upregulation comprised the Notch inhibitor, Numbl homolog, which acts to inhibit Notch signaling. This is thus consistent with our *in vitro* findings where NNI-7 and NNI-8 oligodendroglial GPCs were more sensitive to Notch pathway inhibitors (**Figure 4.3Aii and Bii**).

Furthermore, we analyzed a panel of primary tumors by immunohistochemical staining and observed similar pathway regulation (**Figure 4.7**); that is, GBM tumors exhibited elevated p-SMAD2 expression ($P = 0.0122$) whereas oligodendroglial tumors displayed elevated NICD expression ($P = 0.0331$) and a trend toward elevated active β-catenin (3 of 4 tumors). We also analyzed the enrichment of core stem cell programs (embryonic, hematopoietic, and neural stem cell) in the patient cohorts (Shats et al, 2011). The (+) patients display an enrichment of progenitor-like behaviour with lower tumor grade, whereas (-) patients resemble the CD34+ leukemia-initiating and propagating cells (**Table 4.2**). These data, derived in large patient glioma datasets, independently suggest that core stem cell programs do contribute to the survival-correlated (+) and (-) patient cohorts. Collectively, we show that predictions made by our oligodendroglial GPC signature produced congruent data in GPCs, primary tumors, and patient databases. This thus supports our hypothesis that GPCs mirror their primary tumors and contribute to disease progression and survival outcome.

Table 4.2. Summary of gene set enrichment analysis (GSEA)

Genesets	Description	Size	Normalized enrichment Score	FDR q-value	CMAP Class Association
ST_WNT_BETA_CATENIN_PATHWAY	Wnt/beta-catenin Pathway (N=31)	28	1.45	1	
JAZAG_TGFB1_SIGNALING_VIA_SMAD4_DN	Genes down-regulated in PANC-1-S4KD cells (pancreatic cancer; SMAD4 knocked down by RNAi) after stimulation by TGFB1 for 2 h (N=64)	51	1.4	0.978	Wnt pathway is upregulated, while TGFβ1 signaling is downregulated in Gravendeel (+) patients
VERRECCHIA_RESPONSE_TO_TGFB1_C1	ECM related genes up-regulated in dermal fibroblasts within 30 min after TGFB1 addition, and which kept increasing with time (N=18)	16	-1.58	0.704	
VERRECCHIA_EARLY_RESPONSE_TO_TGFB1	ECM related genes up-regulated early (within 30 min) in dermal fibroblasts after addition of TGFB1 (N=51)	47	-1.53	0.73	TGFβ1 signaling and Nutt GBM versus Anaplastic Oligodendroglioma (AO) are upregulated in Gravendeel (-) patients
NUTT_GBM_VS_AO_GLIOMA_UP	Top 50 marker genes for glioblastoma multiforme (GBM), a class of high grade glioma (N=47)	42	-1.52	0.746	
KEGG_NOTCH_SIGNALING_PATHWAY	Notch signaling pathway (N=47)	40	-1.66	1	
VERRECCHIA_EARLY_RESPONSE_TO_TGFB1	ECM related genes up-regulated early (within 30 min) in dermal fibroblasts after addition of TGFB1 (N=51)	47	-1.53	0.972	
VERRECCHIA_RESPONSE_TO_TGFB1_C5	ECM related genes up-regulated in dermal fibroblasts within 30 min after TGFB1 addition, and which kept increasing with time (N=22)	18	-1.47	0.63	Notch signaling is downregulated (due to Numbl) while TGFβ1 pathway is upregulated in REMBRANDT (-) patients.
VERRECCHIA_RESPONSE_TO_TGFB1_C1	ECM related genes up-regulated in dermal fibroblasts within 30 min after TGFB1 addition, and which kept increasing with time (N=18)	16	-1.43	0.559	

Table 4.2. Summary of gene set enrichment analysis (GSEA) (Cont'd)

Genesets	Description	Size	Normalized enrichment Score	FDR q-value	CMAP Class Association
BENPORATH_ES_WITH_H3K27ME3	Genes posessing the trimethylated H3K27 (H3K27me3) mark in their promoters in human embryonic stem cells, associated with lower grade tumour expression and poor stemness nature (N=1117)	8	1.38	0.16	
BENPORATH_EED_TARGETS	Eed targets genes identified by ChIP on chip as targets of the Polycomb protein EED in human embryonic stem cell, associated with lower grade tumour expression and poor stemness nature (N=1062)	6	1.34	0.13	Stem cell core programs enriched in REMBRANDT (+) patients
DIAZ_CHRONIC_MEYLOGENOUS_LEUKEMIA_UP	Genes up-regulated in CD34+ cells isolated from bone marrow of CML (chronic myelogenous leukemia) patients, compared to those from normal donors (N=1398)	5	-1.07	0.52	
RIGGI_EWING_SARCOMA_PROGENITOR_UP	Genes up-regulated in mesenchymal stem cells (MSC) engineered to express EWS-FLI1 fusion protein (N=421)	5	-0.71	0.89	Stem cell core programs enriched in REMBRANDT (-) patients
BENPORATH_ES_WITH_H3K27ME3	Genes posessing the trimethylated H3K27 (H3K27me3) mark in their promoters in human embryonic stem cells, associated with lower grade tumour expression and poor stemness nature (N=1117)	8	1.12	1	
BENPORATH_EED_TARGETS	Eed targets genes identified by ChIP on chip as targets of the Polycomb protein EED in human embryonic stem cell, associated with lower grade tumour expression and poor stemness nature (N=1062)	6	1.01	0.93	Stem cell core programs enriched in Gravendeel (+) patients
DIAZ_CHRONIC_MEYLOGENOUS_LEUKEMIA_UP	Genes up-regulated in CD34+ cells isolated from bone marrow of CML (chronic myelogenous leukemia) patients, compared to those from normal donors (N=1398)	5	-1.09	0.76	
BENPORATH_NANOG_TARGETS	genes upregulated and identified by ChIP on chip as Nanog transcription factor targets in human embryonic stem cells (N=988)	5	-1.01	0.48	Stem cell core programs enriched in Gravendeel (-) patients

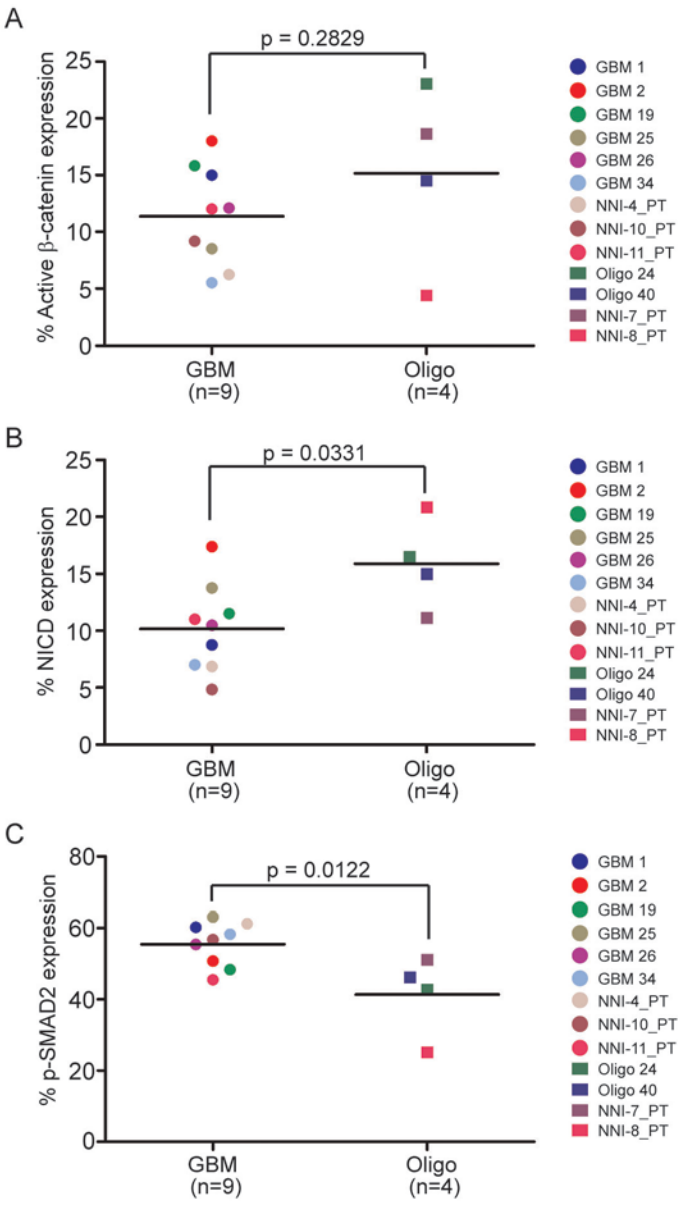

Figure 4.7. Analysis of Wnt, Notch and TGFβ signaling pathways in primary patient tumors. A, active β-catenin; **B**, Notch intracellular domain (NICD); and **C**, p-Smad2 were immunohistochemically detected in patient tumors of GBM and oligodendroglial features.

4.7 The oligodendroglial GPC signature defines molecular heterogeneity within oligodendroglial tumors

Among the major subtypes of gliomas, oligodendrogliomas are distinguished by their remarkable sensitivity to chemotherapy, with approximately two thirds of anaplastic (malignant) oligodendrogliomas responding dramatically to combination treatment with procarbazine, lomustine, and vincristine (termed PCV). Anaplastic oligodendrogliomas are also distinguished by a unique constellation of molecular genetic alterations, including coincident loss of chromosomal arms 1p and 19q in 50-70% of tumors (Cairncross et al, 1998). Cairncross *et al*. demonstrated that combined loss involving chromosomes 1p and 19q is statistically significantly associated with both chemosensitivity and longer recurrence-free survival after chemotherapy.

Accordingly, we interrogated this GPC gene signature in patients with oligodendroglial tumors. The (+) class enriched for lower grades associated with the 1p/19q co-deletion (**Figure 4.8**). Interestingly, patients without loss-of-heterozygosity (LOH) at 1p/19q (yellow) were spread throughout both classes, indicating that our oligodendroglial gene signature detected molecular heterogeneity and survival profiles that cannot be accounted for by the 1p/19q status alone. Although these retrospective data cannot determine whether the gene signature is an independent predictor of survival; furthermore, the 1p/19q status is specifically related to PCV chemotherapy; nevertheless, these data do suggest that the signature is a positive prognostic factor for glioma patients.

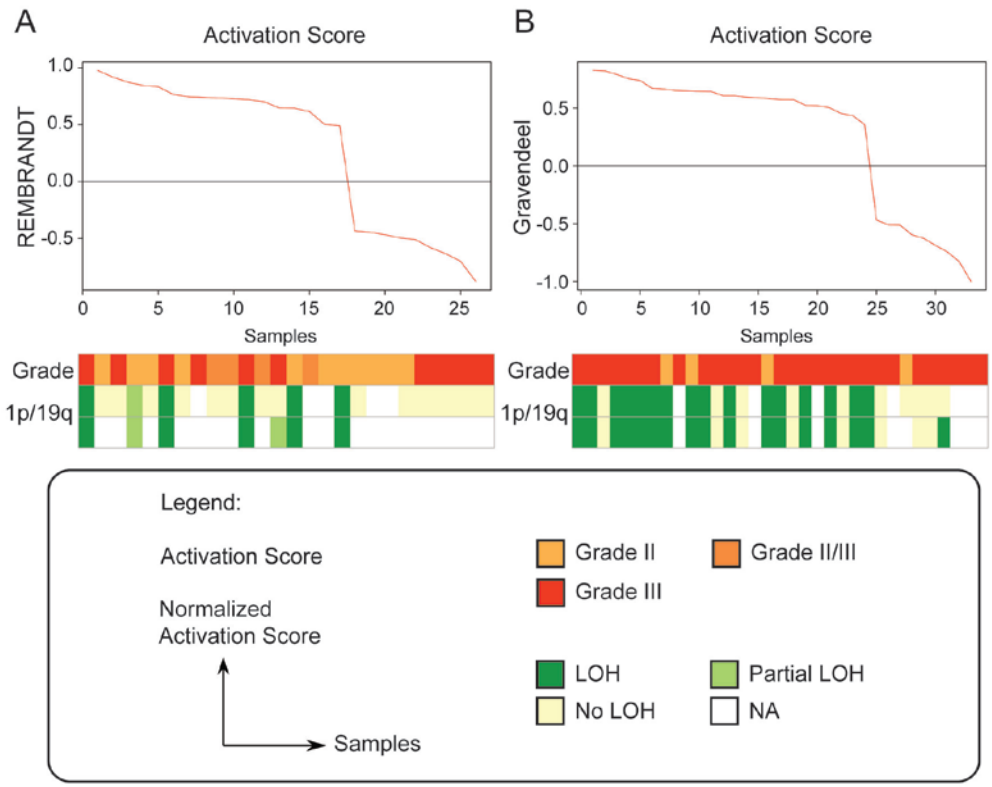

Figure 4.8. Oligodendroglial GPC gene signature is associated with lower tumor grade and 1p/19q co-deletion. Patient survival is shown in all glioma patients in **A**, REMBRANDT; and **B**, Gravendeel databases. Tumor grade ('Grade') and 1p/19q co-deletion distribution corresponding to (+) and (-) classes are shown below the activation score graphs. Of note, patients without loss of heterozygosity (LOH) at 1p/19q were spread throughout both classes, indicating that the oligodendroglial gene signature can detect molecular heterogeneity and survival profiles that cannot be accounted for by the 1p/19q status alone.

4.8 Summary

GPCs mirror the phenotypic and molecular fingerprint of the primary tumors (Lee et al, 2006; Wakimoto et al, 2012). Consequently, they serve as a useful *in vitro* platform to carry out further investigations. However, much less is known about their direct contribution to disease progression and survival outcome. In this chapter, we attempted to address this gap in knowledge by: (i) Tapping into our own and publicly available GPC gene expression and determining the differential gene list between 2 major variants, oligodendroglial GPCs versus GBM GPCs for which distinct patient survival patterns are seen in their primary tumors; (ii) Using a rank-based, pattern-matching approach, the Connectivity Map (CMAP), to interrogate the strength of association between the oligodendroglial gene signature and individual patient gene expression profiles, as gene expression drives glioma disease outcome (Verhaak et al, 2010); (iii) Drawing connections between (+) or (-) patients, tumor grade, and primary tumor molecular classification.

We found that oligodendroglial GPCs could be distinguished from GBM GPCs by Wnt, Notch, and TGFβ regulation. Although these findings are not entirely novel in that these pathways were previously implicated in GBM GPCs, their relation between the 2 major variants – oligodendroglial versus GBM GPCs is unclear. Our *in vitro* analysis showed that Wnt and Notch pathways were upregulated in NNI-7 and NNI-8 oligodendroglial GPCs, whereas TGFβ signaling was upregulated in GBM GPCs. Moreover, these pathways were similarly detected in primary tumors. Interestingly, Lottaz and colleagues showed that mesenchymal GPCs map into the mesenchymal class of primary tumors and exhibit upregulated TGFβ signaling pathway (Lottaz et al, 2010). In recognizing that a limited number of patient specimens were available for our *in vitro* and primary tumor analyses, we sought to tap

into major patient glioma gene expression and molecular signature databases to substantiate our hypothesis that GPCs contribute to disease outcome. Indeed, using our oligodendroglial gene signature, our GSEA study indicated that patients with GBM (i.e. CMAP-) are enriched in the TGFβ signaling module, whereas patients with oligodendroglial tumors (i.e. CMAP+) are enriched in the Wnt and Notch signaling pathways. Moreover, CMAP+ patients display a progenitor-like transcriptomic program that correlates with lower tumor grade, consistent with the idea previously established in a transgenic mouse model of oligodendroglioma that identified the more lineage-committed oligodendrocyte progenitor cell as the tumor cell-of-origin (Persson et al, 2010). Furthermore, these cells are more sensitive to standard chemotherapeutic drugs than neural stem cells or astrocytes.

In summary, our study is important because it provides clinical evidence that *GPCs contain signaling pathways that dictate primary tumor progression, consequently impacting on survival outcome*. These findings emphasize the relevance of *in vitro* cultured GPCs as investigational tools. Interestingly, our oligodendroglial gene signature stratified survival of oligodendroglial tumor patients without 1p/19q LOH, suggesting that the previously “untreatable” class can now be further subdivided into drug-sensitive and –resistant patients. This indicates that our gene signature detects molecular heterogeneity in patients with oligodendroglial tumors that cannot be accounted for by the 1p/19q status alone. This further highlights the limitation of morphology-based histological analyses to diagnose and treat patients. Although oligodendroglial tumors are traditionally more chemosensitive than GBM tumors and would seemingly render our findings expected, our study is important because we provide *a direct clinical link between these controversial GPCs and their primary tumors*. Essentially, we

show that GPCs of different histologies not only mirror the phenotype and molecular fingerprint of their primary tumor, but also contain transcriptomic profiles that reflect the different survival outcomes. Therefore, clinically amendable molecular tests may be developed by profiling unsorted bulk tumor cells because disease progression is in part, a manifest of the activation of stemness-related pathways. Our findings further suggest effective glioma treatment by targeting these signalling pathways which operate at the level of self-renewing GPCs. Taken together, we provide evidence that patient-derived GPCs are clinically relevant.

CHAPTER 5

RESULTS

CHAPTER 5 – SMALL MOLECULE INHIBITORS OF THE WNT PATHWAY TARGET GLIOMASPHERE FREQUENCY AND PROLIFERATION

5.1 Introduction and objectives

The Wnt/β-catenin signaling pathway has been implicated in various cancers (Barker & Clevers, 2006; Polakis, 2007). More importantly, Wnt signaling has been reported to play a role in the establishment and maintenance of cancer stem cells (CSCs) of the hematological and gastrointestinal systems (Reya & Clevers, 2005). Increasing reports for the existence of rare CSCs that initiate and sustain tumors have spurred efforts to identify novel therapeutic strategies for selectively targeting these cells. CSCs have been shown to be resistant to several chemotherapeutic agents (Eyler & Rich, 2008). Hence, identifying compounds that target signal transduction pathways (e.g. Wnt, Notch, TGFβ) controlling CSC self-renewal and maintenance would open up new possibilities for combinatorial therapeutic options that may improve current large majority of strategies that target general mechanisms of rapid cell growth. It may be that the often slow-growing, long-term self-renewing cellular fraction may be responsible for initiating and sustaining tumor growth.

There is much evidence for a cellular hierarchy in cancers of the hematopoietic and colorectal origins and recent studies implicate a role for Wnt in maintaining their pluripotency. Jamieson *et al.* showed that excessive Wnt signaling was present in the granulocyte-macrophage progenitors isolated from patients with chronic myelogenous leukemia (CML), and their self-renewing and proliferation capacity was attenuated by ectopic expression of Axin, an inhibitor of the Wnt pathway (Jamieson et al, 2004). In addition, Vermeulen and colleagues showed that Wnt signaling activity level in colon

CSCs was heterogeneous and that cells with high Wnt signaling activity possessed stem cell-like clonogenic potential (Vermeulen et al, 2010). Importantly, the authors further demonstrated that high Wnt activity was observed preferentially in colon CSCs located close to stromal myofibroblasts, suggesting that microenvironmental cues regulated Wnt signaling activity in these cells. Earlier, we and others showed that Wnt signaling is active and is required for the survival and maintenance of GPCs (Ng et al, 2012; Zhang et al, 2011; Zheng et al, 2010). These studies form the rationale for the development of new therapeutic agents targeting the Wnt signaling pathway in glioma.

In recent years, several small molecule inhibitors of the Wnt pathway have been identified (**Table 5.1**). Lepourcelet *et al.* identified several antagonists that disrupt the β-catenin/TCF complex of the Wnt signaling pathway via a high throughput screening (HTS) of 7000 natural compounds for inhibitory activity (Lepourcelet et al, 2004). Notably, they identified two fungal derivatives, PKF115-854 and CGP049090 (also known as Cercosporin), both of which disrupted the interaction of TCF and β-catenin and consequently inhibited colon cancer cell proliferation and interfered with β-catenin-mediated axis duplication *in vivo*. In another study, Emami *et al.* screened a small molecule library of 5000 compounds using a cell-based assay and identified a small molecule ICG-001 that showed activity in downregulating β-catenin/TCF target genes (Emami et al, 2004). The authors showed that ICG-001 bound to the CREB-binding protein (CBP, a transcriptional activator of the Wnt pathway that binds to β-catenin) and competed for binding to β-catenin.

Table 5.1. Small-Molecule Wnt Pathway inhibitors.

Wnt inhibitor	Molecular target	Reference
CGP049090 (Cercosporin)	TCF/β-catenin complex	Lepourcelet et al. 2004
ICG-001	Creb-binding protein (CBP)	Emami et al. 2004
IWP2	Porcupine	Chen et al. 2009
IWR1	Axin	Chen et al. 2009
XAV939	Tankyrase/Axin	Huang et al. 2009
CCT036477	TCF/β-catenin complex	Ewan et al. 2010

More recently, Chen *et al.* conducted a screen of 200, 000 compounds using mouse L-cells stably expressing the Super (8x) TOPFLASH Wnt reporter and a Wnt3A expression vector via multiple cell-based screening strategy (Chen et al, 2009). Compounds with inhibitory activity were further subcategorized into two groups based on their site of action within the Wnt/β-catenin signaling pathway: (i) inhibitors of Wnt production (IWPs), and (ii) inhibitors of Wnt response (IWRs). IWPs inhibit the secretion of the Wnt ligands through binding to porcupine (Porcn), an important component of the Wnt ligand secretion that mediates addition of a palmitoyl group to Wnt ligand proteins in the endoplasmic reticulum. IWRs, on the other hand, bind directly to Axin and stabilize it, which eventually leads to β-catenin degradation.

In addition, Huang *et al.* also demonstrated that stabilization of Axin by a small molecule inhibitor, XAV939 mediates Wnt signaling inhibition (Huang et al, 2009). Using a protein affinity capture technique, they identified Tankyrases (TNKS1 and 2) as targets of XAV939. Axin is stabilized through destruction of Tankyrases. Disruption of Tankyrase-mediated ADP-ribosylation activity resulted in increased Axin protein stability, possibly through changes in Axin ubiquitinylation status. Furthermore, the authors showed that the mode of action of IWR-1, previously reported by Chen *et al.*, is similar to XAV939. In addition, Ewan *et al.* identified several novel small

molecules that target distinct levels of the Wnt signal transduction pathway (Ewan et al, 2010). Of note, they identified CCT036477 that blocks transcription at the β-catenin/TCF level and showed the strongest phenotypic effects *in vivo* where it blocked development of zebrafish and *Xenopus* embryos and expression of Wnt target genes.

In this chapter, we explore the use of Wnt inhibitors to study the effects of pharmacological inhibition of Wnt/β-catenin signaling in GPCs.

5.2 Screening for potential Wnt inhibitors

To quantify compounds that specifically inhibit Wnt/β-catenin pathway, we screened a modest but well-characterized collection of small molecules using L-Wnt-STF cells (kind gift of A/Prof. Lawrence Lum, Southwestern Medical Center, USA) that stably express a well-characterized Wnt-responsive firefly luciferase (FL) reporter plasmid (SuperTopFlash or STF), control reporter Renilla luciferase (RL), and an expression construct encoding for the Wnt protein (Wnt3A) (**Figure 5.1A**) (Chen et al, 2009).

L-Wnt-STF cells were exposed to Wnt inhibitory molecules for 24 hours prior to measurement of reporter activities using standard luciferase assay. We procured several well-published small molecule inhibitors of Wnt (Cercosporin, IWP2, IWR1, XAV939, and CCT036477) that have well-described mechanisms of action (Chen et al, 2009; Ewan et al, 2010; Huang et al, 2009; Lepourcelet et al, 2004).

We observed that all small molecules showed dose-dependent inhibition of luciferase expression (**Figure 5.1B**). We then proceeded to determine the half maximal inhibitory concentrations (IC_{50}) for all Wnt

inhibitors on our GPC lines so as to determine working concentrations for downstream *in vitro* assays (**Table 5.2**).

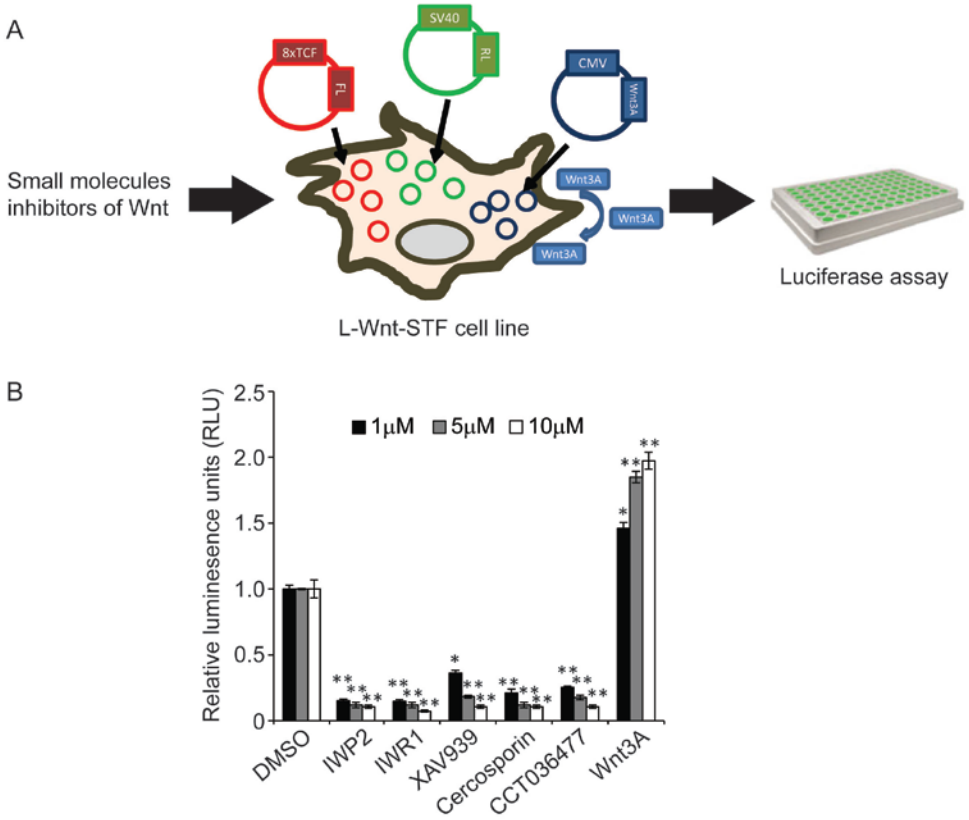

Figure 5.1. Screening of small molecule inhibitors of the Wnt/β-catenin signal transduction pathway. A, Schematic diagram illustrating the identification of potential Wnt/β-catenin antagonists using L-Wnt-STF cells. Compounds of known concentrations were incubated with L-Wnt-STF cells that stably harbor Wnt-responsive firefly luciferase (FL) and internal control Renilla luciferase (RL) reporters for 24 hours prior to measurement of luciferase activity. **B**, Well-described Wnt inhibitors showed concentration-dependent inhibition of FL activity that was normalized to control RL activity. *p<0.05, **p<0.01 compared to DMSO control (n=4).

Specifically, we adopted the method published by Diamandis *et al.* to determine the IC_{50} of the Wnt inhibitors (**Figure 5.2A**) (Diamandis et al, 2007). We observed that well-characterized Wnt inhibitors targeting the production of Wnt ligands (IWP2) and the stabilization of Axin-destruction complex (IWR1 and XAV939) did not affect the cell viability of GPCs up to a

maximal concentration of 10 µM (**Table 5.2**). In contrast, compounds (Cercosporin and CCT036477) that target the downstream components of the Wnt signaling pathway i.e. the β-catenin/TCF complex significantly reduced the cell viability of GPCs with oligodendroglial GPCs demonstrating lower IC_{50} values compared to GBM GPCs (**Figures 5.2B and C**). This data is consistent with our earlier findings that oligodendroglial GPCs possess an elevated Wnt pathway compared to GBM GPCs.

Table 5.2. Half-maximal inhibitory concentrations (IC_{50}) of several well-characterized Wnt inhibitors in gliomaspheres. IC_{50} values are presented in micromolar units; N.D., Not determined at maximal concentration of 10 µM from dose-response curves.

	Compound	IC_{50} of gliomasphere line			
		NNI-4	NNI-8	NNI-11	NNI-12
Well-characterized Wnt inhibitors	IWP1	N.D.	N.D.	N.D.	N.D.
	IWR1	N.D.	N.D.	N.D.	N.D.
	XAV939	N.D.	N.D.	N.D.	N.D.
	Cercosporin	1.8	0.8	1.5	1.2
	CCT036477	5.5	4.2	17.6	7.5

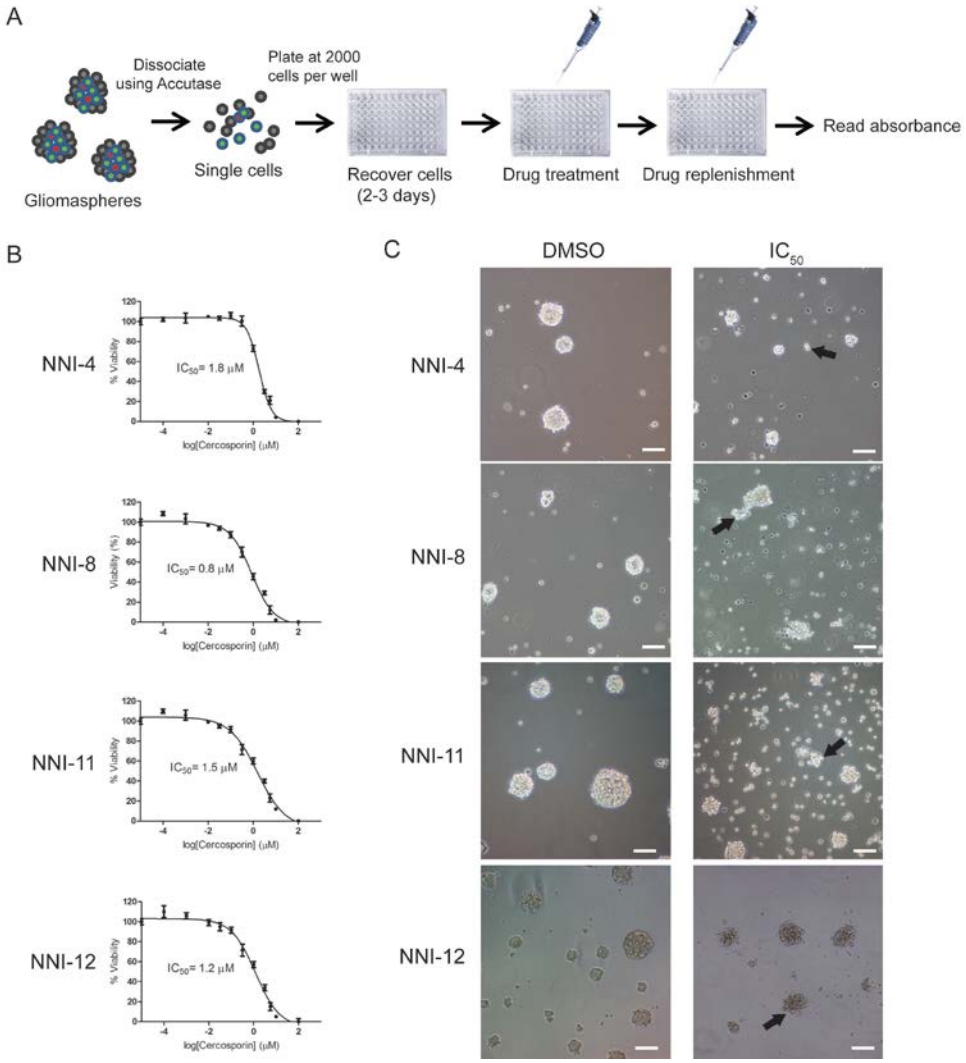

Figure 5.2. Standard assay for measuring half-maximal inhibitory concentrations (IC_{50}) and dose-response curves in GPCs. A, Schematic diagram illustrating the generation of dose-response curves and IC_{50} values for Wnt compounds of GPC lines. Briefly, gliomaspheres (100-150 µm) were collected and enzymatically digested for 5 min at 37°C using Accutase. Viable cells were plated at cell densities (20 cells/µl) in 96-well plates and recovered for two to three days prior to drug treatment. After two days of initial drug treatment, cells were supplemented with additional fresh aliquots of drug and growth medium and incubated for an additional three days before quantification of viability by standard alamarBlue™ assay. **B**, Dose-response curves of Wnt inhibitor, Cercosporin for four GPC lines (NNI-4, 8, 11, and 12). Cercosporin concentrations were titrated across a series of ten half-log dilutions, n=4. **C**, Representative images of GPCs treated with Cercosporin at their respective IC_{50} concentrations after 5 days. Note the disintegration of gliomaspheres after Wnt inhibitor treatment (arrows). Scale bar = 50µm.

5.3 Wnt inhibitors mitigate GPC frequency and proliferation *in vitro*

Several surface markers such as CD133, CD15 (SSEA-1) and nestin have been shown to enrich for GPCs (Bar et al, 2007b; Singh et al, 2004; Son et al, 2009). However, surface markers often do not reflect the *bona fide* properties of cancer stem cells as marker expression has been shown to change with disease state and progression (Quintana et al, 2008; Shackleton et al, 2009). In addition, conventional short-term viability assays also detect the majority of fast-growing progenitors and thus mask the minority frequency of *bona fide* cancer stem cells. Consequently, there is a need to rely on *functional* assays such as the neurosphere assay described earlier to measure GPC frequency (Rich & Eyler, 2009).

We plated GPCs at clonal density (30 cells/well of a 96-well plate) to allow spheres to arise from single GPCs, termed clonogenicity (Kalani et al, 2008). We treated GPCs with Wnt inhibitors over an extended time frame of over 7, 14 and 21 days using their respective IC_{50} values for each GPC line. Interestingly, we observed a variable trend of the Wnt inhibitory effects on our GPCs. Our data illustrated that IWR1 and XAV939, both of which inhibit Wnt signaling by stabilizing the Axin-degradation complex and IWP2 which inhibits Wnt signaling via the blocking of Wnt ligand production in cells had barely any effect on the gliomasphere-forming capacity and proliferation (**Figures 5.3B and C**). In contrast, using Cercosporin and CCT036477 which target the β-catenin/TCF complex, we effectively abrogated the self-renewal and proliferation capacity of GPCs (**Figures 5.3B and C**). This observation corroborates with a recent work demonstrating that FoxM1 directly interacts with β-catenin and is necessary and sufficient for its nuclear localization and transcriptional activation in glioma cells (Zhang et al, 2011).

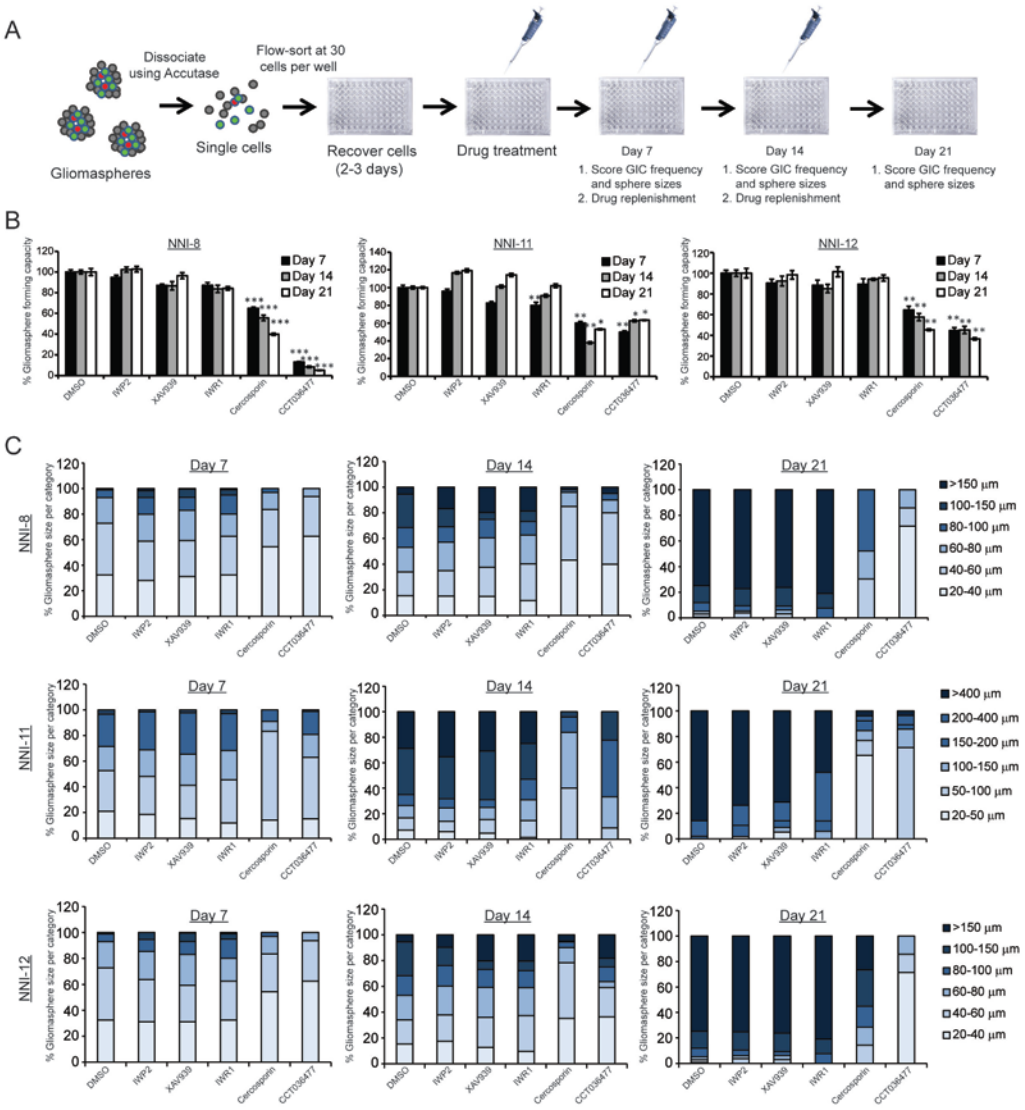

Figure 5.3. Well-characterized small molecule inhibitors of Wnt/β-catenin pathway abrogates gliomasphere-forming ability and proliferation *in vitro*. **A**, Schematic diagram demonstrating the measurement of gliomasphere-forming capacity and proliferation using the neurosphere assay. Gliomaspheres were collected and enzymatically dissociated prior to plating into 96-well plates at clonal density (0.3 cells/µl) via fluorescent-activated cell sorting (FACS). Cells were allowed to recover prior to initial drug treatment at their IC_{50} doses. The number and size of secondary gliomaspheres formed were quantified 7, 14, and 21 days post drug treatment and replenishment. **B**, Gliomasphere-forming capacity of GPCs was measured after 7, 14, and 21 days post incubation with respective well-characterized Wnt inhibitors. Notably, Wnt inhibitors targeting β-catenin/TCF complex (Cercosporin and CCT036477) were more effective at reducing GPC frequency. *p<0.05, **p<0.01, ***p<0.001 compared to respective DMSO controls (n=5). **C**, Individual gliomasphere sizes (an approximate of proliferation) were measured and categorized post incubation with respective Wnt inhibitors at days 7, 14, and 21.

Furthermore, we also observed that oligodendroglial GPCs (NNI-8) were more sensitive to Wnt inhibitors that target the β-catenin/TCF complex (i.e. Cercosporin and CCT036477) as compared to the GBM GPCs (NNI-11 and NNI-12). This is consistent with the levels of active β-catenin (nuclear-localized) detected as previously shown in chapter 4. In summary, our data show that GPCs can be effectively targeted specifically at the terminal stages of Wnt signaling, rather than at the Wnt ligand production stage. This finding is important to grasp as the site of inhibition likely points to the genetic lesion in glioma cells that maintains elevated Wnt signaling. Knowing the genetic lesion is important for effective glioma therapeutic design.

5.4 Common activating mutations of the Wnt pathway are not present in GPCs

We earlier demonstrated that GPCs were more sensitive to pharmacological compounds that disrupt the β-catenin/TCF complex, suggesting that genetic lesion that resulted in the hyperactivated Wnt activity in GPCs may lie between the destruction complex (Axin-GSK3β-APC) and the β-catenin/TCF complex. In addition, we also showed that inhibition of the upstream components of the Wnt pathway that involves Wnt ligand production did not affect GPC frequency and proliferation. Since mutations in the Wnt pathway should serve as a guide in determining where the prospective lesion(s) may be located and where inhibitors would be expected to work, we sought to determine the commonly known Wnt pathway mutations in cancers that resulted in hyperactivation of the Wnt pathway via direct sequencing.

Activating mutations in the Wnt pathway have been described in various cancers (Polakis, 1999; Polakis, 2000). Loss-of-function mutations in

the tumor suppressor, adenomatous polyposis coli (APC) and gain-of-function mutations in the amino-terminal region of the proto-oncogene *CTNNB1* that encodes for β-catenin are two commonly found mutations in colorectal and gastric cancers (Clements et al, 2002; Rowan et al, 2000). Interestingly, it was observed that in colorectal cancer, β-catenin mutations are mutually exclusive to those that harbor APC mutations and the frequency of detecting a mutation in *CTNNB1* increases in colorectal tumors lacking APC mutations (Iwao et al, 1998; Sparks et al, 1998).

CTNNB1 mutations commonly occur at serine/ threonine residues encoded in exon 3 of the β-catenin gene (Hart et al, 1998; Polakis, 2000). These mutations abrogate the phosphorylation-dependent interaction of β-catenin with β-TrCP, a component of an E3 ubiquitin ligase that makes direct contact with amino terminal sequence in β-catenin. Hence, β-catenin is stabilized and allowed to accumulate in the nucleus and activate Wnt signaling. We specifically screened for these "hotspot" mutations (in exon 3) by direct PCR sequencing of 6 GPC lines and observed absence of common *CTNNB1* mutations when compared to the human wild-type *CTNNB1* exon 3 DNA sequence (**Figure 5.4**).

Mutations of the APC protein are frequently located in the mutation cluster region (MCR) (codon 1286-1513) on exon 15 (Miyoshi et al, 1992; Polakis, 2000). Since the majority of somatic mutations in APC occur within the MCR, we sequenced the MCR as 3 overlapping fragments. Again, no mutations were identified between codons 1286 and 1513 (**Supplementary Figure S2**).

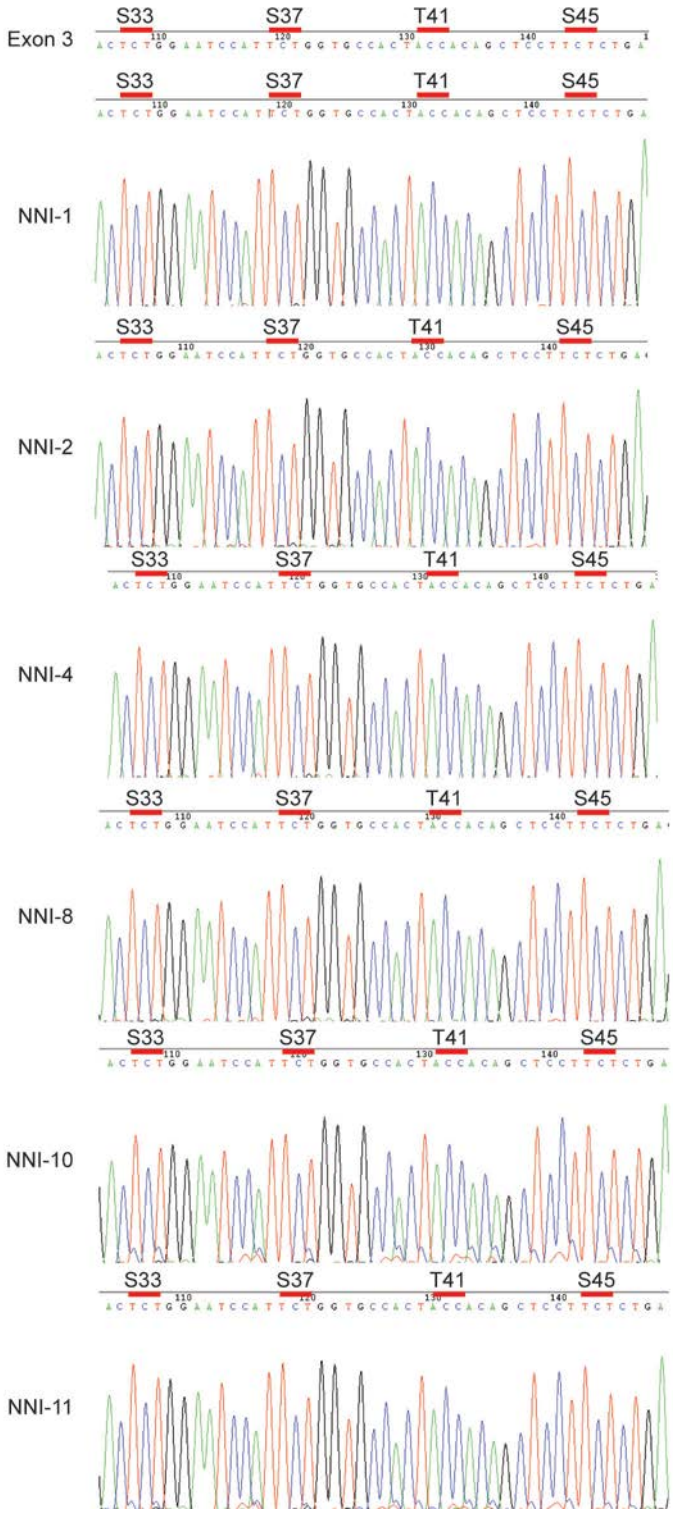

Figure 5.4. Common activating "hotspot" mutations of *CTNNB1* are absent in GPCs. Electropherograms showing absence of common mutations located at serine-33 (S33), serine-37 (S37), threonine (Thr41), and serine-45 (S45) of β-catenin.

5.5 Summary

Taken together, our data demonstrate that GPCs are sensitive to small molecule inhibitors of Wnt pathway that target the β-catenin/TCF complex. In addition, we also show that oligodendroglial GPCs are more sensitive to Wnt inhibition compared to GBM GPCs. Common APC and *CTNNB1* hyperactivating mutations are absent, suggesting that novel mechanism(s) modulating the β-catenin/TCF complex exist in GPCs. This lays the groundwork for our analysis of likely mechanisms in chapter 7.

CHAPTER 6

RESULTS

CHAPTER 6 – GENETIC KNOCKDOWN OF BETA-CATENIN ABOLISHES *IN VITRO* AND *IN VIVO* TUMORIGENIC POTENTIAL

6.1 Introduction and objectives

Earlier, we showed that oligodendroglial GPCs are more sensitive to β-catenin/TCF inhibition than GBM GPCs, suggesting the possibility of effectively eradicating GPCs via the Wnt pathway. Although this therapeutic approach may seem redundant in the case of oligodendrogliomas which are typically chemosensitive and already have a better prognosis, the important finding we wish to point out is: The oligodendroglial gene signature detected Wnt sensitive and resistant patients within the cohort that does not have the 1p/19q co-deletion status. This essentially means that the previously "untreatable" class is now amenable to Wnt inhibitory therapy if the patients demonstrate positive association with the signature despite lack of LOH at the 1p/19q locus (CMAP+).

The Wnt/β-catenin signaling pathway has been shown to be the predominant driving force of stem cells of the colonic crypt, hematopoietic and central nervous systems (Barker et al, 2007; Kalani et al, 2008; Reya et al, 2003). In particular, cancer stem cells of the colon (Barker et al, 2009), breast (Chen et al, 2007; Woodward et al, 2007) and hematopoietic system (Zhao et al, 2007) have been shown to cause tumorigenesis via aberrant Wnt signaling. Wnt activation has been shown to play a role in the progression of gliomas (Sareddy et al, 2009a) although clarification of its role at the level of GPCs has only recently begun. Here, using genetic approaches, we seek to understand the role and function of the Wnt/β-catenin pathway in GPCs. Functional assays to measure GPC frequency and mouse models were utilized. Additionally, this would serve as validation of our previous findings that Wnt/β-catenin is active in a subset of GPCs.

6.2 GPCs are effectively transduced by lentiviruses

For the purpose of our study, we selected lentiviruses as a genetic manipulation tool to investigate Wnt regulation in GPCs. Lentiviruses are highly efficient at infection and stable integration of the desired target gene of interest or short hairpin RNA (shRNA) into a cell system (Fuerer & Nusse, 2010). Lentiviral particles infect both dividing and quiescent cells efficiently as their pre-integration complex (i.e. viral shell) can enter the intact membrane of the nucleus of the target cell. This makes them ideal for genetic manipulations in slowly-dividing stem-like GPCs. In addition, lentiviral-mediated transduction has frequently been used as a tool in the study of GPC survival and tumorigenesis (Clement et al, 2007; Eyler et al, 2008; Wang et al, 2008).

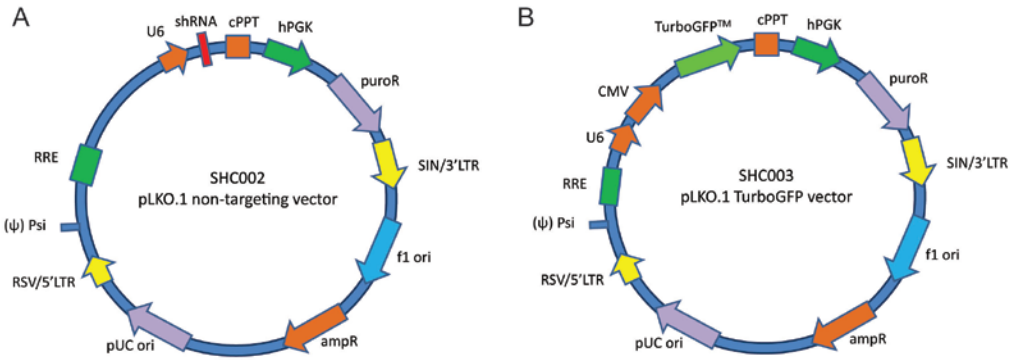

Figure 6.1. pLKO.1-based lentiviral vector maps. A, pLKO.1-puro non-targeting control vector containing a shRNA insert that does not target human and mouse genes, serving as a negative control in experiments. **B**, pLKO.1-puro-CMV-TurboGFP^{TM} vector containing a gene encoding TurboGFP, under the control of the CMV promoter. It is useful as a positive transduction control in experiments. Abbreviations: U6, U6 promoter; cPPT, central polypurine tract; hPGK, human phosphoglycerate kinase eukaryotic promoter; puroR, puromycin resistance gene for mammalian selection; WPRE, Woodchuck Hepatitis Post-Transcriptional Regulatory Element; SIN/3'LTR, 3' self-inactivating long terminal repeat; f1 ori, f1 origin of replication; ampR, Ampicillin resistance gene for bacterial selection; pUC ori, pUC origin of replication; 5' LTR, 5' long terminal repeat; Psi, RNA packaging signal; RRE, Rev response element.

As initial optimization and monitoring of the transduction efficiency of the lentiviral transduction system using the pLKO.1-puro-based vector (**Figure 6.1A**), we performed our knockdown in parallel with a control clone SHC003 (**Figure 6.1B**), a TurboGFP-containing, non-targeting lentiviral vector of similar backbone as pLKO.1. This enables visualization of the green fluorescent protein (GFP) that can be quantified by immunofluorescent methods (**Figure 6.2**).

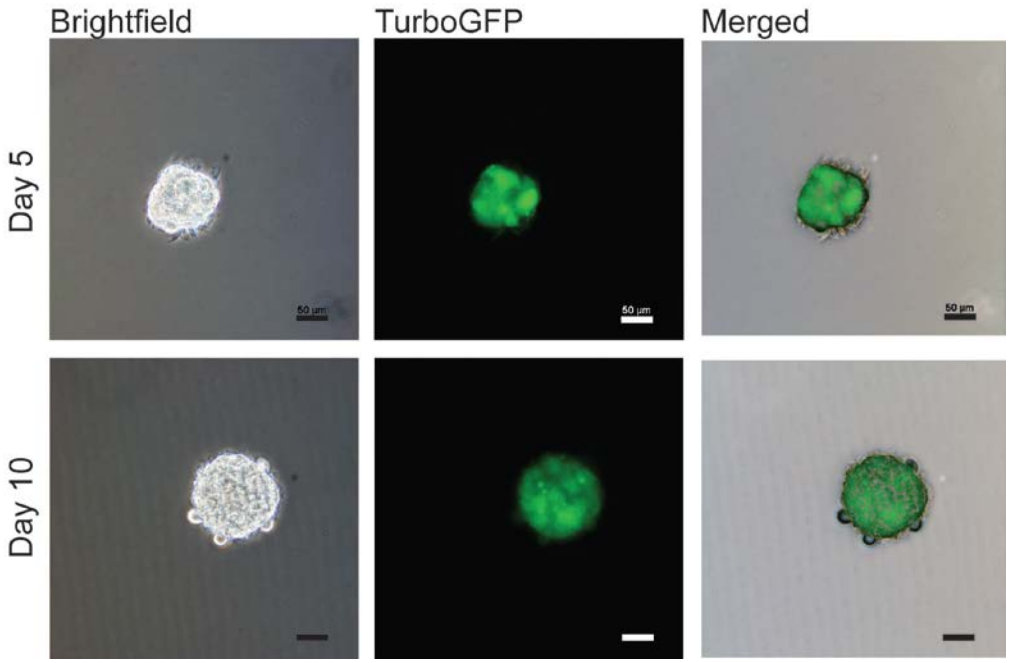

Figure 6.2. pLKO.1-based lentiviral vector effectively transduces GPCs. GPCs were transduced with pLKO.1-puro-CMV-TurboGFP vector and transduction efficiency monitored by visualization of green fluorescent protein (GFP). Scale bar = 50 µm.

6.3 Wnt/β-catenin signaling is active in GPCs

To investigate the biological function of Wnt/β-catenin regulation of GPCs, we first determined expression of active β-catenin, the key downstream effector of the canonical Wnt signaling pathway. We ascertained the protein expression levels of nuclear-localized activated β-catenin (dephosphorylated on Ser-37 or Thr41) and demonstrated that oligodendroglial GPC, NNI-8 and a subset of GBM GPCs possessed active Wnt/β-catenin signaling pathway (**Figure 6.3A**). In addition, we show, by immunofluorescent staining of active β-catenin *in vitro* that active β-catenin was nuclear-localized (**Figure 6.3B**), a key hallmark of active Wnt/β-catenin signalling (Ganesan et al, 2008).

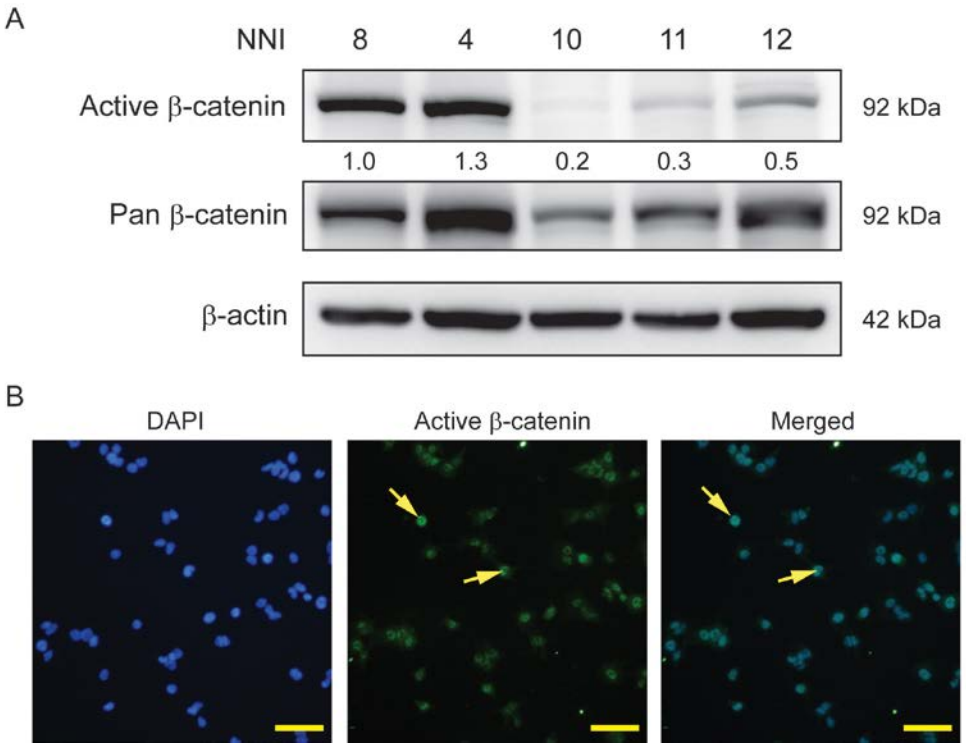

Figure 6.3. Wnt/β-catenin signaling is active in GPCs. A (Similar to Figure 4.3 A(i)), Representative immunoblot analyses of active β-catenin (dephosphorylated at Ser-37 and Thr-41) in oligodendroglial (NNI-8) and GBM (NNI-4, 10, 11, 12) GPCs; n=3. **B**, Representative immunofluorescent staining images of active β-catenin in GPCs showed distinct nuclear localization (arrows); n =2; Scale bar = 50 µm.

In addition, we assessed the activity of Wnt signaling *in vivo* using a selectable, fluorescent detectable lentiviral vector (7TGC) that can monitor successfully transduced GPCs with mCherry, and the status of Wnt activity by eGFP expression driven by the TCF promoter (Fuerer & Nusse, 2010). Specifically, we transduced GPCs with 7TGC and transplanted the cells into immunocompromised mice (NOD-SCID gamma, NSG) and harvested the brains after the mice displayed neurological deficits. Interestingly, we observed significant active Wnt signaling *in vivo*, as indicated by the presence of both mCherry- and eGFP-positive cells in the glioma xenografts (**Figure 6.4**). Collectively, we demonstrate strong evidence that Wnt/β-catenin signaling is active in GPCs and their resultant xenograft tumors.

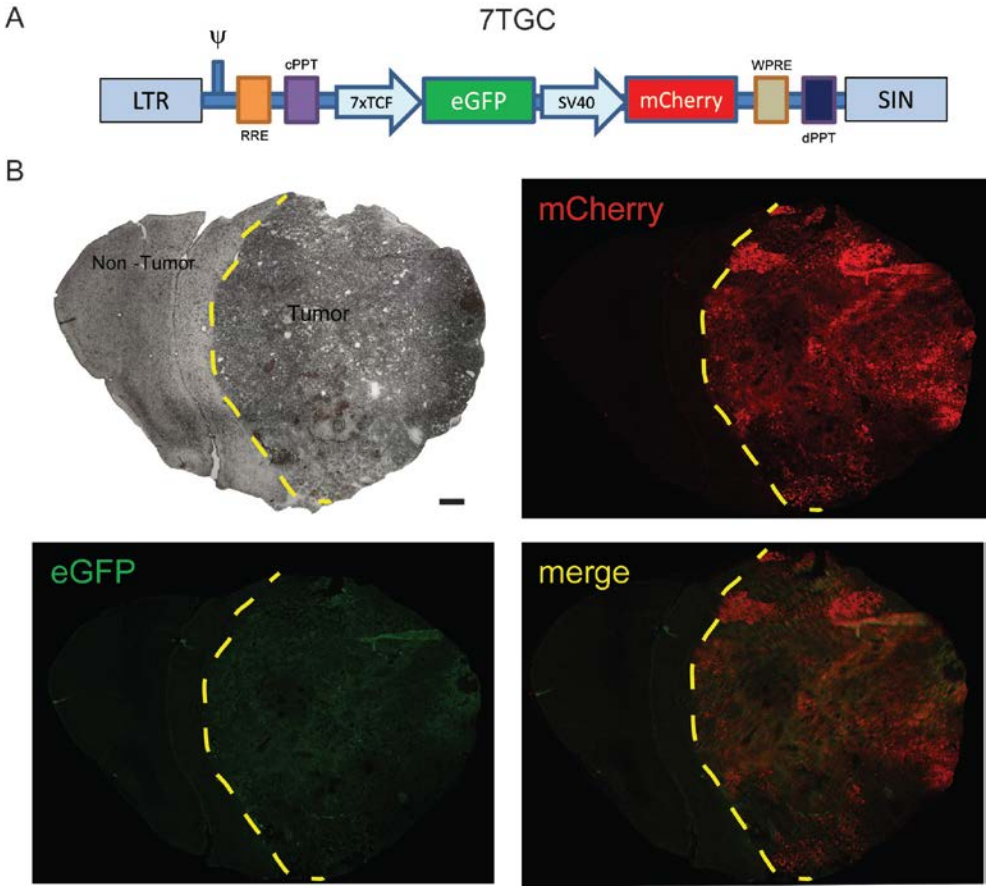

Figure 6.4. Wnt signaling is active in human xenografted gliomas. **A**, Schematic diagram of the 7xTCF-eGFP//SV40-mCherry vector (7TGC) LTR: Long Terminal Repeat, H: packaging signal, RRE: Rev Response Element, cPPT: central PolyPurine Tract, WPRE: Woodchuck hepatitis Post-transcriptional Regulatory Element, dPPT: distal PolyPurine Tract, SIN: Self Inactivated (LTR). **B**, Mouse brains implanted with GPCs expressing 7TGC were harvested and examined under immunofluorescence for mCherry (detecting successfully transduced cells) and eGFP (detecting cells with Wnt activity). Scale bar = 200 µm.

6.4 Wnt/β-catenin activity is diminished in shβ-catenin-transduced GPCs

To investigate if the Wnt signaling pathway is crucial in the survival and maintenance of GPCs, we carried out β-catenin knockdown by utilizing lentiviral short hairpin RNAs (shRNAs) to achieve high multiplicity of infection (MOI). We have selected β-catenin as the knockdown target because it represents the key downstream effector of the canonical Wnt signaling pathway. Two different sequences of shRNA directed against β-catenin, and a non-targeting (NT) shRNA were used for each experiment to control for potential off-target shRNA effects. Both β-catenin shRNA constructs (shβcat1 and shβcat2) significantly and effectively knocked down the protein levels of β-catenin in GPCs compared to non-targeting control (**Figure 6.5A**).

In addition, we performed qRT-PCR analyses of known downstream Wnt target genes to determine the effectiveness of the knockdown constructs on canonical Wnt/β-catenin signaling pathways. *AXIN2*, *TCF7L2*, and *BIRC5* are classic examples of known direct downstream target genes of the Wnt signaling pathway (Roose et al, 1999; Yan et al, 2001; Zhang et al, 2001). Accordingly, we demonstrated that knockdown of β-catenin significantly down-regulated the expression of these Wnt target genes after 48 hours post-transduction compared to non-targeting control, providing evidence that the lentiviral constructs shβcat1 and shβcat2 are effective at down-regulating the Wnt/β-catenin signaling pathway in GPCs (**Figure 6.5B**).

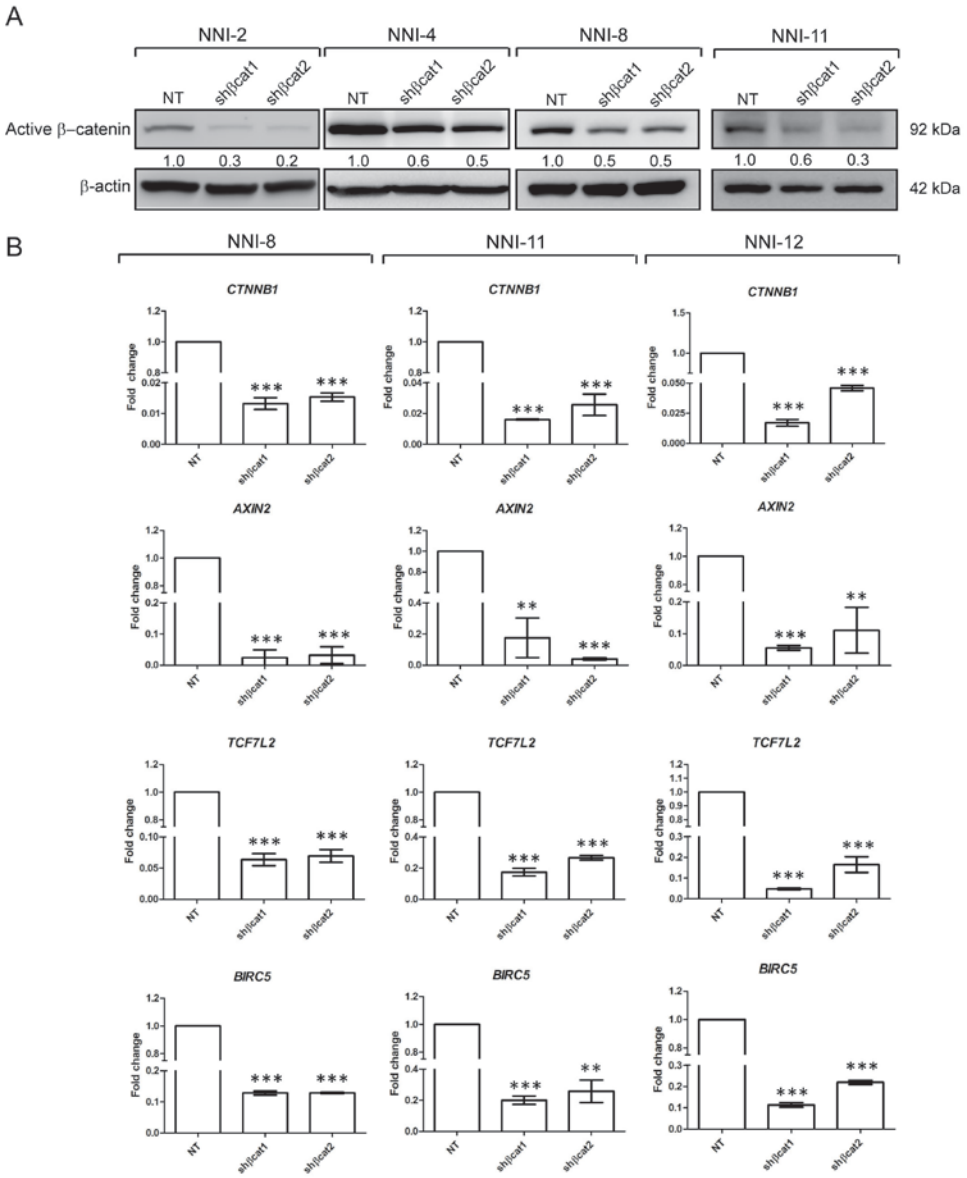

Figure 6.5. Targeting β-catenin using lentiviral shRNAs effectively reduces β-catenin protein expression and associated Wnt-target genes. A, Representative immunoblot analyses of active β-catenin protein expression of 4 GPC lines expressing NT, shβcat1, or shβcat2 constructs. Densitometric values of active β-catenin protein normalized to β-actin are shown from representative immunoblots; n=3. **B**, Quantitative real-time RT-PCR analyses of Wnt-target genes in 3 representative GPC lines expressing NT, shβcat1, or shβcat2 constructs. All values were given as the mean ± SEM (n=3) and were normalized to HRPT control. NT control vectors were set as 1 and expression profiles of shβcat1 or shβcat2 vectors were presented as a multiple (fold change) of target gene expression. **p<0.01; ***p<0.001 compared to NT control.

6.5 β-catenin depletion reduces self-renewal capability and viability of GPCs

As gliomasphere formation is a key behavior of GPCs and is used as a measure of stem cell self-renewal, we proceeded to investigate the effects of Wnt inactivation in GPCs by scoring for secondary gliomasphere formation (an estimation of self-renewing GPCs) and assessing gliomasphere number (GPC frequency) and size (an indication of proliferation potential). Targeting β-catenin expression markedly decreased the ability of GPCs to form gliomaspheres as indicated by the reduction in gliomasphere-forming number and consequently efficiency (**Figure 6.6A**) and the size of the gliomaspheres formed (**Figure 6.6B**). Gliomaspheres that formed from β-catenin-targeted GPCs were significantly smaller than those forming from non-targeting (NT) GPCs, suggesting decreased proliferation (**Figure 6.6B**). In addition, β-catenin knockdown resulted in significant decrease in GPC viability compared to NT control as determined by the cell viability assay (**Figure 6.6C**). These data provide firm evidence for the role of β-catenin in maintaining the self-renewal properties of GPCs and suggest that targeting β-catenin decreases GPC self-renewal due to decreased survival.

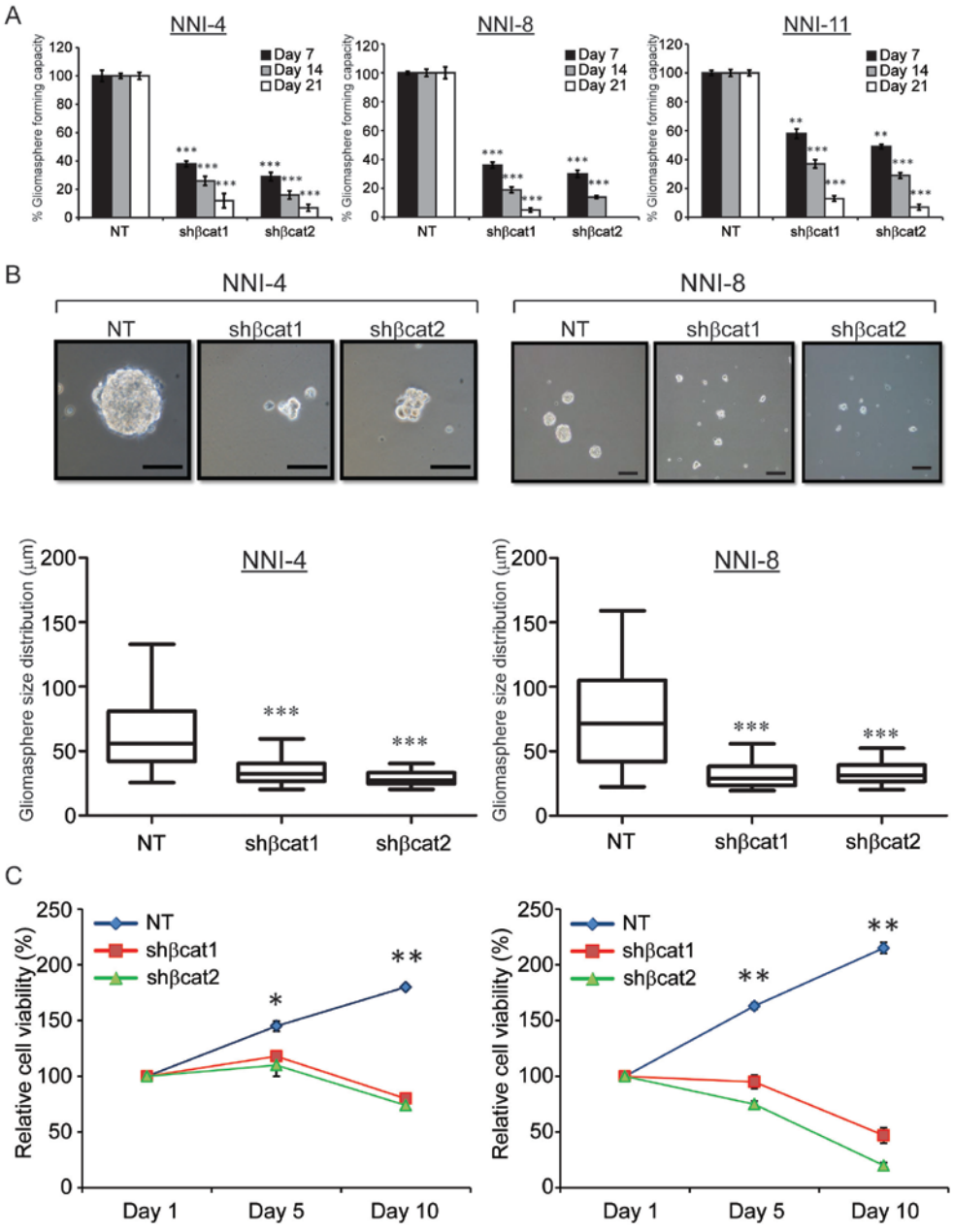

Figure 6.6. Targeting β-catenin expression in GPCs reduces cell growth associated with decreased proliferation and gliomasphere-forming capacity. A, Targeting β-catenin expression significantly attenuated the efficiency of GPCs to form gliomaspheres; **p<0.01, ***p<0.001 (n=3). **B**, Upper panels, representative images demonstrating reduced gliomasphere sizes and formation in GPCs transduced with β-catenin targeting shRNAs (shβcat1 or 2) constructs compared to non-targeting (NT) control. Scale bar = 50 μm. Lower panels, gliomasphere size distribution of GPCs transduced with β-catenin targeting shRNAs (shβcat1 or 2) constructs compared to non-targeting (NT) control after 14 days. ***p<0.001 compared to NT control. **C**, β-catenin knockdown with 2 distinct lentiviral shRNA constructs resulted in decreased cell viability as assessed by the cell titer assay. *p<0.05, **p<0.01 compared to NT control at the same time point (n=3).

6.6 Targeting β-catenin increases survival of mice bearing xenografts established from patient-derived GPCs

Based on the requirement of β-catenin for self-renewal, growth and survival in GPCs *in vitro*, we examined the role of β-catenin expression in tumorigenicity. GPCs were infected with NT control lentivirus or lentivirus targeting β-catenin (shβcat1 and 2). Five hundred thousand cells of each group were injected into the right frontal lobes of NOD-SCID gamma (NSG) mice. Our data showed a significant, improved survival in all mice implanted with GPCs expressing shβcat1 and shβcat2 compared to NT control (**Figure 6.7A**). All mice bearing NT infected cells developed neurological deficits after 2.5 months and displayed large tumors with pleomorphic cells, consistent with high grade glial malignancy (**Figure 6.7B**). Collectively, these data demonstrate that β-catenin is required for maintaining the tumorigenic capacity of GPCs *in vivo*.

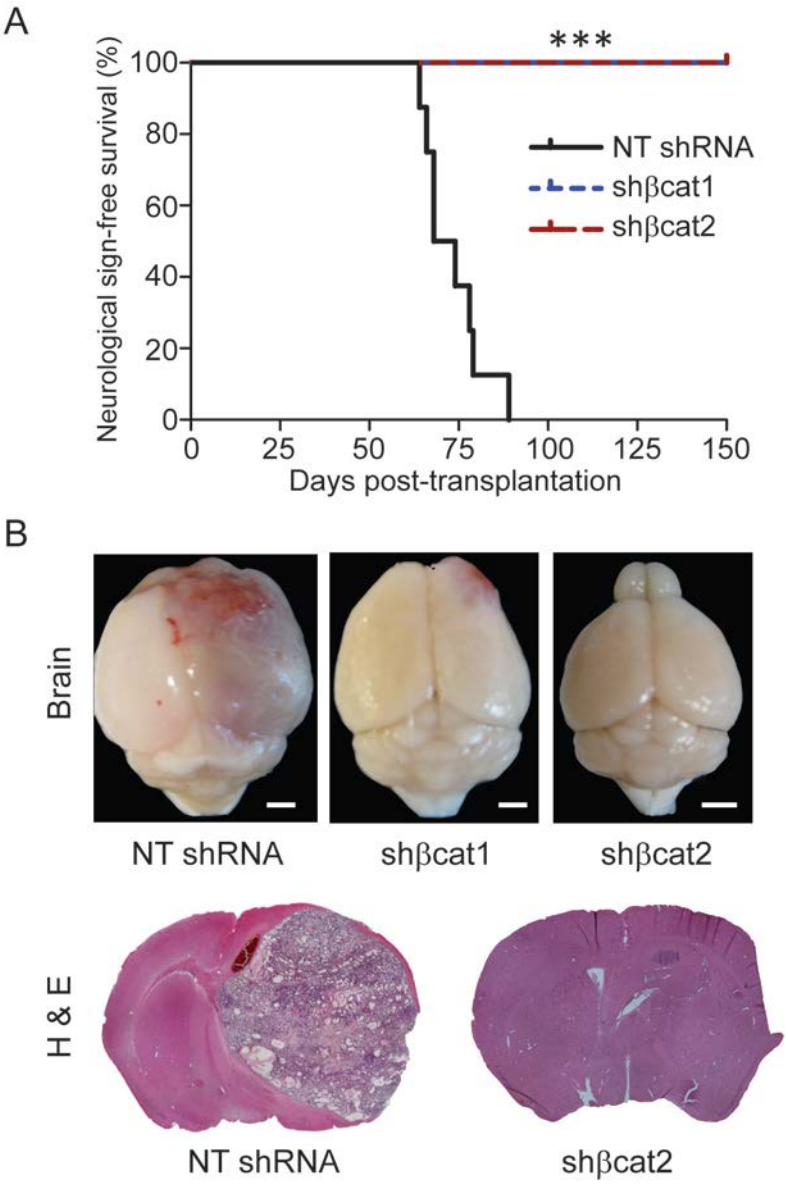

Figure 6.7. Targeting β-catenin decreases GPC tumorigenic potential and increases the survival of mice bearing intracranial human glioma xenografts. A, Kaplan-Meier curves demonstrate increased survival with β-catenin targeting in NSG mice injected with 500,000 GPCs. ***p<0.001 for shβcat1 or 2 groups compared to NT group with log-rank analysis of survival curves (n=8). **B**, Representative images of mice brains bearing NT, shβcat1 or 2; n=8; Scale bar = 0.2 cm.

6.7 Summary

The Wnt/β-catenin signaling pathway is aberrantly activated in human cancers and is critical for cancer formation and maintenance. A key feature of Wnt signaling activation is the nuclear localization of β-catenin. In this chapter, we identified Wnt/β-catenin signaling pathway as being active in GPCs, consistent with observations made by other investigators (Zhang et al, 2011; Zheng et al, 2010). In addition, we demonstrated that targeting β-catenin expression in GPCs using shRNAs significantly reduces proliferation and gliomasphere-forming capacity. More importantly, targeting β-catenin expression increases the survival of mice bearing intracranial patient-derived, glioma xenografts. Taken together, our findings provide evidence for targeting the Wnt pathway as a therapeutic strategy; and more importantly, an effective approach that eradicates the slow-growing, self-renewing tumor-initiating and sustaining cellular fraction.

CHAPTER 7

RESULTS

CHAPTER 7 – MITF/BETA-CATENIN/LEF-1 AXIS REGULATES SELF-RENEWAL AND PROLIFERATION POTENTIAL OF GLIOMA-PROPAGATING CELLS THROUGH WNT SIGNALING

7.1 Introduction and objectives

In previous chapters, we demonstrated that Wnt signaling is crucial in the maintenance of self-renewal and proliferation of GPCs. In addition, we showed that oligodendroglial GPCs present higher sensitivity towards β-catenin/TCF pathway inhibition compared to the majority of GBM GPCs. We attempted to address this higher β-catenin/TCF activation status in GPCs by screening for common "hotspot" mutations reported to cause Wnt signaling dysregulation in cancers. However, we did not observe any common hotspot mutations in *CTNNB1* and *APC* in GPCs. To further elucidate the mechanism by which oligodendroglial GPCs display higher Wnt/β-catenin status compared to GBM GPCs, we further analyzed our initial differential gene list (shown in chapter 4) and observed that microphthalmia-associated transcription factor (*MITF*) was among the top most differentially regulated genes with a significant $\log_2$ fold change of 2.33 (absolute fold change, 5.03) between the oligodendroglial and GBM GPCs (**Supplementary Table 2**). In addition, we looked at the individual expression levels of *MITF* of oligodendroglial and GBM GPCs across 3 GPC databases (Chong et al, 2009; Gunther et al, 2008; Pollard et al, 2009) and observed that *MITF* is upregulated in oligodendroglial GPCs compared to majority of GBM GPCs (**Figure 7.1A**). To confirm our observations, we performed a qRT-PCR for *MITF* and validated that *MITF* is significantly upregulated in the oligodendroglial GPC (NNI-8) compared to GBM GPCs (NNI-1, 2, 3, 4, and 5) (**Figure 7.1B**).

MITF is a transcription factor belonging to the family of basic helix-loop-helix and leucine-zipper (bHLH/LZ) proteins and is a master regulator of melanocyte development and function (Hodgkinson et al, 1993). In addition, it has been demonstrated that MITF is a frequently amplified oncogene in melanomas (Ugurel et al, 2007). Importantly, MITF has been shown to interact with LEF-1, a nuclear mediator of Wnt signaling, to enhance the transcription from the dopachrome tautomerase (*DCT*) gene promoter, an early melanoblast marker (Yasumoto et al, 2002). It has also been demonstrated that β-catenin is a significant regulator of melanoma cell growth, with MITF as a critical downstream target (Widlund et al, 2002).

These observations suggest that MITF may play an important role in the differential regulation of Wnt signaling between the oligodendroglial and GBM GPCs. In this chapter, we explore the role of MITF as an important mediator of the Wnt/β-catenin signaling in GPCs.

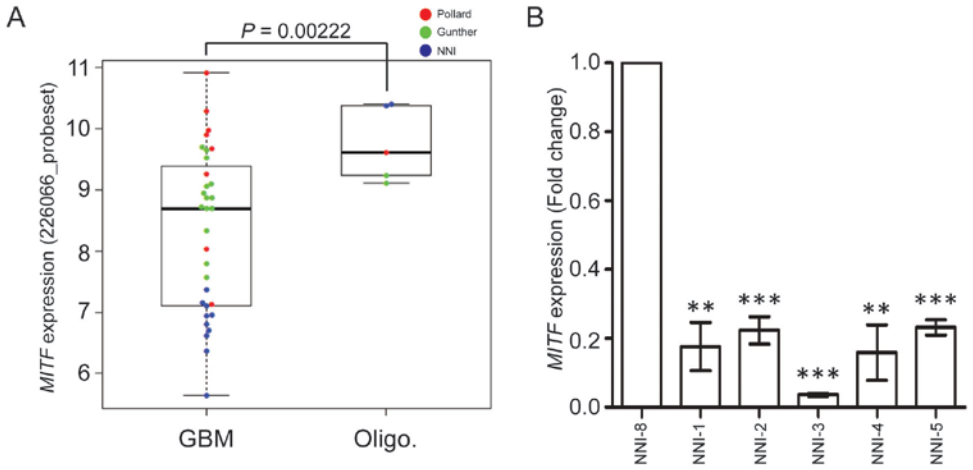

Figure 7.1. *MITF* expression is higher in oligodendroglial GPCs compared to GBM GPCs. A, *MITF* gene expression of oligodendroglial and GBM GPCs in 3 major GPC databases; p=0.00222. **B**, Quantitative real time RT-PCR analysis of *MITF* mRNA expression in oligodendroglial (NNI-8) and GBM (NNI-1, 2, 3, 4, and 5) GPCs. **p<0.01, ***p<0.001 compared to NNI-8 GPC; n=3.

7.2 *MITF* positively correlates and interacts with *CTNNB1* in oligodendroglial GPCs

We performed genome-wide pair-wise correlation coefficient analysis to evaluate potential genes having inverse relationship in oligodendroglial and GBM GPCs collated from 3 GPC databases (including ours) to enhance statistical power. Specifically, we identified 160 genes having entirely opposite correlation in GBM and oligodendroglial GPCs. Interestingly, among these 160 genes, we identified that the *MITF* gene has a positive correlation of coefficient 0.7 with *CTNNB1* in the oligodendroglial GPCs but with a negative correlation of -0.6 in GBM GPCs (**Figure 7.2**). This data provides further support that the β-catenin/LEF1-MITF signaling axis is inversely correlated in oligodendroglial and GBM GPCs.

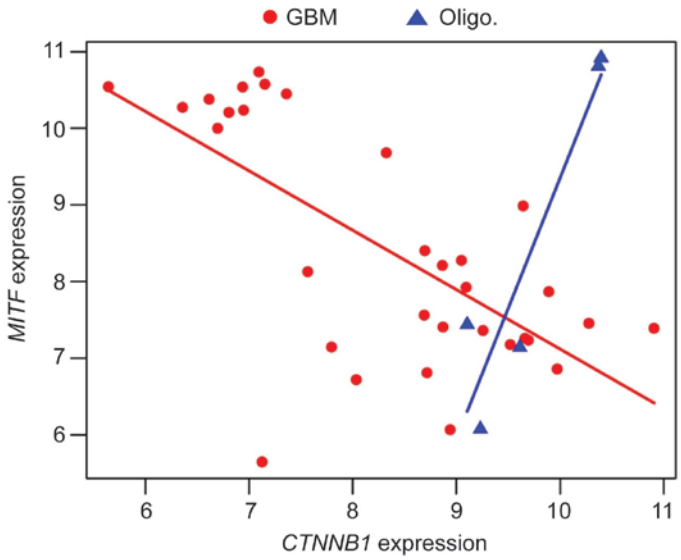

Figure 7.2. *MITF* correlates positively and negatively with *CTNNB1* in oligodendroglial and GBM GPCs respectively. Pair-wise correlation of *MITF* and *CTNNB1* in GPCs reveal positive correlation of 0.7 in oligodendroglial GPCs and a negative correlation of -0.6 in GBM GPCs.

In addition, we also detected the endogenous levels of MITF protein by immunoblot analysis in a panel of GPCs and demonstrated that oligodendroglial GPC (NNI-8) possesses higher MITF protein expression compared to the GBM GPCs (**Figure 7.3**). This suggests that MITF may play an important role in the differential regulation of Wnt/β-catenin signaling between the oligodendroglial and GBM GPCs. Interestingly, NNI-11, a GBM GPC, demonstrated high MITF protein level. This may suggest that MITF protein level stratifies a group of GBM and oligodendroglial GPCs independently of histology. This is an exciting avenue to be followed up in future directions.

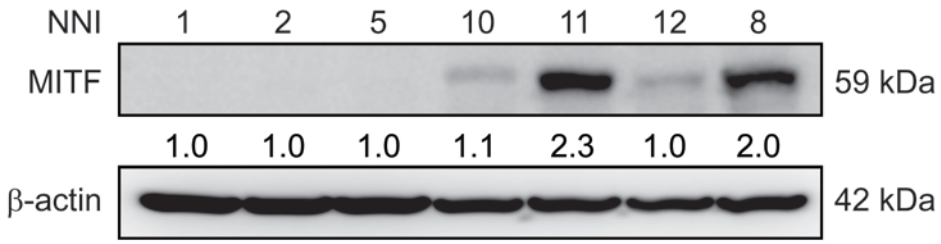

Figure 7.3. Endogenous MITF protein expression is higher in oligodendroglial GPC compared to majority of GBM GPCs. Representative immunoblot analyses of MITF protein expression of oligodendroglial (NNI-8) and GBM (NNI-1, 2, 5, 10, 11, and 12) GPC lines. Densitometric values of MITF protein normalized to β-actin are shown from representative immunoblots; n = 3.

Furthermore, to confirm observations made by others that MITF interacts with components of the Wnt signaling pathway i.e. β-catenin and LEF-1, we performed a co-immunoprecipitation (co-IP) between the three proteins in lysates of NNI-8 oligodendroglial GPCs where endogenous MITF is relatively higher than majority of the GBM GPCs. MITF formed a complex with β-catenin (**Figure 7.4A**) and LEF-1 (**Figure 7.4B**) in NNI-8 oligodendroglial GPCs, consistent with published literature (Schepsky et al, 2006; Yasumoto et al, 2002).

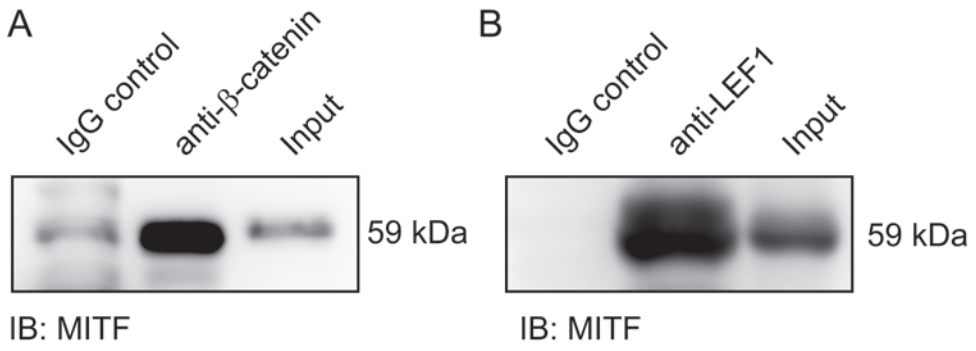

Figure 7.4. Co-immunoprecipitation of MITF with β-catenin and LEF-1 in GPCs. Co-immunoprecipitation assays were performed to test the interaction between **A**, MITF and β-catenin and **B**, MITF and LEF-1.

7.3 MITF expression is higher in patients with oligodendroglial tumors

To demonstrate that GPCs contribute to primary tumor progression, we analyzed a panel of patient tumors by immunohistochemical staining and observed similar trend of higher MITF expression in oligodendroglial tumors compared to GBM tumors (**Figure 7.5A and B**). This is consistent with earlier observations where we detected higher *MITF* mRNA and protein expression in oligodendroglial versus GBM GPCs. Once again, we show that GPCs mirror their primary tumors and contribute to disease progression.

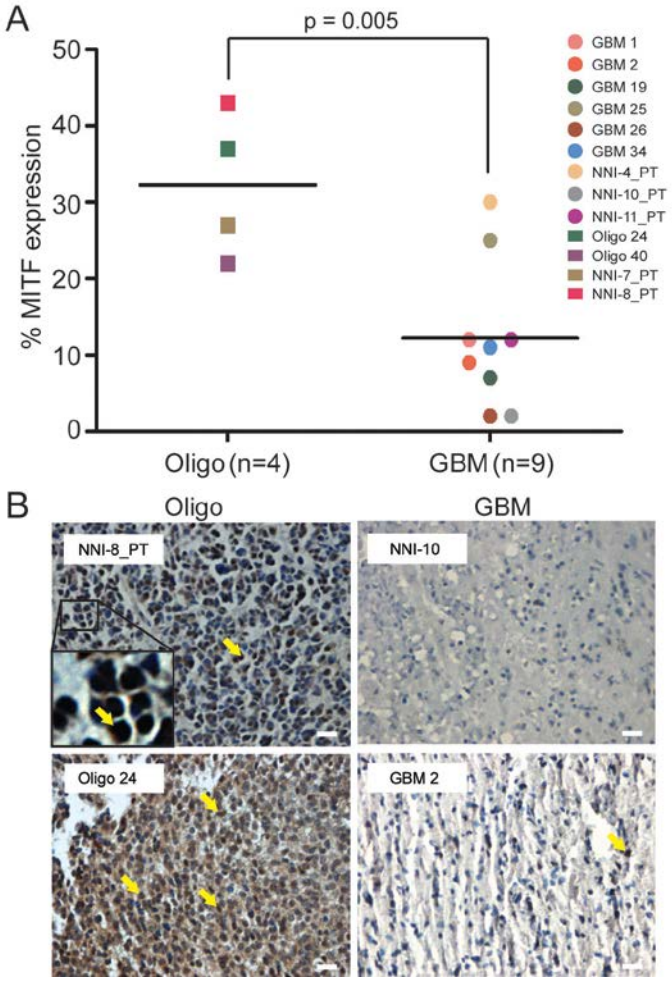

Figure 7.5. MITF expression is higher in oligodendroglial patient tumors. A, MITF protein expression was immunohistochemically detected and scored in patient tumors of GBM and oligodendroglial features. **B**, Representative immunohistochemical staining sections of MITF in primary patient tumors (arrows indicate positive MITF staining). Scale bar = 50 µm.

In addition, we also looked into patient glioma database – REMBRANDT, to determine the levels of *MITF* in CMAP+ and CMAP- patients (described in chapter 4). Interestingly, CMAP+ patients (more oligodendroglial GPC association) significantly exhibit higher levels of *MITF* compared to CMAP- patients (more GBM GPC association) in REMBRANDT glioma database (**Figure 7.6**). This indicates that patient tumors with oligodendroglial features are more likely to express more *MITF*. Collectively, these results suggest that *MITF* is differentially regulated between oligodendroglial and GBM tumors.

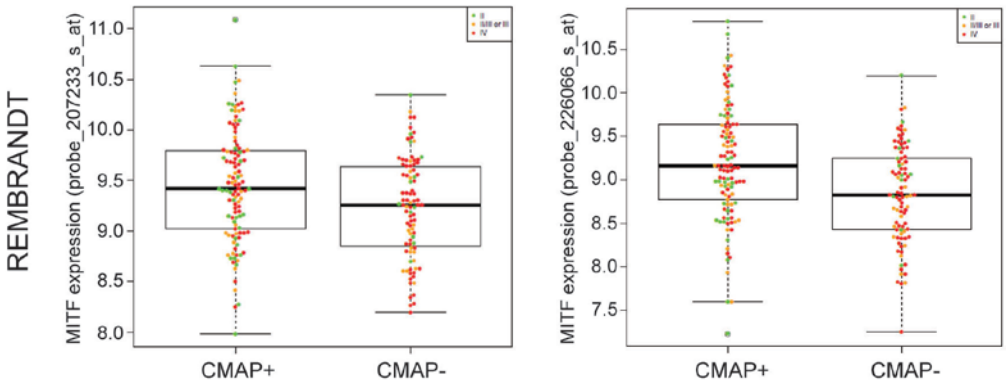

Figure 7.6. *MITF* microarray gene expression is higher in CMAP+ patients. CMAP+ patients (consisting mainly of lower grade oligodendroglial tumors) expressed higher *MITF* expression compared to CMAP- patients (consisting mainly of higher grades III and IV astrocytic and GBM tumors) in REMBRANDT (p-values = 0.00386 and 1.47E-05 for MITF probes 207233 and 226066 respectively) database.

7.4 Lentiviral-mediated knockdown of MITF strongly abrogates self-renewal and proliferation in oligodendroglial GPCs

Although our findings demonstrate that MITF is significantly up-regulated in oligodendroglial GPCs, no studies to-date have suggested a functional role for MITF in GPCs. As MITF physically interacts with β-catenin and LEF-1, the crucial mediators of the Wnt/β-catenin signaling pathway, we first assessed the ability of MITF to regulate GPC cell growth by targeting *MITF* expression using lentiviral transduced short hairpin RNAs (shRNAs).

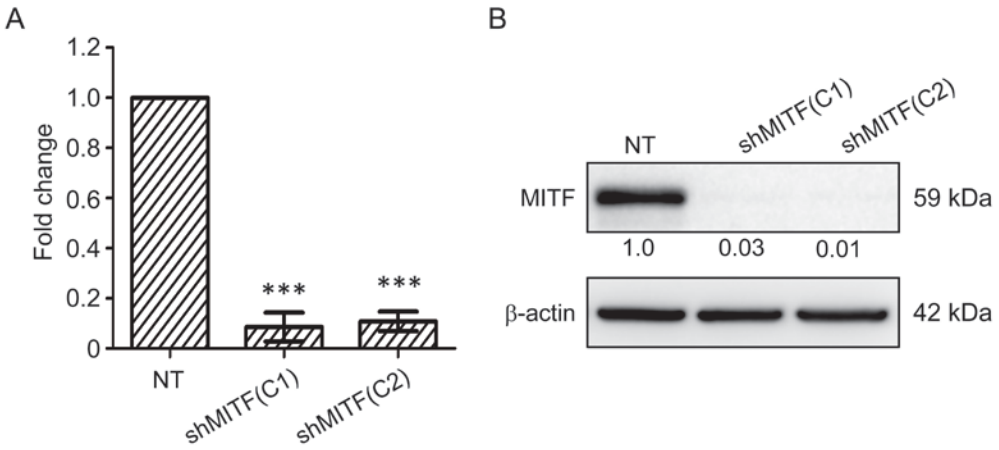

Figure 7.7. Targeting MITF using lentiviral shRNAs effectively reduces *MITF* mRNA and protein expression. A, Quantitative real-time RT-PCR analyses of *MITF* mRNA in GPC expressing NT, shMITF(C1), or shMITF(C2) constructs. All values were given as the mean ± SEM (n=3) and were normalized to HRPT control. NT control vectors were set as 1 and expression profiles of shMITF(C1) or shMITF(C2) vectors were presented as a multiple (fold change) of target gene expression. ***p<0.001 compared to NT control. **B**, Representative immunoblot analyses of active β-catenin protein expression of NNI-8 GPC expressing NT, shMITF(C1), or shMITF(C2) constructs. Densitometric values of MITF protein normalized to β-actin are shown from representative immunoblots; n=3.

To control for potential off-target shRNA effects, two different sequences of shRNA directed against *MITF* and a non-targeting (NT) shRNA were used. Transduction with *MITF* shRNA reduced *MITF* mRNA and protein level in GPCs in comparison to the non-targeting control (**Figure 7.7**). MITF targeting profoundly impacted GPC growth in oligodendroglial GPC (NNI-8)

as demonstrated by the marked reduction in viability over time (**Figure 7.8**) compared to GBM GPCs (NNI-12).

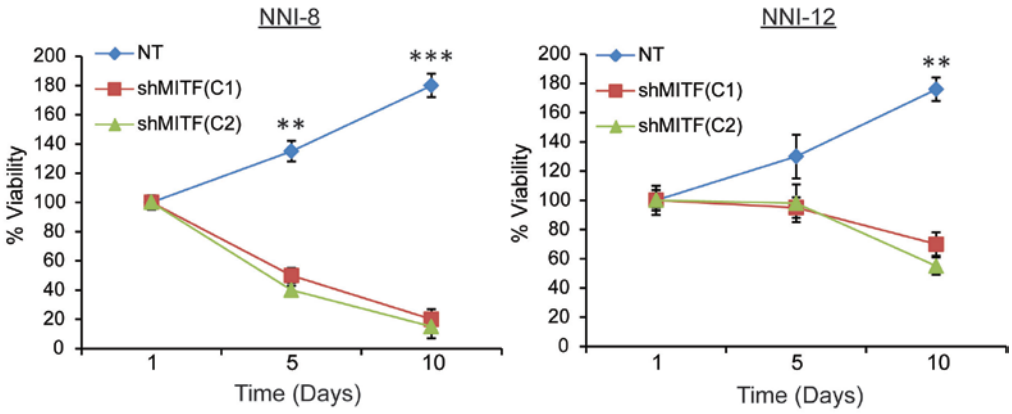

Figure 7.8. Targeting MITF decreases GPC growth. MITF knockdown with 2 distinct lentiviral shRNA constructs (C1 and C2) resulted in decreased cell viability as assessed by the cell titer assay. **p<0.01, ***p<0.001 compared to NT control at the same time point (n=3). Note the more pronounced cell death in oligodendroglial GPC (NNI-8) compared to GBM GPC (NNI-12) at similar time points assessed.

Cancer stem cells are functionally defined through their capacity for sustained self-renewal. As the growth and survival of GPCs was affected by *MITF* knockdown, we next examined whether MITF was crucial for self-renewal. To more definitively evaluate this possibility, we utilized the *in vitro* indicator of self-renewal in normal and cancer stem cells as described before - the neurosphere assay. We found that targeting MITF in GPCs decreased gliomasphere formation more profoundly in oligodendroglial GPCs than GBM GPCs in comparison to their respective non-targeting controls (**Figure 7.9A**). Gliomaspheres that did form from MITF-targeted GPCs were much smaller in oligodendroglial GPCs than GBM GPCs when compared to those forming from their respective non-targeting GPCs (**Figure 7.9B**), suggesting decreased proliferation. Hence, the formation of gliomaspheres is significantly

mitigated by the loss of MITF, especially in oligodendroglial GPCs, indicating a more important role for MITF in oligodendroglial GPC self-renewal.

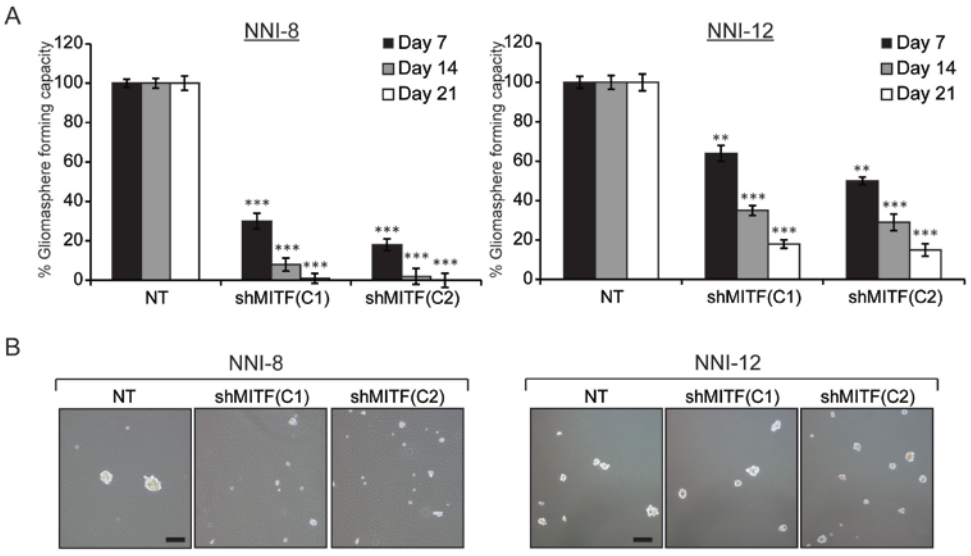

Figure 7.9. Targeting MITF expression in GPCs reduces gliomasphere-forming capacity and proliferation. **A**, Targeting MITF expression significantly attenuated the efficiency of GPCs to form gliomaspheres (effect was especially more prominent in NNI-8 oligodendroglial GPCs); **p<0.01, ***p<0.001 (n=3). **B**, Representative images demonstrating reduced gliomasphere sizes and formation in NNI-8 GPCs transduced with MITF targeting shRNAs (C1 or C2) constructs compared to non-targeting (NT) control. Scale bar = 100 µm.

7.5 Summary

Taken together, our results demonstrate that MITF is implicated in the differential regulation of Wnt/β-catenin signaling between oligodendroglial and GBM GPCs through interaction with β-catenin and LEF-1. In addition, we demonstrate that oligodendroglial GPCs are more sensitive to MITF inhibition compared to GBM GPCs as shown by the marked reduction in self-renewal capacity and proliferation. Our findings present MITF as a novel target molecule that is crucial in the maintenance of self-renewal and growth through the Wnt signaling pathway in oligodendroglial tumors.

CHAPTER 8

GENERAL DISCUSSION

CHAPTER 8 – GENERAL DISCUSSION

8.1 Discussion

When we first explored the field of glioma-propagating cells (GPCs), there was considerable attention to their importance. First, several teams showed that clinically derived GPCs contain phenotypic and karyotypic hallmarks found in the primary tumor (Lee et al, 2006; Wakimoto et al, 2012). Second, xenografts established from GPCs recapitulate the patient's original pathophysiology. Such findings emphasize that GPCs may present a relevant cellular platform for further studies. However, we also noted that at the National Neuroscience Institute which sees most of the brain tumor cases in Singapore, we lacked a constant supply of clinical material that would be typically found in larger populations such as China or USA. Moreover, to serially passage such tumors in immune-compromised mice would mean gene expression drifts towards mesenchymal and proliferative features (Hodgson et al, 2009). This is further compounded by a lack of a constant supply of mice at the right age for individual tumors that come along. To address this issue, with knowledge that extensive serial passage changes karyotype of cells and effects transformation, we evaluated several cryopreservation techniques with a few criteria in mind:

1. Svendsen *et al*. have elegantly documented the need to passage normal neural stem cells (NSCs) as spheroid structures in serum-free medium (Svendsen et al, 1998). Essentially, they showed that if NSC spheroids were dissociated into single cells, senescence eventually occurred with loss of proliferation. In contrast, if spheroid structures were cut into smaller spherical structures using a mechanical method, the spheres proliferated exponentially. These findings highlight the importance of cell-cell contact in promoting the survival of NSCs. We now know that

intercellular contact through integrins and extracellular matrix proteins such as laminin are vital to maintaining clinically derived GPCs in culture (Lathia et al, 2010; Pollard et al, 2009).

2. Effective freezing and thawing techniques should enable the efficient preservation of stocks of early passage cells, as well as the conservation of specific clones that are developed from the original cell lines such as genetically modified clones. Slow-freezing and rapid thawing methods are most commonly used; however, while these methods are sufficiently adequate for mouse cells, they perform very poorly with cells of human origin, and most cells either differentiate or die (Reubinoff et al, 2001).
3. We explored vitrification because it has been used successfully to preserve embryos and embryoid bodies (spherical structures), and has been highly efficient in bovine species, pig and hamster, all of which poorly withstand freezing and thawing by other methods (Lane et al, 1999; Yokota et al, 2000).

With the vitrification approach, a glass-like solidification of the freezing solution is achieved by using a high concentration of cryoprotectant and rapid cooling. While this approach can eliminate cell injury due to ice crystal formation, the high concentration of cryoprotectant may induce significant toxic and osmotic damage. The concentrations of cryoprotectants required to achieve vitrification are inversely related to the rate of cooling. Therefore, an increased speed of cooling can lessen the cryoprotectant-induced toxicity, as it minimizes the exposure time to these toxic compounds and allows their use at reduced concentrations. Our data illustrates for the first time the effective cryopreservation of clinically derived GPCs by vitrification (Chong et al, 2009). Importantly, we characterized preservation of essential features similar to the primary tumor, such as marker expression, GPC frequency, karyotype and

transcriptomic profiles. The advance we made in our *Stem Cells* publication include documenting gene expression changes and xenograft morphologies, compared to an earlier work which focused on only phenotypic features of cryopreserved NSC spheroid structures (Tan et al, 2007). This is an important approach since in 1996, The Cancer Genome Atlas project was initiated, which subsequently proved that gene expression drives brain tumor disease progression and clinical outcome (Atlas, 2008; Verhaak et al, 2010). Essentially, we showed that histologically similar tumors could yield GPCs with very different transcriptomic profiles, possibly accounting for the frequently observed inter-patient heterogeneity to treatment response. Indeed, we now know that genome-informed therapeutic decisions have proven to be valid in several cancers (Ooi et al, 2009; Wiedemeyer et al, 2010).

It is with this knowledge that we continued to ask if our GPCs, besides showing primary tumor hallmarks, contain gene expression-driven activation pathways that dictate primary tumor behavior. We rationalized that this would be a major advance, since we would directly connect GPCs (or “cancer stem cells”) to their primary tumor. If this were so, individual patient-derived GPCs (and their matching xenografts) would be an extremely valuable resource to recapitulate the entire patient molecular heterogeneity spectrum. We hypothesized that GPCs could contribute to brain tumor disease progression and patient survival outcome. For this, we chose to study 2 major brain tumor variants with disparate clinical outcomes: oligodendroglial versus glioblastoma multiforme (GBM) tumors. Recognizing that no number of GPC lines collected would be meaningful; we sought to increase our statistical power by combining GPC information from several investigators. This serves 2 purposes: First, we have a bigger dataset to work with, improving

robustness of conclusions, and second, by aligning our GPC collection with others (Gunther et al, 2008; Pollard et al, 2009), we could validate our cell line repository using published molecular classification systems. Indeed, our data highlights that transcriptomic programs in oligodendroglial GPCs dictate signaling pathways that confer better prognosis compared to GBM tumors. Importantly, our gene signature prognosticated patient survival independently of current clinical indicators of age and histology, underscoring that GPCs contain molecular patterns that contribute to the heterogeneity of tumors. This highlights the limitation of relying solely on morphology-based histological methods to diagnose and subsequently treat patients. Our bioinformatical method using the Connectivity Map (CMAP) was first executed successfully in a collaborative work with A/Prof. Lim Kah Leong on evaluating the tumor suppressor role of Parkin in glioma (Yeo et al, 2012). Here, our study taps into the multi-data platform capability of CMAP and we analyzed patterns of association between our GPC gene signature and individual patient gene expression information. This approach assumes that patients with gene expression likeness to the GPC gene signature will demonstrate features related to for example, the oligodendroglial or GBM GPCs, and be linked to performance of that signature in patient tumors. This thus provides a direct connection of cancer stem cells in the context of their primary tumor. We therefore show that GPCs are clinically relevant and contribute to clinical profiles, and most importantly, gene expression drives brain tumor disease progression and patient survival outcomes. This message of molecular heterogeneity as defined by gene expression is well-supported in the analyses of primary tumors by large efforts such as TCGA, the Phillips classification scheme and that by Fine and colleagues (Li et al, 2009; Phillips et al, 2006a; Verhaak et al, 2010). It should be noted that it is no trivial task to assess these schemes compared to one another to determine superiority,

simply because while the signatures hold true in prognostic databases, no true predictive datasets are available to query each classification method appropriately. Thus, our study utilized the most common Phillips classification scheme applicable to gliomas of all grades (Phillips et al, 2006a). We had attempted to align our GPC gene signature to TCGA classification scheme but the CMAP was not significantly associated, most likely arising from our internal observations that CMAP usually works well with only databases of heterogeneous histologies (TCGA contains only GBM tumors). This was also seen in Ooi *et al*. which used CMAP to interrogate against different gastric cancer subtypes (Ooi et al, 2009). Our data showed that the gene signature prognosticated survival independently of the 1p/19q co-deletion status of oligodendrogliomas, the latter of which confers enhanced sensitivity to chemotherapeutic agents. Although this finding would seemingly render our work less meaningful, given that oligodendrogliomas are already well-treatable with PCV therapy, we want to highlight that we could further detect sensitive and resistant patient cohorts without LOH at 1p/19q. This means that the previously “untreatable” patients could now be treated according to their pathway activation if they fell into the sensitive profile. This is a significant advance as incomplete surgical resection of brain tumors often means that chemotherapy is the remaining option to combat the infiltrative and recurrent nature of the disease.

Our GPC gene signature enriched for the Wnt, TGFβ and Notch signaling pathways. Wnt and Notch are upregulated in oligodendroglial tumors, while TGFβ is upregulated in GBM tumors. Although there is significant knowledge that these pathways do regulate glioma growth, their activation between these 2 major variants is unknown (Fan et al, 2010; Penuelas et al, 2009; Zheng et al, 2010). The knowledge gleaned from our

study includes: (1) GPCs contribute to disease progression, (2) Tumors can now be viewed as manifestations of their pathway activation as defined by gene expression information, and (3) Genome-informed approaches may guide therapeutic choices. To prove point (3), we subjected GPCs to small molecules targeting each of these pathways and showed GPC response as predicted. Next, to draw the link between GPC response and primary tumor behavior, we interrogated large patient databases and showed that pathway activation, in terms of core programs, mapped similarly. We then focused on the Wnt pathway because its role in GPCs is relatively unknown. We adopted the approach of using well-characterized small molecule Wnt pathway inhibitors to assess GPC response. We highlight that although our study did not investigate the GPC-specificity of these inhibitors, these published Wnt-inhibitors has been shown to be effective and specific to cancer cell lines harboring hyperactivated Wnt/β-catenin signaling pathway as compared to their normal counterparts (Ewan et al, 2010; Lepourcelet et al, 2004). Furthermore, Chen *et al.* reported that the *in vivo* use of the Wnt inhibitor, IWR1, did not incur permanent damage of normal stem cell function with transient repression of Wnt signaling. This suggests the practicability of these inhibitors in a clinical setting (Chen et al, 2009). Notably, any inhibitors targeting Wnt secretion were ineffective, while inhibitors targeting the β-catenin stage were highly effective against GPC proliferation. This is an interesting result for a few reasons: (1) Cancers of the breast, for instance, are typically responsive to Wnt secretion inhibition (Proffitt et al, 2012), while (2) Glioma cells are most likely to manifest genetic lesions leading to Wnt pathway activation late in the pathway, at the β-catenin/TCF stage. Knowing this is important to select the appropriate Wnt pathway inhibitor for the treatment of gliomas. Indeed, during the progress of our work, 2 other publications arose on assessing β-catenin/TCF role in gliomas (Zhang et al,

2011; Zheng et al, 2010). We add incremental knowledge in demonstrating Wnt regulation in specifically GPCs, the cells that sustain tumor growth. In addition, the dependence on the downstream Wnt signaling pathway in GPCs, more specifically, the β-catenin/TCF cascade, suggests that β-catenin/TCF complex formation may be uncoupled from Wnt ligand production and the Axin degradation complex activity. Furthermore, as β-catenin mutations are not the cause of heightened β-catenin/TCF activity in GPCs, these lead us to suggest that β-catenin signaling activity can be modulated by Wnt-independent mechanisms including post-translational modifications or regulation of nuclear localization of β-catenin. The forkhead box M1 (FoxM1) transcription factor has been shown to interact with β-catenin and directs its nuclear import in glioma formation (Zhang et al, 2011). In addition, insulin growth factor-2 (IGF-2) can induce redistribution of β-catenin from the plasma membrane to the nucleus and cause transcriptional activation of β-catenin/TCF target genes (Morali et al, 2001). Novak *et al.* demonstrated that increased expression of integrin-linked kinase (ILK), an ankyrin repeat containing serine-threonine protein kinase leads to translocation of β-catenin into the nucleus and transactivates β-catenin/LEF activity of intestinal and mammary epithelial cells (Novak et al, 1998). Other mediators of Wnt-independent mechanisms that result in modulation of β-catenin signaling activity include IGF-1 , growth factor Gas6, vascular endothelial growth factor (VEGF), hepatocyte growth factor (HGF) and G-proteins (Carmeliet et al, 1999; Goruppi et al, 2001; Hiscox & Jiang, 1999; Kawasaki et al, 2000; Papkoff & Aikawa, 1998; Playford et al, 2000).

Moving forward, we then validated these findings genetically both *in vitro* and *in vivo* and implicated MITF as a downstream effector of β-catenin/TCF. Importantly, we showed that β-catenin and MITF are both

upregulated in oligodendroglial tumors compared to GBM tumors, providing clinical evidence for our GPC-driven hypothesis that cancer stem cells dictate primary tumor behavior.

8.2 Future Directions

Our study has been described in 2 manuscripts of which I am co-first author of (Chong et al, 2009; Ng et al, 2012). We plan to perform the following experiments to complete and publish the work on MITF as a downstream effector of β-catenin/TCF activation. Briefly:

1. We will determine that MITF is downstream of β-catenin/TCF activation by assessing the rescue ability of MITF overexpression in a TCF- or LEF-dominant negative (dn) background. We have these plasmids from our collaboration with Prof. David Virshup. We will assess effects on GPC frequency and proliferation.
2. We will determine these similar rescue effects *in vivo* using the orthotopic xenograft mouse model, using NOD-SCID gamma mice. We expect to see poor survival for implanted vehicle cells, and best survival with MITF knockdown (2 clones plus 1 non-targeting control), TCF- or LEF-dn expression. In contrast, this good survival should be reversed with MITF overexpression (**Figure 8.1**). Briefly, we will stereotaxically implant 10 NOD-SCID gamma mice per arm and monitor the time to development of neurological deficits. We calculated the number of mice we need on http://www.biomath.info/power/index.htm. We will sacrifice the animals by transcardiac perfusion with 4% paraformaldehyde. Mouse brains will be embedded in paraffin sections and analyzed as previously described (Ng et al, 2012). Kaplan-Meier survival curves will be calculated using the log-rank test in GraphPad Prism software (www.graphpad.com).

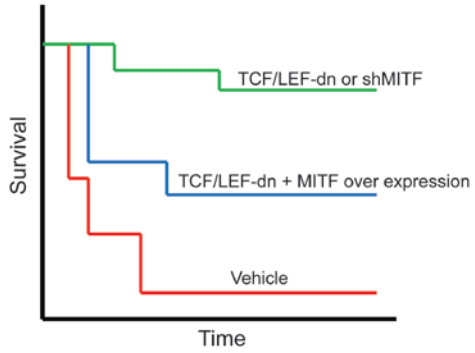

Figure 8.1. Hypothetical Kaplan-Meier survival analysis to determine rescue effects using overexpression of MITF *in vivo.*

3. Recognizing that no number of GPC lines or the animal model is perfect at recapitulating the tumorigenic process, we will assess MITF role in patient tumor databases with gene expression information. We will determine MITF-associated core modules and determine patient cohorts associated with favorable or worse profiles, correlating with low and high MITF respectively, as shown by our earlier gene expression and immunohistochemistry data. We have previously successfully performed such a bioinformatical approach when evaluating PLK1 role in glioma (Foong et al, 2012). This MITF-associated gene module approach enables us to examine gene events upstream and downstream of β-catenin/TCF. We will also identify patient molecular subclasses amenable to MITF inhibitory therapy. Notably, we had observed that oligodendroglial or GBM GPCs that exhibited high MITF could be effectively targeted, suggesting that MITF may be a better predictor of response than histology, albeit a modest pool of cells. This approach that we will employ will present a significant advance in that we will have statistical power of hundreds of patients in the database to verify our hypothesis that patient subclasses can be identified who will be amenable to anti-MITF therapeutic approaches.

8.3 Conclusion

We show that GPCs contain transcriptomic programs that dictate pathway activation in the primary tumor. This genome-informed approach can direct treatment strategies and identify patient cohorts most likely to receive treatment benefit. Collectively, our work establishes that GPCs are clinically relevant, and contribute to glioma disease progression and patient survival outcome. Furthermore, our data highlight the limitation of current morphology-based histologic analyses in tumor classification, consequently impacting on treatment decisions. In addition, given the importance of Wnt/β-catenin signaling pathway in human cancers in general, our findings not only improved the understanding of the molecular mechanisms underlying β-catenin/TCF activation but also suggest additional targets for therapeutic intervention.

9. REFERENCES

Abdouh M, Facchino S, Chatoo W, Balasingam V, Ferreira J, Bernier G (2009) BMI1 sustains human glioblastoma multiforme stem cell renewal. *J Neurosci* **29:** 8884-8896

Al-Hajj M, Wicha MS, Benito-Hernandez A, Morrison SJ, Clarke MF (2003) Prospective identification of tumorigenic breast cancer cells. *Proc Natl Acad Sci U S A* **100:** 3983-3988

Alcantara Llaguno S, Chen J, Kwon CH, Jackson EL, Li Y, Burns DK, Alvarez-Buylla A, Parada LF (2009) Malignant astrocytomas originate from neural stem/progenitor cells in a somatic tumor suppressor mouse model. *Cancer Cell* **15:** 45-56

Ali J, Shelton JN (1993) Successful vitrification of day-6 sheep embryos. *J Reprod Fertil* **99:** 65-70

Anido J, Saez-Borderias A, Gonzalez-Junca A, Rodon L, Folch G, Carmona MA, Prieto-Sanchez RM, Barba I, Martinez-Saez E, Prudkin L, Cuartas I, Raventos C, Martinez-Ricarte F, Poca MA, Garcia-Dorado D, Lahn MM, Yingling JM, Rodon J, Sahuquillo J, Baselga J, Seoane J (2010) TGF-beta Receptor Inhibitors Target the CD44(high)/Id1(high) Glioma-Initiating Cell Population in Human Glioblastoma. *Cancer Cell* **18:** 655-668

Atlas TCG (2008) Comprehensive genomic characterization defines human glioblastoma genes and core pathways. *Nature* **455:** 1061-1068

Bandyopadhyay D, Mandal M, Adam L, Mendelsohn J, Kumar R (1998) Physical interaction between epidermal growth factor receptor and DNA-dependent protein kinase in mammalian cells. *J Biol Chem* **273:** 1568-1573

Bao S, Wu Q, McLendon RE, Hao Y, Shi Q, Hjelmeland AB, Dewhirst MW, Bigner DD, Rich JN (2006) Glioma stem cells promote radioresistance by preferential activation of the DNA damage response. *Nature* **444:** 756-760

Bar EE, Chaudhry A, Farah MH, Eberhart CG (2007a) Hedgehog signaling promotes medulloblastoma survival via Bc/II. *Am J Pathol* **170:** 347-355

Bar EE, Chaudhry A, Lin A, Fan X, Schreck K, Matsui W, Piccirillo S, Vescovi AL, DiMeco F, Olivi A, Eberhart CG (2007b) Cyclopamine-mediated hedgehog pathway inhibition depletes stem-like cancer cells in glioblastoma. *Stem Cells* **25:** 2524-2533

Barker N, Clevers H (2006) Mining the Wnt pathway for cancer therapeutics. *Nat Rev Drug Discov* **5:** 997-1014

Barker N, Ridgway RA, van Es JH, van de Wetering M, Begthel H, van den Born M, Danenberg E, Clarke AR, Sansom OJ, Clevers H (2009) Crypt stem cells as the cells-of-origin of intestinal cancer. *Nature* **457:** 608-611

Barker N, van Es JH, Kuipers J, Kujala P, van den Born M, Cozijnsen M, Haegebarth A, Korving J, Begthel H, Peters PJ, Clevers H (2007) Identification of stem cells in small intestine and colon by marker gene Lgr5. *Nature* **449:** 1003-1007

Beatus P, Jhaveri DJ, Walker TL, Lucas PG, Rietze RL, Cooper HM, Morikawa Y, Bartlett PF (2011) Oncostatin M regulates neural precursor activity in the adult brain. *Dev Neurobiol* **71:** 619-633

Becher OJ, Hambardzumyan D, Fomchenko EI, Momota H, Mainwaring L, Bleau AM, Katz AM, Edgar M, Kenney AM, Cordon-Cardo C, Blasberg RG, Holland EC (2008) Gli activity correlates with tumor grade in platelet-derived growth factor-induced gliomas. *Cancer Res* **68:** 2241-2249

Beier D, Hau P, Proescholdt M, Lohmeier A, Wischhusen J, Oefner PJ, Aigner L, Brawanski A, Bogdahn U, Beier CP (2007) CD133(+) and CD133(-) glioblastoma-derived cancer stem cells show differential growth characteristics and molecular profiles. *Cancer Res* **67:** 4010-4015

Blaskovich MA, Sun J, Cantor A, Turkson J, Jove R, Sebti SM (2003) Discovery of JSI-124 (cucurbitacin I), a selective Janus kinase/signal transducer and activator of transcription 3 signaling pathway inhibitor with potent antitumor activity against human and murine cancer cells in mice. *Cancer Res* **63:** 1270-1279

Bleau AM, Hambardzumyan D, Ozawa T, Fomchenko EI, Huse JT, Brennan CW, Holland EC (2009) PTEN/PI3K/Akt pathway regulates the side population phenotype and ABCG2 activity in glioma tumor stem-like cells. *Cell Stem Cell* **4:** 226-235

Bonnet D, Dick JE (1997) Human acute myeloid leukemia is organized as a hierarchy that originates from a primitive hematopoietic cell. *Nat Med* **3:** 730-737

Brandes AA, Franceschi E, Tosoni A, Hegi ME, Stupp R (2008) Epidermal growth factor receptor inhibitors in neuro-oncology: hopes and disappointments. *Clin Cancer Res* **14:** 957-960

Brennan C, Momota H, Hambardzumyan D, Ozawa T, Tandon A, Pedraza A, Holland E (2009) Glioblastoma subclasses can be defined by activity among signal transduction pathways and associated genomic alterations. *PLoS One* **4:** e7752

Burkhardt JK, Riina HA, Shin BJ, Moliterno JA, Hofstetter CP, Boockvar JA (2011) Intra-arterial chemotherapy for malignant gliomas: a critical analysis. *Interv Neuroradiol* **17:** 286-295

Cai J, Wu Y, Mirua T, Pierce JL, Lucero MT, Albertine KH, Spangrude GJ, Rao MS (2002) Properties of a fetal multipotent neural stem cell (NEP cell). *Dev Biol* **251:** 221-240

Cairncross JG, Ueki K, Zlatescu MC, Lisle DK, Finkelstein DM, Hammond RR, Silver JS, Stark PC, Macdonald DR, Ino Y, Ramsay DA, Louis DN (1998) Specific genetic predictors of chemotherapeutic response and survival in patients with anaplastic oligodendrogliomas. *J Natl Cancer Inst* **90:** 1473-1479

Carmeliet P, Lampugnani MG, Moons L, Breviario F, Compernolle V, Bono F, Balconi G, Spagnuolo R, Oosthuyse B, Dewerchin M, Zanetti A, Angellilo A, Mattot V, Nuyens D, Lutgens E, Clotman F, de Ruiter MC, Gittenberger-de Groot A, Poelmann R, Lupu F, Herbert JM, Collen D, Dejana E (1999) Targeted deficiency or cytosolic truncation of the VE-cadherin gene in mice impairs VEGF-mediated endothelial survival and angiogenesis. *Cell* **98:** 147-157

Chakravarti A, Zhai G, Suzuki Y, Sarkesh S, Black PM, Muzikansky A, Loeffler JS (2004) The prognostic significance of phosphatidylinositol 3-kinase pathway activation in human gliomas. *J Clin Oncol* **22:** 1926-1933

Chen B, Dodge ME, Tang W, Lu J, Ma Z, Fan CW, Wei S, Hao W, Kilgore J, Williams NS, Roth MG, Amatruda JF, Chen C, Lum L (2009) Small molecule-mediated disruption of Wnt-dependent signaling in tissue regeneration and cancer. *Nat Chem Biol* **5:** 100-107

Chen MS, Woodward WA, Behbod F, Peddibhotla S, Alfaro MP, Buchholz TA, Rosen JM (2007) Wnt/beta-catenin mediates radiation resistance of Sca1+ progenitors in an immortalized mammary gland cell line. *J Cell Sci* **120:** 468-477

Chong YK, Toh TB, Zaiden N, Poonepalli A, Leong SH, Ong CE, Yu Y, Tan PB, See SJ, Ng WH, Ng I, Hande MP, Kon OL, Ang BT, Tang C (2009) Cryopreservation of neurospheres derived from human glioblastoma multiforme. *Stem Cells* **27:** 29-39

Chua C, Zaiden N, Chong KH, See SJ, Wong MC, Ang BT, Tang C (2008) Characterization of a side population of astrocytoma cells in response to temozolomide. *J Neurosurg* **109:** 856-866

Clement V, Sanchez P, de Tribolet N, Radovanovic I, Ruiz i Altaba A (2007) HEDGEHOG-GLI1 signaling regulates human glioma growth, cancer stem cell self-renewal, and tumorigenicity. *Curr Biol* **17:** 165-172

Clements WM, Lowy AM, Groden J (2003) Adenomatous polyposis coli/beta-catenin interaction and downstream targets: altered gene expression in gastrointestinal tumors. *Clin Colorectal Cancer* **3:** 113-120

Clements WM, Wang J, Sarnaik A, Kim OJ, MacDonald J, Fenoglio-Preiser C, Groden J, Lowy AM (2002) beta-Catenin mutation is a frequent cause of Wnt pathway activation in gastric cancer. *Cancer Res* **62:** 3503-3506

Collins AT, Berry PA, Hyde C, Stower MJ, Maitland NJ (2005) Prospective identification of tumorigenic prostate cancer stem cells. *Cancer Res* **65:** 10946-10951

Cui D, Xu Q, Wang K, Che X (2010) Gli1 is a potential target for alleviating multidrug resistance of gliomas. *J Neurol Sci* **288:** 156-166

Curtis SJ, Sinkevicius KW, Li D, Lau AN, Roach RR, Zamponi R, Woolfenden AE, Kirsch DG, Wong KK, Kim CF (2010) Primary tumor genotype is an important determinant in identification of lung cancer propagating cells. *Cell Stem Cell* **7:** 127-133

Dahlstrand J, Collins VP, Lendahl U (1992) Expression of the class VI intermediate filament nestin in human central nervous system tumors. *Cancer Res* **52:** 5334-5341

Dai C, Celestino JC, Okada Y, Louis DN, Fuller GN, Holland EC (2001) PDGF autocrine stimulation dedifferentiates cultured astrocytes and induces oligodendrogliomas and oligoastrocytomas from neural progenitors and astrocytes in vivo. *Genes Dev* **15:** 1913-1925

Diamandis P, Wildenhain J, Clarke ID, Sacher AG, Graham J, Bellows DS, Ling EK, Ward RJ, Jamieson LG, Tyers M, Dirks PB (2007) Chemical genetics reveals a complex functional ground state of neural stem cells. *Nat Chem Biol* **3:** 268-273

Dittmann K, Mayer C, Fehrenbacher B, Schaller M, Raju U, Milas L, Chen DJ, Kehlbach R, Rodemann HP (2005) Radiation-induced epidermal growth factor receptor nuclear import is linked to activation of DNA-dependent protein kinase. *J Biol Chem* **280:** 31182-31189

Doetsch F, Caille I, Lim DA, Garcia-Verdugo JM, Alvarez-Buylla A (1999) Subventricular zone astrocytes are neural stem cells in the adult mammalian brain. *Cell* **97:** 703-716

Dreesen O, Brivanlou AH (2007) Signaling pathways in cancer and embryonic stem cells. *Stem Cell Rev* **3:** 7-17

Ehtesham M, Sarangi A, Valadez JG, Chanthaphaychith S, Becher MW, Abel TW, Thompson RC, Cooper MK (2007) Ligand-dependent activation of the hedgehog pathway in glioma progenitor cells. *Oncogene* **26:** 5752-5761

Emami KH, Nguyen C, Ma H, Kim DH, Jeong KW, Eguchi M, Moon RT, Teo JL, Kim HY, Moon SH, Ha JR, Kahn M (2004) A small molecule inhibitor of beta-catenin/CREB-binding protein transcription [corrected]. *Proc Natl Acad Sci U S A* **101:** 12682-12687

Eppert K, Takenaka K, Lechman ER, Waldron L, Nilsson B, van Galen P, Metzeler KH, Poeppl A, Ling V, Beyene J, Canty AJ, Danska JS, Bohlander SK, Buske C, Minden MD, Golub TR, Jurisica I, Ebert BL, Dick JE (2011) Stem cell gene expression programs influence clinical outcome in human leukemia. *Nat Med* **17:** 1086-1093

Ewan K, Pajak B, Stubbs M, Todd H, Barbeau O, Quevedo C, Botfield H, Young R, Ruddle R, Samuel L, Battersby A, Raynaud F, Allen N, Wilson S, Latinkic B, Workman P, McDonald E, Blagg J, Aherne W, Dale T (2010) A useful approach to identify novel small-molecule inhibitors of Wnt-dependent transcription. *Cancer Res* **70:** 5963-5973

Eyler CE, Foo WC, LaFiura KM, McLendon RE, Hjelmeland AB, Rich JN (2008) Brain cancer stem cells display preferential sensitivity to Akt inhibition. *Stem Cells* **26:** 3027-3036

Eyler CE, Rich JN (2008) Survival of the fittest: cancer stem cells in therapeutic resistance and angiogenesis. *J Clin Oncol* **26:** 2839-2845

Fan X, Khaki L, Zhu TS, Soules ME, Talsma CE, Gul N, Koh C, Zhang J, Li YM, Maciaczyk J, Nikkhah G, Dimeco F, Piccirillo S, Vescovi AL, Eberhart CG (2010) NOTCH pathway blockade depletes CD133-positive glioblastoma cells and inhibits growth of tumor neurospheres and xenografts. *Stem Cells* **28:** 5-16

Fomchenko EI, Dougherty JD, Helmy KY, Katz AM, Pietras A, Brennan C, Huse JT, Milosevic A, Holland EC (2011) Recruited cells can become transformed and overtake PDGF-induced murine gliomas in vivo during tumor progression. *PLoS One* **6:** e20605

Foong CS, Ng FS, Phong M, Toh TB, Chong YK, Tucker-Kellogg G, Campbell RM, Ang BT, Tang C (2011) Cryopreservation of cancer-initiating cells derived from glioblastoma. *Front Biosci (Elite Ed)* **3:** 698-708

Foong CS, Sandanaraj E, Brooks HB, Campbell RM, Ang BT, Chong YK, Tang C (2012) Glioma-Propagating Cells as an In Vitro Screening Platform: PLK1 as a Case Study. *J Biomol Screen* **17:** 1136-1150

French PJ, Swagemakers SM, Nagel JH, Kouwenhoven MC, Brouwer E, van der Spek P, Luider TM, Kros JM, van den Bent MJ, Sillevis Smitt PA (2005) Gene expression profiles associated with treatment response in oligodendrogliomas. *Cancer Res* **65:** 11335-11344

Friedmann-Morvinski D, Bushong EA, Ke E, Soda Y, Marumoto T, Singer O, Ellisman MH, Verma IM (2012) Dedifferentiation of neurons and astrocytes by oncogenes can induce gliomas in mice. *Science* **338:** 1080-1084

Fuerer C, Nusse R (2010) Lentiviral vectors to probe and manipulate the Wnt signaling pathway. *PLoS One* **5:** e9370

Gal H, Makovitzki A, Amariglio N, Rechavi G, Ram Z, Givol D (2007) A rapid assay for drug sensitivity of glioblastoma stem cells. *Biochem Biophys Res Commun* **358:** 908-913

Galli R, Binda E, Orfanelli U, Cipelletti B, Gritti A, De Vitis S, Fiocco R, Foroni C, Dimeco F, Vescovi A (2004) Isolation and characterization of tumorigenic, stem-like neural precursors from human glioblastoma. *Cancer Res* **64:** 7011-7021

Ganesan K, Ivanova T, Wu Y, Rajasegaran V, Wu J, Lee MH, Yu K, Rha SY, Chung HC, Ylstra B, Meijer G, Lian KO, Grabsch H, Tan P (2008) Inhibition of gastric cancer invasion and metastasis by PLA2G2A, a novel beta-catenin/TCF target gene. *Cancer Res* **68:** 4277-4286

Gangemi RM, Griffero F, Marubbi D, Perera M, Capra MC, Malatesta P, Ravetti GL, Zona GL, Daga A, Corte G (2009) SOX2 silencing in glioblastoma tumor-initiating cells causes stop of proliferation and loss of tumorigenicity. *Stem Cells* **27:** 40-48

Gautier L, Cope L, Bolstad BM, Irizarry RA (2004) affy--analysis of Affymetrix GeneChip data at the probe level. *Bioinformatics* **20:** 307-315

Gentleman R CV, Dudoit S, Irizarry R, Huber W (ed) (2005) *Smyth, G.K.Limma: linear models for microarray data. In: 'Bioinformatics and Computational Biology Solutions using R and Bioconductor'*: Springer, New York, 397-420pp

Gerlinger M, Rowan AJ, Horswell S, Larkin J, Endesfelder D, Gronroos E, Martinez P, Matthews N, Stewart A, Tarpey P, Varela I, Phillimore B, Begum S, McDonald NQ, Butler A, Jones D, Raine K, Latimer C, Santos CR, Nohadani M, Eklund AC, Spencer-Dene B, Clark G, Pickering L, Stamp G,

Gore M, Szallasi Z, Downward J, Futreal PA, Swanton C (2012) Intratumor heterogeneity and branched evolution revealed by multiregion sequencing. *N Engl J Med* **366:** 883-892

Goruppi S, Chiaruttini C, Ruaro ME, Varnum B, Schneider C (2001) Gas6 induces growth, beta-catenin stabilization, and T-cell factor transcriptional activation in contact-inhibited C57 mammary cells. *Mol Cell Biol* **21:** 902-915

Graham V, Khudyakov J, Ellis P, Pevny L (2003) SOX2 functions to maintain neural progenitor identity. *Neuron* **39:** 749-765

Gravendeel LA, Kouwenhoven MC, Gevaert O, de Rooi JJ, Stubbs AP, Duijm JE, Daemen A, Bleeker FE, Bralten LB, Kloosterhof NK, De Moor B, Eilers PH, van der Spek PJ, Kros JM, Sillevis Smitt PA, van den Bent MJ, French PJ (2009) Intrinsic gene expression profiles of gliomas are a better predictor of survival than histology. *Cancer Res* **69:** 9065-9072

Gritti A, Parati EA, Cova L, Frolichsthal P, Galli R, Wanke E, Faravelli L, Morassutti DJ, Roisen F, Nickel DD, Vescovi AL (1996) Multipotential stem cells from the adult mouse brain proliferate and self-renew in response to basic fibroblast growth factor. *J Neurosci* **16:** 1091-1100

Grygielko ET, Martin WM, Tweed C, Thornton P, Harling J, Brooks DP, Laping NJ (2005) Inhibition of gene markers of fibrosis with a novel inhibitor of transforming growth factor-beta type I receptor kinase in puromycin-induced nephritis. *J Pharmacol Exp Ther* **313:** 943-951

Gunther HS, Schmidt NO, Phillips HS, Kemming D, Kharbanda S, Soriano R, Modrusan Z, Meissner H, Westphal M, Lamszus K (2008) Glioblastoma-derived stem cell-enriched cultures form distinct subgroups according to molecular and phenotypic criteria. *Oncogene* **27:** 2897-2909

Ha SY, Jee BC, Suh CS, Kim HS, Oh SK, Kim SH, Moon SY (2005) Cryopreservation of human embryonic stem cells without the use of a programmable freezer. *Hum Reprod* **20:** 1779-1785

Hambardzumyan D, Becher OJ, Rosenblum MK, Pandolfi PP, Manova-Todorova K, Holland EC (2008) PI3K pathway regulates survival of cancer stem cells residing in the perivascular niche following radiation in medulloblastoma in vivo. *Genes Dev* **22:** 436-448

Hancock CR, Wetherington JP, Lambert NA, Condie BG (2000) Neuronal differentiation of cryopreserved neural progenitor cells derived from mouse embryonic stem cells. *Biochem Biophys Res Commun* **271:** 418-421

Hart MJ, de los Santos R, Albert IN, Rubinfeld B, Polakis P (1998) Downregulation of beta-catenin by human Axin and its association with the APC tumor suppressor, beta-catenin and GSK3 beta. *Curr Biol* **8:** 573-581

Hatanpaa KJ, Burma S, Zhao D, Habib AA (2010) Epidermal growth factor receptor in glioma: signal transduction, neuropathology, imaging, and radioresistance. *Neoplasia* **12:** 675-684

He XC, Zhang J, Tong WG, Tawfik O, Ross J, Scoville DH, Tian Q, Zeng X, He X, Wiedemann LM, Mishina Y, Li L (2004) BMP signaling inhibits intestinal stem cell self-renewal through suppression of Wnt-beta-catenin signaling. *Nat Genet* **36:** 1117-1121

Hemmati HD, Nakano I, Lazareff JA, Masterman-Smith M, Geschwind DH, Bronner-Fraser M, Kornblum HI (2003) Cancerous stem cells can arise from pediatric brain tumors. *Proc Natl Acad Sci U S A* **100:** 15178-15183

Hiscox S, Jiang WG (1999) Hepatocyte growth factor/scatter factor disrupts epithelial tumour cell-cell adhesion: involvement of beta-catenin. *Anticancer Res* **19:** 509-517

Hodgkinson CA, Moore KJ, Nakayama A, Steingrimsson E, Copeland NG, Jenkins NA, Arnheiter H (1993) Mutations at the mouse microphthalmia locus are associated with defects in a gene encoding a novel basic-helix-loop-helix-zipper protein. *Cell* **74:** 395-404

Hodgson JG, Yeh RF, Ray A, Wang NJ, Smirnov I, Yu M, Hariono S, Silber J, Feiler HS, Gray JW, Spellman PT, Vandenberg SR, Berger MS, James CD (2009) Comparative analyses of gene copy number and mRNA expression in glioblastoma multiforme tumors and xenografts. *Neuro Oncol* **11:** 477-487

Hovinga KE, Shimizu F, Wang R, Panagiotakos G, Van Der Heijden M, Moayedpardazi H, Correia AS, Soulet D, Major T, Menon J, Tabar V (2010) Inhibition of notch signaling in glioblastoma targets cancer stem cells via an endothelial cell intermediate. *Stem Cells* **28:** 1019-1029

Hu X, Pandolfi PP, Li Y, Koutcher JA, Rosenblum M, Holland EC (2005) mTOR promotes survival and astrocytic characteristics induced by Pten/AKT signaling in glioblastoma. *Neoplasia* **7:** 356-368

Huang SM, Mishina YM, Liu S, Cheung A, Stegmeier F, Michaud GA, Charlat O, Wiellette E, Zhang Y, Wiessner S, Hild M, Shi X, Wilson CJ, Mickanin C, Myer V, Fazal A, Tomlinson R, Serluca F, Shao W, Cheng H, Shultz M, Rau C, Schirle M, Schlegl J, Ghidelli S, Fawell S, Lu C, Curtis D, Kirschner MW, Lengauer C, Finan PM, Tallarico JA, Bouwmeester T, Porter JA, Bauer A, Cong F (2009) Tankyrase inhibition stabilizes axin and antagonizes Wnt signalling. *Nature* **461:** 614-620

Inda MM, Bonavia R, Mukasa A, Narita Y, Sah DW, Vandenberg S, Brennan C, Johns TG, Bachoo R, Hadwiger P, Tan P, Depinho RA, Cavenee W, Furnari F (2010) Tumor heterogeneity is an active process maintained by a mutant EGFR-induced cytokine circuit in glioblastoma. *Genes Dev* **24:** 1731-1745

Ivanova N, Dobrin R, Lu R, Kotenko I, Levorse J, DeCoste C, Schafer X, Lun Y, Lemischka IR (2006) Dissecting self-renewal in stem cells with RNA interference. *Nature* **442:** 533-538

Iwao K, Nakamori S, Kameyama M, Imaoka S, Kinoshita M, Fukui T, Ishiguro S, Nakamura Y, Miyoshi Y (1998) Activation of the beta-catenin gene by interstitial deletions involving exon 3 in primary colorectal carcinomas without adenomatous polyposis coli mutations. *Cancer Res* **58:** 1021-1026

Jacques TS, Swales A, Brzozowski MJ, Henriquez NV, Linehan JM, Mirzadeh Z, C OM, Naumann H, Alvarez-Buylla A, Brandner S (2010) Combinations of genetic mutations in the adult neural stem cell compartment determine brain tumour phenotypes. *Embo J* **29:** 222-235

Jamieson CH, Ailles LE, Dylla SJ, Muijtjens M, Jones C, Zehnder JL, Gotlib J, Li K, Manz MG, Keating A, Sawyers CL, Weissman IL (2004) Granulocyte-macrophage progenitors as candidate leukemic stem cells in blast-crisis CML. *N Engl J Med* **351:** 657-667

Jiang X, Yu Y, Yang HW, Agar NY, Frado L, Johnson MD (2010) The imprinted gene PEG3 inhibits Wnt signaling and regulates glioma growth. *J Biol Chem* **285:** 8472-8480

Kalani MY, Cheshier SH, Cord BJ, Bababeygy SR, Vogel H, Weissman IL, Palmer TD, Nusse R (2008) Wnt-mediated self-renewal of neural stem/progenitor cells. *Proc Natl Acad Sci U S A* **105:** 16970-16975

Kaneko Y, Sakakibara S, Imai T, Suzuki A, Nakamura Y, Sawamoto K, Ogawa Y, Toyama Y, Miyata T, Okano H (2000) Musashi1: an evolutionally conserved marker for CNS progenitor cells including neural stem cells. *Dev Neurosci* **22:** 139-153

Kasai M, Hamaguchi Y, Zhu SE, Miyake T, Sakurai T, Machida T (1992) High survival of rabbit morulae after vitrification in an ethylene glycol-based solution by a simple method. *Biol Reprod* **46:** 1042-1046

Kasai M, Komi JH, Takakamo A, Tsudera H, Sakurai T, Machida T (1990) A simple method for mouse embryo cryopreservation in a low toxicity vitrification solution, without appreciable loss of viability. *J Reprod Fertil* **89:** 91-97

Kawasaki Y, Senda T, Ishidate T, Koyama R, Morishita T, Iwayama Y, Higuchi O, Akiyama T (2000) Asef, a link between the tumor suppressor APC and G-protein signaling. *Science* **289:** 1194-1197

Kemper K, Sprick MR, de Bree M, Scopelliti A, Vermeulen L, Hoek M, Zeilstra J, Pals ST, Mehmet H, Stassi G, Medema JP (2010) The AC133 epitope, but not the CD133 protein, is lost upon cancer stem cell differentiation. *Cancer Res* **70:** 719-729

Kotliarova S, Pastorino S, Kovell LC, Kotliarov Y, Song H, Zhang W, Bailey R, Maric D, Zenklusen JC, Lee J, Fine HA (2008) Glycogen synthase kinase-3 inhibition induces glioma cell death through c-MYC, nuclear factor-kappaB, and glucose regulation. *Cancer Res* **68:** 6643-6651

Kwon CH, Zhao D, Chen J, Alcantara S, Li Y, Burns DK, Mason RP, Lee EY, Wu H, Parada LF (2008) Pten haploinsufficiency accelerates formation of high-grade astrocytomas. *Cancer Res* **68:** 3286-3294

Lamb J, Crawford ED, Peck D, Modell JW, Blat IC, Wrobel MJ, Lerner J, Brunet JP, Subramanian A, Ross KN, Reich M, Hieronymus H, Wei G, Armstrong SA, Haggarty SJ, Clemons PA, Wei R, Carr SA, Lander ES, Golub TR (2006) The Connectivity Map: using gene-expression signatures to connect small molecules, genes, and disease. *Science* **313:** 1929-1935

Lane M, Schoolcraft WB, Gardner DK (1999) Vitrification of mouse and human blastocysts using a novel cryoloop container-less technique. *Fertil Steril* **72:** 1073-1078

Lathia JD, Gallagher J, Heddleston JM, Wang J, Eyler CE, Macswords J, Wu Q, Vasanji A, McLendon RE, Hjelmeland AB, Rich JN (2010) Integrin alpha 6 regulates glioblastoma stem cells. *Cell Stem Cell* **6:** 421-432

Lathia JD, Hitomi M, Gallagher J, Gadani SP, Adkins J, Vasanji A, Liu L, Eyler CE, Heddleston JM, Wu Q, Minhas S, Soeda A, Hoeppner DJ, Ravin R, McKay RD, McLendon RE, Corbeil D, Chenn A, Hjelmeland AB, Park DM, Rich JN (2011) Distribution of CD133 reveals glioma stem cells self-renew through symmetric and asymmetric cell divisions. *Cell Death Dis* **2:** e200

Lathia JD, Mattson MP, Cheng A (2008) Notch: from neural development to neurological disorders. *J Neurochem* **107:** 1471-1481

Lee C, Fotovati A, Triscott J, Chen J, Venugopal C, Singhal A, Dunham C, Kerr JM, Verreault M, Yip S, Wakimoto H, Jones C, Jayanthan A, Narendran A, Singh SK, Dunn SE (2012) Polo-Like Kinase 1 (PLK1) Inhibition Kills Glioblastoma Multiforme Brain Tumour Cells in Part Through Loss of SOX2 and Delays Tumour Progression in Mice. *Stem Cells* **30:** 1064-1075

Lee J, Kotliarova S, Kotliarov Y, Li A, Su Q, Donin NM, Pastorino S, Purow BW, Christopher N, Zhang W, Park JK, Fine HA (2006) Tumor stem cells derived from glioblastomas cultured in bFGF and EGF more closely mirror the phenotype and genotype of primary tumors than do serum-cultured cell lines. *Cancer Cell* **9:** 391-403

Lee SM, Tole S, Grove E, McMahon AP (2000) A local Wnt-3a signal is required for development of the mammalian hippocampus. *Development* **127:** 457-467

Lee Y, Scheck AC, Cloughesy TF, Lai A, Dong J, Farooqi HK, Liau LM, Horvath S, Mischel PS, Nelson SF (2008) Gene expression analysis of glioblastomas identifies the major molecular basis for the prognostic benefit of younger age. *BMC Med Genomics* **1:** 52

Lei L, Sonabend AM, Guarnieri P, Soderquist C, Ludwig T, Rosenfeld S, Bruce JN, Canoll P (2011) Glioblastoma models reveal the connection between adult glial progenitors and the proneural phenotype. *PLoS One* **6:** e20041

Lepourcelet M, Chen YN, France DS, Wang H, Crews P, Petersen F, Bruseo C, Wood AW, Shivdasani RA (2004) Small-molecule antagonists of the oncogenic Tcf/beta-catenin protein complex. *Cancer Cell* **5:** 91-102

Lessard J, Sauvageau G (2003) Bmi-1 determines the proliferative capacity of normal and leukaemic stem cells. *Nature* **423:** 255-260

Li A, Walling J, Ahn S, Kotliarov Y, Su Q, Quezado M, Oberholtzer JC, Park J, Zenklusen JC, Fine HA (2009) Unsupervised analysis of transcriptomic profiles reveals six glioma subtypes. *Cancer Res* **69:** 2091-2099

Li A, Walling J, Kotliarov Y, Center A, Steed ME, Ahn SJ, Rosenblum M, Mikkelsen T, Zenklusen JC, Fine HA (2008) Genomic changes and gene expression profiles reveal that established glioma cell lines are poorly representative of primary human gliomas. *Mol Cancer Res* **6:** 21-30

Li C, Heidt DG, Dalerba P, Burant CF, Zhang L, Adsay V, Wicha M, Clarke MF, Simeone DM (2007) Identification of pancreatic cancer stem cells. *Cancer Res* **67:** 1030-1037

Li C, Wong WH (2001) Model-based analysis of oligonucleotide arrays: expression index computation and outlier detection. *Proc Natl Acad Sci U S A* **98:** 31-36

Lie DC, Colamarino SA, Song HJ, Desire L, Mira H, Consiglio A, Lein ES, Jessberger S, Lansford H, Dearie AR, Gage FH (2005) Wnt signalling regulates adult hippocampal neurogenesis. *Nature* **437:** 1370-1375

Lim E, Vaillant F, Wu D, Forrest NC, Pal B, Hart AH, Asselin-Labat ML, Gyorki DE, Ward T, Partanen A, Feleppa F, Huschtscha LI, Thorne HJ, Fox SB, Yan M, French JD, Brown MA, Smyth GK, Visvader JE, Lindeman GJ (2009) Aberrant luminal progenitors as the candidate target population for basal tumor development in BRCA1 mutation carriers. *Nat Med* **15:** 907-913

Lin M, Wei LJ, Sellers WR, Lieberfarb M, Wong WH, Li C (2004) dChipSNP: significance curve and clustering of SNP-array-based loss-of-heterozygosity data. *Bioinformatics* **20:** 1233-1240

Liu C, Sage JC, Miller MR, Verhaak RG, Hippenmeyer S, Vogel H, Foreman O, Bronson RT, Nishiyama A, Luo L, Zong H (2011a) Mosaic analysis with double markers reveals tumor cell of origin in glioma. *Cell* **146:** 209-221

Liu C, Tu Y, Sun X, Jiang J, Jin X, Bo X, Li Z, Bian A, Wang X, Liu D, Wang Z, Ding L (2011b) Wnt/beta-Catenin pathway in human glioma: expression pattern and clinical/prognostic correlations. *Clin Exp Med* **11:** 105-112

Liu X, Wang L, Zhao S, Ji X, Luo Y, Ling F (2011c) beta-Catenin overexpression in malignant glioma and its role in proliferation and apoptosis in glioblastma cells. *Med Oncol* **28:** 608-614

Lo HW, Cao X, Zhu H, Ali-Osman F (2008) Constitutively activated STAT3 frequently coexpresses with epidermal growth factor receptor in high-grade gliomas and targeting STAT3 sensitizes them to Iressa and alkylators. *Clin Cancer Res* **14:** 6042-6054

Lottaz C, Beier D, Meyer K, Kumar P, Hermann A, Schwarz J, Junker M, Oefner PJ, Bogdahn U, Wischhusen J, Spang R, Storch A, Beier CP (2010) Transcriptional profiles of CD133+ and CD133- glioblastoma-derived cancer stem cell lines suggest different cells of origin. *Cancer Res* **70:** 2030-2040

Louis DN, Ohgaki H, Wiestler OD, Cavenee WK, Burger PC, Jouvet A, Scheithauer BW, Kleihues P (2007) The 2007 WHO classification of tumours of the central nervous system. *Acta Neuropathol* **114:** 97-109

Ma S, Lee TK, Zheng BJ, Chan KW, Guan XY (2008) CD133+ HCC cancer stem cells confer chemoresistance by preferential expression of the Akt/PKB survival pathway. *Oncogene* **27:** 1749-1758

Madhavan S, Zenklusen JC, Kotliarov Y, Sahni H, Fine HA, Buetow K (2009) Rembrandt: helping personalized medicine become a reality through integrative translational research. *Mol Cancer Res* **7:** 157-167

Mannino M, Chalmers AJ (2011) Radioresistance of glioma stem cells: intrinsic characteristic or property of the 'microenvironment-stem cell unit'? *Mol Oncol* **5:** 374-386

Mazzoleni S, Politi LS, Pala M, Cominelli M, Franzin A, Sergi Sergi L, Falini A, De Palma M, Bulfone A, Poliani PL, Galli R (2010) Epidermal growth factor receptor expression identifies functionally and molecularly distinct tumor-initiating cells in human glioblastoma multiforme and is required for gliomagenesis. *Cancer Res* **70:** 7500-7513

McMahon AP, Bradley A (1990) The Wnt-1 (int-1) proto-oncogene is required for development of a large region of the mouse brain. *Cell* **62:** 1073-1085

Milosevic J, Storch A, Schwarz J (2005) Cryopreservation does not affect proliferation and multipotency of murine neural precursor cells. *Stem Cells* **23:** 681-688

Miyoshi Y, Nagase H, Ando H, Horii A, Ichii S, Nakatsuru S, Aoki T, Miki Y, Mori T, Nakamura Y (1992) Somatic mutations of the APC gene in colorectal tumors: mutation cluster region in the APC gene. *Hum Mol Genet* **1:** 229-233

Molyneux G, Geyer FC, Magnay FA, McCarthy A, Kendrick H, Natrajan R, Mackay A, Grigoriadis A, Tutt A, Ashworth A, Reis-Filho JS, Smalley MJ (2010) BRCA1 basal-like breast cancers originate from luminal epithelial progenitors and not from basal stem cells. *Cell Stem Cell* **7:** 403-417

Morali OG, Delmas V, Moore R, Jeanney C, Thiery JP, Larue L (2001) IGF-II induces rapid beta-catenin relocation to the nucleus during epithelium to mesenchyme transition. *Oncogene* **20:** 4942-4950

Mountford P, Nichols J, Zevnik B, O'Brien C, Smith A (1998) Maintenance of pluripotential embryonic stem cells by stem cell selection. *Reprod Fertil Dev* **10:** 527-533

Mukaida T, Wada S, Takahashi K, Pedro PB, An TZ, Kasai M (1998) Vitrification of human embryos based on the assessment of suitable conditions for 8-cell mouse embryos. *Hum Reprod* **13:** 2874-2879

Murphy M, Loosemore A, Ferrer I, Wesseling P, Wilkins PR, Bell BA (2002) Neuropathological diagnostic accuracy. *Br J Neurosurg* **16:** 461-464

Ng FS, Toh TB, Ting E, Koh GR, Sandanaraj E, Phong M, Wong SS, Leong SH, Kon OL, Tucker-Kellogg G, Ng WH, Ng I, Tang C, Ang BT (2012) Progenitor-Like Traits Contribute to Patient Survival and Prognosis in Oligodendroglial Tumors. *Clin Cancer Res* **18:** 4122-4135

Novak A, Hsu SC, Leung-Hagesteijn C, Radeva G, Papkoff J, Montesano R, Roskelley C, Grosschedl R, Dedhar S (1998) Cell adhesion and the integrin-linked kinase regulate the LEF-1 and beta-catenin signaling pathways. *Proc Natl Acad Sci U S A* **95:** 4374-4379

Nusse R, Brown A, Papkoff J, Scambler P, Shackleford G, McMahon A, Moon R, Varmus H (1991) A new nomenclature for int-1 and related genes: the Wnt gene family. *Cell* **64:** 231

Nusse R, Varmus HE (1982) Many tumors induced by the mouse mammary tumor virus contain a provirus integrated in the same region of the host genome. *Cell* **31:** 99-109

O'Brien CA, Pollett A, Gallinger S, Dick JE (2007) A human colon cancer cell capable of initiating tumour growth in immunodeficient mice. *Nature* **445:** 106-110

Ooi CH, Ivanova T, Wu J, Lee M, Tan IB, Tao J, Ward L, Koo JH, Gopalakrishnan V, Zhu Y, Cheng LL, Lee J, Rha SY, Chung HC, Ganesan K, So J, Soo KC, Lim D, Chan WH, Wong WK, Bowtell D, Yeoh KG, Grabsch H, Boussioutas A, Tan P (2009) Oncogenic pathway combinations predict clinical prognosis in gastric cancer. *PLoS Genet* **5:** e1000676

Panhuysen M, Vogt Weisenhorn DM, Blanquet V, Brodski C, Heinzmann U, Beisker W, Wurst W (2004) Effects of Wnt1 signaling on proliferation in the developing mid-/hindbrain region. *Mol Cell Neurosci* **26:** 101-111

Papkoff J, Aikawa M (1998) WNT-1 and HGF regulate GSK3 beta activity and beta-catenin signaling in mammary epithelial cells. *Biochem Biophys Res Commun* **247:** 851-858

Park IK, Qian D, Kiel M, Becker MW, Pihalja M, Weissman IL, Morrison SJ, Clarke MF (2003) Bmi-1 is required for maintenance of adult self-renewing haematopoietic stem cells. *Nature* **423:** 302-305

Penuelas S, Anido J, Prieto-Sanchez RM, Folch G, Barba I, Cuartas I, Garcia-Dorado D, Poca MA, Sahuquillo J, Baselga J, Seoane J (2009) TGF-beta increases glioma-initiating cell self-renewal through the induction of LIF in human glioblastoma. *Cancer Cell* **15:** 315-327

Persson AI, Petritsch C, Swartling FJ, Itsara M, Sim FJ, Auvergne R, Goldenberg DD, Vandenberg SR, Nguyen KN, Yakovenko S, Ayers-Ringler J, Nishiyama A, Stallcup WB, Berger MS, Bergers G, McKnight TR, Goldman SA, Weiss WA (2010) Non-stem cell origin for oligodendroglioma. *Cancer Cell* **18:** 669-682

Phillips HS, Kharbanda S, Chen R, Forrest WF, Soriano RH, Wu TD, Misra A, Nigro JM, Colman H, Soroceanu L, Williams PM, Modrusan Z, Feuerstein BG, Aldape K (2006a) Molecular subclasses of high-grade glioma predict prognosis, delineate a pattern of disease progression, and resemble stages in neurogenesis. *Cancer Cell* **9:** 157-173

Phillips TM, McBride WH, Pajonk F (2006b) The response of CD24(-/low)/CD44+ breast cancer-initiating cells to radiation. *J Natl Cancer Inst* **98:** 1777-1785

Playford MP, Bicknell D, Bodmer WF, Macaulay VM (2000) Insulin-like growth factor 1 regulates the location, stability, and transcriptional activity of beta-catenin. *Proc Natl Acad Sci U S A* **97:** 12103-12108

Polakis P (1999) The oncogenic activation of beta-catenin. *Curr Opin Genet Dev* **9:** 15-21

Polakis P (2000) Wnt signaling and cancer. *Genes Dev* **14:** 1837-1851

Polakis P (2007) The many ways of Wnt in cancer. *Curr Opin Genet Dev* **17:** 45-51

Pollard SM, Yoshikawa K, Clarke ID, Danovi D, Stricker S, Russell R, Bayani J, Head R, Lee M, Bernstein M, Squire JA, Smith A, Dirks P (2009) Glioma stem cell lines expanded in adherent culture have tumor-specific phenotypes and are suitable for chemical and genetic screens. *Cell Stem Cell* **4:** 568-580

Proffitt KD, Madan B, Ke Z, Pendharkar V, Ding L, Lee MA, Hannoush RN, Virshup DM (2012) Pharmacological inhibition of the Wnt acyltransferase PORCN prevents growth of WNT-driven mammary cancer. *Cancer Res*

Pu P, Zhang Z, Kang C, Jiang R, Jia Z, Wang G, Jiang H (2009) Downregulation of Wnt2 and beta-catenin by siRNA suppresses malignant glioma cell growth. *Cancer Gene Ther* **16:** 351-361

Purow BW, Haque RM, Noel MW, Su Q, Burdick MJ, Lee J, Sundaresan T, Pastorino S, Park JK, Mikolaenko I, Maric D, Eberhart CG, Fine HA (2005) Expression of Notch-1 and its ligands, Delta-like-1 and Jagged-1, is critical for glioma cell survival and proliferation. *Cancer Res* **65:** 2353-2363

Quintana E, Shackleton M, Sabel MS, Fullen DR, Johnson TM, Morrison SJ (2008) Efficient tumour formation by single human melanoma cells. *Nature* **456:** 593-598

Rall WF, Wood MJ, Kirby C, Whittingham DG (1987) Development of mouse embryos cryopreserved by vitrification. *J Reprod Fertil* **80:** 499-504

Reilly KM, Loisel DA, Bronson RT, McLaughlin ME, Jacks T (2000) Nf1;Trp53 mutant mice develop glioblastoma with evidence of strain-specific effects. *Nat Genet* **26:** 109-113

Reubinoff BE, Pera MF, Vajta G, Trounson AO (2001) Effective cryopreservation of human embryonic stem cells by the open pulled straw vitrification method. *Hum Reprod* **16:** 2187-2194

Reya T, Clevers H (2005) Wnt signalling in stem cells and cancer. *Nature* **434:** 843-850

Reya T, Duncan AW, Ailles L, Domen J, Scherer DC, Willert K, Hintz L, Nusse R, Weissman IL (2003) A role for Wnt signalling in self-renewal of haematopoietic stem cells. *Nature* **423:** 409-414

Reya T, Morrison SJ, Clarke MF, Weissman IL (2001) Stem cells, cancer, and cancer stem cells. *Nature* **414:** 105-111

Reynolds BA, Rietze RL (2005) Neural stem cells and neurospheres--re-evaluating the relationship. *Nat Methods* **2:** 333-336

Reynolds BA, Tetzlaff W, Weiss S (1992) A multipotent EGF-responsive striatal embryonic progenitor cell produces neurons and astrocytes. *J Neurosci* **12:** 4565-4574

Rich JN, Eyler CE (2009) Cancer Stem Cells in Brain Tumor Biology. *Cold Spring Harb Symp Quant Biol*

Richards M, Fong CY, Tan S, Chan WK, Bongso A (2004) An efficient and safe xeno-free cryopreservation method for the storage of human embryonic stem cells. *Stem Cells* **22:** 779-789

Rietze RL, Valcanis H, Brooker GF, Thomas T, Voss AK, Bartlett PF (2001) Purification of a pluripotent neural stem cell from the adult mouse brain. *Nature* **412:** 736-739

Roose J, Huls G, van Beest M, Moerer P, van der Horn K, Goldschmeding R, Logtenberg T, Clevers H (1999) Synergy between tumor suppressor APC and the beta-catenin-Tcf4 target Tcf1. *Science* **285:** 1923-1926

Rowan AJ, Lamlum H, Ilyas M, Wheeler J, Straub J, Papadopoulou A, Bicknell D, Bodmer WF, Tomlinson IP (2000) APC mutations in sporadic colorectal tumors: A mutational "hotspot" and interdependence of the "two hits". *Proc Natl Acad Sci U S A* **97:** 3352-3357

Saha S, Otoi T, Takagi M, Boediono A, Sumantri C, Suzuki T (1996) Normal calves obtained after direct transfer of vitrified bovine embryos using ethylene glycol, trehalose, and polyvinylpyrrolidone. *Cryobiology* **33:** 291-299

Sakariassen PO, Prestegarden L, Wang J, Skaftnesmo KO, Mahesparan R, Molthoff C, Sminia P, Sundlisaeter E, Misra A, Tysnes BB, Chekenya M, Peters H, Lende G, Kalland KH, Oyan AM, Petersen K, Jonassen I, van der Kogel A, Feuerstein BG, Terzis AJ, Bjerkvig R, Enger PO (2006) Angiogenesis-independent tumor growth mediated by stem-like cancer cells. *Proc Natl Acad Sci U S A* **103:** 16466-16471

Sareddy GR, Challa S, Panigrahi M, Babu PP (2009a) Wnt/beta-catenin/Tcf signaling pathway activation in malignant progression of rat gliomas induced by transplacental N-ethyl-N-nitrosourea exposure. *Neurochem Res* **34:** 1278-1288

Sareddy GR, Panigrahi M, Challa S, Mahadevan A, Babu PP (2009b) Activation of Wnt/beta-catenin/Tcf signaling pathway in human astrocytomas. *Neurochem Int* **55:** 307-317

Schepsky A, Bruser K, Gunnarsson GJ, Goodall J, Hallsson JH, Goding CR, Steingrimsson E, Hecht A (2006) The microphthalmia-associated transcription factor Mitf interacts with beta-catenin to determine target gene expression. *Mol Cell Biol* **26:** 8914-8927

Shackleton M, Quintana E, Fearon ER, Morrison SJ (2009) Heterogeneity in cancer: cancer stem cells versus clonal evolution. *Cell* **138:** 822-829

Shats I, Gatza ML, Chang JT, Mori S, Wang J, Rich J, Nevins JR (2011) Using a stem cell-based signature to guide therapeutic selection in cancer. *Cancer Res* **71:** 1772-1780

Shen R, Mo Q, Schultz N, Seshan VE, Olshen AB, Huse J, Ladanyi M, Sander C (2012) Integrative subtype discovery in glioblastoma using iCluster. *PLoS One* **7:** e35236

Shih AH, Dai C, Hu X, Rosenblum MK, Koutcher JA, Holland EC (2004) Dose-dependent effects of platelet-derived growth factor-B on glial tumorigenesis. *Cancer Res* **64:** 4783-4789

Shinojima N, Tada K, Shiraishi S, Kamiryo T, Kochi M, Nakamura H, Makino K, Saya H, Hirano H, Kuratsu J, Oka K, Ishimaru Y, Ushio Y (2003) Prognostic value of epidermal growth factor receptor in patients with glioblastoma multiforme. *Cancer Res* **63:** 6962-6970

Singec I, Knoth R, Meyer RP, Maciaczyk J, Volk B, Nikkhah G, Frotscher M, Snyder EY (2006) Defining the actual sensitivity and specificity of the neurosphere assay in stem cell biology. *Nat Methods* **3:** 801-806

Singh SK, Clarke ID, Terasaki M, Bonn VE, Hawkins C, Squire J, Dirks PB (2003) Identification of a cancer stem cell in human brain tumors. *Cancer Res* **63:** 5821-5828

Singh SK, Hawkins C, Clarke ID, Squire JA, Bayani J, Hide T, Henkelman RM, Cusimano MD, Dirks PB (2004) Identification of human brain tumour initiating cells. *Nature* **432:** 396-401

Son MJ, Woolard K, Nam DH, Lee J, Fine HA (2009) SSEA-1 is an enrichment marker for tumor-initiating cells in human glioblastoma. *Cell Stem Cell* **4:** 440-452

Sparks AB, Morin PJ, Vogelstein B, Kinzler KW (1998) Mutational analysis of the APC/beta-catenin/Tcf pathway in colorectal cancer. *Cancer Res* **58:** 1130-1134

Subramanian A, Tamayo P, Mootha VK, Mukherjee S, Ebert BL, Gillette MA, Paulovich A, Pomeroy SL, Golub TR, Lander ES, Mesirov JP (2005) Gene set enrichment analysis: a knowledge-based approach for interpreting genome-wide expression profiles. *Proc Natl Acad Sci U S A* **102:** 15545-15550

Svendsen CN, ter Borg MG, Armstrong RJ, Rosser AE, Chandran S, Ostenfeld T, Caldwell MA (1998) A new method for the rapid and long term growth of human neural precursor cells. *J Neurosci Methods* **85:** 141-152

Takahashi K, Yamanaka S (2006) Induction of pluripotent stem cells from mouse embryonic and adult fibroblast cultures by defined factors. *Cell* **126:** 663-676

Tan FC, Lee KH, Gouk SS, Magalhaes R, Poonepalli A, Hande MP, Dawe GS, Kuleshova LL (2007) Optimization of cryopreservation of stem cells cultured as neurospheres: comparison between vitrification, slow-cooling and rapid cooling freezing protocols. *Cryo Letters* **28:** 445-460

Tanaka K, Kitagawa Y, Kadowaki T (2002) Drosophila segment polarity gene product porcupine stimulates the posttranslational N-glycosylation of wingless in the endoplasmic reticulum. *J Biol Chem* **277:** 12816-12823

Team RDC (2009) R: A language and environment for statistical computing; version 2.10.1. *R Foundation for Statistical Computing, Vienna, Austria ISBN 3-900051-07-0*

Tibshirani R, Hastie T, Narasimhan B, Chu G (2002) Diagnosis of multiple cancer types by shrunken centroids of gene expression. *Proc Natl Acad Sci U S A* **99:** 6567-6572

Tohyama T, Lee VM, Rorke LB, Marvin M, McKay RD, Trojanowski JQ (1992) Nestin expression in embryonic human neuroepithelium and in human neuroepithelial tumor cells. *Lab Invest* **66:** 303-313

Uchida N, Buck DW, He D, Reitsma MJ, Masek M, Phan TV, Tsukamoto AS, Gage FH, Weissman IL (2000) Direct isolation of human central nervous system stem cells. *Proc Natl Acad Sci U S A* **97:** 14720-14725

Ugurel S, Houben R, Schrama D, Voigt H, Zapatka M, Schadendorf D, Brocker EB, Becker JC (2007) Microphthalmia-associated transcription factor gene amplification in metastatic melanoma is a prognostic marker for patient survival, but not a predictive marker for chemosensitivity and chemotherapy response. *Clin Cancer Res* **13:** 6344-6350

Uhrbom L, Dai C, Celestino JC, Rosenblum MK, Fuller GN, Holland EC (2002) Ink4a-Arf loss cooperates with KRas activation in astrocytes and neural progenitors to generate glioblastomas of various morphologies depending on activated Akt. *Cancer Res* **62:** 5551-5558

Verhaak RG, Hoadley KA, Purdom E, Wang V, Qi Y, Wilkerson MD, Miller CR, Ding L, Golub T, Mesirov JP, Alexe G, Lawrence M, O'Kelly M, Tamayo P, Weir BA, Gabriel S, Winckler W, Gupta S, Jakkula L, Feiler HS, Hodgson JG, James CD, Sarkaria JN, Brennan C, Kahn A, Spellman PT, Wilson RK, Speed TP, Gray JW, Meyerson M, Getz G, Perou CM, Hayes DN (2010) Integrated genomic analysis identifies clinically relevant subtypes of glioblastoma characterized by abnormalities in PDGFRA, IDH1, EGFR, and NF1. *Cancer Cell* **17:** 98-110

Vermeulen L, De Sousa EMF, van der Heijden M, Cameron K, de Jong JH, Borovski T, Tuynman JB, Todaro M, Merz C, Rodermond H, Sprick MR, Kemper K, Richel DJ, Stassi G, Medema JP (2010) Wnt activity defines colon cancer stem cells and is regulated by the microenvironment. *Nat Cell Biol* **12:** 468-476

Vescovi AL, Galli R, Reynolds BA (2006) Brain tumour stem cells. *Nat Rev Cancer* **6:** 425-436

Visvader JE (2011) Cells of origin in cancer. *Nature* **469:** 314-322

Wakimoto H, Mohapatra G, Kanai R, Curry WT, Jr., Yip S, Nitta M, Patel AP, Barnard ZR, Stemmer-Rachamimov AO, Louis DN, Martuza RL, Rabkin SD (2012) Maintenance of primary tumor phenotype and genotype in glioblastoma stem cells. *Neuro Oncol* **14:** 132-144

Wang HM, Yang XJ, Dong XT, Li Y, Wang W, Ming HL, Zhang B, Yu SP (2011) [Correlation between the distribution of CD133-positive cells and the proliferation of microvessels in glioblastoma multiforme]. *Zhonghua Yi Xue Za Zhi* **91:** 781-785

Wang J, Miletic H, Sakariassen PO, Huszthy PC, Jacobsen H, Brekka N, Li X, Zhao P, Mork S, Chekenya M, Bjerkvig R, Enger PO (2009) A reproducible brain tumour model established from human glioblastoma biopsies. *BMC Cancer* **9:** 465

Wang J, Wakeman TP, Lathia JD, Hjelmeland AB, Wang XF, White RR, Rich JN, Sullenger BA (2010) Notch promotes radioresistance of glioma stem cells. *Stem Cells* **28:** 17-28

Wang J, Wang H, Li Z, Wu Q, Lathia JD, McLendon RE, Hjelmeland AB, Rich JN (2008) c-Myc is required for maintenance of glioma cancer stem cells. *PLoS One* **3:** e3769

Widlund HR, Horstmann MA, Price ER, Cui J, Lessnick SL, Wu M, He X, Fisher DE (2002) Beta-catenin-induced melanoma growth requires the downstream target Microphthalmia-associated transcription factor. *J Cell Biol* **158:** 1079-1087

Wiedemeyer WR, Dunn IF, Quayle SN, Zhang J, Chheda MG, Dunn GP, Zhuang L, Rosenbluh J, Chen S, Xiao Y, Shapiro GI, Hahn WC, Chin L (2010) Pattern of retinoblastoma pathway inactivation dictates response to CDK4/6 inhibition in GBM. *Proc Natl Acad Sci U S A* **107:** 11501-11506

Willert K, Brown JD, Danenberg E, Duncan AW, Weissman IL, Reya T, Yates JR, 3rd, Nusse R (2003) Wnt proteins are lipid-modified and can act as stem cell growth factors. *Nature* **423:** 448-452

Wolfe MS, Citron M, Diehl TS, Xia W, Donkor IO, Selkoe DJ (1998) A substrate-based difluoro ketone selectively inhibits Alzheimer's gamma-secretase activity. *J Med Chem* **41:** 6-9

Woodward WA, Chen MS, Behbod F, Alfaro MP, Buchholz TA, Rosen JM (2007) WNT/beta-catenin mediates radiation resistance of mouse mammary progenitor cells. *Proc Natl Acad Sci U S A* **104:** 618-623

Yan D, Wiesmann M, Rohan M, Chan V, Jefferson AB, Guo L, Sakamoto D, Caothien RH, Fuller JH, Reinhard C, Garcia PD, Randazzo FM, Escobedo J, Fantl WJ, Williams LT (2001) Elevated expression of axin2 and hnkd mRNA provides evidence that Wnt/beta -catenin signaling is activated in human colon tumors. *Proc Natl Acad Sci U S A* **98:** 14973-14978

Yan X, Ma L, Yi D, Yoon JG, Diercks A, Foltz G, Price ND, Hood LE, Tian Q (2011) A CD133-related gene expression signature identifies an aggressive glioblastoma subtype with excessive mutations. *Proc Natl Acad Sci U S A* **108:** 1591-1596

Yasumoto K, Takeda K, Saito H, Watanabe K, Takahashi K, Shibahara S (2002) Microphthalmia-associated transcription factor interacts with LEF-1, a mediator of Wnt signaling. *Embo J* **21:** 2703-2714

Yauch RL, Gould SE, Scales SJ, Tang T, Tian H, Ahn CP, Marshall D, Fu L, Januario T, Kallop D, Nannini-Pepe M, Kotkow K, Marsters JC, Rubin LL, de Sauvage FJ (2008) A paracrine requirement for hedgehog signalling in cancer. *Nature* **455:** 406-410

Yeo CW, Ng FS, Chai C, Tan JM, Koh GR, Chong YK, Koh LW, Foong CS, Sandanaraj E, Holbrook JD, Ang BT, Takahashi R, Tang C, Lim KL (2012) Parkin pathway activation mitigates glioma cell proliferation and predicts patient survival. *Cancer Res* **72:** 2543-2553

Yokota Y, Sato S, Yokota M, Ishikawa Y, Makita M, Asada T, Araki Y (2000) Successful pregnancy following blastocyst vitrification: case report. *Hum Reprod* **15:** 1802-1803

Yuan X, Curtin J, Xiong Y, Liu G, Waschsmann-Hogiu S, Farkas DL, Black KL, Yu JS (2004) Isolation of cancer stem cells from adult glioblastoma multiforme. *Oncogene* **23:** 9392-9400

Zhang N, Wei P, Gong A, Chiu WT, Lee HT, Colman H, Huang H, Xue J, Liu M, Wang Y, Sawaya R, Xie K, Yung WK, Medema RH, He X, Huang S (2011) FoxM1 promotes beta-catenin nuclear localization and controls Wnt target-gene expression and glioma tumorigenesis. *Cancer Cell* **20:** 427-442

Zhang T, Otevrel T, Gao Z, Ehrlich SM, Fields JZ, Boman BM (2001) Evidence that APC regulates survivin expression: a possible mechanism contributing to the stem cell origin of colon cancer. *Cancer Res* **61:** 8664-8667

Zhao C, Blum J, Chen A, Kwon HY, Jung SH, Cook JM, Lagoo A, Reya T (2007) Loss of beta-catenin impairs the renewal of normal and CML stem cells in vivo. *Cancer Cell* **12:** 528-541

Zhao C, Deng W, Gage FH (2008) Mechanisms and functional implications of adult neurogenesis. *Cell* **132:** 645-660

Zheng H, Ying H, Wiedemeyer R, Yan H, Quayle SN, Ivanova EV, Paik JH, Zhang H, Xiao Y, Perry SR, Hu J, Vinjamoori A, Gan B, Sahin E, Chheda MG, Brennan C, Wang YA, Hahn WC, Chin L, DePinho RA (2010) PLAGL2

regulates Wnt signaling to impede differentiation in neural stem cells and gliomas. *Cancer Cell* **17:** 497-509

Zheng H, Ying H, Yan H, Kimmelman AC, Hiller DJ, Chen AJ, Perry SR, Tonon G, Chu GC, Ding Z, Stommel JM, Dunn KL, Wiedemeyer R, You MJ, Brennan C, Wang YA, Ligon KL, Wong WH, Chin L, DePinho RA (2008) p53 and Pten control neural and glioma stem/progenitor cell renewal and differentiation. *Nature* **455:** 1129-1133

Zhou F, Cui C, Ge Y, Chen H, Li Q, Yang Z, Wu G, Sun S, Chen K, Gu J, Jiang J, Wei Y (2010) Alpha2,3-Sialylation regulates the stability of stem cell marker CD133. *J Biochem* **148:** 273-280

Zhu H, Acquaviva J, Ramachandran P, Boskovitz A, Woolfenden S, Pfannl R, Bronson RT, Chen JW, Weissleder R, Housman DE, Charest A (2009) Oncogenic EGFR signaling cooperates with loss of tumor suppressor gene functions in gliomagenesis. *Proc Natl Acad Sci U S A* **106:** 2712-2716

Zhu TS, Costello MA, Talsma CE, Flack CG, Crowley JG, Hamm LL, He X, Hervey-Jumper SL, Heth JA, Muraszko KM, DiMeco F, Vescovi AL, Fan X (2011) Endothelial cells create a stem cell niche in glioblastoma by providing NOTCH ligands that nurture self-renewal of cancer stem-like cells. *Cancer Res* **71:** 6061-6072

Zhu Y, Guignard F, Zhao D, Liu L, Burns DK, Mason RP, Messing A, Parada LF (2005) Early inactivation of p53 tumor suppressor gene cooperating with NF1 loss induces malignant astrocytoma. *Cancer Cell* **8:** 119-130

10. SUPPLEMENTARY FIGURES AND TABLES

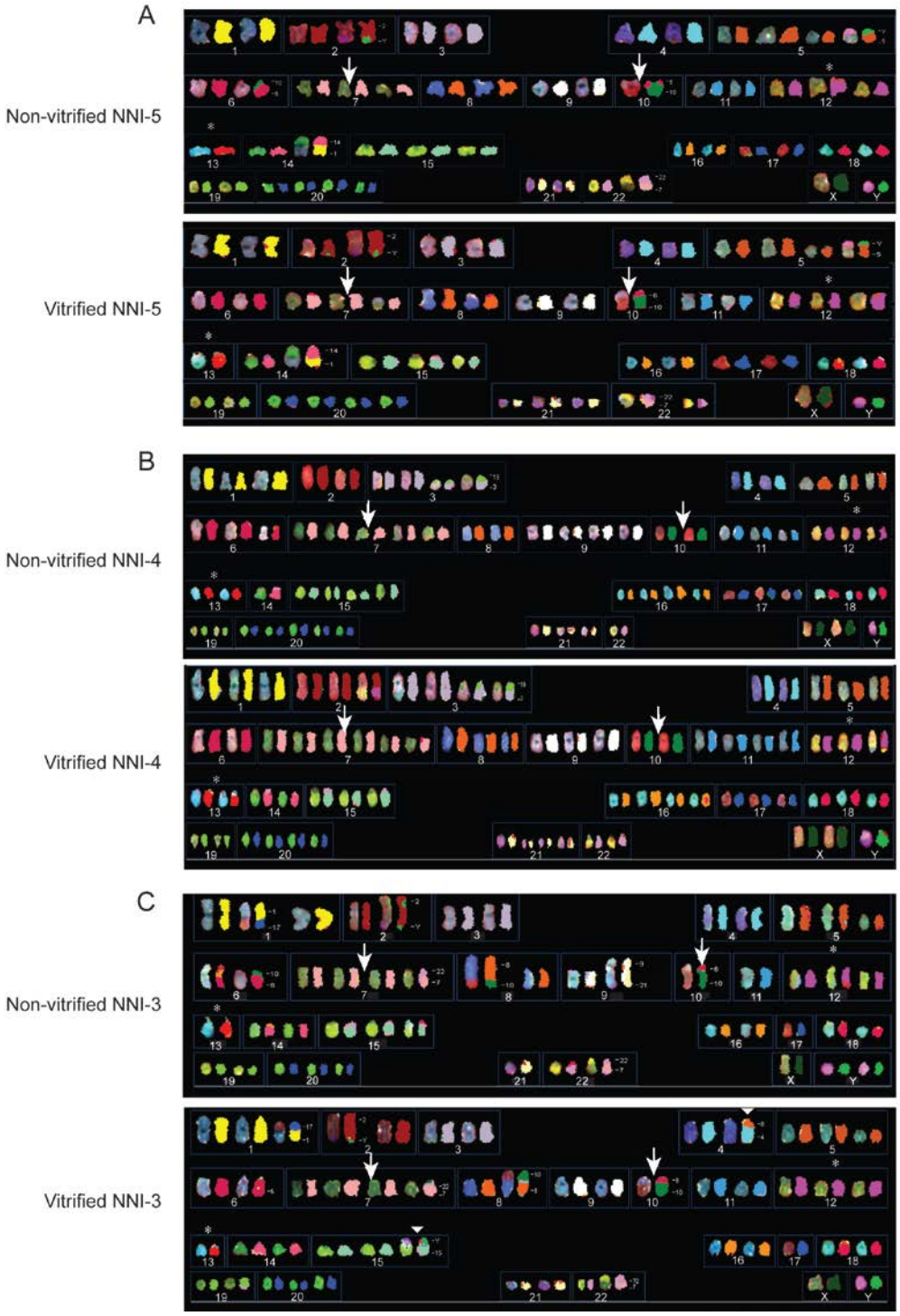

Supplementary Figure S1. Spectral karyotyping analyses. Data for all other patients' gliomaspheres are shown. A total of 15-20 metaphases were karyotyped for each sample. Arrows indicate polysomy of chromosome 7 and loss of chromosome 10. Asterisks indicate aneusomy of chromosomes 12 and 13. Karyotypic changes were observed in NNI-3 non-vitrified sample and these are indicated with arrowheads: t(15;y), t(4;8).

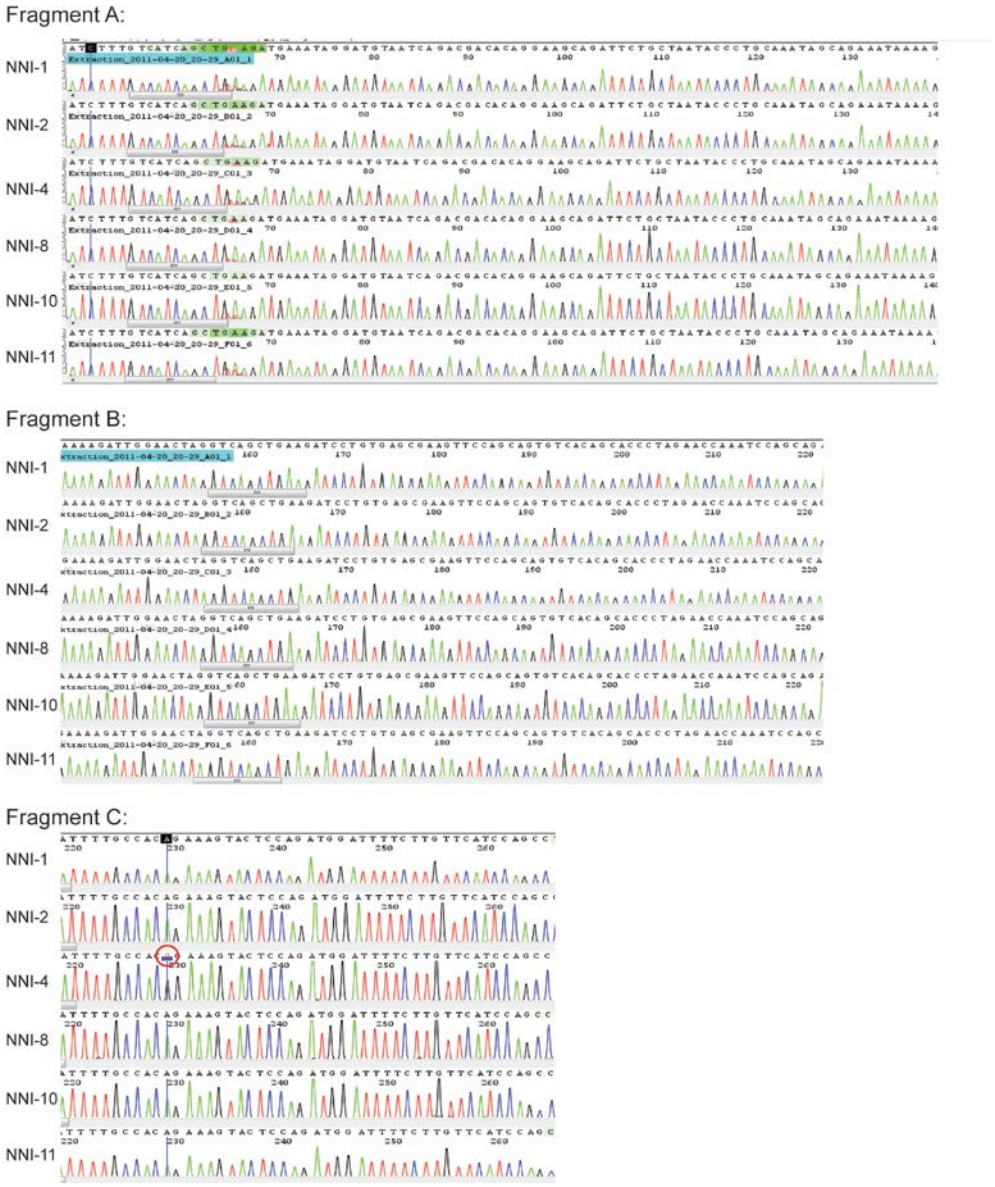

Supplementary Figure S2. Common mutations of APC in the mutation cluster region (MCR) are absent in GPCs. Electropherograms showing absence of mutations in majority of GPCs sequenced between codons 1255 and 1513 (Fragments A-C). We observed a degenrate base substitution (circled in red) on codon 1493 (ACG --> ACA) for NNI-4 GPC that does not result in change in amino acid sequence.

Supplementary Table S1. Confusion Matrix for cross-validation of Phillips classification signature. Mes, Mesenchymal; PN, Proneural; Prolif, Proliferative.

		Predicted			
		Mes	**PN**	**Prolif**	**Class Error Rate**
Actual	**Mes**	30	0	5	0.14285714
	PN	2	34	1	0.08108108
	Prolif	4	0	24	0.14285714
Overall Error Rate				0.12	

Supplementary Table S2. Probesets in the oligodendroglial GPC gene signature.

Probeset ID	Entrez Gene ID	Gene Symbol	Description	Log Fold-Change
212507_at	23505	TMEM131	transmembrane protein 131	-0.931307621
241612_at	27022	FOXD3	forkhead box D3	1.372986027
201368_at	678	ZFP36L2	zinc finger protein 36, C3H type-like 2	-1.105289687
201369_s_at	678	ZFP36L2	zinc finger protein 36, C3H type-like 2	-0.904474969
201564_s_at	6624	FSCN1	fascin homolog 1, actin-bundling protein (Strongylocentrotus purpuratus)	-1.072722937
220231_at	10842	C7orf16	chromosome 7 open reading frame 16	2.645835821
228035_at	65975	STK33	serine/threonine kinase 33	-1.243243529
215241_at	63982	ANO3	anoctamin 3	1.090294876
218163_at	28985	MCTS1	malignant T cell amplified sequence 1	1.017692402
231840_x_at	90624	LYRM7	Lyrm7 homolog (mouse)	0.891245471
206067_s_at	7490	WT1	Wilms tumor 1	0.827289917
218988_at	55508	SLC35E3	solute carrier family 35, member E3	1.67648345
205386_s_at	4193	MDM2	Mdm2 p53 binding protein homolog (mouse)	1.884030655
211832_s_at	4193	MDM2	Mdm2 p53 binding protein homolog (mouse)	1.788934315
1553426_at	285668	C5orf64	chromosome 5 open reading frame 64	-1.147145398
211138_s_at	8564	KMO	kynurenine 3-monooxygenase (kynurenine 3-hydroxylase)	1.260883191
205306_x_at	8564	KMO	kynurenine 3-monooxygenase (kynurenine 3-hydroxylase)	1.335650833
241765_at	1368	CPM	carboxypeptidase M	3.226405764
243403_x_at	1368	CPM	carboxypeptidase M	2.660052824
225591_at	26260	FBXO25	F-box protein 25	1.023236638

1557260_a_at	84911	ZNF382	zinc finger protein 382	1.763574339
209565_at	7737	RNF113A	ring finger protein 113A	0.993408597
235502_at	5515	PPP2CA	protein phosphatase 2, catalytic subunit, alpha isozyme	1.026294597
243282_at	54520	CCDC93	coiled-coil domain containing 93	-0.893187785
226462_at	29091	STXBP6	syntaxin binding protein 6 (amisyn)	1.408107909
236290_at	220164	DOK6	docking protein 6	0.808537521
214440_at	9	NAT1	N-acetyltransferase 1 (arylamine N-acetyltransferase)	1.762236745
50400_at	196743	PAOX	polyamine oxidase (exo-N4-amino)	1.059361819
237029_at	3081	HGD	homogentisate 1,2-dioxygenase	0.971522564
244829_at	--	C6orf218	chromosome 6 open reading frame 218	1.411926375
227109_at	120227	CYP2R1	cytochrome P450, family 2, subfamily R, polypeptide 1	1.414119526
225846_at	54845	ESRP1	epithelial splicing regulatory protein 1	1.270624793
219121_s_at	54845	ESRP1	epithelial splicing regulatory protein 1	1.120675543
213638_at	221692	PHACTR1	phosphatase and actin regulator 1	1.535840464
215000_s_at	9637	FEZ2	fasciculation and elongation protein zeta 2 (zygin II)	-0.957606762
242989_at	6801	STRN	striatin, calmodulin binding protein	-1.055129989
204077_x_at	9583	ENTPD4	ectonucleoside triphosphate diphosphohydrolase 4	0.815264939
218870_at	55843	ARHGAP15	Rho GTPase activating protein 15	1.017607164
221427_s_at	81669	CCNL2	cyclin L2	-0.850386591
222999_s_at	81669	CCNL2	cyclin L2	-0.954468271
205512_s_at	9131	AIFM1	apoptosis-inducing factor, mitochondrion-associated, 1	0.954516011
207344_at	10566	AKAP3	A kinase (PRKA) anchor protein 3	2.654311598
244825_at	57477	SHROOM4	shroom family member 4	1.054431061
205281_s_at	5277	PIGA	phosphatidylinositol glycan anchor biosynthesis, class A	0.836793751
226764_at	152485	ZNF827	zinc finger protein 827	-0.996757033

1554509_a_at	80013	FAM188A	family with sequence similarity 188, member A	1.293780634
206334_at	8513	LIPF	lipase, gastric	1.947198374
204644_at	10495	ENOX2	ecto-NOX disulfide-thiol exchanger 2	0.879076665
218807_at	10451	VAV3	vav 3 guanine nucleotide exchange factor	-1.573828653
223423_at	26996	GPR160	G protein-coupled receptor 160	1.266788929
215153_at	9722	NOS1AP	nitric oxide synthase 1 (neuronal) adaptor protein	-0.882741057
1563512_at	9722	NOS1AP	nitric oxide synthase 1 (neuronal) adaptor protein	-1.07867364
37512_at	8630	HSD17B6	hydroxysteroid (17-beta) dehydrogenase 6 homolog (mouse)	1.128384226
212631_at	8417	STX7	syntaxin 7	1.113525058
225308_s_at	85461	TANC1	tetratricopeptide repeat, ankyrin repeat and coiled-coil containing 1	-0.854227497
200665_s_at	6678	SPARC	secreted protein, acidic, cysteine-rich (osteonectin)	-1.027737524
229000_at	58492	ZNF77	zinc finger protein 77	0.944812365
204759_at	1102	RCBTB2	regulator of chromosome condensation (RCC1) and BTB (POZ) domain containing protein 2	-1.668131465
221289_at	1750	DLX6	distal-less homeobox 6	1.041848794
206552_s_at	6863	TAC1	tachykinin, precursor 1	1.705027503
222767_s_at	79794	C12orf49	chromosome 12 open reading frame 49	0.808709328
204713_s_at	2153	F5	coagulation factor V (proaccelerin, labile factor)	1.431619627
204714_s_at	2153	F5	coagulation factor V (proaccelerin, labile factor)	1.504311671
206426_at	2315	MLANA	melan-A	0.890635292
206427_s_at	2315	MLANA	melan-A	1.431212371
206135_at	9705	ST18	suppression of tumorigenicity 18 (breast carcinoma) (zinc finger protein)	1.131230985
206058_at	6539	SLC6A12	solute carrier family 6 (neurotransmitter transporter, betaine/GABA), member 12	1.091850355
1561969_at	131368	ZPLD1	zona pellucida-like domain containing 1	1.316003453

224999_at	1956	EGFR	epidermal growth factor receptor	-1.990616663
201983_s_at	1956	EGFR	epidermal growth factor receptor	-2.165112816
204238_s_at	10591	C6orf108	chromosome 6 open reading frame 108	1.111934072
242727_at	221079	ARL5B	ADP-ribosylation factor-like 5B	1.32300753
235356_at	374354	NHLRC2	NHL repeat containing 2	0.931504627
231569_at	203562	TMEM31	transmembrane protein 31	1.032880572
205647_at	5893	RAD52	RAD52 homolog (S. cerevisiae)	-0.833601355
202746_at	9452	ITM2A	integral membrane protein 2A	3.632094429
202747_s_at	9452	ITM2A	integral membrane protein 2A	3.720860606
228891_at	10507	SEMA4D	sema domain, immunoglobulin domain (Ig), transmembrane domain (TM) and short cytoplasmic domain, (semaphorin) 4D	0.981611103
207540_s_at	6850	SYK	spleen tyrosine kinase	1.381598219
204011_at	10253	SPRY2	sprouty homolog 2 (Drosophila)	-0.96891126
221035_s_at	56155	TEX14	testis expressed 14	0.988947099
209848_s_at	6490	PMEL	premelanosome protein	1.830948971
215643_at	223117	SEMA3D	sema domain, immunoglobulin domain (Ig), short basic domain, secreted, (semaphorin) 3D	0.977345169
203122_at	51112	TTC15	tetratricopeptide repeat domain 15	-1.208989641
231068_at	146802	SLC47A2	solute carrier family 47, member 2	-1.501602291
239738_at	117154	DACH2	dachshund homolog 2 (Drosophila)	1.361110621
225651_at	7325	UBE2E2	ubiquitin-conjugating enzyme E2E 2 (UBC4/5 homolog, yeast)	1.451235296
244419_at	2487	FRZB	frizzled-related protein	1.045474278
219212_at	51182	HSPA14	heat shock 70kDa protein 14	0.825224502
206375_s_at	8988	HSPB3	heat shock 27kDa protein 3	1.769496044
219099_at	57103	C12orf5	chromosome 12 open reading frame 5	1.237422609

222613_at	57102	C12orf4	chromosome 12 open reading frame 4	1.105505079
212954_at	8798	DYRK4	dual-specificity tyrosine-(Y)-phosphorylation regulated kinase 4	1.57075808
226066_at	4286	MITF	microphthalmia-associated transcription factor	2.334568409
208606_s_at	54361	WNT4	wingless-type MMTV integration site family, member 4	0.859407907

Supplementary Table S3A. Activation scores, associated p-value and metadata of REMBRANDT samples identified as (+) or (-) based on the oligodendroglial GPC signature.

Samples	Activation Score	Normalized Score	p-value	Age	Survival (mths)	Status	Histology	Grade
HF0505	0.749457969	1	0.0271	35	3.2	1	GBM	IV
HF1246	0.732100118	0.976839461	0.003	65	0.2	1	ASTROCYTOMA	II
E08021	0.731966357	0.976660984	0.0097	40	81.5	1	OLIGODENDROGLIOMA	III
HF1269	0.694346941	0.926465486	0.0014	55	13	1	GBM	IV
HF0599	0.688132241	0.918173226	0.0444	70	42.8	1	OLIGODENDROGLIOMA	II
E10193	0.680597094	0.908119098	0.0269	50	34.2	NA	GBM	IV
HF1502	0.654386806	0.873146771	0.0595	70	6.4	1	OLIGODENDROGLIOMA	III
HF1032	0.640376005	0.854452194	0.0471	40	28.1	1	ASTROCYTOMA	III
HF1227	0.632969918	0.844570269	0.018	50	251.7	0	OLIGODENDROGLIOMA	II
E09688	0.624472362	0.833232	0.0144	55	50.8	1	MIXED	II
E09787	0.622652421	0.830803657	6.00E-04	55	86.5	0	GBM	IV
HF0180	0.616102353	0.822063916	0.0479	35	0.3	1	GBM	IV
E09956	0.603754355	0.805588012	0.001	70	21	1	GBM	IV
HF1587	0.590356299	0.787711017	0.0511	30	75.3	0	ASTROCYTOMA	III
E10184	0.586292819	0.782289125	0.0947	30	28.3	1	GBM	IV
HF0087	0.586151619	0.782100723	0.0099	60	78.8	1	ASTROCYTOMA	III
E09606	0.584952923	0.780501305	0.0162	30	13.3	1	GBM	IV
E09515	0.584812915	0.780314493	0.0474	35	65.4	0	ASTROCYTOMA	II/III
E09278	0.58381164	0.778978494	0.0363	40	36.6	0	GBM	IV

HF0963	0.575711213	0.768170114	0.04	10	10.6	1	GBM	IV
HF1493	0.57332728	0.764989237	0.0684	65	41.9	1	OLIGODENDROGLIOMA	III
E10252	0.569847595	0.760346302	0.0644	55	53	1	GBM	IV
E09670	0.566785165	0.756260108	0.0575	75	14.2	1	GBM	IV
E09454	0.565155368	0.754085474	0.0828	55	18	1	GBM	IV
E09846	0.559234143	0.746184798	0.0508	65	14.3	1	GBM	IV
HF0285	0.558833826	0.745650656	0.0393	80	14.4	1	OLIGODENDROGLIOMA	II
E10312	0.557733116	0.744181981	0.0856	35	37.9	1	GBM	IV
HF1677	0.557606793	0.744013429	0.0491	50	63.5	0	ASTROCYTOMA	II
E09930	0.557353343	0.743675251	0.0686	50	5.1	1	GBM	IV
HF0026	0.554987055	0.740517919	0.0633	60	57.1	1	ASTROCYTOMA	II
HF0252	0.554987055	0.740517919	0.0552	35	123.1	0	ASTROCYTOMA	II
E09938	0.554812915	0.740285564	0.0303	45	25.2	1	GBM	IV
E09893	0.554807183	0.740277916	0.0153	40	111.9	1	OLIGODENDROGLIOMA	III
E10072	0.550695692	0.734791963	0.0179	65	37.2	0	OLIGODENDROGLIOMA	II/III
E09513	0.544168132	0.726082255	0.0911	55	13.4	1	OLIGODENDROGLIOMA	II/III
HF0251	0.5391027	0.719323462	0.0012	65	22.7	1	OLIGODENDROGLIOMA	III
E09920	0.537674994	0.717418476	0.0367	25	59.4	1	ASTROCYTOMA	III
HF1058	0.530737231	0.708161435	0.0242	40	18	1	GBM	IV
HF1511	0.526839197	0.702960298	0.0256	25	56.6	1	ASTROCYTOMA	II
E09262	0.525938162	0.701758049	0	50	13.6	1	MIXED	II/III
HF0434	0.52223726	0.696819944	0.0083	60	6.1	1	ASTROCYTOMA	II
HF1667	0.519023712	0.692532115	0.0019	60	2.5	1	GBM	IV
HF0445	0.515744412	0.688156552	0.0388	40	47.2	1	GBM	IV

E09212	0.507821892	0.677585553	0	40	7.1	1	ASTROCYTOMA	II/III
E09601	0.503894105	0.672344716	0.0034	70	13.2	1	GBM	IV
E09921	0.497126104	0.663314188	0.0602	40	36.4	0	ASTROCYTOMA	II/III
HF1489	0.496517546	0.662502191	0.0539	50	68.3	1	ASTROCYTOMA	II
E10258	0.488339677	0.651590479	0.0539	50	20.6	1	GBM	IV
HF0936	0.488324253	0.651569899	0.0039	55	5.1	1	ASTROCYTOMA	II
E09988	0.484443639	0.646392006	0.0127	70	64.6	1	OLIGODENDROGLIOMA	III
HF0962	0.483030037	0.644505839	0.0278	45	116.5	0	OLIGODENDROGLIOMA	II
E09605	0.480872441	0.641626964	0.0053	45	59.3	1	GBM	IV
HF1492	0.468710079	0.625398754	0.0344	30	2.2	1	GBM	IV
HF0953	0.466790317	0.622837219	0.0829	35	44.6	1	ASTROCYTOMA	II
E09818	0.464049666	0.619180375	0.0338	30	38.1	0	ASTROCYTOMA	II/III
E09531	0.462403898	0.61698443	8.00E-04	55	19.3	1	ASTROCYTOMA	II/III
E09664	0.461318096	0.615535648	0.0155	40	27.1	1	OLIGODENDROGLIOMA	II/III
HF0022	0.459908744	0.613655152	0.0678	20	133.9	0	ASTROCYTOMA	II
HF0914	0.452628786	0.603941522	0.032	40	146.9	0	ASTROCYTOMA	II
E10551	0.451868661	0.602927288	0.0669	65	12.3	1	GBM	IV
E09907B	0.443791064	0.59214937	0.0024	60	55.2	1	GBM	IV
HF1345	0.433641331	0.578606606	0.0145	15	83.5	0	ASTROCYTOMA	II
HF1588	0.431310239	0.575496235	0.0735	40	75.2	0	ASTROCYTOMA	II
E09802	0.429940365	0.573668415	0.0306	80	32.2	1	GBM	IV
HF1585	0.425210527	0.567357403	0.031	25	19.9	1	GBM	IV
HF0520	0.422798129	0.564138546	0.0122	40	8.7	1	GBM	IV
E09852	0.422437933	0.563657938	0.0288	50	48.3	1	GBM	IV

HF0108	0.420665649	0.561293184	0.0404	35	132	0	ASTROCYTOMA	III
E09192	0.404265925	0.53941107	0.0641	75	13.4	1	GBM	IV
HF0024	0.4034404	0.538309574	0.0562	45	5.8	1	GBM	IV
E09471	0.399568094	0.533142766	0.0065	70	27.2	1	ASTROCYTOMA	II
E10026	0.398363859	0.531535958	0.0281	65	15.4	1	GBM	IV
HF0608	0.398032902	0.531094363	0.0107	50	10.6	1	ASTROCYTOMA	II
E09690	0.389382233	0.519551795	0.0354	75	62.3	0	GBM	IV
E09647	0.382230723	0.510009552	0.0426	55	19.3	1	GBM	IV
E10144	0.380705674	0.507974683	0.0099	50	25.9	1	GBM	IV
HF1409	0.379186615	0.505947806	0.0143	50	12.7	1	ASTROCYTOMA	III
E09661	0.376503249	0.502367397	0.0076	65	48.5	0	OLIGODENDROGLIOMA	II
E09867	0.368241369	0.49134359	0.0267	75	38.7	0	OLIGODENDROGLIOMA	II
HF0778	0.363984009	0.485663005	0.0013	65	8.1	1	ASTROCYTOMA	II
HF1262	0.357766443	0.477366921	0.0163	30	23.7	1	GBM	IV
HF1178	0.356451664	0.475612614	0.0369	35	15.8	1	GBM	IV
HF0152	0.341086864	0.455111398	0.0564	30	131.5	0	ASTROCYTOMA	III
HF0543	0.334896186	0.44685119	0.049	30	67.6	0	GBM	IV
HF0996	0.322142945	0.429834571	0.0493	50	120.5	0	GBM	IV
HF0138	0.306071311	0.408390229	0.0594	60	1.2	1	GBM	IV
HF1509	-0.299523658	-0.386689141	0.0852	40	2.7	1	GBM	IV
HF1517	-0.304781874	-0.393477569	0.0358	55	8.3	1	GBM	IV
HF1078	-0.31280225	-0.403831985	0.0685	50	22.8	1	GBM	IV
HF0790	-0.317019359	-0.40927633	0.0439	45	7.5	1	GBM	IV
HF0855	-0.323567174	-0.417729649	0.0293	55	13.7	1	ASTROCYTOMA	II

HF0510	-0.336784038	-0.434792801	0.0494	45	19.6	1	OLIGODENDROGLIOMA	II
HF0894	-0.337132125	-0.435242187	0.0477	40	14.1	1	GBM	IV
HF0835	-0.34490649	-0.445278998	0.0021	20	45.3	1	OLIGODENDROGLIOMA	II
E10031	-0.352909446	-0.455610923	0.0213	55	27.5	1	GBM	IV
HF0327	-0.362469071	-0.467952531	0.0057	75	19.6	1	OLIGODENDROGLIOMA	II
E09917	-0.367243861	-0.47411685	0.0036	50	6.1	1	GBM	IV
HF0960	-0.383971676	-0.495712688	0.033	45	88.7	1	OLIGODENDROGLIOMA	II
HF0408	-0.387273163	-0.499974953	4.00E-04	30	15.8	1	GBM	IV
HF1090	-0.395275411	-0.510305964	0.0306	50	8.5	1	OLIGODENDROGLIOMA	III
HF0450	-0.407202966	-0.525704601	0.0508	30	29.5	1	ASTROCYTOMA	II
E09791	-0.416213927	-0.537337876	0.0619	60	13.4	1	GBM	IV
E09730	-0.419038557	-0.540984511	0.0168	40	61.7	1	GBM	IV
HF0442.5	-0.422172569	-0.545030563	0.0252	30	19.6	1	GBM	IV
HF1122	-0.440157815	-0.568249762	0.0091	40	7.3	1	GBM	IV
HF1534	-0.445761091	-0.575483669	0.0165	20	7.8	1	GBM	IV
HF1057	-0.450285554	-0.581324812	1.00E-04	55	24.5	1	OLIGODENDROGLIOMA	III
HF1671	-0.453315816	-0.585236922	0.0711	50	13.3	1	GBM	IV
HF0031	-0.462637223	-0.597270985	0.0601	35	0.5	1	GBM	IV
E10300	-0.46358746	-0.598497754	0.0218	60	9.4	1	GBM	IV
HF0702	-0.480207693	-0.619954703	0.0205	50	8.5	1	ASTROCYTOMA	III
E10102	-0.485464009	-0.626740679	0.014	45	38.8	0	GBM	IV
E10271	-0.485974839	-0.627400166	0.0716	30	12.5	1	GBM	IV
HF0460	-0.491378375	-0.634376206	0.0796	45	10.7	1	OLIGODENDROGLIOMA	III
E09348	-0.496743594	-0.641302777	0.0536	35	18.5	1	GBM	IV

E09139	-0.497586056	-0.642390407	0.028	45	36.5	1	GBM	IV
HF1186	-0.500533627	-0.646195762	0.0111	30	20.1	1	ASTROCYTOMA	III
HF1185	-0.506307341	-0.653649705	0.0285	25	95.2	0	ASTROCYTOMA	III
HF1344	-0.506640166	-0.654079386	0.061	60	9	1	ASTROCYTOMA	II
HF0990	-0.508177096	-0.656063585	0	NA	88.3	1	GBM	IV
HF1608	-0.510846262	-0.659509514	0.0827	60	7.9	1	GBM	IV
E10483	-0.513600598	-0.663065399	0.0754	25	66.4	1	ASTROCYTOMA	II
HF1538	-0.521697579	-0.673518713	0.0756	55	3.2	1	GBM	IV
HF1286	-0.530642368	-0.685066558	0.0333	75	13.2	1	ASTROCYTOMA	III
HF1618	-0.537184	-0.693511895	0.022	50	2.4	1	GBM	IV
HF0816	-0.543687185	-0.701907595	0.0361	60	46.7	1	OLIGODENDROGLIOMA	III
E50074	-0.546405102	-0.705416463	0.0368	50	5.4	1	GBM	IV
HF1382	-0.551104735	-0.711483754	0.0141	35	48.3	1	GBM	IV
E09967	-0.574153706	-0.741240291	0.002	45	4.4	1	GBM	IV
E09610	-0.57500937	-0.742344965	0.0061	55	12.5	1	GBM	IV
E10227	-0.601182757	-0.776135166	0.008	45	12.6	1	GBM	IV
HF0066	-0.601470694	-0.776506897	0.0016	50	9.1	1	GBM	IV
HF0986	-0.603858685	-0.779589825	2.00E-04	15	62.4	1	GBM	IV
HF1139	-0.628805522	-0.811796533	0.0117	40	15.8	1	GBM	IV
HF1191	-0.64276171	-0.829814163	7.00E-04	25	0.3	1	GBM	IV
HF1150	-0.651136485	-0.840626112	0	70	21.2	1	ASTROCYTOMA	III
HF0142	-0.6526464	-0.842575432	0.0021	25	0.3	1	GBM	IV
E09833B	-0.661856328	-0.854465576	0.0192	45	20.8	1	GBM	IV
HF1297	-0.665978187	-0.859786953	0	60	17.2	1	GBM	IV

E09966	-0.678273537	-0.875660417	0.0042	55	17.7	1	ASTROCYTOMA	III
HF0184	-0.681526594	-0.879860159	0	65	12	1	OLIGODENDROGLIOMA	III
HF1628	-0.684914765	-0.884234334	0.084	70	14.6	1	GBM	IV
E10284	-0.686683443	-0.886517721	0.0026	55	4.8	1	GBM	IV
E10267	-0.686925784	-0.886830587	0.004	75	12	1	GBM	IV
HF1077	-0.702421737	-0.906836074	5.00E-04	45	73.4	1	GBM	IV
HF1490	-0.722523361	-0.932787546	0.073	65	4	1	ASTROCYTOMA	III
HF1589	-0.774585129	-1	0.0162	25	3.3	1	GBM	IV

Supplementary Table S3B. Activation scores, associated p-value and metadata of Gravendeel samples identified as (+) or (-) based on the oligodendroglial GPC signature.

Samples	Activation Score	Normalized Score	p-value	Age	Survival (yrs)	Status	Histology	Grade	CHR1p	CHR19q	EGFR
GSM405355	0.801064034	1	0.0074	73	1.19	1	ASTROCYTOMA	II	NA	NA	NA
GSM405256	0.737876569	0.921120582	0.0866	38	4.79	1	ASTROCYTOMA	II	no LOH	no LOH	wild type
GSM405461	0.716299484	0.894185051	0.0947	49	0.76	1	GBM	IV	LOH	LOH	wild type
GSM405246	0.682859857	0.852441038	0.0305	33	6.31	1	GBM	IV	LOH	LOH	NA
GSM405203	0.66280444	0.827405066	0.0025	39	8.92	1	OLIGODENDROGLIOMA	III	LOH	LOH	wild type
GSM405212	0.658658913	0.82223004	0.02	23	17.49	1	OLIGODENDROGLIOMA	III	LOH	LOH	wild type
GSM405370	0.643329952	0.803094291	0.0192	47	1.61	1	GBM	IV	no LOH	no LOH	wild type
GSM405318	0.634974336	0.792663644	0.0118	62	6.21	0	OLIGODENDROGLIOMA	III	no LOH	no LOH	NA
GSM405216	0.615021607	0.76775586	0.0045	52	3.28	1	GBM	IV	NA	no LOH	wild type
GSM405207	0.605455573	0.755814201	0.0052	44	8.12	1	OLIGODENDROGLIOMA	III	LOH	LOH	wild type
GSM405409	0.59181949	0.738791739	0.0477	54	10.36	1	OLIGODENDROGLIOMA	III	LOH	LOH	NA
GSM405324	0.566705887	0.707441431	0.0436	14	0.67	1	GBM	IV	no LOH	no LOH	amplification
GSM405234	0.554016145	0.691600324	4.00E-04	58	0.62	1	GBM	IV	NA	NA	NA
GSM405283	0.538231934	0.671896267	0.0183	38	4.07	1	OLIGOASTROCYTOMA	III	LOH	LOH	wild type
GSM405205	0.533253927	0.665682023	0.0317	48	3.24	1	OLIGODENDROGLIOMA	III	LOH	LOH	wild type
GSM405386	0.521886757	0.651491935	0.0114	54	3.76	1	OLIGODENDROGLIOMA	II	LOH	LOH	wild type

GSM405325	0.519420906	0.648413715	0.0449	43	3.65	1	OLIGOASTROCYTOMA	III	NA	NA	wild type
GSM405441	0.517104497	0.64552205	0.0178	45	3.27	0	OLIGODENDROGLIOMA	II	LOH	LOH	wild type
GSM405204	0.516167462	0.644352312	0.0954	34	8.59	1	OLIGODENDROGLIOMA	III	LOH	LOH	wild type
GSM405320	0.515438603	0.643442448	0.017	70	0.6	1	GBM	IV	NA	NA	wild type
GSM405411	0.507483079	0.633511251	5.00E-04	38	0.05	1	ASTROCYTOMA	III	LOH	no LOH	NA
GSM405217	0.506733901	0.632576024	0.0389	33	6.77	0	GBM	IV	NA	no LOH	wild type
GSM405314	0.504431242	0.629701523	2.00E-04	54	0.65	1	GBM	IV	no LOH	LOH	wild type
GSM405343	0.489292619	0.610803379	0.0816	67	NA	0	GBM	IV	NA	NA	wild type
GSM405457	0.486971348	0.607905645	0.0523	71	0.3	1	OLIGODENDROGLIOMA	III	no LOH	no LOH	wild type
GSM405287	0.486856457	0.607762221	0.0345	44	6.87	1	OLIGODENDROGLIOMA	III	LOH	LOH	wild type
GSM405330	0.483717775	0.603844081	0.0869	33	0.71	1	GBM	IV	no LOH	NA	wild type
GSM405261	0.476668599	0.595044314	0.0015	60	0.98	1	OLIGODENDROGLIOMA	III	no LOH	no LOH	NA
GSM405227	0.47341699	0.590985202	0.07	48	4.77	1	OLIGODENDROGLIOMA	III	NA	NA	NA
GSM405243	0.470390141	0.587206667	0.0156	61	0.88	1	GBM	IV	NA	NA	NA
GSM405395	0.464586642	0.579961928	0.0425	55	3.76	1	OLIGOASTROCYTOMA	II	LOH	LOH	wild type
GSM405382	0.459041423	0.573039611	0.0015	44	4.86	1	OLIGOASTROCYTOMA	III	LOH	LOH	NA
GSM405420	0.458788616	0.572724023	0.0413	50	3	1	OLIGODENDROGLIOMA	III	no LOH	no LOH	wild type
GSM405278	0.458173812	0.571956538	2.00E-04	58	0.73	1	GBM	IV	NA	NA	amplification
GSM405462	0.454461768	0.567322647	0.0601	50	7.52	1	ASTROCYTOMA	II	LOH	LOH	NA
GSM405415	0.438470443	0.547360042	0.0062	67	0.5	1	GBM	IV	no LOH	no LOH	NA

GSM405301	0.426132041	0.531957526	0.0979	65	0.3	1	GBM	IV	NA	NA	NA
GSM405465	0.420244949	0.524608435	0.0242	69	0.63	1	GBM	IV	NA	no LOH	NA
GSM405211	0.419707136	0.523937062	0.0445	35	1.83	1	OLIGODENDROGLIOMA	III	LOH	LOH	NA
GSM405342	0.417912408	0.521696632	0.0872	47	2.99	1	OLIGODENDROGLIOMA	III	NA	NA	wild type
GSM405396	0.416841065	0.520359231	0.0331	77	0.02	1	GBM	IV	no LOH	no LOH	NA
GSM405403	0.415940255	0.519234715	0.0034	38	0.04	1	ASTROCYTOMA	III	NA	NA	NA
GSM405333	0.40417074	0.504542362	0.0697	58	9.11	1	OLIGODENDROGLIOMA	III	LOH	LOH	wild type
GSM405249	0.40304092	0.503131964	0.002	23	0.04	1	GBM	IV	NA	NA	wild type
GSM405475	0.39505561	0.493163584	0.0501	34	1.05	1	GBM	IV	NA	NA	wild type
GSM405481	0.392048822	0.489410092	0.0018	34	10.37	0	PILOCYTIC ASTROCYTOMA	I	NA	NA	NA
GSM405268	0.385988137	0.481844298	0.0039	48	0.64	1	GBM	IV	no LOH	no LOH	amplification
GSM405311	0.381022431	0.47564541	0.0427	43	7.48	0	ASTROCYTOMA	II	NA	NA	NA
GSM405265	0.377448173	0.471183522	0.0795	32	1.81	1	ASTROCYTOMA	III	NA	NA	wild type
GSM405483	0.373761793	0.466581668	0.0012	32	0.19	0	PILOCYTIC ASTROCYTOMA	I	NA	NA	NA
GSM405334	0.364091978	0.454510454	0.0214	57	1.47	1	OLIGODENDROGLIOMA	III	no LOH	no LOH	wild type
GSM405321	0.363960116	0.454345846	0.0406	34	3.97	1	ASTROCYTOMA	III	NA	NA	wild type
GSM405459	0.36310793	0.453282028	0.0099	64	1.14	1	GBM	IV	no LOH	no LOH	NA
GSM405210	0.348355938	0.434866532	0.0782	39	10.28	1	OLIGODENDROGLIOMA	III	LOH	LOH	wild type
GSM405464	0.340105521	0.424567209	0.0132	55	0.56	1	GBM	IV	NA	NA	NA
GSM405250	0.317464016	0.39630292	0.0848	31	1.48	1	ASTROCYTOMA	II	NA	NA	NA
GSM405466	0.302478925	0.377596437	0.0725	67	0.28	1	GBM	IV	no	no LOH	NA

									LOH		
GSM405377	0.28692836	0.35818405	0.0854	42	0.6	1	OLIGODENDROGLIOMA	III	LOH	LOH	NA
GSM405356	-0.342749828	-0.460064457	0.0371	43	0.18	1	GBM	IV	NA	no LOH	wild type
GSM405298	-0.349169162	-0.468680968	0.0271	43	1.96	1	OLIGOASTROCYTOMA	III	no LOH	no LOH	NA
GSM405240	-0.351520541	-0.471837164	0.0206	33	6.62	0	GBM	IV	no LOH	no LOH	NA
GSM405391	-0.371763333	-0.499008553	0.0328	56	1.05	1	GBM	IV	no LOH	no LOH	NA
GSM405339	-0.373760087	-0.501688746	0.0043	78	NA	0	GBM	IV	NA	NA	amplification
GSM405436	-0.375071936	-0.503449608	0.0199	79	0.48	1	GBM	IV	NA	NA	NA
GSM405450	-0.379106436	-0.508865015	0.0134	37	13.3	0	OLIGOASTROCYTOMA	III	NA	NA	NA
GSM405372	-0.380450453	-0.510669056	0.0961	37	3.32	1	GBM	IV	LOH	LOH	NA
GSM405439	-0.381414955	-0.511963683	0.0096	33	3.7	0	OLIGOASTROCYTOMA	II	no LOH	NA	wild type
GSM405384	-0.383888277	-0.515283561	0.0174	70	0.02	0	GBM	IV	no LOH	no LOH	NA
GSM405424	-0.401716738	-0.539214255	0.0365	33	3.2	1	ASTROCYTOMA	II	no LOH	no LOH	wild type
GSM405230	-0.430676082	-0.578085652	0.0297	63	0.47	1	GBM	IV	no LOH	no LOH	NA
GSM405438	-0.433696491	-0.582139871	0.0301	43	2.3	1	GBM	IV	LOH	LOH	NA
GSM405388	-0.444215467	-0.596259227	0.0413	79	0.53	1	OLIGOASTROCYTOMA	III	no LOH	no LOH	amplification
GSM405337	-	-	0.0197	15	0.28	1	GBM	IV	NA	NA	amplification

	0.445057768	0.597389827									
GSM405440	-0.445411877	-0.597865138	0.0352	70	0.53	1	GBM	IV	NA	NA	wild type
GSM405326	-0.450820952	-0.605125604	0.0235	75	0.27	1	GBM	IV	NA	NA	amplification
GSM405422	-0.459443511	-0.616699447	0.034	71	0.91	1	GBM	IV	no LOH	no LOH	NA
GSM405294	-0.465957579	-0.625443117	0.0319	56	0.8	1	GBM	IV	partial LOH	partial LOH	amplification
GSM405476	-0.466653593	-0.626377359	0.0131	65	1.31	1	OLIGOASTROCYTOMA	III	no LOH	no LOH	amplification
GSM405443	-0.486639715	-0.653204227	0.0605	57	0.98	1	GBM	IV	NA	NA	amplification
GSM405312	-0.491071311	-0.659152647	0.0293	61	1.02	1	GBM	IV	NA	NA	amplification
GSM405226	-0.512661405	-0.688132486	0.0028	49	0.28	1	OLIGOASTROCYTOMA	III	no LOH	LOH	amplification
GSM405474	-0.524231599	-0.703662865	0.0344	61	0.29	1	GBM	IV	NA	NA	amplification
GSM405390	-0.554141148	-0.743809699	0.0917	70	0.02	1	OLIGOASTROCYTOMA	III	NA	NA	NA
GSM405405	-0.581116167	-0.780017587	0.0126	71	0.61	1	GBM	IV	no LOH	LOH	NA
GSM405267	-0.591581464	-0.794064892	0.0358	53	0.65	1	GBM	IV	no LOH	NA	NA
GSM405292	-0.605376456	-0.812581563	0	66	1.11	1	GBM	IV	NA	NA	amplification
GSM405347	-0.616268217	-0.827201299	0.0143	43	0.19	1	OLIGOASTROCYTOMA	III	NA	NA	amplification
GSM405428	-0.622239739	-0.835216722	0.0052	71	0.79	1	GBM	IV	no LOH	no LOH	amplification

GSM405376	-0.637951306	-0.856305963	0.016	53	1.85	1	GBM	IV	no LOH	NA	amplification
GSM405289	-0.67705098	-0.908788469	0.003	37	0.19	1	ASTROCYTOMA	III	NA	NA	amplification
GSM405352	-0.715537781	-0.960448333	0.0752	70	0.4	1	GBM	IV	NA	NA	amplification
GSM405341	-0.745003928	-1	0.0565	71	0.63	1	OLIGOASTROCYTOMA	III	NA	NA	amplification

Supplementary Table S4. Contingency tables for classification of (+) and (-) patient based on Phillips molecular subtypes.

(a) REMBRANDT Dataset

	Mesenchymal	**Proneural**	**Proliferative**	**Total**
(-)	32	5	24	61
(+)	16	60	10	86
Total	48	65	34	147

X-squared = 9.609, df = 2, p-value = 0.008193

(b) Gravendeel Dataset

	Mesenchymal	**Proneural**	**Proliferative**	**Total**
(-)	8	5	21	34
(+)	8	27	23	58
Total	16	32	44	92

X-squared = 54.9748, df = 2, p-value = 1.154e-12

Supplementary Table S5. Probesets in the NNI-8 GPC versus Primary Tumor stemness gene signature.

Probeset ID	Entrez Gene ID	Gene Symbol	Description	Log Fold Change
1553635_s_at	200132	TCTEX1D1	Tctex1 domain containing 1	-6.215791136
209156_s_at	1292	COL6A2	collagen, type VI, alpha 2	-6.493620158
209448_at	10553	HTATIP2	HIV-1 Tat interactive protein 2, 30kDa	-6.42297587
222484_s_at	9547	CXCL14	chemokine (C-X-C motif) ligand 14	-8.105582051
202018_s_at	4057	LTF	lactotransferrin	-8.54583883
230422_at	2359	FPR3	formyl peptide receptor 3	-7.35868863
203032_s_at	2271	FH	fumarate hydratase	6.389162912
204122_at	7305	TYROBP	TYRO protein tyrosine kinase binding protein	-7.451463342
213975_s_at	4069	LYZ	lysozyme	-8.567997622
204570_at	1346	COX7A1	cytochrome c oxidase subunit VIIa polypeptide 1 (muscle)	-6.10959307
204158_s_at	10312	TCIRG1	T-cell, immune regulator 1, ATPase, H+ transporting, lysosomal V0 subunit A3	-6.005341469
209183_s_at	11067	C10orf10	chromosome 10 open reading frame 10	-6.05532165
209047_at	358	AQP1	aquaporin 1 (Colton blood group)	-6.969067359
205572_at	285	ANGPT2	angiopoietin 2	-7.511111563
236034_at	285	ANGPT2	angiopoietin 2	-6.482834194
235639_at	28513	CDH19	cadherin 19, type 2	6.235154529
209901_x_at	199	AIF1	allograft inflammatory factor 1	-6.32542485
213095_x_at	199	AIF1	allograft inflammatory factor 1	-7.499645133
215051_x_at	199	AIF1	allograft inflammatory factor 1	-7.64616928

1555460_a_at	25800	SLC39A6	solute carrier family 39 (zinc transporter), member 6	6.466383357
220311_at	29104	N6AMT1	N-6 adenine-specific DNA methyltransferase 1 (putative)	6.090119758
203240_at	8857	FCGBP	Fc fragment of IgG binding protein	-6.279670112
202628_s_at	5054	SERPINE1	serpin peptidase inhibitor, clade E (nexin, plasminogen activator inhibitor type 1), member 1	-6.169187776
201743_at	929	CD14	CD14 molecule	-9.061228844
225400_at	116461	TSEN15	tRNA splicing endonuclease 15 homolog (S. cerevisiae)	6.564806667
219386_s_at	56833	SLAMF8	SLAM family member 8	-6.439653705
218345_at	55365	TMEM176A	transmembrane protein 176A	-7.028336131
219167_at	51285	RASL12	RAS-like, family 12	-7.447403055
225502_at	81704	DOCK8	dedicator of cytokinesis 8	-6.431728356
234023_s_at	55835	CENPJ	centromere protein J	6.500186173
209619_at	972	CD74	CD74 molecule, major histocompatibility complex, class II invariant chain	-6.392605538
223434_at	2635	GBP3	guanylate binding protein 3	-7.428950443
207054_at	3617	IMPG1	interphotoreceptor matrix proteoglycan 1	-7.236493758
205374_at	6588	SLN	sarcolipin	-6.139099986
203535_at	6280	S100A9	S100 calcium binding protein A9	-6.508034002
203571_s_at	10974	C10orf116	chromosome 10 open reading frame 116	-6.322842462
204128_s_at	5983	RFC3	replication factor C (activator 1) 3, 38kDa	6.363690078
218559_s_at	9935	MAFB	v-maf musculoaponeurotic fibrosarcoma oncogene homolog B (avian)	-6.671432912
201842_s_at	2202	EFEMP1	EGF containing fibulin-like extracellular matrix protein 1	-6.040243322
212268_at	1992	SERPINB1	serpin peptidase inhibitor, clade B (ovalbumin), member 1	-6.972772922
209723_at	5272	SERPINB9	serpin peptidase inhibitor, clade B (ovalbumin), member 9	-6.55138368
223620_at	2857	GPR34	G protein-coupled receptor 34	-7.926594277

219607_s_at	51338	MS4A4A	membrane-spanning 4-domains, subfamily A, member 4	-8.180055654
226034_at	1846	DUSP4	dual specificity phosphatase 4	6.838468179
225314_at	132299	OCIAD2	OCIA domain containing 2	-8.275917817
204990_s_at	3691	ITGB4	integrin, beta 4	-6.364422156
203854_at	3426	CFI	complement factor I	-6.363714998
202310_s_at	1277	COL1A1	collagen, type I, alpha 1	-7.130038944
1556499_s_at	1277	COL1A1	collagen, type I, alpha 1	-9.238542552
213566_at	6039	RNASE6	ribonuclease, RNase A family, k6	-7.823580016
204482_at	7122	CLDN5	claudin 5	-6.460963571
221816_s_at	51131	PHF11	PHD finger protein 11	-6.825731298
239132_at	4842	NOS1	nitric oxide synthase 1 (neuronal)	-6.386282534
209395_at	1116	CHI3L1	chitinase 3-like 1 (cartilage glycoprotein-39)	-10.14439331
209396_s_at	1116	CHI3L1	chitinase 3-like 1 (cartilage glycoprotein-39)	-9.362700349
219719_at	51751	HIGD1B	HIG1 hypoxia inducible domain family, member 1B	-6.669433848
203540_at	2670	GFAP	glial fibrillary acidic protein	-7.35128303
201721_s_at	7805	LAPTM5	lysosomal protein transmembrane 5	-6.25877809
232887_at	644139	PIRT	phosphoinositide-interacting regulator of transient receptor potential channels	-6.331567906
204787_at	11326	VSIG4	V-set and immunoglobulin domain containing 4	-7.189520229
208161_s_at	8714	ABCC3	ATP-binding cassette, sub-family C (CFTR/MRP), member 3	-6.929235405
210055_at	7253	TSHR	thyroid stimulating hormone receptor	-6.141153984
202859_x_at	3576	IL8	interleukin 8	-8.035544596
235417_at	90853	SPOCD1	SPOC domain containing 1	-6.444542888

203835_at	2615	LRRC32	leucine rich repeat containing 32	-6.267902391
202238_s_at	4837	NNMT	nicotinamide N-methyltransferase	-6.6617682
202237_at	4837	NNMT	nicotinamide N-methyltransferase	-7.208303354
229391_s_at	441168	FAM26F	family with sequence similarity 26, member F	-6.297620939
223467_at	51655	RASD1	RAS, dexamethasone-induced 1	-8.103012345
239461_at	117248	GALNTL2	UDP-N-acetyl-alpha-D-galactosamine:polypeptide N-acetylgalactosaminyltransferase-like 2	-7.696742518
228501_at	117248	GALNTL2	UDP-N-acetyl-alpha-D-galactosamine:polypeptide N-acetylgalactosaminyltransferase-like 2	-6.995008809
205786_s_at	3684	ITGAM	integrin, alpha M (complement component 3 receptor 3 subunit)	-6.272756493
208747_s_at	716	C1S	complement component 1, s subcomponent	-8.132346089
201859_at	5552	SRGN	serglycin	-8.765885577
201858_s_at	5552	SRGN	serglycin	-8.111413158
207397_s_at	3239	HOXD13	homeobox D13	6.35025642
1568604_a_at	8618	CADPS	Ca++-dependent secretion activator	-7.030383795
231068_at	146802	SLC47A2	solute carrier family 47, member 2	-8.52812485
215049_x_at	9332	CD163	CD163 molecule	-7.402833043
218729_at	56925	LXN	latexin	-6.457187984
209875_s_at	6696	SPP1	secreted phosphoprotein 1	-7.285379742
200986_at	710	SERPING1	serpin peptidase inhibitor, clade G (C1 inhibitor), member 1	-8.060359753
225353_s_at	714	C1QC	complement component 1, q subcomponent, C chain	-7.877615852
202953_at	713	C1QB	complement component 1, q subcomponent, B chain	-9.175565222

Supplementary Table S6. Results from Pathway Activation Score, Log Rank and Cox Regression analysis (NNI-8 GPC versus Primary Tumor gene signature). (+) represents patients with concordance to GPC signature; (-) represents patients with inverse gene expression relationship to GPC signature.

Dataset	Connectivity Maps Analysis						Log Rank p-value	Multivariate Cox		Univariate Cox	
	# of probes	# of samples	(+)	(-)	total(+)(-)	%(+)(-)		Hazard Ratio	p-value	Hazard Ratio	p-value
REMBRANDT	84	298	80	54	134	44.97	0.007	0.671 (0.455 - 0.989)	0.044	0.596 (0.406 - 0.874)	0.008
Gravendeel	84	276	86	77	163	59.06	0.0007	0.691 (0.488 - 0.977)	0.036	0.567 (0.407 - 0.791)	0.0008

Multivariate Cox Regression:
REMBRANDT: coxph(formula = Surv(survival, status) ~ age + grade + class, data = dat)
Gravendeel: coxph(formula = Surv(survival, status) ~ age + grade + class, data = dat)

Univariate Cox Regression:
REMBRANDT: coxph(formula = Surv(survival, status) ~ class, data = dat)
Gravendeel: coxph(formula = Surv(survival, status) ~ class, data = dat)

Supplementary Table S7A. Activation scores, associated p-value and metadata of REMBRANDT samples identified as (+) or (-) based on the NNI-8 stemness signature.

Samples	Activation Score	Normalized Score	p-value	Age	Survival (mths)	Status	Histology	Grade
E08021	1.522597165	1	0	40	81.5	1	OLIGODENDROGLIOMA	III
E09448	1.422752629	0.934424851	0	60	229.1	1	OLIGODENDROGLIOMA	III
HF0891	1.303831733	0.856320873	0	35	28.8	1	GBM	IV
HF0142	1.288468221	0.84623054	0	25	0.3	1	GBM	IV
HF0066	1.216406036	0.798902076	0	50	9.1	1	GBM	IV
E10110	1.176753544	0.772859408	0	50	23.1	1	GBM	IV
HF0996	1.119487883	0.735248895	0	50	120.5	0	GBM	IV
E09804	1.103850023	0.724978378	0	70	42.4	0	OLIGODENDROGLIOMA	II
HF1136	1.084938272	0.712557659	0	35	45.3	1	ASTROCYTOMA	III
HF0108	1.077128487	0.707428407	0	35	132	0	ASTROCYTOMA	III
HF1227	1.074604481	0.705770709	0	50	251.7	0	OLIGODENDROGLIOMA	II
E10105	1.067544582	0.701133961	0	40	1.1	NA	ASTROCYTOMA	III
E09278	1.050937357	0.690226792	0	40	36.6	0	GBM	IV
HF0920	1.049199817	0.689085624	0	40	1	1	OLIGODENDROGLIOMA	II
E09867	1.04340192	0.685277724	0	75	38.7	0	OLIGODENDROGLIOMA	II
E09690	1.029117513	0.675896118	0	75	62.3	0	GBM	IV
E09893	1.027983539	0.675151355	0	40	111.9	1	OLIGODENDROGLIOMA	III
E09394	1.019807956	0.669781857	0	30	51.7	1	MIXED	III

HF1628	1.007590306	0.66175764	0	70	14.6	1	GBM	IV
E09802	0.99482396	0.653373054	0	80	32.2	1	GBM	IV
HF0184	0.987032465	0.648255814	0	65	12	1	OLIGODENDROGLIOMA	III
HF0975	0.978033836	0.642345762	0	60	36.5	1	ASTROCYTOMA	III
HF0251	0.974357567	0.63993129	0	65	22.7	1	OLIGODENDROGLIOMA	III
HF1382	0.962780064	0.632327503	0	35	48.3	1	GBM	IV
HF1511	0.960128029	0.63058572	0	25	56.6	1	ASTROCYTOMA	II
E09722	0.958006401	0.629192293	0	50	28.5	1	GBM	IV
HF1587	0.919524463	0.603918412	0	30	75.3	0	ASTROCYTOMA	III
HF0180	0.911165981	0.598428791	0.0105	35	0.3	1	GBM	IV
HF1677	0.903978052	0.593707957	0	50	63.5	0	ASTROCYTOMA	II
E09656	0.891229995	0.585335383	0	65	34.1	1	OLIGODENDROGLIOMA	III
HF1551	0.888523091	0.583557563	0	30	70.9	0	ASTROCYTOMA	II
E10299	0.878079561	0.576698539	0	40	44.6	0	ASTROCYTOMA	II/III
HF1613	0.870233196	0.571545262	0	35	66.8	1	ASTROCYTOMA	III
E10013	0.860045725	0.564854411	5.00E-04	55	4.9	1	GBM	IV
E09855	0.850022862	0.55827167	0.0247	25	38.4	0	ASTROCYTOMA	III
E10252B	0.846566072	0.556001345	0	55	53	1	GBM	IV
E09988	0.84526749	0.555148472	0	70	64.6	1	OLIGODENDROGLIOMA	III
HF0702	0.831184271	0.545899001	0.0011	50	8.5	1	ASTROCYTOMA	III
E09818	0.829263832	0.544637709	0	30	38.1	0	ASTROCYTOMA	II/III
E09997	0.827471422	0.543460504	0	35	46.9	0	ASTROCYTOMA	II/III
E09966	0.822496571	0.540193158	0.002	55	17.7	1	ASTROCYTOMA	III
HF1469	0.821326017	0.539424371	0	25	22.2	1	GBM	IV

HF1640	0.81911294	0.537970882	0	50	5.5	1	GBM	IV
HF1295	0.80175583	0.526571209	0	55	19.1	1	ASTROCYTOMA	III
E09688	0.800877915	0.525994618	0	55	50.8	1	MIXED	II
E10267	0.789062643	0.518234672	0	75	12	1	GBM	IV
HF0408	0.770900777	0.506306458	0.0032	30	15.8	1	GBM	IV
E09454	0.760987654	0.499795791	0	55	18	1	GBM	IV
HF1344	0.758536808	0.498186143	0	60	9	1	ASTROCYTOMA	II
E10262	0.755884774	0.496444359	0.0074	50	18	1	GBM	IV
E09569	0.738052126	0.484732366	0	70	37.4	1	GBM	IV
E10211	0.736131687	0.483471074	0	85	28.4	1	GBM	IV
E09920	0.725761317	0.4766601	0.0074	25	59.4	1	ASTROCYTOMA	III
E10271	0.722981253	0.47483423	0.0044	30	12.5	1	GBM	IV
HF1191	0.715116598	0.469668941	6.00E-04	25	0.3	1	GBM	IV
E09959	0.713580247	0.468659908	0	50	46.4	1	ASTROCYTOMA	III
HF0966	0.709958848	0.466281472	2.00E-04	50	137.7	0	ASTROCYTOMA	III
E50123	0.674183813	0.442785412	0	30	17.5	1	GBM	IV
E10001	0.672610882	0.441752354	0	50	8.7	1	OLIGODENDROGLIOMA	III
HF0960	0.669666209	0.439818374	0	45	88.7	1	OLIGODENDROGLIOMA	II
E10252	0.666575217	0.437788295	0	55	53	1	GBM	IV
HF1490	0.665532693	0.437103594	0.0025	65	4	1	ASTROCYTOMA	III
HF0990	0.651906722	0.42815443	0	NA	88.3	1	GBM	IV
E09860	0.621490626	0.408177974	0	40	36.8	0	OLIGODENDROGLIOMA	II
HF1338	0.604572474	0.397066596	0	35	5.9	1	GBM	IV
E09956	0.604444444	0.39698251	0	70	21	1	GBM	IV

HF0963	0.566035665	0.371756679	0.009	10	10.6	1	GBM	IV
E09610	0.565743027	0.371564482	0.0243	55	12.5	1	GBM	IV
HF1057	0.554513032	0.364188929	0.0021	55	24.5	1	OLIGODENDROGLIOMA	III
E09623	0.547379973	0.359504132	3.00E-04	50	20.7	1	GBM	IV
E10184	0.541033379	0.355335864	0	30	28.3	1	GBM	IV
HF1487	0.530132602	0.348176533	0	50	9.9	1	OLIGODENDROGLIOMA	II
E09921	0.511476909	0.335923986	0	40	36.4	0	ASTROCYTOMA	II/III
HF0442.5	0.509044353	0.33432635	0.0137	30	19.6	1	GBM	IV
HF0992	0.496607225	0.326157986	2.00E-04	30	20	1	GBM	IV
E10144	0.477750343	0.313773304	0.0012	50	25.9	1	GBM	IV
E10138	0.459789666	0.301977225	2.00E-04	25	46.9	0	ASTROCYTOMA	II/III
E09801	0.459021491	0.301472708	5.00E-04	30	42.5	1	ASTROCYTOMA	III
HF0654	0.387965249	0.25480492	0.0299	20	14.6	1	GBM	IV
HF1357	0.382094193	0.250948972	0.0141	40	30.8	1	OLIGODENDROGLIOMA	III
HF0816	-0.432245085	-0.40731102	0.0376	60	46.7	1	OLIGODENDROGLIOMA	III
E09471	-0.454631916	-0.428406467	0.0028	70	27.2	1	ASTROCYTOMA	II
HF1534	-0.478372199	-0.450777291	7.00E-04	20	7.8	1	GBM	IV
E10226	-0.53223594	-0.501533901	0.0285	65	18.7	1	GBM	IV
E10031	-0.545569273	-0.514098101	0.0032	55	27.5	1	GBM	IV
HF0316	-0.551641518	-0.519820068	0	40	73.4	1	ASTROCYTOMA	II
HF0954.2	-0.593379058	-0.559149978	0	70	11	1	ASTROCYTOMA	III
HF0606	-0.612821216	-0.577470615	0	30	76.8	1	ASTROCYTOMA	II
E09451	-0.636707819	-0.599979318	0	60	5.3	1	GBM	IV
HF0024	-0.649272977	-0.611819655	0	45	5.8	1	GBM	IV

E09664	-0.661088249	-0.622953363	0.0094	40	27.1	1	OLIGODENDROGLIOMA	II/III
E09673	-0.665441244	-0.627055255	0	45	213.8	0	ASTROCYTOMA	II
E10158	-0.667142204	-0.628658095	0	70	40.6	0	GBM	IV
HF0844	-0.672281664	-0.633501086	0	30	63.8	1	ASTROCYTOMA	II
HF1538	-0.68349337	-0.644066044	0	55	3.2	1	GBM	IV
E10193	-0.687242798	-0.647599187	0	50	34.2	NA	GBM	IV
HF1671	-0.689437586	-0.649667368	0	50	13.3	1	GBM	IV
E10284	-0.691687243	-0.651787253	0	55	4.8	1	GBM	IV
HF1077	-0.697960677	-0.657698804	0	45	73.4	1	GBM	IV
HF1137	-0.711074531	-0.670056186	0	35	18.3	1	GBM	IV
E09430	-0.715354367	-0.674089139	0	45	32	1	GBM	IV
HF0543	-0.715628715	-0.674347661	0	30	67.6	0	GBM	IV
E09483	-0.715829904	-0.674537244	0	65	10.3	1	GBM	IV
E10514	-0.716671239	-0.675330047	0	75	23.7	1	GBM	IV
HF0089	-0.72698674	-0.685050498	0	65	7.9	1	ASTROCYTOMA	III
E10551	-0.734192958	-0.691841026	0	65	12.3	1	GBM	IV
E09661	-0.739515318	-0.696856365	0	65	48.5	0	OLIGODENDROGLIOMA	II
E10488	-0.758774577	-0.715004653	0	55	21.9	1	GBM	IV
E10103	-0.764389575	-0.72029575	0	50	3.3	1	ASTROCYTOMA	II/III
E09930	-0.772565158	-0.727999724	0	50	5.1	1	GBM	IV
E09531	-0.773699131	-0.729068284	0	55	19.3	1	ASTROCYTOMA	II/III
HF1178	-0.788367627	-0.742890628	0	35	15.8	1	GBM	IV
HF0936	-0.797567444	-0.751559753	0	55	5.1	1	ASTROCYTOMA	II
E09649	-0.804773663	-0.758350281	0	70	9.7	1	GBM	IV

HF0757	-0.813644262	-0.766709179	0	40	74.9	1	ASTROCYTOMA	II
HF0460	-0.816899863	-0.769776981	0	45	10.7	1	OLIGODENDROGLIOMA	III
HF1246	-0.829721079	-0.781858605	0	65	0.2	1	ASTROCYTOMA	II
E09602	-0.841481481	-0.792940609	0	60	4.1	1	GBM	IV
E10227	-0.845834476	-0.797042501	0	45	12.6	1	GBM	IV
E09239	-0.849419296	-0.80042053	0	30	63.3	1	ASTROCYTOMA	III
E09331	-0.864618198	-0.814742684	0	55	38.9	0	GBM	IV
E10290	-0.880951075	-0.830133398	0	30	6.9	1	GBM	IV
E10077	-0.88698674	-0.835820896	0	55	25.8	1	GBM	IV
E10300	-0.88870599	-0.837440971	0	60	9.4	1	GBM	IV
E09334	-0.89223594	-0.840767295	0	50	85.2	1	MIXED	III
E10305	-0.90434385	-0.852176761	0	40	10.1	1	GBM	IV
HF1585	-0.910068587	-0.857571266	0	25	19.9	1	GBM	IV
HF0953	-0.940283493	-0.886043225	0	35	44.6	1	ASTROCYTOMA	II
E09348	-0.942075903	-0.887732239	0	35	18.5	1	GBM	IV
E10002	-0.944691358	-0.890196822	0	55	8.4	1	GBM	IV
HF1356	-1.01733882	-0.958653614	0	50	13.5	1	GBM	IV
HF0608	-1.035354367	-0.975629933	0	50	10.6	1	ASTROCYTOMA	II
HF1220	-1.039433013	-0.979473303	0	35	10.4	1	GBM	IV
E09759	-1.061216278	-1	0	45	20.1	1	GBM	IV

Supplementary Table S7B. Activation scores, associated p-value and metadata of Gravendeel samples identified as (+) or (-) based on the NNI-8 stemness signature.

Samples	Activation Score	Normalized Score	p-value	Age	Survival (yrs)	Status	Histology	Grade	CHR1p	CHR19q	IDH1	EGFR
GSM405467	1.226995885	1	0	43.9	1.34	1	OLIGODENDROGLIOMA	III	no LOH	no LOH	mutation	wild type
GSM405476	1.216186557	0.991190412	0	64.97	1.31	1	OLIGOASTROCYTOMA	III	no LOH	no LOH	no mutation	amplification
GSM405475	1.200091449	0.978072921	0	33.74	1.05	1	GBM	IV	NA	NA	no mutation	wild type
GSM405431	1.147946959	0.935575232	0	80.65	0.92	1	GBM	IV	no LOH	no LOH	no mutation	wild type
GSM405210	1.13399177	0.924201771	0	38.53	10.28	1	OLIGODENDROGLIOMA	III	LOH	LOH	mutation	wild type
GSM405399	1.132766347	0.923203053	0	52.07	1.18	1	OLIGOASTROCYTOMA	III	no LOH	NA	no mutation	amplification
GSM405349	1.128376772	0.919625555	0	24.42	2.41	1	GBM	IV	NA	NA	no mutation	wild type
GSM405246	1.126127115	0.917792088	0	32.59	6.31	1	GBM	IV	LOH	LOH	mutation	NA
GSM405369	1.106776406	0.902021286	0	50.34	4.13	1	GBM	IV	LOH	LOH	mutation	wild type
GSM405201	1.089437586	0.887890171	0	44.57	9.82	1	OLIGODENDROGLIOMA	III	LOH	LOH	mutation	NA
GSM405208	1.088834019	0.887398265	0	51.4	3.04	1	OLIGODENDROGLIOMA	III	LOH	LOH	mutation	wild type
GSM405338	1.064581619	0.867632591	0	50.23	7.96	1	OLIGODENDROGLIOMA	II	LOH	LOH	mutation	wild type

GSM405370	1.054485597	0.859404347	0	46.52	1.61	1	GBM	IV	no LOH	no LOH	no mutation	wild type
GSM405323	1.005102881	0.819157499	0	58.78	0.62	1	GBM	IV	NA	NA	no mutation	amplification
GSM405319	1.003950617	0.818218406	0	53.65	5.62	1	OLIGODENDROGLIOMA	III	LOH	LOH	mutation	NA
GSM405257	1.000164609	0.815132815	0	46.04	10.86	0	OLIGODENDROGLIOMA	III	LOH	LOH	mutation	wild type
GSM405437	0.981545496	0.799958263	0	51.63	3.44	0	OLIGODENDROGLIOMA	II	NA	NA	mutation	NA
GSM405378	0.975290352	0.794860329	0	57.22	0	1	OLIGODENDROGLIOMA	II	NA	NA	no mutation	wild type
GSM405382	0.972491998	0.792579674	0	44.15	4.86	1	OLIGOASTROCYTOMA	III	LOH	LOH	NA	NA
GSM405227	0.967773205	0.788733864	0	48.1	4.77	1	OLIGODENDROGLIOMA	III	NA	NA	NA	NA
GSM405449	0.95820759	0.780937901	0	45.39	2.02	1	OLIGODENDROGLIOMA	III	LOH	LOH	no mutation	wild type
GSM405247	0.941362597	0.767209254	0	39.36	1.59	1	GBM	IV	no LOH	no LOH	no mutation	NA
GSM405420	0.939899406	0.766016755	0	49.94	3	1	OLIGODENDROGLIOMA	III	no LOH	no LOH	mutation	wild type
GSM405327	0.937796068	0.764302537	0	66.86	3.3	1	OLIGODENDROGLIOMA	III	LOH	LOH	mutation	wild type
GSM405329	0.936406036	0.763169663	0	60.33	5.02	1	OLIGODENDROGLIOMA	III	LOH	LOH	mutation	NA
GSM405212	0.936296296	0.763080225	0	23.33	17.49	1	OLIGODENDROGLIOMA	III	LOH	LOH	no mutation	wild type
GSM405204	0.929382716	0.757445667	0	33.89	8.59	1	OLIGODENDROGLIOMA	III	LOH	LOH	no mutation	wild type
GSM405283	0.896223137	0.730420654	0	38.07	4.07	1	OLIGOASTROCYTOMA	III	LOH	LOH	NA	wild type

GSM405234	0.882725194	0.719419849	0	57.68	0.62	1	GBM	IV	NA	NA	NA	NA
GSM405347	0.875793324	0.713770384	0	43.11	0.19	1	OLIGOASTROCYTOMA	III	NA	NA	mutation	amplification
GSM405441	0.871568358	0.710327043	0	44.74	3.27	0	OLIGODENDROGLIOMA	II	LOH	LOH	no mutation	wild type
GSM405308	0.868696845	0.707986763	0	47.4	3.1	0	GBM	IV	NA	NA	mutation	NA
GSM405377	0.859625057	0.700593268	0.0071	41.98	0.6	1	OLIGODENDROGLIOMA	III	LOH	LOH	no mutation	NA
GSM405434	0.848870599	0.691828399	0	67.01	0.24	1	GBM	IV	NA	NA	NA	NA
GSM405386	0.84528578	0.688906776	0	53.85	3.76	1	OLIGODENDROGLIOMA	II	LOH	LOH	mutation	wild type
GSM405232	0.844078647	0.687922965	0	35.7	0.98	1	GBM	IV	no LOH	no LOH	mutation	wild type
GSM405223	0.839561043	0.684241123	0	53.26	1.92	1	GBM	IV	NA	NA	no mutation	amplification
GSM405207	0.835976223	0.6813195	0	44.41	8.12	1	OLIGODENDROGLIOMA	III	LOH	LOH	no mutation	wild type
GSM405366	0.833836305	0.67957547	0	75.13	2.21	1	OLIGODENDROGLIOMA	III	LOH	LOH	mutation	wild type
GSM405388	0.817704618	0.666428167	0	78.52	0.53	1	OLIGOASTROCYTOMA	III	no LOH	no LOH	no mutation	amplification
GSM405337	0.816479195	0.665429449	0	15.02	0.28	1	GBM	IV	NA	NA	no mutation	amplification
GSM405344	0.81571102	0.664803387	0	34.71	1.19	1	OLIGODENDROGLIOMA	II	partial LOH	no LOH	no mutation	wild type
GSM405253	0.794549611	0.647556867	4.00E-04	34.84	12.56	0	GBM	IV	no LOH	no LOH	no mutation	NA
GSM405330	0.794494742	0.647512149	0	33.12	0.71	1	GBM	IV	no LOH	NA	mutation	wild type

GSM405380	0.786465478	0.640968309	0	39.99	6.04	1	OLIGODENDROGLIOMA	III	LOH	LOH	mutation	wild type
GSM405289	0.767480567	0.625495632	0	37.44	0.19	1	ASTROCYTOMA	III	NA	NA	no mutation	amplification
GSM405341	0.766620942	0.624795039	0.072	71.11	0.63	1	OLIGOASTROCYTOMA	III	NA	NA	mutation	amplification
GSM405316	0.742386831	0.605044272	0	40.06	10.34	1	OLIGOASTROCYTOMA	III	NA	NA	no mutation	wild type
GSM405461	0.737997257	0.601466774	0	49.14	0.76	1	GBM	IV	LOH	LOH	no mutation	wild type
GSM405318	0.725358939	0.591166562	0	62.46	6.21	0	OLIGODENDROGLIOMA	III	no LOH	no LOH	mutation	NA
GSM405383	0.711970736	0.580255195	0.029	37.6	1.32	1	ASTROCYTOMA	II	no LOH	no LOH	no mutation	wild type
GSM405231	0.707599451	0.576692604	0.0017	62.96	1.26	1	GBM	IV	no LOH	no LOH	NA	NA
GSM405312	0.697082762	0.568121516	0	61.31	1.02	1	GBM	IV	NA	NA	no mutation	amplification
GSM405292	0.685980796	0.559073428	0	65.52	1.11	1	GBM	IV	NA	NA	no mutation	amplification
GSM405396	0.682414266	0.556166711	2.00E-04	77.31	0.02	1	GBM	IV	no LOH	no LOH	mutation	NA
GSM405309	0.682359396	0.556121993	0.004	54.6	0.26	1	GBM	IV	NA	NA	mutation	NA
GSM405220	0.668971193	0.545210625	0	54.12	1.27	1	GBM	IV	NA	NA	no mutation	wild type
GSM405225	0.667636031	0.54412247	0	31.56	3.47	1	OLIGOASTROCYTOMA	III	no LOH	no LOH	NA	wild type
GSM405249	0.660027435	0.537921474	0	23.02	0.04	1	GBM	IV	NA	NA	mutation	wild type
GSM405468	0.65395519	0.532972602	0	33.48	7.04	0	PILOCYTIC ASTROCYTOMA	I	NA	NA	no mutation	NA

GSM405215	0.651083676	0.530632323	0.0056	51.44	2.3	1	GBM	IV	no LOH	no LOH	no mutation	NA
GSM405460	0.644554184	0.525310795	0	52.52	0.48	1	OLIGODENDROGLIOMA	III	no LOH	no LOH	no mutation	amplification
GSM405303	0.643219021	0.52422264	0.0055	56.64	0.55	1	GBM	IV	NA	NA	no mutation	NA
GSM405352	0.638372199	0.520272486	0	69.95	0.4	1	GBM	IV	NA	NA	no mutation	amplification
GSM405427	0.633763146	0.516516114	0.0014	50.83	1.53	1	GBM	IV	NA	NA	NA	NA
GSM405262	0.63122085	0.514444146	0.0062	43.26	2.89	1	GBM	IV	NA	NA	no mutation	amplification
GSM405392	0.616680384	0.502593686	0.0161	48.35	0.47	1	GBM	IV	NA	no LOH	NA	NA
GSM405284	0.613260174	0.499806219	0	57.7	1.6	1	OLIGOASTROCYTOMA	III	no LOH	no LOH	NA	amplification
GSM405242	0.60696845	0.494678472	0.0119	30.33	0.18	1	GBM	IV	NA	NA	NA	NA
GSM405363	0.605724737	0.493664848	2.00E-04	48.84	9.79	1	GBM	IV	no LOH	no LOH	mutation	wild type
GSM405385	0.602487426	0.491026444	0	34.78	1.26	0	GBM	IV	no LOH	NA	mutation	NA
GSM405391	0.599725652	0.488775601	0.0071	55.55	1.05	1	GBM	IV	no LOH	no LOH	NA	NA
GSM405355	0.598171011	0.487508571	0.013	73.19	1.19	1	ASTROCYTOMA	II	NA	NA	no mutation	NA
GSM405222	0.590507545	0.481262857	0.0074	54.06	1.3	1	GBM	IV	NA	NA	NA	NA
GSM405372	0.572748057	0.466788898	0	37.12	3.32	1	GBM	IV	LOH	LOH	NA	NA
GSM405294	0.565852766	0.461169245	0	56.41	0.8	1	GBM	IV	partial LOH	partial LOH	no mutation	amplification

GSM405281	0.561847279	0.457904779	0	37.12	3.32	1	ASTROCYTOMA	III	NA	NA	no mutation	NA
GSM405205	0.557274806	0.454178219	0.006	48.03	3.24	1	OLIGODENDROGLIOMA	III	LOH	LOH	mutation	wild type
GSM405302	0.543557385	0.442998539	0.0107	41.39	0.74	1	GBM	IV	NA	NA	no mutation	amplification
GSM405339	0.53907636	0.43934651	9.00E-04	78.08	NA	0	GBM	IV	NA	NA	no mutation	amplification
GSM405419	0.518829447	0.422845303	0.0073	36.27	2.93	1	GBM	IV	NA	NA	mutation	wild type
GSM405483	0.50780064	0.41385684	6.00E-04	32.35	0.19	0	PILOCYTIC ASTROCYTOMA	I	NA	NA	no mutation	NA
GSM405362	0.507123914	0.41330531	4.00E-04	38.11	1.06	1	GBM	IV	no LOH	no LOH	no mutation	NA
GSM405422	0.494759945	0.403228692	1.00E-04	70.67	0.91	1	GBM	IV	no LOH	no LOH	no mutation	NA
GSM405325	0.468020119	0.381435769	4.00E-04	42.98	3.65	1	OLIGOASTROCYTOMA	III	NA	NA	mutation	wild type
GSM405203	0.458655693	0.373803774	0	38.58	8.92	1	OLIGODENDROGLIOMA	III	LOH	LOH	no mutation	wild type
GSM405452	-0.405048011	-0.352486153	0.0119	71.02	0.35	1	GBM	IV	NA	NA	no mutation	wild type
GSM405464	-0.452857796	-0.394091806	1.00E-04	54.72	0.56	1	GBM	IV	NA	NA	no mutation	NA
GSM405299	-0.475189758	-0.413525817	0.0032	54.94	1.75	1	GBM	IV	NA	NA	NA	NA
GSM405238	-0.516140832	-0.449162794	0.056	37.25	0.94	1	GBM	IV	NA	NA	no mutation	NA
GSM405417	-0.530644719	-0.461784555	2.00E-04	77.31	0.02	1	GBM	IV	no LOH	no LOH	NA	NA
GSM405361	-0.531028807	-0.462118801	0	79.19	1.64	1	OLIGODENDROGLIOMA	III	no LOH	no LOH	no mutation	wild type

GSM405368	-0.55473251	-0.482746546	0	32.14	1.81	1	GBM	IV	NA	NA	NA	NA
GSM405321	-0.555390947	-0.483319539	0	33.83	3.97	1	ASTROCYTOMA	III	NA	NA	mutation	wild type
GSM405446	-0.558408779	-0.485945757	0.0111	68.18	0.73	1	GBM	IV	NA	no LOH	mutation	NA
GSM405470	-0.56354824	-0.490418285	0	31.72	1.92	1	GBM	IV	NA	NA	mutation	NA
GSM405445	-0.563712849	-0.490561533	7.00E-04	56.15	3.33	0	OLIGODENDROGLIOMA	III	no LOH	no LOH	no mutation	NA
GSM405304	-0.570132602	-0.496148214	0	66.39	0.56	1	GBM	IV	NA	NA	no mutation	NA
GSM405340	-0.574833105	-0.500238747	0.0366	52.88	5.56	0	GBM	IV	no LOH	no LOH	mutation	wild type
GSM405455	-0.587288523	-0.511077863	0	55.49	0.23	1	GBM	IV	NA	NA	mutation	NA
GSM405277	-0.590525834	-0.513895079	0	43.89	2.76	1	ASTROCYTOMA	III	NA	NA	mutation	wild type
GSM405450	-0.593854595	-0.516791876	1.00E-04	36.66	13.3	0	OLIGOASTROCYTOMA	III	NA	NA	NA	NA
GSM405443	-0.610992227	-0.531705609	0.0318	56.62	0.98	1	GBM	IV	NA	NA	no mutation	amplification
GSM405402	-0.611028807	-0.531737442	0	23.72	4.55	0	ASTROCYTOMA	II	no LOH	NA	no mutation	amplification
GSM405263	-0.611394604	-0.532055771	0	61.74	1.55	1	GBM	IV	NA	NA	no mutation	wild type
GSM405453	-0.612985825	-0.533440504	0	70.23	0.21	1	GBM	IV	NA	no LOH	no mutation	amplification
GSM405296	-0.614302698	-0.53458649	0.0168	41.09	0.29	1	GBM	IV	no LOH	no LOH	no mutation	wild type
GSM405400	-0.630855053	-0.548990896	0.0028	49.64	0.45	1	ASTROCYTOMA	III	no LOH	NA	no mutation	wild type

GSM405268	-0.631458619	-0.549516139	0	48.04	0.64	1	GBM	IV	no LOH	no LOH	no mutation	amplification
GSM405273	-0.632556013	-0.550471128	0	56.42	0.54	1	OLIGOASTROCYTOMA	III	NA	NA	no mutation	NA
GSM405271	-0.643895748	-0.560339339	0	69.89	0.3	1	GBM	IV	NA	NA	NA	NA
GSM405365	-0.66085048	-0.575093907	0	64.29	2.66	1	GBM	IV	no LOH	no LOH	no mutation	NA
GSM405211	-0.661234568	-0.575428153	0.0023	34.93	1.83	1	OLIGODENDROGLIOMA	III	LOH	LOH	mutation	NA
GSM405214	-0.664252401	-0.578054371	0	37.84	1.5	1	GBM	IV	no LOH	no LOH	no mutation	wild type
GSM405348	-0.674659351	-0.587110842	0.0011	11.72	0.03	0	PILOCYTIC ASTROCYTOMA	I	NA	NA	NA	NA
GSM405295	-0.679890261	-0.591662953	0.0011	41.77	1.99	1	ASTROCYTOMA	III	NA	NA	NA	NA
GSM405218	-0.693315043	-0.603345642	0	32.36	0.64	1	GBM	IV	no LOH	no LOH	no mutation	amplification
GSM405334	-0.700429813	-0.609537149	0	57.01	1.47	1	OLIGODENDROGLIOMA	III	no LOH	no LOH	NA	wild type
GSM405393	-0.701874714	-0.61079455	0	70.67	0.08	1	GBM	IV	NA	NA	no mutation	NA
GSM405390	-0.70266118	-0.611478958	0.0261	70.07	0.02	1	OLIGOASTROCYTOMA	III	NA	NA	no mutation	NA
GSM405375	-0.706191129	-0.614550837	0	67.03	0.06	1	GBM	IV	no LOH	NA	no mutation	NA
GSM405463	-0.710983082	-0.618720952	0	65.53	2.22	1	GBM	IV	NA	no LOH	no mutation	wild type
GSM405261	-0.71303155	-0.620503597	0	60.46	0.98	1	OLIGODENDROGLIOMA	III	no LOH	no LOH	mutation	NA
GSM405477	-0.71478738	-0.622031578	0	73.64	0.11	1	GBM	IV	NA	NA	NA	NA

GSM405471	-0.721572931	-0.627936589	0	78.12	0.15	1	GBM	IV	NA	NA	mutation	NA
GSM405290	-0.738692273	-0.642834405	0	45.5	1.16	1	GBM	IV	NA	NA	NA	NA
GSM405288	-0.742021033	-0.645731203	0	41.93	1.53	1	OLIGOASTROCYTOMA	III	no LOH	no LOH	NA	wild type
GSM405364	-0.746977595	-0.650044566	0	37.61	9.85	1	OLIGODENDROGLIOMA	III	LOH	LOH	mutation	wild type
GSM405397	-0.748861454	-0.651683963	0.0187	60.36	0.35	1	GBM	IV	no LOH	no LOH	no mutation	amplification
GSM405240	-0.771504344	-0.671388553	0.0049	33.09	6.62	0	GBM	IV	no LOH	no LOH	mutation	NA
GSM405447	-0.782130773	-0.680636022	0	59.03	2.79	1	GBM	IV	no LOH	no LOH	NA	NA
GSM405301	-0.785788752	-0.683819316	0	65.35	0.3	1	GBM	IV	NA	NA	NA	NA
GSM405233	-0.79310471	-0.690185904	0	51.64	0.86	1	GBM	IV	NA	NA	no mutation	wild type
GSM405472	-0.796360311	-0.693019036	0	62.11	0.34	1	GBM	IV	NA	NA	mutation	NA
GSM405241	-0.811650663	-0.706325205	0	55.98	0.16	1	GBM	IV	NA	NA	NA	NA
GSM405236	-0.829208962	-0.721605017	0	52.2	1.03	1	GBM	IV	NA	NA	no mutation	NA
GSM405407	-0.844938272	-0.735293181	0	81.18	0.82	1	ASTROCYTOMA	III	no LOH	no LOH	no mutation	NA
GSM405259	-0.864252401	-0.752100974	0	64.01	0.41	1	ASTROCYTOMA	III	NA	NA	no mutation	NA
GSM405442	-0.866758116	-0.754281531	0	63.61	0.3	1	GBM	IV	NA	NA	no mutation	wild type
GSM405243	-0.868221308	-0.755554848	0	61.33	0.88	1	GBM	IV	NA	NA	NA	NA

GSM405423	-0.871129401	-0.758085567	0	35.67	6.12	1	ASTROCYTOMA	III	LOH	no LOH	mutation	NA
GSM405421	-0.872812071	-0.759549882	0	38.4	6.08	0	ASTROCYTOMA	III	no LOH	no LOH	no mutation	wild type
GSM405457	-0.879048925	-0.764977399	0	70.98	0.3	1	OLIGODENDROGLIOMA	III	no LOH	no LOH	no mutation	wild type
GSM405282	-0.889638775	-0.774193035	0	51.92	0.12	1	GBM	IV	NA	NA	no mutation	NA
GSM405412	-0.897759488	-0.781259948	0	55.71	0.65	1	GBM	IV	NA	no LOH	no mutation	NA
GSM405320	-0.902039323	-0.784984402	0	70.28	0.6	1	GBM	IV	NA	NA	no mutation	wild type
GSM405416	-0.912757202	-0.794311453	0	64.26	0.34	1	GBM	IV	NA	NA	NA	NA
GSM405353	-0.918573388	-0.799372891	0	55.39	0.7	1	GBM	IV	NA	NA	no mutation	amplification
GSM405426	-0.920859625	-0.80136245	0	67.1	0.05	1	GBM	IV	NA	NA	mutation	wild type
GSM405415	-0.933004115	-0.811930986	0	67.48	0.5	1	GBM	IV	no LOH	no LOH	no mutation	NA
GSM405374	-0.940448102	-0.81840899	0	58.58	1.21	1	GBM	IV	LOH	LOH	no mutation	wild type
GSM405456	-0.94083219	-0.818743236	0	52.5	NA	0	GBM	IV	NA	NA	no mutation	NA
GSM405278	-0.947105624	-0.824202585	0	58.23	0.73	1	GBM	IV	NA	NA	no mutation	amplification
GSM405313	-0.963090992	-0.83811358	0	32.5	3.31	1	GBM	IV	NA	NA	mutation	wild type
GSM405235	-0.969108368	-0.843350099	0	71.09	0.21	1	GBM	IV	NA	NA	no mutation	NA
GSM405245	-0.97561957	-0.849016362	0	37.98	1.4	1	GBM	IV	no LOH	NA	no mutation	NA

GSM405293	-1.006474623	-0.875867448	0	63.73	0.88	1	GBM	IV	NA	NA	mutation	amplification
GSM405403	-1.025624143	-0.892531992	0	38.42	0.04	1	ASTROCYTOMA	III	NA	NA	NA	NA
GSM405430	-1.052967535	-0.916327115	0	61.1	0.35	1	GBM	IV	no LOH	no LOH	no mutation	wild type
GSM405265	-1.082524005	-0.942048131	0	32.14	1.81	1	ASTROCYTOMA	III	NA	NA	no mutation	wild type
GSM405459	-1.102222222	-0.95919017	0	64.28	1.14	1	GBM	IV	no LOH	no LOH	no mutation	NA
GSM405479	-1.102807499	-0.959699497	0	63.3	0.38	1	GBM	IV	NA	NA	mutation	amplification
GSM405440	-1.149117513	-1	0	69.88	0.53	1	GBM	IV	NA	NA	NA	wild type